22nd Iranian Physical Chemistry Conference

20-22 August 2019

بیست و دومین کنفرانس شیمی فیزیک انجمن شیمی ایران

محورهای کنفرانس

- نانوشیمی فیزیک
- بیوشیمی فیزیک
- ترمودینامیک کلاسیک
- مکانیک آماری
- مکانیک کوانتومی
- طیف‌سنجی
- الکتروشیمی
- طراحی محاسباتی دارو
- سینتیک شیمیایی
- شیمی فیزیک کاربردی
- شیمی محاسباتی
- شیمی سطح و حالت جامد
- شیمی فیزیک پلیمرها

۲۹ الی ۳۱ مرداد

دانشگاه زنجان

شروع ثبت نام و ارسال مقاله: ۱ اردیبهشت ۹۸

آخرین مهلت ارسال مقاله: ۱۷ خرداد ۹۸

اعلام نتایج داوری مقالات: ۱۰ تیر ۹۸

آخرین مهلت ثبت نام: ۱۰ مرداد ۹۸

آدرس دبیرخانه: زنجان، بلوار دانشگاه، دانشگاه زنجان
دانشکده علوم ، گروه شیمی، دبیرخانه کنفرانس
تلفن : ۰۲۴-۳۳۰۵۲۶۳۱ تلفکس: ۰۲۴-۳۳۰۵۲۴۷۷

http://physchem22.ir
E-mail:ipcc22@znu.ac.ir

حامیان بیست و دومین کنفرانس شیمی فیزیک ایران

۱-دانشگاه زنجان

۲- انجمن شیمی ایران

۳- پایگاه استنادی علوم جهان اسلام

۴- مرکز منطقه ای اطلاع رسانی علوم و فناوری

۵- وزارت علوم، تحقیقات و فناوری

۶- شرکت روی پرور

۷-انجمن صنایع و معادن سرب و روی ایران

۸- دانشگاه تحصیلات تکمیلی در علوم پایه زنجان

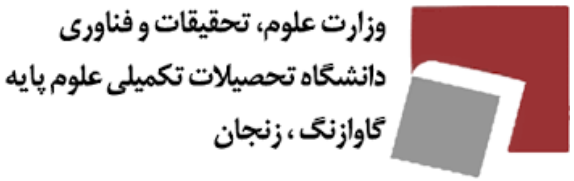

۹- دانشگاه آزاد اسلامی واحد زنجان

دانشگاه آزاد اسلامی
زنجان

۱۰- شرکت ملی سرب و روی ایران

شرکت ملی سرب و روی ایران

۱۱- شرکت آنا کیمیا منگنز

KIMIA MANGANESE 9262

۱۲- شرکت فرآوری مواد معدنی ایران

شرکت فرآوری
مواد معدنی ایران

۱۳- شرکت شمش روی میهن

MZINC
ingot Co.

۱۴- شرکت سپید اکسید زنجان

Sepid Oxide Zanjan Co.
شرکت سپید اکسید زنجان

۱۵- شرکت ترکیب پردازان زنجان

۱۶- اداره کل استاندارد استان زنجان

۱۷- شرکت توزیع نیروی برق استان زنجان

شرکت توزیع نیروی برق استان زنجان
Zanjan Electricity Distribution Company

۱۸- شرکت برق منطقه ای زنجان

برق منطقه ای زنجان

کمیته علمی بیست و دومین کنفرانس شیمی فیزیک انجمن شیمی ایران

عکس	دانشگاه/پژوهشگاه/مرکز تحقیقات	نام و نام خانوادگی
	زنجان	(دبیرعلمی) دکتر مرتضی واحدپور
	خواجه نصیرالدین طوسی	دکتر سیف اله جلیلی
	خوارزمی	دکتر غلامرضا اسلامپور
	اصفهان	دکتر عبدالخالق بردبار

	فردوسی مشهد	دکتر محمدرضا حسین دخت
	کردستان	دکتر رحمت صادقی
	بوعلی سینا-همدان	دکتر سعید عزیزیان
	علم و صنعت ایران	دکتر سیدمرتضی موسوی خوشدل
	محقق اردبیلی	دکتر عزیز حبیبی

	صنعتی امیرکبیر	دکتر محمد حسن موسی زاده
	جیرفت	دکتر راضیه رضوی
	شهید باهنر کرمان	دکتر مریم دهستانی
	زنجان	دکتر جمال داودی
	علوم پزشکی تهران	دکتر مسعود امانلو

	سیستان و بلوچستان	دکتر علی اکبر میرزائی
	تهران	دکتر علی مقاری
	خلیج فارس	دکتر حسین اسلامی
	شهید باهنرکرمان	دکتر سیدمحمدعلی حسینی
	تحصیلات تکمیلی زنجان	دکتر محسن لشگری

	مازندران	دکتر سعید یگانگی
	سیستان و بلوچستان	دکتر سیدمصطفی حبیبی خراسانی
	سمنان	دکتر مصطفی فضلی
	شیراز	دکتر سید حسین موسوی پور
	تهران	دکتر حسن به نژاد

	شهید بهشتی	دکتر شانت شهبازیان
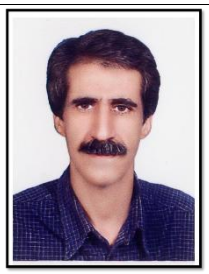	رازی-کرمانشاه	دکتر شهرام رنجبر
	کاشان	دکتر مسعود همدانیان
	یاسوج	دکتر شاپور رمضانی
	شیراز	دکتر علی حیدرپاکیاری

	بیوشیمی و بیوفیزیک	دکتر علی‌اکبر موسوی موحدی
	شیمی و مهندسی شیمی ایران	دکتر زهرا جمشیدی
	تحصیلات تکمیلی زنجان	دکتر فخری السادات محمدی
	علوم پزشکی زنجان	دکتر سعید قنبرزاده
	فردوسی مشهد	دکتر محمدحسن انتظاری

	دامغان	دکتر داود عاجلو
	شهید بهشتی	دکتر محمدحسن پیروی
	صنعتی اصفهان	دکتر محمود تبریزچی
	شیراز	دکتر افشان مهاجری
	تحصیلات تکمیلی زنجان	دکتر محمدحسین کوثری

	فردوسی مشهد	دکتر الهه کفشدارگوهرشادی
	تربیت مدرس	دکتر حسین غریبی
	گیلان	دکتر علی قنادزاده
	شریف	دکتر محسن تفضلی
	کردستان	دکتر خالد عزیزی

	اصفهان	دکتر حسن سبزیان
	شیراز	دکتر مجتبی علی پور
	مازندران	دکتر عبداله عمرانی
	بیوشیمی و بیوفیزیک	دکتر محمد حسین کریمی جعفری
	علم و صنعت ایران	دکتر سید مجید هاشمیان زاده

	تبریز	دکتر حمایت شکاری
	تربیت مدرس	دکترناصر هادی پور لاکمه سری
	شریف	دکتر افشین شفیعی
	علوم و فنون هسته ای	دکتر یاور تقی پور آذر
	شهید بهشتی	دکتر سیدشهاب الدین نقوی

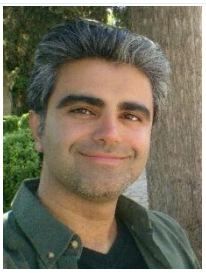	علوم پزشکی اصفهان	دکتر محمود میرزایی
	بیوشیمی و بیوفیزیک	دکتر سجاد قرقانی
	یزد	دکتر محمد کمالوند
	مازندران	دکتر داود فرمان زاده
	صنعتی شیراز	دکتر محمد مهدی علویان مهر

	گیلان	دکتر بهرام قلمی چوبر
	امیرکبیر	دکتر سعیده سرآبادانی تفرشی
	گیلان	دکتر محمدحسن لقمانی
	سیستان و بلوچستان	دکتر علی ابراهیمی
	تحصیلات تکمیلی زنجان	دکتر فریبا نظری

	صنعتی اصفهان	دکتر عزت کشاورزی
	نیشابور	دکتر بهزاد حقیقی
	حکیم سبزواری	دکتر حامد اکبر زاده
	صنعتی شاهرود	دکتر حسین نیکوفرد
	مازندران	دکتر عفت کیانپور

	پیام نور	دکتر رضا بهجت منش اردکانی
	شهیدبهشتی	دکتر کریم زارع
	آزاد اسلامی	دکتر علی مهری زاد
	آزاد اسلامی	دکتر سمیه مجیدی
	آزاد اسلامی	دکتر مسعود درویش گنجی

	آزاد اسلامی	دکتر مسعود گیاهی سراوانی
	آزاد اسلامی	دکتر سید محمد شعاعی
	آزاد اسلامی	دکتر الهام تازیکه لمسکی
	گناباد	دکتر علیرضا برنجی
	فنی و حرفه ای	دکتر مریم عابدی

	زنجان	دکتر منیژه توضیحی
	زنجان	دکتر محبوبه بهروزی
	زنجان	دکتر فرهاد خوئینی

کمیته اجرایی بیست و دومین کنفرانس شیمی فیزیک انجمن شیمی ایران

	دانشگاه	نام و نام خانوادگی
	زنجان	دکتر حامد بهرامی (دبیر اجرائی)
	زنجان	دکتر میر سعید سید دراجی (پذیرش)
	زنجان	دکتر حسن شایانی جم (تغذیه)

	زنجان	دکتر محمد شادمان (وبسایت، کتابچه کنفرانس و مدیریت سخنرانی ها)
	زنجان	دکتر سهراب رحمانی (ارائه پوستر ها)
	زنجان	مهندس حمید ارجمندفر (میزگردهای تخصصی صنعتی)
	زنجان	دکتر فرهاد کبیری اصفهانی (روابط عمومی، هماهنگی سالن ها)

	زنجان	دکتر رحمت اله پورعطا (اسکان)
	زنجان	دکتر بهمن فرجمند (کارگاه ها)
	زنجان	خانم دکتر منیژه توضیحی (مدیریت داوری مقالات و صدور گواهی ها)
	زنجان	دکتر محمد علی رضوانی (غرفه ها)
	زنجان	دکتر محبوبه بهروزی (داوری پوسترها)

	زنجان	جناب آقای احسان حریری (پذیرایی میان وعده)
	زنجان	جناب آقای حسین حمزه لو (گردشگری)
	زنجان	سرکار خانم ستاره حسن وند (مجری)
	تحصیلات تکمیلی علوم پایه زنجان	جناب آقای کریم واحدپور (سمعی و بصری)

	مسولیت	زیر مجموعه	نام و نام خانوادگی
	ارتباط با صنعت	دبیرخانه	آقای رضا احمدی
	سالن های سخنرانی	دبیرخانه	آقای دکتر سعید تقوی فردود
	مدیریت مقالات -چاپ پوستر- ارائه پوستر	دبیرخانه	خانم معصومه قهرمانی
	مدیریت مقالات	دبیرخانه	خانم فهیمه خوئینی

	ارائه پوسترها	دبیرخانه	خانم سحر افشاری
	پشتیبانی	دبیرخانه	آقای حامد درودگری
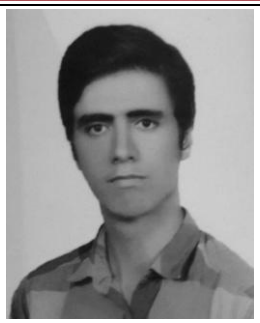	پشتیبانی- اسکان	دبیرخانه	آقای فرشاد نوری
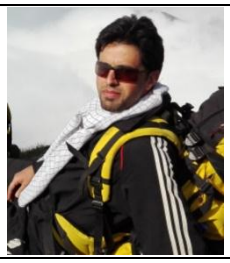	گردشگری	گردشگری	آقای دکتر بابک پاشایی

	پشتیبانی – سالن ها	دبیرخانه	خانم شیوا یحیی زاده
	خوابگاه خواهران	اسکان	خانم مینا امیری
	خوابگاه خواهران	اسکان	خانم نرگس سعیدی
	خوابگاه برادران و متاهلین	اسکان	آقای هادی زارع پور

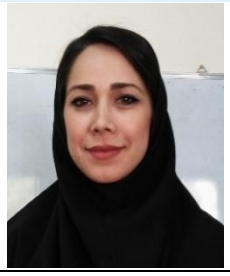	سالن های سخنرانی	دبیرخانه	خانم پریا اسدی
	سالن های سخنرانی	دبیرخانه	خانم شبنم برجی
	میزپذیرش	دبیرخانه	سوده المعی
	میزپذیرش	دبیرخانه	هدا دانشور
	میز پذیرش	دبیرخانه	سیده فاطمه حسینی

	میزپذیرش	دبیرخانه	نیما محمودی
	کارگاه ها	کارگاه ها	الهه احدی
	کارگاه ها	کارگاه ها	معصومه اقمشه
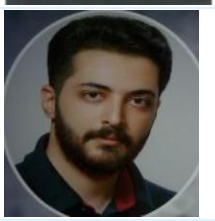	میز پذیرش	دبیرخانه	پیمان پارسیان
	میز پذیرش	دبیرخانه	سینا رحمنی

	هماهنگی سالن ها	سالن ها	پیام ویسی
	میز پذیرش	دبیرخانه	فرناز یوسفیان
	میز پذیرش	دبیرخانه	بهاره نویدی
	میز پذیرش	دبیرخانه	فاطمه عسکری

Section:

Applied Physical Chemistry

Physical Properties of Choline chloride+K_3PO_4+H_2O System

E. Norouzi*[a], *A. Roosta*[a]
Department of Chemical, Petroleum and Gas Engineering, Shiraz University of Technology, Shiraz, Iran
**Email: aa.roosta@sutech.ac.ir*

Abstract: Aqueous two-phase systems (ATPSs) are used for separating biological compounds. Recently, ATPSs consisting of choline chloride and a kosmotropic salt as very efficient systems have been attracted due to its superiority and application in various industries, researchers have recently focused their attention on physical properties such as density, viscosity, and surface tension. In this study, some physical properties of an aqueous two-phase system consisting of choline chloride, tri-potassium phosphate and water have been measured and the effect of the concentration of phosphate salt on the physical properties has been investigated. The results show that the density and viscosity increase with an increase in the concentration of phosphate salt while the surface tension decreases with the increase in the phosphate concentration. Furthermore, the viscosity of the current system is significantly lower than the viscosity of polymer-based ATPSs.

Keywords: aqueous two-phase systems, choline chloride, physical properties, tri-potassium phosphate.

I. INTRODUCTION

There are different methods for separation and purification of biological compounds, such as adsorption, precipitation, membrane separation crystallization, column chromatography, organic solvent extraction, and liquid-liquid extraction [1,2]. An aqueous two-phase system (ATPS) is a liquid-liquid extraction technique and has gained interest because of great potential for the extraction, separation, purification, and enrichment of proteins, viruses, enzymes, nucleic acids, and other biomolecules industries [3,4]. This method has some advantages over conventional extraction techniques such as environmentally friendly, low cost, ease of scaling up, capable of continuous operation [5].
In 1896, Beijerinck accidentally found the ATPS while mixing an aqueous solution of starch and gelatin [6]. However, in 1958, its real application was discovered by Albertsson, who employed these systems to distribute a wide range of biomolecules [7]. ATPSs consist of various components such as polymer-polymer, polymer-salt, alcohol-salt, salt-salt or polymer- ionic liquids [2]. The problems of polymer systems and ionic liquids are their high cost and viscosity [6]. Fortunately, these problems are solved by salt-salt systems. Some physical properties of these systems, including density, surface tension and viscosity are important properties in designing the separation process. Thus, in this study, the physical properties of an aqueous two-phase system consisting of choline chloride, tri-potassium phosphate, and water have been investigated.

II. METHODS

In this study, the density, surface tension, kinematic viscosity and dynamic viscosity of the ternary system of choline chloride + tripotassium phosphate + water were experimentally determined at 300 K and different concentrations of the constituents. In this regard, different mixtures of the ternary systems were prepared on the binodal curve of the system, by using an analytical scale with an accuracy of 0.0001 g. To measure the density, 1 mL of each sample was removed by a sampler (with an accuracy of 0.001 mL) and was scaled by an analytical scale (with an accuracy of 0.0001 g). The kinematic viscosity was measured using an Ostwald viscometer placed in a water bath. The surface tension of the samples was determined using a surface tensiometer based on Du-Nouy Method ASTM 1331 (Novin Shimyar Company). Finally, the dynamic viscosity was calculated by multiplying the kinematic viscosity in the density.

III. RESULTS AND DISCUSSION

The experimental data of density, kinematic viscosity, dynamic viscosity, and surface tension as a function of the concentration of K_3PO_4 are illustrated in Figures 1 to 4, respectively.
As can be seen in Figure 1, the density of the mixtures increases with the increase in the concentration of K_3PO_4 or decrease in the choline chloride concentration. The density varied between 1100 $kg.m^{-3}$ to 1570 $kg.m^{-3}$ where the mass percent of K_3PO_4 increased from 6% to 56%.
As seen in Figure 2, the kinematic viscosity increases with the increase in the phosphate salt concentration, especially for the salt concentrations more than 40 (%w/w). The dynamic viscosity was calculated by multiplying the kinematic viscosity in the density, as shown in Figure 3. The

dependence of the dynamic viscosity on the salt concentration is almost the same as the kinematic viscosity. It is worth mentioning that the viscosity of this system is significantly lower than the conventional polymer-based ATPSs.

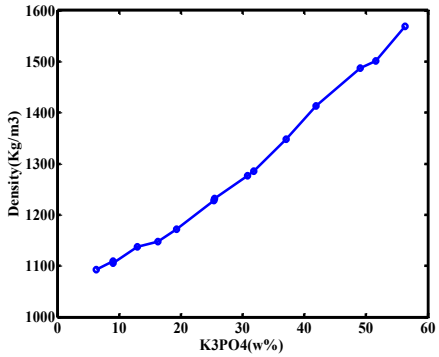

Fig.1: Density of the system vs. phosphate mass percentage at 300 K.

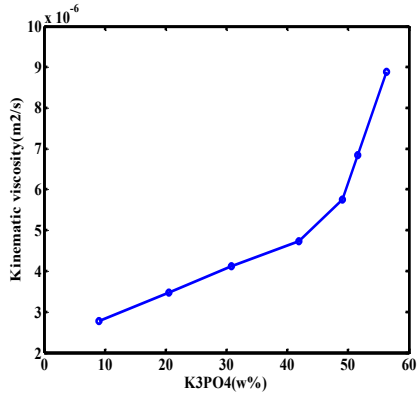

Fig.2: Kinematic of the system vs. phosphate mass percentage at 300 K.

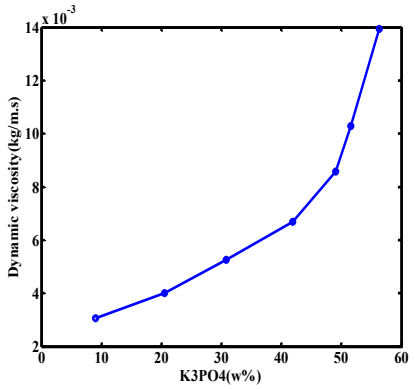

Fig.3: Dynamic viscosity of the system vs. phosphate mass percentage at 300 K.

Furthermore, the surface tension of the system as a function of K_3PO_4 concentration is illustrated in Figure 4. The surface tension decreases as the salt concentration is increased. In addition, the surface tension of the system is lower than the surface tension of distilled water (71.7 mN/m at 300 K) for all concentrations of K_3PO_4.

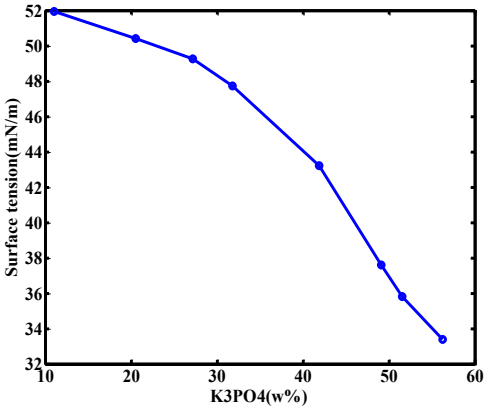

Fig.4: Surface tension of the system vs. phosphate mass percentage at 300 K.

IV. CONCLUSION

In this study, the physical properties of the ATPS of choline chloride+tri-potassium phosphate+ water were measured at 300 K. The low viscosity of this system compared to conventional ATPSs is an advantage of the current system. In addition, the significant change in density with the salt concentration leads to a better separation of two phases.

REFERENCES

[1] N.Li, Y.Wang, K. Xu, Talanta, vol. 152, pp. 23-32, **2016**.
[2] A. Roosta, A. Rabieenezhad, The Journal of Chemical Thermodynamics, vol. 120, pp. 54-59, **2018**.
[3] I.N. Souza, M.M. Pereira, M.G. Freire, Separation and purification technology, vol. 136, pp. 74-8, **2014**.
[4] R. Sankaran, P.L. Show, Y.J. Yap, H.L. Lam, J. Clean. Prod, Vol. 184, pp. 938–948, **2018**.
[5] G. Pazuki, M. Vossoughi, V. Taghikhani, J. Chem. Eng, Data., vol. 55, pp. 243-248. **2009.**
[6] S. Raja, V. R Murty, V. Thivaharan, Sci Technol, vol. 1, pp. 7-16, **2011**.
[7] P.A. Albertsson, Adv. Protein Chem, Vol. 24, pp. 309-341, **1970**.

The Investigation of Adsorptive Performance of Co3O4 Nanoparticles in the Removal of Cd^{2+} ions

Mitra Rafizadeh*[a], Narges Samadani Langeroodia, Mahnaz Khalafi[b]

[a]*Department of Chemistry, Faculty of Sciences, Golestan University, Gorgan, Iran*
[b]*Department of Statistics, Faculty of Sciences, Golestan University, Gorgan, Iran*

Abstract: In this study Co3O4 nanoparticles was synthesized by sol-gel technique and was examined as sorbent to remove of Cd2+. The obtained nanoparticles were characterized using FTIR, and XRD. BET surface area of nanoparticles was 21.39 m2/g. The effect of adsorbent weight and contact time on adsorption capacity and removal ratio of the Cd2+ ions was investigated as well. The results revealed that prepared nanoparticles can be used as an effective adsorbent for the removal of Cd2+ ions.

Keywords: heavy metals; Nanoparticles; Adsorption

I. INTRODUCTION

Water contamination by heavy metals such as Cd, Pb and Cu is a serious environmental problem. These metals pose a serious threat to organisms, living species and human beings because of their bioaccumulation, no biodegradable property and toxicity. Cadmium is one of the most toxic metals and has negative effects on the environment [1-3]. Our objectives in this work are the synthesis of Co3O4 nanoparticle and its application for adsorption of Cd2+ ions.

II. METHODS

FTIR (Perkin-Elmer Model System 2000 using KBr pellet method), and X-ray diffractometer (XRD) (X′ Pert Pro, Panalytical, Netherlands) were employed in this study. Cd2+ remaining unabsorbed in the supernatant liquid were determined with atomic absorption spectrometer (model Shimadzu, AA-7000). Surface area was determined by N2-BET method.

A certain weight of CO (NO3)2 · 6H2O was dissolved in deionized water. Then 1 M NaOH solution was added drop wise into above mixture with mechanical stirring to pH to 13. Then, the stirrer was turned off and the obtained solution was kept at room temperature for 24 hours. After this time, wet powders were dried at 70 °C for 18 hours. The obtained dry powder was heated in a quartz tube furnace at 250°C for 3 hours and finally, was calcination at 600 °C for 3 hours.

Adsorption experiments were performed by mixing a certain amount of adsorbent with 50 mL of 50 mg/L the Cd (NO3)2 · 4H2O solution. The amount of Cd2+ adsorbed per unit mass of adsorbent at different times, qt (mg/g), was calculated according to equation (1):

$$q_t = \frac{(C_0 - C_t)V}{W} \quad (1)$$

The removal ratio (R%) of Cd2+ was calculated using the following equation:

$$R = \frac{C_0 - C_e}{C_0} \times 100 \quad (2)$$

Where C0 (mg.L-1) and Ce (mg.L-1) are the initial and equilibrium concentrations of the adsorbate, respectively.

III. RESULTS AND DISCUSSION

A. *FT-IR spectroscopy*

The FTIR spectrum of Co3O4 nanoparticles shows the adsorption bond at 632 cm-1and 538 cm-1. The band located at 632 cm-1 corresponds to the stretching vibration of CoII-O in tetrahedral hole and 538 cm-1 was assigned to the stretching vibration mode of CoIII-O in octahedral hole [4, 5].

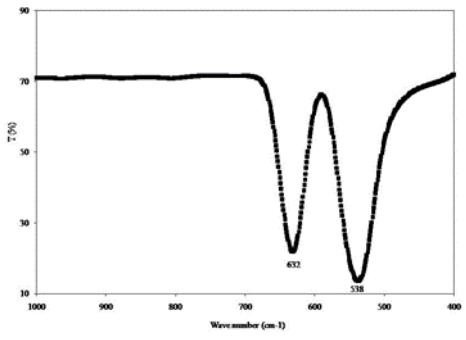

Fig. 1. FT-IR spectra ofCo3O4

B. X-ray diffraction

The XRD plot of prepared nanoparticles is shown in Fig. 2. The average crystallite size, based on the intense diffraction peak is about 48 nm. The observed peaks at 2θ =19.08, 31.35, 36.93, 38.66, 44.89, 59.41 and 65.31° confirmed the preparation of Co3O4 nanoparticles with a cubic structure that is fully consistent with the standard spectrum (JCPDS: 43-1003). XRD result showed that the prepared nanoparticle is well crystalline frameworks.

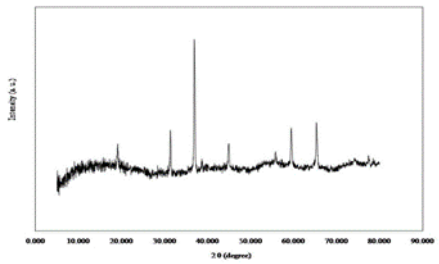

Fig. 2. XRD patterns ofCo3O4

Effect of adsorbent weight

It could be seen from the Fig. 3 that adsorption capacity decreased with increasing adsorbent weight, due to the unsaturation of some of the active sites in the adsorption process. Fig. 3 demonstrates the removal ratio of Cd2+ increases with increase in adsorbent weight due to increase in the number of adsorption sites.

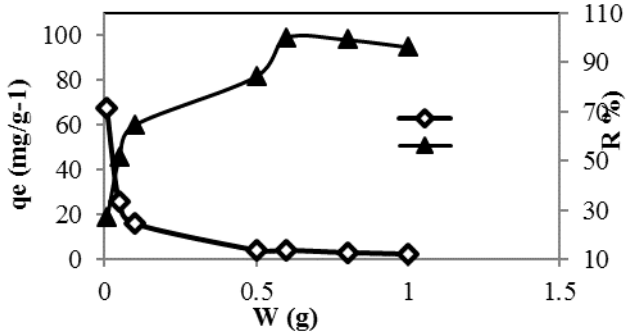

Fig. 3. Effect of adsorbent weight on adsorption capacity and removal ratio of Cd 2+

Effect of contact time

It should be noted that adsorption capacity of Cd2+ is increased with contact time and finally attained equilibrium in approximately 60 min (Fig.4).

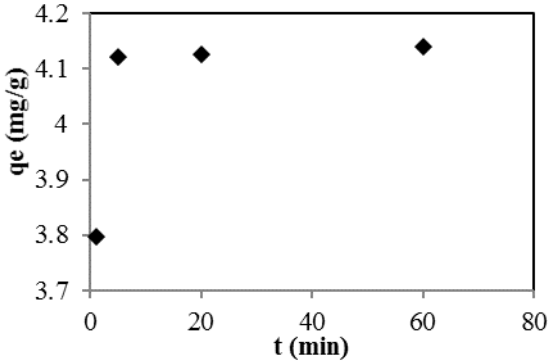

Fig.4. Effect of time on adsorption capacity of Cd 2+

IV. CONCLUSION

In this study Co3O4 nanoparticle was synthesized by sol-gel method and were characterized by IR and XRD methods. Co3O4 nanoparticle in the adsorption process was effective in removing Cd2+ ions from aqueous solution because of suitable crystallinity of nanoparticles

REFERENCES

[1] . N. N. Nassar, J. Hazard. Mater. 184 (1-3), 538 (2010).
[2] Y, Feng, J. L. Gong, G. M. Zeng, Q. Y. Niu, H.Y. Zhang, and C. G. Niu, J. H. Deng, M. Yan, Chem. Eng. J. 162, 487 (2010).
[3] P. Trivedi, L. Axe, Modeling Cd and Zn sorption to hydrous metal oxides, Enviroci. Technol. 34, 2215(2000).
[4] R. Manigandan, K. Giribabu, R. Suresh, L. Vigayalakshmi, A. Stephen, and V. Narayanan, Chem. Sci. Trans. 2 (S1), S47 (2013).
[5] M. Ghiasi, A. Malekzadeh, and H. Mardani,Mater. Sci. Semiconduc. Procc. 42, 311 (2016).
[6]
[7]

Direct Conversion of Chlorella Vulgaris Microalgae to Biodiesel Under Supercritical Methanol Condition in The Presence of Heterogeneous Nano-photocatalyst

***Maryam Aghilinategh*[1], *Mohammad Barati*[2,*], *Masood Hamadanian*[1,3]**

[1] *Department of Physical Chemistry, Faculty of Chemistry, University of Kashan, Kashan, Iran*

[2] *Department of Applied Chemistry, Faculty of Chemistry, University of Kashan, Kashan, Iran*

[3] *Institute of Nanosciences and Nanotechnology, University of Kashan, Kashan, Iran*

*Corresponding author, Email: barati.m@kashanu.ac.ir

Abstract: The CaO/TiO2 nanocatalyst was synthetized via photochemical method. This work illustrates an increase in total product yield Consequently, the presence of nanocatalysts in reaction medium that is include direct conversion of Chlorella vulgaris microalgae to biodiesel in supercritical methanol. No CaO was found in products and no color change happen for product over time which is due to the strong bonding of CaO to TiO2. The effects of nanocatalysts on products were described via reaction mechanisms.

Keywords: Biodiesel, Microalgae, Nano-photocatalyst, Supercritical methanol, Chlorella vulgaris.

I. INTRODUCTION

Alkali metal oxides have been widely used as heterogeneous catalysts for transesterification reactions. Calcium oxide is one of the most noteworthy heterogeneous catalysts for biodiesel production that has a low preparation cost and high basicity [1, 2]. Trace dissolving of some metal oxides in the produced biodiesel has a negative effect on fuel quality over time [3, 4]. The metal oxides SrO, ZnO, CaO, ZrO_2, and TiO_2 have been used as catalysts for biodiesel production in supercritical and subcritical methanol. Results confirm the presence of SrO and CaO in the final product, in contrast to ZnO, TiO_2 and ZrO_2 which were insoluble in biodiesel [5]. CaO solubility in biodiesel has also been reported by some other researchers [6, 7]. Product washing with a methanol-Na_2CO_3 mixture has been reported as an efficient method for eliminating calcium soaps in biodiesel produced in the presence of CaO as a heterogeneous catalyst [6]. In this research, the photochemical method was used for the preparation of CaO/ TiO_2 catalysts for biodiesel production from microalgae biomass in supercritical methanol to investigate the stability of photochemical-synthetized CaO in a supercritical process.

II. METHOD

Materials: Methanol (Samchun Chemical Co., Ltd., Korea). Ethyl tridecanoat (99% pure, Sigma–Aldrich Korea, Co.). n-Hexane (99.0% pure, Samchun Chemical Co., Ltd., Korea). Titanium tetraisopropoxide (TTIP), glacial acetic acid, ethanol and $CaCl_2.2H_2O$ were all purchased from Merck.

Catalysts preparation: The TiO_2 nanocatalyst was prepared by a modified sol-gel (SG) method using TTIP, glacial acetic acid, ethanol and water. Afterwards, it was dried and finally calcined at 550.0 ˚C for 1 h. The CaO/ TiO_2 nanocatalyst was prepared by photochemical method.

Experimental procedure: The reaction was performed in a cylindrical reactor made of 316 stainless steel with 60mL volume. The reaction temperature was controlled using an electrical furnace and a PID temperature controller. For all experiments, the reactor was charged with *Chlorella vulgaris* dry powder, methanol and catalyst. Then, the reactor was sealed firmly, the electric furnace was heated to achieve the desired temperature, 260.0 ˚C, and the reaction was initiated for 1 h at a constant pressure of 9.0-10.0 MPa. Finally, the reactor was put into a water bath to cool to room temperature and the reaction was terminated. The final mixture was centrifuged to remove solid residue. A volume of n-hexane was added to the liquid product. The upper layer containing FAMEs was recovered and analyzed by GC–MS during which ethyl tridecanoat was used as an internal standard. The production yield of FAMEs was defined as a ratio of produced FAMEs weight to microalgae weight.

III. RESULTS AND DISCUSSION

Catalysts characterization: The detection of calcium in the catalysts was performed for the CaO/ TiO_2 catalyst with ICP-OES. The calculations showed 19.6 wt.% of calcium oxide on the CaO/ TiO_2 catalyst that was close to the expected value of 20.0 wt.%.

The FT-IR spectra CaO/ TiO_2 compared with pure TiO_2, no obvious additional peaks appeared which might be

because of the overlapping associated with calcium oxide and titanium dioxide.

Since the peaks on the XRD pattern of CaO overlaps with TiO_2 in 2θ values of 37.66°, 54.35°, and 67.99° [8]. As a result, the intensity of the corresponding peaks has increased, indicating that calcium oxide is well formed on the TiO_2.

the SEM photographs and corresponding EDX of the pure TiO_2, and CaO/ TiO_2 nanocatalysts shows, the peaks related to Ca appear on the spectrum and confirm the presence of calcium oxide on the surface of titanium dioxide. The elemental distribution of titanium, calcium and oxygen in the CaO/ TiO_2 nanocatalyst was probed using SEM-EDX to measure the intensity of the Kα line across the catalyst. All three elemental images show relatively good distributions.

Liquid product analysis: the ICP-OES analysis was performed to determine the amount of catalyst dissolved in the products. Results showed no calcium trace in the final biodiesel. It can be concluded that the leaching of CaO, did not occur during such high temperature and pressure conditions. It seems that, the photochemical synthesis of calcium particles on TiO_2 causes a good attachment and subsequently prevents CaO release into the product.

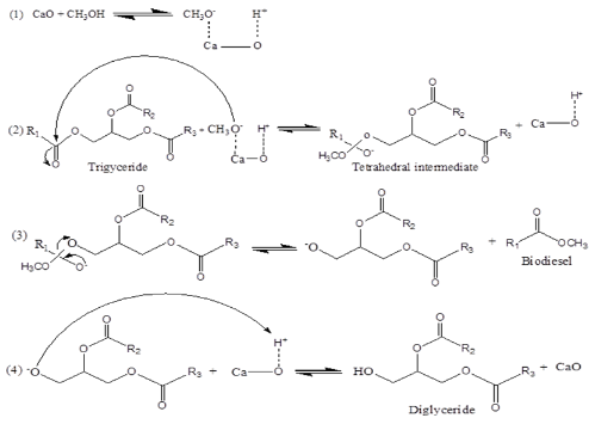

Fig. 1. The mechanism of transesterification of triglycerides for production of FAMEs in the presence of methanol [2].

The results of the chemical composition of products in different reaction media (catalyst free, TiO_2 catalyst and CaO/ TiO_2 catalyst) shows that the major compounds achieved in biodiesel can be classified into three groups: hydrocarbons, esters, and oxygenates. The total product yield increased with the addition of CaO and TiO_2 to the supercritical medium. Well-distributed calcium oxide on titanium dioxide and the relatively high basic strength of calcium oxide increased the catalytic activity in the reaction and consequently enhanced the yield of FAMEs in the presence CaO/ TiO_2 catalyst. Hydrocarbon production showed a similar behavior with FAMEs. The presence of hydrocarbons in the product is related to their extraction from the microalgae structure and not the chemical reaction.

Fig. 1 displays a reaction mechanism for CaO catalyzed transesterification of triglyceride using methanol [2].

IV. CONCLUSION

The CaO/ TiO_2 nanocatalyst was synthetized via photochemical method in order to check the physical stability of CaO on TiO_2. TiO2, CaO/ TiO2 nanocatalyst remarkably increased the total product yield in supercritical methanol. An increase in the yield of FAMEs produced in the presence of CaO is due to the good distribution on TiO_2 and its high basic property. The results depicted no CaO traces released into the product and this is good evidence for high physical stability of the synthetized photochemical- catalyst.

REFERENCES

[1] A.K. Endalew, Y. Kiros, R. Zanzi, Energy, vol. 36, pp. 2693-2700, 2011.
[2] M.E. Borges, L. Díaz, Renewable and Sustainable Energy Reviews, vol. 16, pp. 2839-2849, 2012.
[3] A.P.S. Chouhan, A.K. Sarma, Renewable and Sustainable Energy Reviews, vol. 15, pp. 4378-4399, 2011.
[4] P. Andreo-Martínez, N. García-Martínez, M.d.M. Durán-del-Amor, J. Quesada-Medina, Energy Conversion and Management, vol. 173, pp. 187-196, 2018.
[5] S.J. Yoo, H.-s. Lee, B. Veriansyah, J. Kim, J.-D. Kim, Y.-W. Lee, Bioresource Technology, vol. 101, pp. 8686-8689,2010.
[6] A.C. Alba-Rubio, M.L. Alonso Castillo, M.C.G. Albuquerque, R. Mariscal, C.L. Cavalcante, M. López Granados, Fuel, vol. 95, pp. 464-470, 2012.
[7] S. Hu, Y. Guan, Y. Wang, H. Han, Applied Energy, vol. 88, pp. 2685-2690, 2011.
[8] X. Liu, H. He, Y. Wang, S. Zhu, X. Piao, Fuel, vol. 87, pp. 216-221, 2008.

Removal of Direct Red Photocatalytic under Visible Light Radiation by Magnetic Spinel $CoFe_2O_4$

Zahra Soudi, Parvaneh Nakhostin-Panahi*, Mohammad-Hosein Rasouli-Fard

Department of Chemistry, University of Zanjan, Iran

Email: panahi@znu.ac.ir

Abstract: In this study, $CoFe_2O_4$ with spinel structure was synthesized by sol-gel method with different calcination temperatures and their photocatalytic activity studied in the process of direct red removal under visible light radiation. The results indicated that $CoFe_2O_4$ synthesized at calcination temperature 600°C has the most photocatalytic activity in the removal of direct red pollutant.

Keywords*:* spinel, photocatalyt, sol-gel, direct red 23

I. Introduction

Organic dyes are one of the important groups of pollutants in waste water produced from textile and other industrial processes. These wastewaters have an intense coloration and cause many damages to the ecological system of the receiving surface water and create many disturbances to the groundwater resources [1]. Nowadays, many techniques have been developed to remove dye pollutants from wastewater. The photocatalytic oxidation is a promising method for degradation of organic dyes and remediation of polluted water. In recent years, spinel ferrites with the general formula of MFe_2O_4 have been exploited as effective photocatalysts in the visible region. The bulk cobalt ferrite possesses inverse spinel structure. It has half of the Fe^{3+} ions on the A site (tetra-hedral) and remaining half of the Fe^{3+} ions and all the Co^{2+} metal ions situate on the B-site (octahedral). The synthesis of this material in nano-regime induces cation rearrangement over A and B sites in the spinel ferrite that leads to different magnetic properties from its bulk counterpart. Thus, nanosized $CoFe_2O_4$ is neither completely normal nor completely inverse spinel، but has mixed spinel structure. In the pure cobalt ferrite, half of the Fe^{3+} ions exist in the tetrahedral sites while remaining ions try to find to the octahedral sites. Owing to the above properties، it is a promising candidate for bio-medical drug delivery, magnetic resonance imaging, cancer treatment, UV and visible light induced photocatalysts, support for
magnetic fluids, microwave devices، ecc [2, 3]. In the present paper, we report on the preparation of spinel $CoFe_2O_4$ by the sol-gel method with different calcination temperatures and photocatalytic activity of prepared samples compared for the degradation of direct red dye under visible-light irradiation.

II. Experimental

The $CoFe_2O_4$ was synthesized by the sol-gel method with citric acid as a complexing agent and ethylene glycol as a polymerization agent. Briefly, the appropriate amounts of $Co(NO_3)_2$ and $Fe(NO_3)_3$ were dissolved in distilled water and the mixture was stirred magnetically at the room temperature for 15 min. Then, citric acid and ethylene glycol were added and mixture heated at 80°C under the constant stirring until a sticky gel obtained. In the following, gel dried at 200°C for 2 h. Finally, dried gel was grinded and calcined at high temperature (600, 700 and 800 °C) for 4 h to obtain the sample $CoFe_2O_4$.

The photocatalytic activity of the prepared samples was investigated by the degradation of direct red under visible light irradiation. The decolorization of direct red solution was carried out in a glass beaker containing 100 mL direct red aqueous (20 ppm) and 200 ppm of photocatalyst. The suspension was first stirred for 30 min in the dark to establish the adsorption–desorption equilibrium between the photocatalyst and dye. Afterwards the visible light lamp illuminated so that the suspension exposes to visible light irradiation. At regular 1 h intervals of irradiation, about 5 mL of suspension was pipette out and centrifuged to remove the photocatalyst particles. The residual dye concentration in the upper transparent solution was determined using a UV-Visible spectrophotometer and the discoloration percentage (%) was calculated as follows:

$(\%) = (C_0 - C_t) / C_0 \times 100$

Where C_o and C_t represent the initial and final concentration, respectively.

III. Results and discussion

To investigate the effect of calcination temperature on the photocatalytic performance, spinel $CoFe_2O_4$ calcined at the different calcination temperatures (600, 700 and 800°C). The degradation of direct red under visible light irradiation in the presence of spinels $CoFe_2O_4$ prepared at different calcination temperatures is presented in Fig. 1.

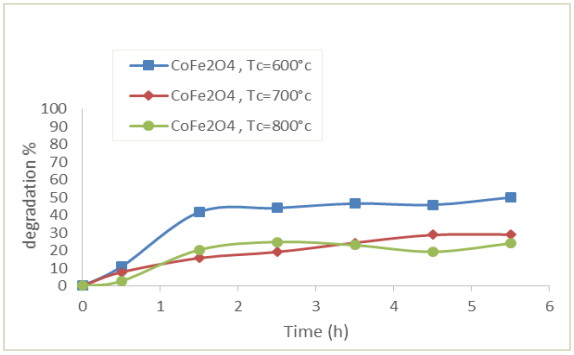

Fig. 1 Photocatalytic degradation of direct red under the visible light radiation by spinels $CoFe_2O_4$ with different calcination temperatures

As shown in this figure, calcination temperature of $CoFe_2O_4$ plays an important role in its photocatalytic properties because it affects particles size of samples which is very effective. The $CoFe_2O_4$ prepared with calcination temperature 600 °C showed the highest photocatalytic activity and discoloration percentage (50% removal). All prepared spinels are also magnetite and consequently, photocatalysts are easily recovered by an external magnet.

I. Conclusions

We have successfully synthesized the $CoFe_2O_4$ by sol-gel method with different calcination temperatures. The photocatalytic activity of samples was evaluated for the removal of direct red under visible light irradiation. The results indicated that calcination temperature is an important factor in photocatalytic performance and $CoFe_2O_4$ synthesized at calcination temperature 600°C showed the most photocatalytic activity in the removal of direct red pollutant.

References

[1] Fathi MR, Asfaram A, Farhangi A. Molecular and Biomolecular Spectroscopy. 364-72. 2015
[2] Casbeer E, Sharma VK, Li XZ. Separation and Purification Technology. 1-4. 2012
[3] Sadeghpour F, Nabiyouni G, Ghanbari D. Journal of Materials Science: Materials in Electronics. (11). 60-73. 2016

Synthesis of Magnetic Spinel $CoFe_2O_4$ by Hydrothermal Method and Study of Photocatalytic Activity

Parvaneh Nakhostin Panahi*, Zahra Soudi
Department Of Chemistry, University Of Zanjan, Iran
** Email: panahi@znu.ac.ir*

Abstract In this study, $CoFe_2O_4$ with spinel structure was synthesized by hydrothermal method with different temperatures and their activity studied in the process of photocatalytic removal of direct red pollutant under visible light. The results indicated that $CoFe_2O_4$ synthesized at temperature 180°C has the most photocatalytic activity in the removal of direct red pollutant.

Keywords: spinel، photocatalyst، direct red 23

I. Introduction

The dyes and pigments have become part of human's life. They are widely used in the textile، paperplastics، leather، food ، and cosmetic industries، and can be released to the environment through colored wastewater from these industries. Such colored effluent can reduce light penetration and photosynthesis causing reduction in oxygen levels in water and also in severe case، result in the suffocation of aquatic flora and fauna. Therefore، they can be called eco-toxic sub-stances، which need to be removed before discharging into receiving water bodies. The many methods have been used to remove dyes from aque-ous environment, such as oxidation، electrocoagulation، nano-filtration، photocatalysis، biosorption, and etc. [1]. Photocatalytic oxidation with semiconducting materials is a promising method for purification and remediation of polluted water and air. In recent years, spinel ferrites with the general formula of MFe_2O_4 have been exploited as effective photocatalysts in the visible region compared to the single component metal oxides [2, 3]. In this paper, spinel $CoFe_2O_4$ was synthesized by the hydrothermal method with different temperatures and their photocatalytic performance compared for the decomposition of direct red dye under visible-light irradiation.

II. Experimental

Synthesis of spinel: The spinel $CoFe_2O_4$ was synthesized by the hydrothermal method with different temperatures and $Co(NO_3)_2$ and Fe $(NO_3)_3$ were used as a precursor. In the typical reaction procedure، $Co(NO_3)_2$ and $Fe(NO_3)_3$ were dissolved in distilled water and the mixture was stirred magnetically at room temperature for 15 min. Then solution NaOH was added as drop until pH reached to 12. The produced precipitates were aged at room temperature for 30 min and then transferred into autoclave. The sealed autoclave was kept at high temperature (140, 160. 180 and 200°C) for 16 h. Subsequently، the autoclave was allowed to cool to room temperature naturally. Finally, the precipitates were filtered and washed with distilled water several times until the pH reached 7. The resulting product was dried in an oven 70°C for 12h.

Photocatalytic activity test: The photocatalytic performance of the synthesized spinels was investigated in the process of color contaminant removal (direct red) under the radiation of visible light. The first، required amount of $CoFe_2O_4$ (200 ppm) was transferred to the reaction vessel containing a direct red dye solution (20 ppm) and while the lamp is off was stirred for 30 min to achieve the adsorption/desorption equilibrium. Then the visible light lamp illuminated so that the suspension exposes to visible light irradiation. At regular 1 h intervals of irradiation, about 5 mL of suspension was pipette out and centrifuged to remove the photocatalyst particles. The supernatant liquid was analyzed by measuring the absorbance at the maximum absorption wavelength of direct red on a spectrophotometer. The efficiency of dye degradation (R) was calculated according to the following equation (Eq. (1))

$$R = (A_0 - A_t) / A_0 \times 100\% \quad (1)$$

Where A_0 and A_t are the absorbance intensities of direct red solution before and after illumination, respectively.

III. Results and discussion

Fig 1 shows the results of photocatalytic activity of spinels $CoFe_2O_4$ prepared by hydrothermal method with different temperatures.

According to this Fig, prepared spinels have photocatalytic activity under the visible light radiation. It could be seen that the $CoFe_2O_4$ prepared at 180 °C led to highest discoloration percentage (70%) and the $CoFe_2O_4$ prepared at 160 °C showed poor photocatalytic activity (30%). As a consequence, temperature of hydrothermal is an important factor in photocatalytic performance of spinels because it affects size of crystals which is very effective. All prepared spinels are magnetite and consequently, photocatalysts are easily recovered by an external magnet. This study provided a promising photocatalyst for cleaning wastewater by using visible light.

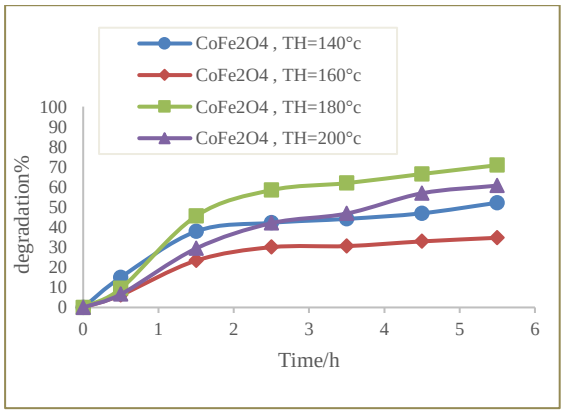

Fig 1: Photocatalytic degradation of direct red under the visible light radiation by $CoFe_2O_4$ syntheses with different hydrothermal temperatures (T_H)

IV. Conclusions

In conclusion, we have successfully synthesized the $CoFe_2O_4$ by hydrothermal method and the activity of samples was evaluated for the removal of direct red by photocatalytic process. The results indicated that temperature of hydrothermal is an important factor in photocatalytic performance and $CoFe_2O_4$ synthesized at temperature 180°C showed the most photocatalytic activity in the removal of direct red pollutant under the radiation of visible light (70% removal).

References

[1] Yavari S, Mahmodi NM, Teymouri P, Shahmoradi B, Maleki A. Journal of the Taiwan institute of chemical engineers. 320-9. 2016

[2] Sadeghpour F, Nabiyouni G, Ghanbari D. Journal of Materials Science: Materials in Electronics. (11) . 60-73. 2016

[3] Casbeer E, Sharma VK, Li XZ. Separation and Purification Technology. 1-4. 2012

Photocatalytic Degradation of Direct Blue 14 by Polyaniline/CdS Nanocomposite

A. Mehrizad

Department of Chemistry, Tabriz Branch, Islamic Azad University, Tabriz, Iran.

Email:mehrizad@iaut.ac.ir

Abstract: Polyaniline/cadmium sulfide (PANI/CdS) nanocomposite photocatalyst was used to degrade of Direct Blue 14 (DB 14). Response surface methodology (RSM) was applied to design the experiment, generate a model and optimize the process. Under optimum conditions (initial concentration of DB 14= 5 mg L^{-1}, catalyst concentration= 0.4 g L^{-1}, pH= 3.5, time= 55 min), dye removal efficiency reached to up 83.65.5%.

Keywords: Polyaniline, Cadmium sulfide, Direct Blue 14, Photocatalyst.

I. INTRODUCTION

There are different types of pollutants in water, soil and air that have harmful effects on human, plants and animals' health and affect the eco-environment. One of the major environmental pollutants is chromatic wastewater containing chemicals. The presence of dye in receiver water prevents light infiltration and causes eutrophication phenomenon that disturbs the photosynthesis process and inhibits the growth of aquatic organisms. In addition, studies have shown that dyes used in various industries have carcinogenic, mutagenicity and allergenicity properties [1]. Currently, the application of advanced oxidation processes (AOPs) for the removal of contaminants has a special place, especially from aqueous media [2]. Photocatalytic processes are efficient advanced oxidation processes to remove dye pollutants that play a role by a semiconductor photocatalyst and an energetic light source [3]. In this study, the role of polyaniline/cadmium sulfide (PANI/CdS) nanocomposite was evaluated as a photocatalyst for Direct Blue 14 (DB 14) dye removal from aqueous solutions. Experiments were designed using response surface methodology (RSM).

II. METHODS

All experiments were conducted in a cylindrical glass reactor on a magnetic stirrer by agitation of predetermined amounts of PANI/CdS nanocomposite in 100 mL of DB 14 solution at a given pH. Irradiation was performed using a UV-A lamp, mounted at the top of the reactor in a wooden cabin. After a specific time interval, samples were withdrawn, centrifuged and analyzed spectrophotometrically (UV mini-1240, Shimadzu) at 665 nm. The removal percentage of the dye was computed by equation (1):

$$R\ (\%) = \left(\frac{A_0 - A_t}{A_0} \right) \times 100 \qquad (1)$$

where A_0 and A_t are the absorbance of dye when the reaction time is 0 and t, respectively.

III. RESULTS AND DISCUSSION

Figure (1) shows the photocatalytic degradation of DB14 by PANI/CdS as a function of initial concentration of DB14-pH and PANI/CdS amount-irradiation time.

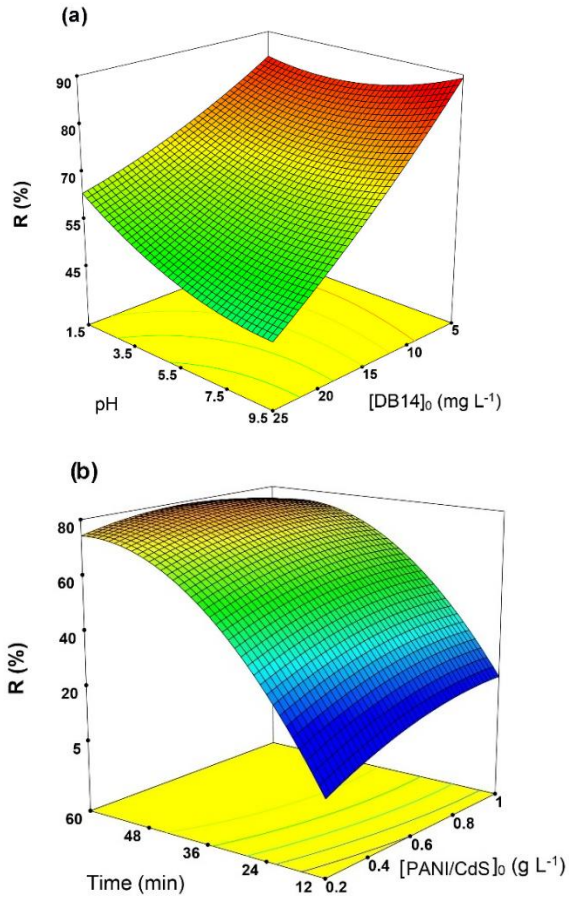

Fig.1: Photocatalytic degradation of DB14 by PANI/CdS as a function of (a) initial concentration of DB14 and pH; (b) PANI/CdS amount and irradiation time

According to figure 1 (a), removal efficiency has a reverse relationship with the initial concentration of the dye. In fact, the solution will become turbid by increasing the amount of dye and thus the dispersal of UV radiation. As seen in this figure, removal efficiency of dye is reduced gradually by increasing the pH of the solution. This result can be explained by the electrostatic interactions between the photocatalyst surface and the dye molecules that can be effective on attacking hydroxyl radicals for the degradation of dye molecules. Measuring the pH of the isoelectric point (pH_{iep}) showed that the amount of pH_{iep} for PANI/CdS is about 4.5 (data not shown here). In other words, the surface of nanoparticles in pH<4.5 have a positive charge and they have a negative charge in other pHs. Since DB14 is an anionic dye, the electrostatic attraction between DB14 and the photocatalyst surface in acidic pHs caused more adsorption; thus, the removal efficiency was increased by increasing the attack of active species on the dye. According to figure 1 (b), removal efficiency is increased by increasing the amount of catalyst. The number of active sites available for the photocatalyst and the number of adsorbed photons are increased by increasing catalyst concentrations. Therefore, more active species are produced for the degradation of dye molecules by producing more e^--h^+. On the other hand, the accessibility to a greater surface area is possible for the maximum adsorption of dye molecules by increasing the amount of catalysts in the solution. Also, this figure shows that the time of irradiation plays a critical role in the photocatalytic degradation of dye. In fact, increasing the time of a photocatalyst process leads to more adsorption of dye molecules on the photocatalyst surface and creates more opportunity for attacking target molecules (dye) by producing greater active species such as hydroxyl radicals.

Finally, the optimum conditions for photocatalytic degradation of DB14 (83.65%) were found to be 5 mg L^{-1} of DB14, 0.4 g L^{-1} of PANI/CdS, at pH=3.5, and an irradiation time of 55 min. This was verified experimentally (80.90%) and is further evidenced from the success of the designed model.

IV. CONCLUSION

In this study, PANI/CdS nanocomposite was used towards photocatalytic degradation of DB 14 under UV-A light irradiation. The effect of operational variables on the removal efficiency of dye was evaluated by RSM. The findings demonstrated that, dye removal efficiency has reverse relation with the initial concentration of dye and pH, whereas it increases with increasing the catalyst amount and the irradiation time. Under optimum conditions (initial DB 14 concentration= 5 mg L^{-1}, PANI/CdS concentration= 0.4 g L^{-1}, pH= 3.5, irradiation time= 55 min), dye removal efficiency reached to up 83.65%.

REFERENCES

[1] M.T. Yagub, T.K. Sen, S. Afroze, H.M. Ang, Dye and its removal from aqueous solution by adsorption: A review, Adv. Colloid Interface Sci. 209 (2014) 172-184.

[2] M.I. Litter, N. Quici, Advanced oxidation processes for water and wastewater treatment, Recent Pat. Eng. 4 (2010) 217-241.

[3] A. Mehrizad, P. Gharbani, Removal of Methylene blue from aqueous solution using nano-TiO_2/UV process: Optimization by Response Surface Methodology, Prog. Color Colorants Coat. 9 (2016) 135-143.

Physical Properties of the Pseudo-Ternary System of Deep Eutectic Solvent (Choline Chloride+ Glucose) + K_2HPO_4 + Water

M. Cheraghi Iranshahi[a], *A. Roosta*[a]*

Department of Chemical, Petroleum and Gas Engineering, Shiraz University of Technology, Shiraz, Iran
** Email: aa.roosta@sutech.ac.ir*

Abstract: In this study, some physical properties (density, viscosity, and surface tension) of an aqueous two-phase system consisting of a DES (choline chloride + glucose with 1:1 mol/mol), di-potassium phosphate and water has been measured at 303.15 K, and the effect of phosphate salt concentration on the physical properties is studied. According to the results, the increase in the phosphate concentration leads to increase in the density and decrease in the surface tension while the viscosity passes through a minimum at 27% (w/w) of phosphate.

Keywords: aqueous two-phase systems, deep eutectic solvent, physical properties.

I. INTRODUCTION

Aqueous two-phase system (ATPS) is an appropriate alternative for organic solvents in separation and purification of biological compounds such as enzymes, proteins, DNA, and antibiotics [1,2]. ATPSs are usually constructed with dissolution of two hydrophilic compounds in water such as two polymers, two salts, or a salt and a polymer [3]. On the other hand, deep eutectic solvents (DESs) as green solvents have attracted the attention of researchers. Recently, a new type of ATPSs has attracted the attention of researchers that is composed of aqueous solution of a salt and a deep eutectic solvent (DES) [4]. These type of ATPSs are very efficient in separation of biological compounds [5]. Deep eutectic solvents (DESs), were firstly introduced by Abbott *et al.* in 2003 [6]. A DES is formed by mixing a hydrogen bond acceptor (HBA), such as a quaternary ammonium salt, and a hydrogen bond donor (HBD), such as amines, carboxylic acids, alcohols, and carbohydrates [6].
By mixing these two components in proper ratios, eutectic mixtures are formed, with a significant decrease in the melting point of the mixture when compared to the melting temperatures of the starting components [6,7]. The physical properties of these ATPSs are important factors in their applications.

II. METHODS

In this study, the density, surface tension, kinematic and dynamic viscosity of a pseudo-ternary ATPS consisting of a DES (choline chloride + glucose with 1:1 mol/mol), di-potassium phosphate and water was measured at 303.15 K. Samples with different concentration of DES and phosphate were prepared to investigate the effect of constituents on the physical properties. To prepare the DES, choline chloride was dried in an oven, then choline chloride and glucose with 1:1 molar ratio was mixed to form a clear liquid. To prepare the ATPS with a given composition, the DES, phosphate, and water were scaled and mixed. The samples were kept at 303.15 K by using a shaker incubator. To measure the density, an analytical scale with a precision of 0.0001 g was used to scale 1 mL of the sample. The kinematic viscosity at 303.15 K was measured using an Ostwald viscometer placed in a water bath. The dynamic viscosity was obtained by multiplying the density by the kinematic viscosity. Furthermore, the surface tension was measured by using a surface tensiometer based on Du-Nouy Method ASTM 1331 (Novin Shimyar Company).

III. RESULTS AND DISCUSSION

The effect of phosphate concentration on the density, dynamic viscosity and surface tension of the pseudo-ternary ATPS are shown in Figs. 1 to 3, respectively. As seen in Fig. 1, the density increases with the increase in the concentration of phosphate (decrease in the DES concentration). For instance, density increases from 1291 $kg.m^{-3}$ for a mixture of 13% (w/w) phosphate to 1551 $kg.m^{-3}$ for a mixture of 44% (w/w) of phosphate.
The effect of phosphate concentration on the dynamic viscosity is illustrated in Fig. 2. According to the results, the minimum dynamic viscosity of the ATPS was observed at a mixture of 27% (w/w) phosphate. Perhaps, the viscosity decreased with increasing phosphate concentration, where the

concentration of phosphate was less than 27% (w/w) and then increased with the increase in the phosphate concentration. It is worth mentioning that increasing the concentration of phosphate was synchronized with the decrease in the DES concentration and vice versa. In the other hand, adding DES or phosphate increases the viscosity of the aqueous solution. Thus, at a lower concentration of phosphate (higher concentration of DES), the increase in the viscosity is due to the high concentration of DES. Another noticeable point is that the viscosity of this system is high compared to the viscosity of pure water; however, the viscosity is low compared to the viscosity of conventional ATPSs (polymer-salt).

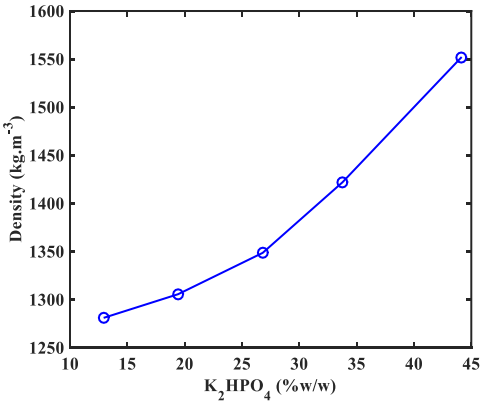

Fig.1. Density of the pseudo-ternary mixture as a function of phosphate concentration.

The surface tension of the ATPS as a function of phosphate concentration is shown in Fig. 3. The results show that increasing phosphate concentration (decreasing DES concentration) reduces the surface tension of the mixture. In addition, the surface tension of the studied ATPS is less than the surface tension of pure water (71.2 mN.m-1 at 303.15 K), except for the mixtures with phosphate concentration less than 15% (w/w).

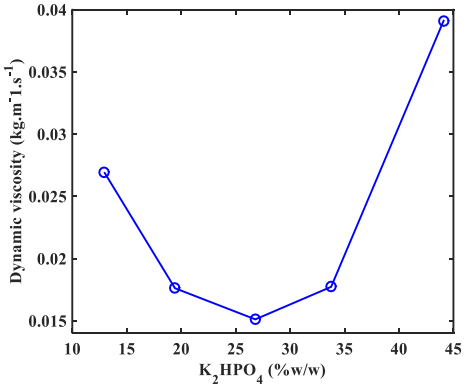

Fig.2. Dynamic viscosity of the pseudo-ternary mixture as a function of phosphate concentration.

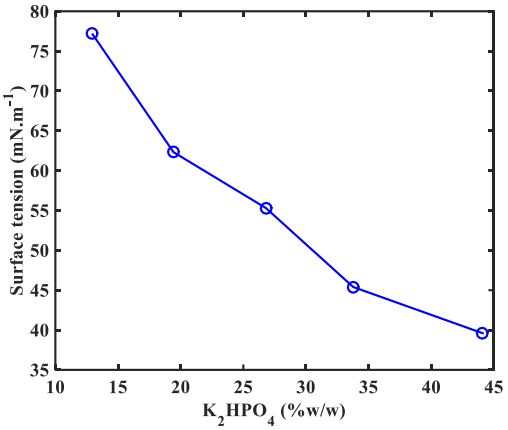

Fig.3. Surface tension of the pseudo-ternary mixture as a function of phosphate concentration.

IV. CONCLUSION

The physical properties of a new ATPS consisting of a DES (choline chloride + glucose with 1:1 mol/mol), di-potassium phosphate and water was measured at 303.15 K. The results showed that the viscosity of the current system is lower than the previous ATPSs. In addition, the density changed with phosphate concentration significantly. These are advantages of this system in the application for separation and purification of biological compounds.

REFERENCES

[1] M. Osloob, A. Roosta, Journal of Molecular Liquids, vol. 279, pp. 171-176, 2019.
[2] A. Roosta, A. Rabieenezhad, The Journal of Chemical Thermodynamics, vol. 120, pp. 54-59, 2018.
[3] R.C.S. Sousa, C.M.S.S. Neves, M.M. Pereira, M.G. Freire, J.A.P. Coutinho, Journal of Chemical Technology and Biotechnology, vol. 93, pp. 1940–1947, 2018.
[4] L.A. Ferreira, V.N. Uversky, B.Y. Zaslavsky, Journal of Chromatography A, vol. 1535, pp. 154–161, 2018.
[5] N. Li, Y. Wang, K. Xu, Y. Huang, Q. Wen, X. Ding Talanta, vol. 152, pp. 23–32, 2016.
[6] A.P. Abbott, G. Capper, D.L. Davies, R.K. Rasheed, Chemical Communications, vol. 2003, pp. 70-71, 2003.
[7] A.P. Abbott, D. Boothby, G. Capper, D.L. Davies, R.K. Rasheed, Journal of the American Chemical Society, vol. 126, pp. 9142-9147, 2004.

Taguchi Design for Indole Remove on CuO loaded Zeolite MCM-41

***S. Amiri Khoshkarvandani*[a], *R. Fazaeli*[a*], *M.Giahi Saravani*[a], *H. Pasdar*[b]**

[a] *Department of Chemistry, South Tehran Branch, Islamic Azad University, Tehran, 11365-4435, Iran*
[b] *Department of chemistry, North Tehran Branch, Islamic Azad University, Tehran, 19136-4711, Iran*
** Email: R_Fazaeli@azad.ac.ir*

Abstract: Indole is considered as an air and water pollutant; therefore, designing and preparation of an operation and inexpensive catalyst for removing it from the ecosystem is essential. MCM-41 is a mesoporous material with various desirable properties, whoever, due to promoting its catalytic activity CuO is loaded on its surface. Based on Taguchi method, indole removal with CuO/MCM-41 under UV irradiation was investigated. By applying this method, operation parameters such as the concentration of H_2O_2 (mM), odor concentration (ppm), and pH were optimized. The results demonstrated that pH in comparison with the other ones plays the most crucial role.

Keywords: CuO/MCM-41, Indole, optimization, Taguchi

I. INTRODUCTION

Indole and its derivatives are hugely poisonous with an unpleasant odor. They can be found widely in the environment and jeopardize the health of earth residents sharply [1]. Unfortunately, the common methods for removing this toxic compound from the environment, have wasted a huge amount of energy and catalysts, since such process requires harsh reaction condition, high temperature and pressure [2].Among all of the mesoporous, MCM-41 seems to be virtually suitable for industrial targets, because their synthesis is relatively easy and economic, have high chemical and thermal stability, uniform pore structure.Yang and Wang modified the surface of MCM-41 with metal oxides, which caused a remarkable enhancement in the yield of the desulfurization process [3].

II. METHODS

Synthesis of CuO/MCM-41:1gr of CTAB was added to a solution of NaOH (2M) and 480 ml water. When the mixture became completely uniform, 5 ml TEOS was steadily added. The resultant mixture was refluxed under 80°C for about 120 minutes. Finally, the suspension was washed for at least 3 times and rested at room temperature overnight. For removing surfactant, it was calcinated for 5 hours at 550°C [4]. For loading of CuOon MCM-41, 4gr of zeolite was added to 100 mL Cu (II) 0.1 M and shaken for 24h. The product was calcined at 450°C for 5 h in the furnace.

Experimental Design Based on the Taguchi Method:Using this method provides a great opportunity to obtain the optimum experimental circumstance with the lowest number of experiences. In this way, by regarding the amounts of factors and levels, various orthogonal arrays as matrix experiments are used. By applying Taguchi methods variability can be shown by signal to noise rate [5]. The highest amount of S/N rate shown the optimal condition. The orthogonal arrays are presented by the formula L_n (X^y), where n is the number of designed experiments, while X is the number of levels and y is the maximum number of factors, investigating by the array. In this work, 3 factors with 3 levels are studied. Table1 presents the investigated factors with their related levels.

Table1: Levels and factors used in DOE.

Number of levels	H2O2 (mM)	Pollutant Concentration (ppm)	pH
1	0	8	4
2	10	16	7
3	100	32	10

Reaction Procedure:1gr of the prepared catalyst was added to 20 ml indole solution with different initial indole concentration, then, the various amounts of H_2O_2 were added to the solution. The obtained suspension was shaken under UV lamp radiation. After 40 minutes it was centrifuged at 10000 rpm for 10 minutes due to separating the catalyst from the solution. For measuring the ratio of indole removal, UV-vis spectrophotometer was used.

III. RESULTS AND DISCUSSION

Cu/MCM-41 Characterization: Low angle XRD patterns of the synthesized silicate structured catalyst support clearly showed that the ordered pore structure of MCM-41 was formed (Fig.1). The main XRD peak observed at a 2θ value of 2.40° (corresponding to d100) and the three reflection peaks at 2θ values 4.08°, 4.66° and 6.19° is a clear indication of MCM-41 structure.

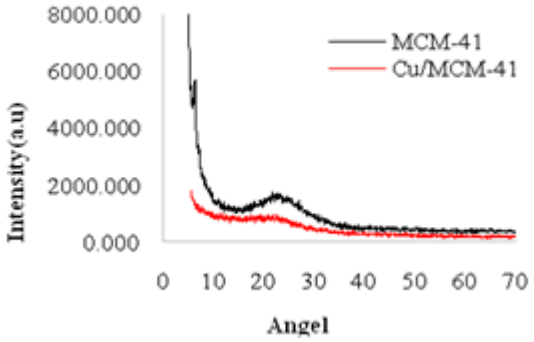

Fig.1: XRD Pattern of Z/CuO Composite Compared to MCM-41 Zeolite

Scanning electron microscopy (SEM) images are shown in fig.3. The SEM images also confirm that MCM-41 and CuO/MCM-41 have a uniform and spherical morphology

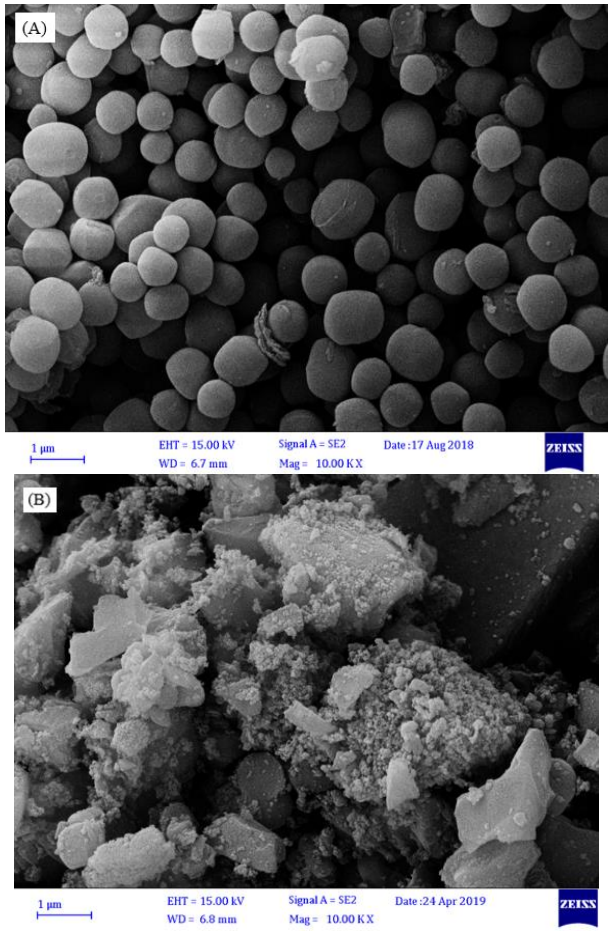

Fig.2: SEM micrograph of a) Cu/MCM-41, b) MCM-41

As shown in Fig.3, the energy dispersive X-ray spectrum (EDS) of the catalyst illustrates the percentage of 1.6% of Cu presence.

Optimum Conditions: By considering the final results, the optimum conditions are obtained: H_2O_2 10mM, indole concentration 8ppm and pH 10. Factors in term of them

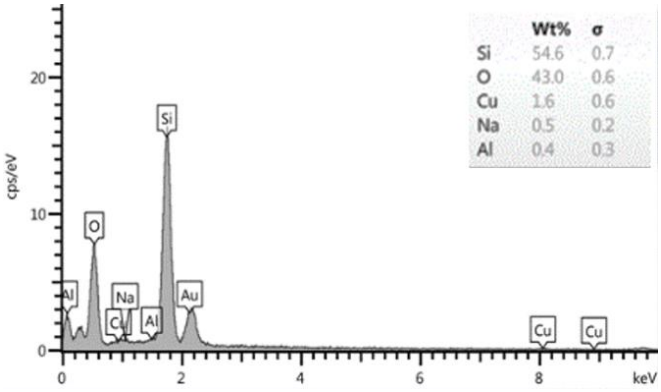

Fig.3: EDS spectrum of Cu (II)/MCM-41

influence is pH>H_2O_2>Concentration. Fig.4 illustrated the mean of S/N ratio graphs.

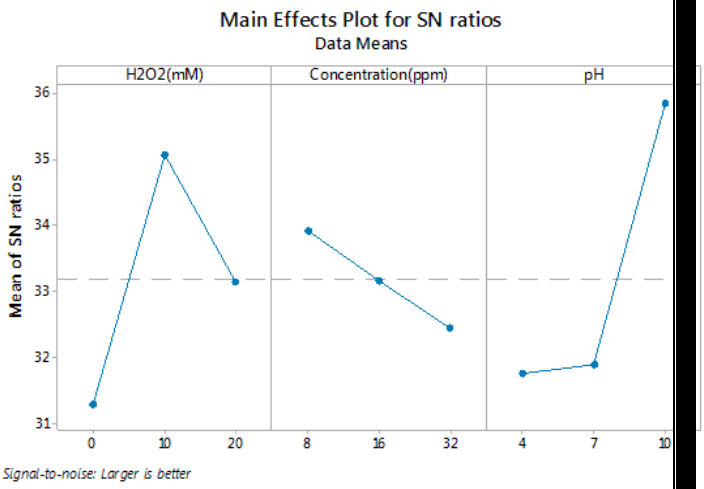

Fig.4: Mean of means graph for H_2O_2, concentration, pH

IV. CONCLUSION

At first, CuO/MCM-41 was prepared,and then, it was examined for indole removal by applying the Taguchi method. The results showed that the catalyst can effectively

remove indole under UV irradiation. By using the Taguchi method, the removal of indole was optimized. Optimal conditions were obtained at pH 10, 8ppm indole

concentration and 10mM H_2O_2. According to the results, pH was the most important factor. It is also predicted that in the optimize condition the efficiency will be 87.66%.

REFERENCES

[1] Y. Liu, L. Wang, and J. Ma. Chemical engineering journal, vol. 331, pp. 31-38, **2018**.
[2] M. Hartman, D. Jung, Journal, vol. 10, pp. 34-39, **1995**.
[3] X. Wei. Y. Hui, K. Fan, Chines Chemical Letters Journal, vol. 27, pp. 335-339,**2016**.
[4] M. Nikoorazm, A. G. Choghamarani, M. Khanmoradi, RSC Advances Journal, vol. 6, pp. 49-61, **2016.**
[5] N. E. Fard, R. Fazaeli, Russioan Journal of Physical Chemistry, vol. 92, pp. 226-237, **2018.**

Section:
Biophysical Chemistry

Application of chaos theory in biological systems

B. Gholami, M.G. Mahjani
Department of Chemistry, K. N. Toosi University of Technology, 19697 64499, Tehran, Iran
Email: Mahjani@kntu.ac.ir

Abstract*:* Complex systems exist at different levels of organization that range from the subatomic realm to individual organisms to whole populations and beyond. Complexity exist between order and disorder behavior that order behavior predictable and disorder behavior unpredictable. A space exist between order and disorder is non-ergodic and we can predict behavior of system with use of stochastic formulas. Growth of cancer cells, brain behavior and logistic equation are examples of complex systems. [1].

Keywords: Chaos, Stable and unstable, Logistic equation, Edge of chaos

I. INTRODUCTION

Chaos theory is a field of study in mathematics, with applications in several disciplines including physics, engineering, economics, biology, and philosophy. Chaos theory is a dynamical behavior that with transition of time exhibit complexity. Chaos theory is highly sensetive to initial condition and popular example for sensitive to initial condition is butterfly effect.

II. METHODS

In this article is used Matlab and Visio applications for plot diagrams and graph. At first is explained conception of words that use in chaos theory and finally is shown chaos theory with logistic equation in the diagram. Population that applicate in an article is a model for recursive function.

III. RESULTS AND DISCUSSION

Chaos is a random behavior exhibited by deterministic dynamical systems. It is a consequence of expansion of the unknowable due to locally unstable but globally stable dynamics.

Because of dynamical systems are considered in chaos theory and it is importance for us, we explain stability.

Locally stable means that we choose points near the equilibrium and with transition of time these points toward equilibrium point and locally unstable means that we choose points near the equilibrium afterward these points faraway of equilibrium point.

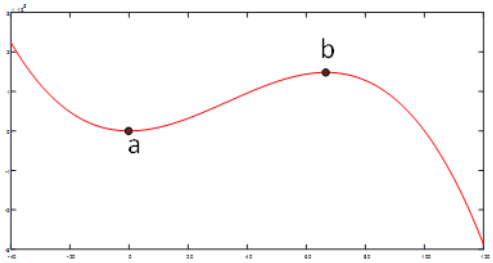

Fig.1: Point a is locally stable and point b is locally unstable

Logistic equation:

The simple logistic equation is a formula for approximating the evolution of an animal population over time. The logistic equation is recursive function and any region has special capacity(r) for species that are live.

Population of any generation are calculated by population of the last generation.

$$A_{n+1} = rA_n(1 - A_n) \qquad (1)$$

Or functional form

$$f(x) = rx\,(1 - x). \qquad (2)$$

If we draw (x) relative to (r) the below diagram is received.

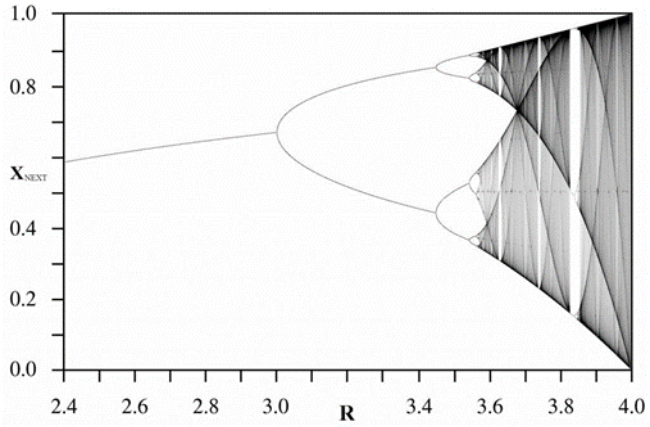

Fig.2: Logistic Map

Bifurcation:

As it can be observed in fig.2 a symmetry breaking is appeared when carrying capacity(r) is changed. In fact bifurcation points is in the regime edge of chaos.

IV. CONCLUSION

Chaotic behavior is unpredictable in principle. We may predict the performance of system if trajectory are embed at the phase space non-ergodic. Phase space non-ergodic appears at the edge of chaos. In the non-ergodic phase space four categories of relationship with past can be observed: 1- We can predict future behavior without considering past trajectories. 2- A partial of future behavior stage can be dependent to past, but when system run to infinity no dependence to past can be observed. 3- In some case full dependence to past might be observed.

REFERENCES

[1]. Mazzocchi, F., Complexity in biology: Exceeding the limits of reductionism and determinism using complexity theory. EMBO reports, 2008. 9(1): p. 10-14.

.

Generating the Supplementary Structure of Dopamine D2 Receptor Based on the X-ray Crystal Structure for Molecular Modeling

***P. Amani*[a], *R. Habibpour*[a] ***

a: Department of Chemical Industries, Iranian Research Organization for Science and Technology, Tehran, Iran

Email: Habibpour@irost.ir

Abstract: There is always a gap between known protein sequences and experimentally determined structures, thus generating a reliable protein model is a milestone that computational physical chemists and bio-molecular modelers are required to pass. As an important main receptor for most antipsychotic drugs, we chose dopamine D2 receptor to generate its supplementary structure.

The structure has been determined with crystallography recently by professor Wang research group, and we treat the structure using Wincoot/Gaussian/Gromacs.

Keywords: Dopamine, Schizophrenia, Supplementary Structure, Dopamine D2 Receptor

I. INTRODUCTION

Dopamine receptors are members of the G-protein coupled receptor family and are prominent in the vertebrate central nervous system (CNS) [1]. Dopamine receptors can be divided into two classes (D1-like and D2-like) on the basis of their biochemical and physiological effects [2]. Dopamine receptor D2 (D2R), is a protein that is the site of action of numerous antipsychotic drugs and several groups. As a protein, the structure of DRD2 in complex with the atypical antipsychotic Risperidone has been determined with purification and crystallography (Figure 1) [3].

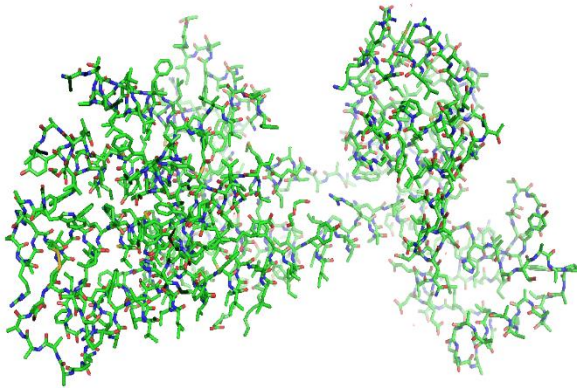

Figure 1: D2R structure, Structure Weight: 50455.63, Atom Count: 3220, Residue Count: 430

Even though the released data was very precious, but the presented structure suffers from missing residues. Missing residues are shown in the figure 2 with Orange color. A scientist, who tries to perform molecular dynamic simulation use to have the holistic structure of the protein receptor. We have done this repair on dopamine D2 receptor.

Figure 2: Dopamine D2 receptor residues, missing residues are shown with orange color

II. METHODS

For the purpose of model generation we used Wincoot [4] software which let us view and edit the structure manually. We determined the missing residues which were as follows:

```
RES C SSSEQI
MET A   140
LEU A   141
TYR A   142
ASN A   143
```

```
LYS A   362
LEU A   363
CYS A   443
```

For each part (part 1: 140-143, part 2: 362-363, part 3: 443) we have determine the residue where the chain was broken and, the next existing residue (visually) to scope the distance between the two and get an idea of what the missing part should look like (helix, strand or just coil/loop). Part one missing residues is shown in the Figure 3.

In each part, missing residues have been designed and optimized in Gaussian [5] (for instance: for the first part: series of MET – LEU – TYR – ASN). Then we overlap two structures manually using the Wincoot facilities (Figure 4). Then we have rotate/refine the models to fit to the vacancy and the bonds were formed. Then we edited Chi angles and then we edited backbone torsions to optimize the structure. Then we regularize the zone (which fixed weird geometries according to the standard dictionaries). After that we performed a MD simulation to minimize the geometrical energy as the last geometrical optimization. The last structure can be seen in the Figure 5.

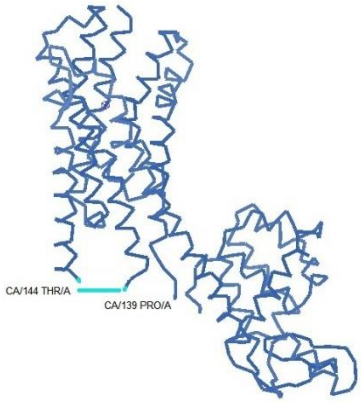

Figure 3: D2R backbone structure. Missing residue location is shown with cyan color.

III. RESULTS AND DISCUSSION

The complete structure of dopamine d2 receptor is obtained using the crystallography structure and correlated pdb structure from protein data bank and manual and computational corrections we have done using Wincoot/Gaussian/Gromacs [6].

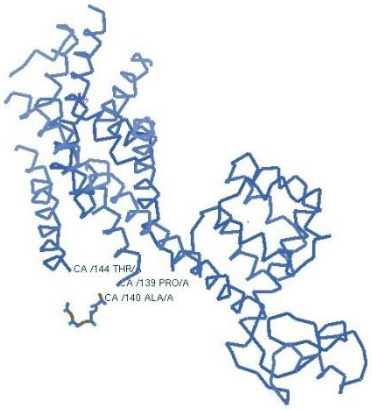

Figure 4: Optimizing the protein/missed residues position manually.

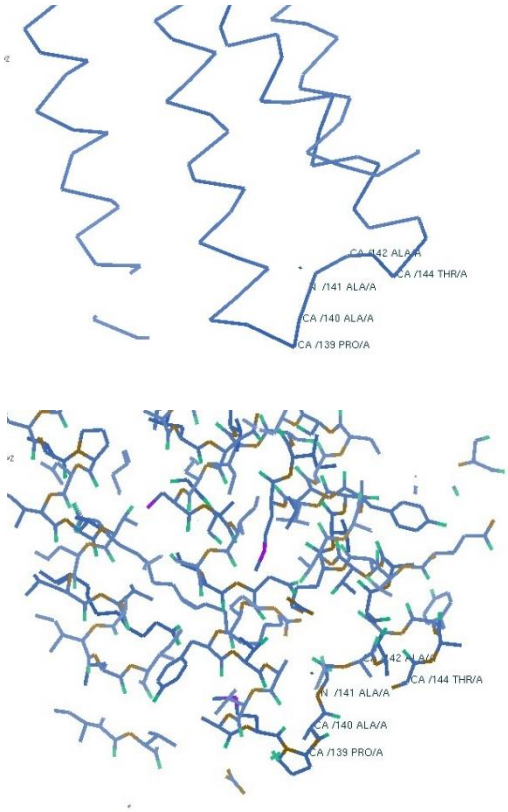

Figure 5: The optimized structure of D2R (backbone and all atom structures)

IV. CONCLUSION

As any bio-molecular dynamic simulation study need a perfect structure of the correlated bimolecular structure , we need the exact/absolut structure of dopamine receptor protein structure for any further studies in this regard. Using Wincoot/Gaussian/Gromacs softwares the intended structure obtained.

Acknowledge

We acknowledge the use of computational facilities at the Institute for Research in Fundamental Sciences (IPM).

REFERENCES

[1] J.-A. Girault and P. Greengard, “The neurobiology of dopamine signaling,” Arch. Neurol., vol. 61, no. 5, pp. 641–644, 2004.

[2] C. Missale, S. R. Nash, S. W. Robinson, M. Jaber, and M. G. Caron, “Dopamine receptors: from structure to function,” Physiol. Rev., vol. 78, no. 1, pp. 189–225, 1998.

[3] S. Wang, T. Che, A. Levit, B. K. Shoichet, D. Wacker, and B. L. Roth, “Structure of the D2 dopamine receptor bound to the atypical antipsychotic drug risperidone,” Nature, vol. 555, no. 7695, p. 269, 2018.

[4] B. Lohkamp, P. Emsley, and K. Cowtan, “Coot news,” CCP4 Newsl., vol. 42, pp. 3–5, 2005.

[5] M. J. Frisch et al., “Gaussian 09, Revision A. 02; Gaussian, Inc: Wallingford, CT, 2009,” There is no Corresp. Rec. this Ref., 2015.

[6] D. Van Der Spoel, E. Lindahl, B. Hess, G. Groenhof, A. E. Mark, and H. J. C. Berendsen, “GROMACS: fast, flexible, and free,” J. Comput. Chem., vol. 26, no. 16, pp. 1701–1718, 2005.

UV-Vis and Molecular Docking Study of the Interaction of Trans Aco Base (curcuminato) Exo Zirconium IV Hydrate and Curcumin with Human Serum Albumin

Z. Shabanzade, H. Dezhampanah*, M. Esmaili
Department of Chemistry, Faculty of Science, University of Guilan, P.O. Box: 19141, Rasht, Iran,
Email: h.dpanah@guilan.ac.ir

ABSTRACT: Curcumin, the bioactive compound has certain drug behavior, that we use this potential for therapeutic. The previous study examined the potential of curcumin, but this product has poor bioavailability and half-life. The chemical scientist can increase the properties of this drug with a change of the structure of components. In this study, we design and examine a new complex of curcumin (Scheme. 1a) for use in medicine. Most of the drugs get moved through the body by binding with Human Serum Albumin (HSA), we use Uv- Vis and molecular docking study to compare the interaction of curcumin (Scheme. 1b) and complex of curcumin with HSA because of its pharmacokinetic and pharmacological importance.

Keywords: HSA, Curcumin, Molecular Docking Study; UV-Vis measurement.

I. INTRODUCTION

HSA is the most plentiful protein in blood plasma, that very important application in the transport of non-esterified fatty acids, hormones, heme, and lipophilic xenobiotics through the bloodstream. The secondary structure of HSA appears in the configuration of a hydrophilic and hydrophobic hole that is effective for the binding of a variety of ligands [1].

Curcumin exhibited features such as anti-inflammatory, anticarcinogenic and antioxidant. Furthermore, Curcumin has proved hopeful in vitro phototoxicity upon various microorganisms and can be utilized as a photosensitizer in antimicrobial photodynamic therapy [2].

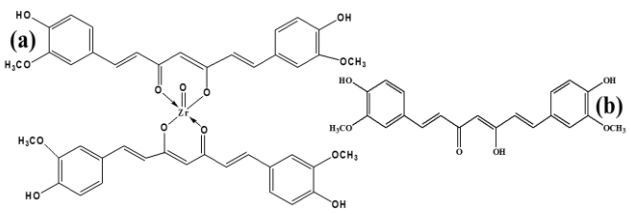

Scheme. 1. Chemical structure of (a) complex of curcumin and (b) curcumin.

II. METHODS

Human serum albumin (HSA) (97%; Sigma–Aldrich, Germany) was dissolved in pH 7.4 phosphate buffer 5.65 mM. Complex of curcumin and curcumin solution prepared by dissolving in dimethyl sulfoxide. Binding analysis for interaction of Complex of curcumin and curcumin with HSA by UV-Vis spectrophotometer was performed.

Docking study was taken out by utilizing AutoDock 4.2. The geometry of curcumin and complex of curcumin was prepared by HyperChem. The crystal structure of HSA (PDB ID: 1BMO) was provided from Protein Data Bank. In docking study, all water molecules were eliminated and polar hydrogen atoms were added at suitable geometry. And the other hand, in docking usually, we expected ligands as flexible molecules and let the docking software to switch all rotatable bonds of ligand to reach the best and optimized conformer of the ligands within the active site of HSA. The lowest energy docked structure was taken by using a grid map with 90×90×90 points and a gridpoint spacing of 0.375 Å. The Lamarckian genetic algorithm was used with the: 150 docking runs and 25,000,000 energy evaluations for each run.

III. RESULTS AND DISCUSSION

Fig. 1, showed the change of the absorbance of complex of curcumin by addition of HSA. The absorbance of a complex of curcumin reduced with the rising concentration of HSA. The UV_vis absorbance spectra of curcumin are similar to the complex of curcumin, which was not plotted in this paper. In these results proposed the curcumin and complex of curcumin with BSA have a good interaction.

UV–Vis absorption measurement is an easy and powerful method for analyzing the interactions of the protein with a small ligand. The absorption spectra of HSA in the presence and absence of complex of curcumin were shown in Fig. 2. The $\pi \rightarrow \pi^*$ transition of a carbonyl group in a peptide bond was shown a strong absorption band at near 205 nm, that refers to the frame structure and the α-helical content of HSA [3]. Fig. 2 showed with the increase of ligand concentration, the intensity of the absorption band at approximately 205 nm

increased.Also, with the increase of the concentration of complex of curcumin the intensity of the absorption band at near 411 nm (related to dye) increased.

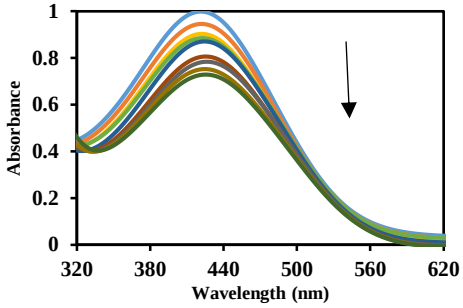

Fi g. 1. UV-Vis spectra of the complex of curcumin (The arrow indicates the absorbance changes with increasing of the HSA).

Meanwhile, when the increases of the concentration of dye, the absorption bands at205 showed about 40 nm red shift and the absorption bands at 411 nm demonstrated about 15 nm the blue shift. In this result proposed the complex of curcumin-HSA was created. The result of the interaction curcumin with HSA showed nearly this conclusion that can't be shown in this paper. All in all both of the absorbance change and wavelength change suggested the complex of protein-dye was formed. In order to achieve a better comprehension of the interaction of curcumin and complex of curcumin to HSA docking study was utilized.

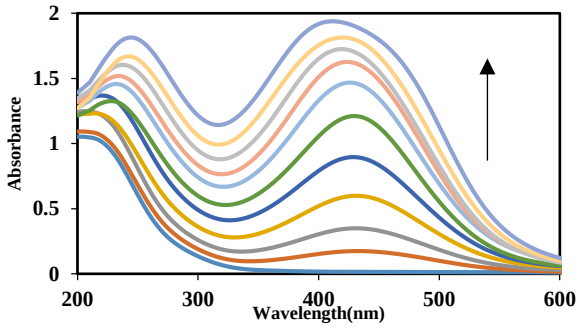

Fig. 2. UV-Vis spectra of the HSA (The arrow indicates the absorbance changes with increasing of the complex of curcumin).

The docking results of minimum binding energy conformations are mention in Table 1. We can see when the interaction of HSA with the complex of curcumin is surrounded by Lys 195, Arg 218, Glu 277 (H bond), Glu292, Val 293, Glu 294, Asn 295 (H bond), Lys 436(H bond), His 440 (π-π interaction), Pro 447, Cys 448, Asp 451, Tyr 452 and Val 455 with the free binding energy of -10.49 kcal/ mol (Fig. 3 and Table 1). In Table 1 assigned that when the interaction of HSA with curcumin is surrounded by Arg114, Leu 115 (H bond),Arg 117 (H bond), Tyr 138, Ile142, Arg145, His 146 (H bond), Tyr 161, Arg 186, Gly 189 and Lys190 with the free binding energy of -8.39 kcal/ mol. It is apparent that several amino acids with polar characteristics are in contact with curcumin and complex of curcumin with HSA. Also, curcumin is found within the binding pocket of domain I and subdomain IB of HSA, as well as the complex of curcumin is found within too close of site II is located in subdomain IIIA of HSA. The docking results reveal that the interaction complex of curcumin with HSA is very stronger than the interaction of curcumin with HSA. Also, these results can present HSA represents a very good binding and entrapment capacity for complex of curcumin. Because this ligand showed an enormous amount of free binding and it can be easily carried by site II.

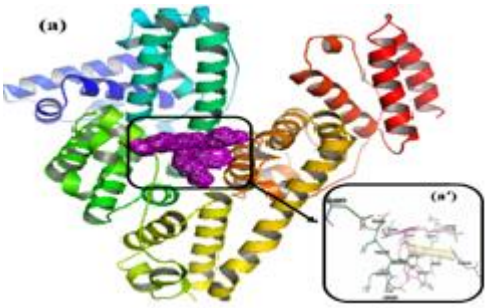

Fi g. 3. (a) Best conformations of the complex of curcumin docked to HSA in cartoon ribbons and (a') binding site represented in sticks.

Table 1. Amino acid residues involved in interaction of ligand and HSA with the free binding energy for the best selected docking positions.

	amino acids involved in ligand - HSA bindings	$\Delta G_{binding}$ (kcal/mol)
Curcumin -HSA	Arg 114, Leu 115*, Arg 117*Tyr138, Ile 142, Arg 145, His 146*, Tyr161, Arg 186, Gly 189 and Lys190	-8.39
complex of curcumin-HSA	Lys 195, Arg 218, Glu 277*, Glu292, Val 293, Glu 294, Asn 295*, Lys 436*, His 440 **, Pro 447, Cys448, Asp 451,Tyr 452 and Val455	-10.49

* Hydrogen bonding was observed with this amino acid.
** π-π interaction was observed with this amino acid.

IV. CONCLUSION

In this work, the interaction between curcumin and complex of curcumin with HSA was examined using molecular docking and UV-Vis technique. These results can provide HSA displays a very good entrapment potential for both drug, but the complex of curcumin better than curcumin and thus may help as a useful carrier for the drug in aqueous preparations for the transfer of it and great reference value for a model of used for drug design.

REFERENCES

[1] T. Kar, P. Basak, S. Sen, R. K. Ghosh, M. Bhattacharyya, Frontiers in Biology, 12, pp. 199-209, **2017**.
[2] M. Vukićević, H. H. Tønnesen, Pharmaceutical development and technology, 21, pp. 428-436, **2016**.
[3] Q. Wang, C. R. Huang, M. Jiang, Y. Y. Zhu, J. Wang, J. Chen, J. H. Shi, Spectrochimica Acta Part A: Molecular and Biomolecular Spectroscopy, 156, pp. 155-163, **2016**.

Spectroscopic Study of the Interaction of Trans_Aco Base (curcuminato) Exo Zirconium (IV) Hydrate and Curcumin with Bovine Serum Albumin

A.Askari, H. Dezhampanah*

Department of Chemistry, Faculty of Science, University of Guilan, P.O. Box: 19141, Rasht, Iran,

Email: ***h.dpanah@guilan.ac.ir***

ABSTRACT: This study was conducted to investigate the mechanism interaction of novel complex of zirconium with curcumin ligand (trans-[ZrO(curcumin)$_2$(H_2O)].H_2O) with bovine serum albumin (BSA), by means of various spectroscopic techniques. The fluorescence quenching measurements revealed that the quenching mechanism was static and the binding site of zirconium complex to BSA was singular. Uv-Vis absorption measurement showed the maximum absorption of complex increases with increasing of BSA concentration.

Keywords: BSA, Curcumin, Flourescence; UV_Vis

I. INTRODUCTION

Bovine serum albumin (BSA) is a globular protein (~66,000 Da) that is used in numerous biochemical applications due to its stability and lack of interference within biological reactions. Bovine is well characterized, abundant and cost effective serum albumin and is homologous to Human Serum Albumin (HSA). The above mentioned properties made BSA a potent tool for protein-drug interaction studies and their specific and firm binding with small molecules rugs and dyes can be used for drug delivery [1]. Curcumin, possesses a variety of remarkable pharmacological activity including anti-inflammatory, anti-carcinogenic, and anti-oxidant activity [2].In this study, the interaction between zirconium curcumin complex (trans-[ZrO(curcumin)$_2$(H_2O)].H_2O) scheme 1 and BSA was investigated by the application of UV–Vis and fluorescence spectroscopic techniques.

II. METHODS

Bovine serum albumin (BSA) (96%; Sigma–Aldrich, Germany) was dissolved in pH 7.4 phosphate buffer.

Trans-[ZrO(curcumin)$_2$(H_2O)].H_2O was synthesized according to a method described by khorshidi in [3]. The stock solution of Zr complex and curcumin were prepared in 5 mM phosphate buffer, pH 7.20 and stored in the dark at 510 ºC.The absorption spectra were recorded on a Cary 500 scan UV-vis-NIR spectrophotometer. The UV-Vis titration experiments were made by addition of the BSA stock solutions into a 1 mL cuvette containing the complex and curcumin solution of appropriate concentration.

The fluorescence measurements were performed using Varian Cary Eclipse spectrofluorimeter equipped with a thermostatic bath, and 1.0 cm quartz cuvette. The excitation wavelength was 290 nm, while the excitation and emission slits were set at 2.5nm .For fluorescence titration experiments, BSA solution (2.5 ml, 7 µM in 20 mM phosphate buffer pH 7.4) in a quartz cuvette was titrated with various amounts of 0.1 mM solution of both compounds.

III. RESULTS AND DISCUSSION

Fig. 1, shows the UV–Vis absorbance spectra of complex of curcumin and BSA. The absorbance of complex of curcumin increased with increasing concentration of BSA. The intensity of absorption spectra for complex of curcumin at 218nm increases gradually with increasing concentrations of added BSA. The absorbance reaches a maximum at 121 µM of BSA.

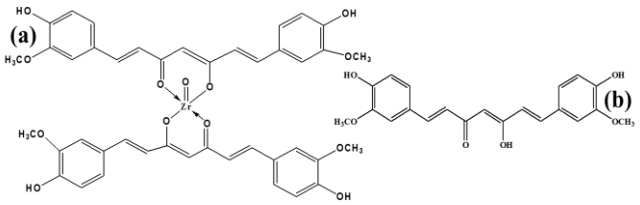

Scheme. 1. Chemical structure of (a) complex of curcumin and (b) curcumin.

The fluorescence emission spectra of BSA upon the addition of zirconium complex were shown in Fig. 2. It can be observed that increasing the concentration of complex led to a decrease in the maximum wavelength of fluorescence intensity in BSA with a 4 nm blue shift. It was suggested that addition of zirconium complex the microenvironment of tryptophan residues, but results demonstrate change in the zirconium complex is more than curcumin. Both static and dynamic processes can be described by the well-known Stern-Volmer equation as follows (Lakowicz 2013):

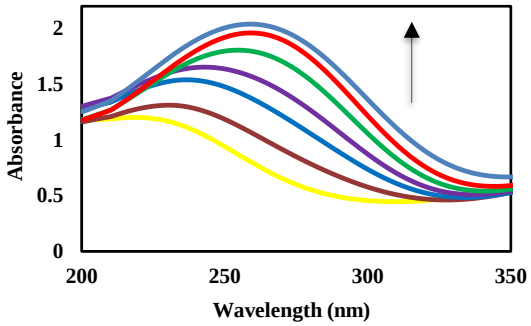

Fig. 1. UV-Vis spectra of the complex of curcumin (The arrow indicates the absorbance changes with increasing of the BSA).

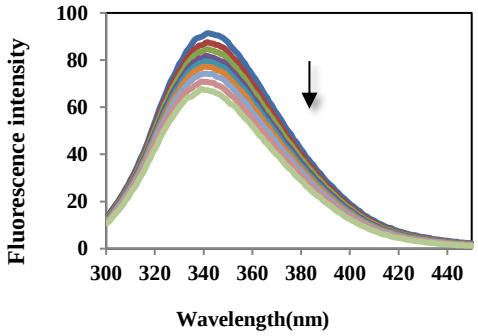

Fig. 2. Fluorescence spectra of BSA in absence and presence various concentrations of complex of curcumin.

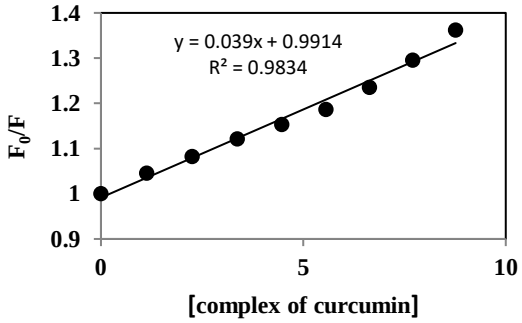

Fig.3 . Stern–Volmer plot for the binding of complex and BSA

The fluorescence quenching data analyzed by Stern-Volmer equation:

$$\frac{F_o}{F} = 1 + K_{SV}[Q] = 1 + K_Q \tau_o [Q]$$

Where F_0 and F are fluorescence intensities in the absence and presence of quenching,[Q] the concentration of quencher,K_{SV} Stern-Volmer constant; K_q the bimolecular quenching rate constant; and τ_0 the mean lifetime of the fluorophore without the quencher and its value is 10 ns for BSA.

The values of K_{SV} and K_q were calculated by slope and intercept of the plot of $\frac{F_o}{F}$ against [Q] of zirconium complex. The quenching rate constant (K_q) are 39023×10^{12} $M^{-1}s^{-1}$ for the complex formation zirconium curcumin-BSA This value is much greater than the maximum collisional quenching constant (2×10^{10}) (Zhang et al. 2013), indicating that the fluorescence quenching mechanism of BSA induced by zirconium curcumin complex was the static quenching due to the formation of zirconium complex–BSA complexes.

IV. CONCLUSION

This research presents spectroscopic study on the interaction of new derivatives of curcumin compound with BSA protein. It was shown that the fluorescence intensity of BSA has been quenched due to interacting with zirconium curcumin complex and the quenching mechanism was characterized as a static process.

These results can provide BSA displays a very good binding and entrapment capacity for this drug, and thus may serve as a useful vehicle for the drug in aqueous preparations for oral delivery of this drug.

REFERENCES

[1] K.Ghosh1,S.Rathi2,D.Arora. Fluorescence spectral studies on interaction of fluorescent probes with Bovine Serum.

[2] N.R. Jana, P. Dikshit, A. Goswami, and N. Nukina, J. Biol. Chem. 279 pp. 11680–11685, **2004.**

[3] N. Kiani, B. Heidari, M. Rassa, M. Kadkhodazadeh, B. Heidari, J. Basic Clin. Physiol.Pharmacol. 25, 367,**2014.**

Binding interaction of disperse azo dye with bovin serum albumin by spectroscopic techniques

S. Shakeri[a], H. Dezhampanah [a]*, R. Firouzi[a]
[a] Department of Chemistry, Faculty of Science, University of Guilan, , Rasht, Iran,
Email:h.dpanah@guilan.ac.ir

Abstract: : The interaction of disperse azo dye with bovine serum albumin (BSA), in 20 mM phosphate buffer pH 7.4 was investigated using fluorescence technique. The results showed that quenching mechanism of BSA with disperse azo dye was of dynamic type. The fluorescence quenching measurements showed a single binding site on BSA for disperse azo dye with the binding constant (K_b) value of $3/39\times10^4$ at 25°C.

Keywords: BSA; Fluorescence; Azo dye; interaction

I. INTRODUCTION

Bovine serum albumin (BSA) is a globular protein that has a wide range of biochemical functions due to its stability and lack of interference within biological reactions. BSA is also a carrier as well as a distributor for several endogenous and exogenous ligands, therefore these types of interactions have been widely studied. BSA is well characterized, cost effective, abundant and homologous to Human Serum Albumin (HSA) [1]. BSA has two tryptophans (Trp-134 and Trp-214), where its Trp-134 is located on the surface of the molecule and the other Trp is in the hydrophobic pocket (like Trp-214 in HSA) [2].
Azo dyes are organic compounds having the functional group R−N=N−R′, in which R and R′ are usually aryl. Compounds containing the linkage C-N=N-C are a commercially important family of azo compounds.
Fluorescence technique is a useful method to study the chemical and biological systems in low concentrations [3]. External molecules added to the fluorescent system can quench fluorescence intensity through dynamic or static methods [4].

II. METHODS

The fluorescence emission spectra were recorded in the range of 300 450 nm at the excitation wavelength of 295 nm by a Cary eclipse spectrofluorimeter. BSA stock solution (1 mM) was prepared in 20 mM sodium phosphate buffer pH 7.4. Azo disperse dye (1 mM) was prepared by dissolving it in DMSO.

III. RESULTS AND DISCUSSION

Variety of processes consisting excited state reactions, energy transfer, complex formation, and collisional quenching can cause quenching [5]. It is known that there are two mechanism of quenching that are dynamic or static quenching. Dynamic quenching is a collisional while static quenching, is due to complex formation. The fluorescence emission spectra of BSA upon the addition of disperse azo dye is shown in Fig. 1. It can be observed that by increasing the concentration of disperse azo dye the fluorescence intensity of BSA decreased with 10 nm a blue shift in the maximum wavelength which suggests that by addition of dye, the microenvironment of tryptophan residue has been changed.

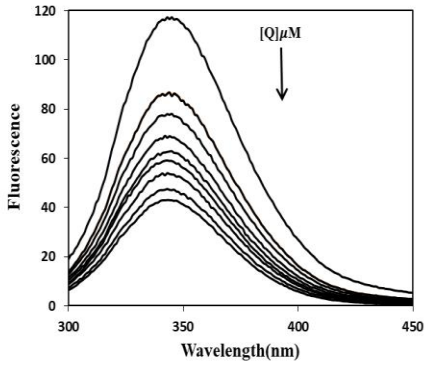

Fig.1: Fluorescence quenching of BSA at different concentrations of disperse azo dye (0 to $8/18\times10^5$ µM).

The fluorescence quenching data were analyzed using Stern-Volmer equation:

$$\frac{F_0}{F} = 1 + K_{SV}[Q]$$

where F_0 and F are fluorescence intensities in the absence and presence of the quencher respectively, K_{SV} is the Stern - Volmer quenching constant and [Q] is the quencher concentration. Table 1 gives the corresponding calculated results which indicates that the quenching mechanism is of dynamic type.

Table 1: Stern–Volmer constant, Binding constants and binding sites.

	K_{SV} $(\mathrm{L}mol^{-1})$	K_b $(\mathrm{L}mol^{-1})$	K_q $(M^{-1}.S^{-1})$	n
Q-BSA	1/934	$3/39\times10^4$	$1/93\times10^7$	1

IV. CONCLUSION

The results showed that quenching mechanism of BSA by disperse azo dye was of dynamic type. The fluorescence quenching measurements showed a single binding site on BSA for disperse azo dye with the binding constant (K_b) value equals to 3.39×10^4 at 25°C.

REFERENCES

[1] K. Ghosh1, S. Rathi2, D. Arora. Fluorescence spectral studies on interaction of fluorescent probes with Bovine Serum Albumin (BSA) Journal of Luminescence.

[2] H. Dezhampanah1,R. Firouzi2 An Investigation on intermolecular interaction between Bis(indolyl)methane and HSA and BSA using multi technique methods. Journal of Biomolecular Structure and Dynamics, 2016

[3] T. Wang, Zh. Zhao, B. Wei, L. Zhang , L. Ji Spectroscopic investigations on the binding of dibazol to bovine serum albumin. Journal of Molecular Structure, 2010

[4] Jihad René Albani Albani. "Fluorescence Quenching", Principles and Applications of Fluorescence Spectroscopy, 2007

[5] H. Dezhampanah, R. Firouzi, L.Hasani. Spectroscopy and Molecular Modeling Study on Binding of Nickel Phthalocyanine to Human Serum Albumin, Protein & Peptide Letters, 2016

Removal Of Vanadium Ion From Industrial WasteWater By Adsorption Using Nano Composite Of Magnesium Oxide/ Chitosan

N.Farhami**, S. Farokhmanesh
Department of Chemistr, Mahshahr Branch, Islamic Azad Univesity, Mahshahr, Iran.
Email:farhami2016@gmail.com

Abstract*:* The main objective of this study was to remove Vanadium ion from industrial waste water by adsorption using nano composite of Magnesium Oxide/chitosan. The adsorption studies performed in a batch system and the effects of various operating parameters such as solution pH(2-11), agitation time(15-300 min), adsorbent dose(1-6 mg/100ml), initial concentration Vanadium(5-30 ppm) were studied . Langmuir isotherm displayed a better fitting model than Freundlich isotherm.

Keywords: adsorption, chitosan adsorbent, vanadium ion.

I. INTRODUCTION

Industrial waste water of oil and petrochemical includes heavy metals such as Vanadium. Vanadium is very toxic and should be removed, before waste water enters into urban waste water or water. According to pervious studies, which have been carried out on the removal of Vanadium with various adsorbents, in addition to extensive studies on chitosan, in this study chitosan- functionalized nano magnesium oxide as adsorbent was used to remove Vanadium. This experimental study was a laboratory experiment that evaluated the effects of parameters on Vanadium removal from a laboratory sample.

II. METHODS

The adsorption test was carried out at a constant temperature of 25^0c. Initial solution of titrazol Vanadium (1000mg/L in H_2SO_4 %8.6) and solution's pH is adjusted by acid (H2SO4 0.2 N) and NaOH (0.1 N) and measured by the pH meter. After preparing the solution to check each parameter, other parameters are considered constant and the absorption of Vanadium solution is measured by the atomic absorption device.

II-I. Preparation adsorbent

Magnesium Oxide(0.75 gr) was added to (100 L of 1 wt %) acetic acid and a few drops of nitric acid were added and then placed on magnetic stirrer after that 1 gr chitosan was added in solution slowly and the solution was placed in ultrasonic apparatus for 30 minutes and while the solution was mixed, Sodium hydroxide was added to reach the solution's pH = 10. Then the mixture was heated for three hours in a Ben-Mari apparatus at a temerature of about 90 ^{0}C, and then the solution should be passed through a filter paper. Then a solid mixture was dried for one hour in a 50^0C Oven dish.

III. RESULTS AND DISCUSSION

The V(IV) concentration of the treated wastewater was analyzed at time interval between 0 and 300 minutes using standard methods recommended for examination of water and wastewater .The removal efficiency(E) of adsorbent on V(IV) was measured as follows:

$$E(\%)= (C_i-C_f/C_i)\times100 \quad (1)$$

Where C_i and C_f are the initial and final equilibrium concentration of V(IV) (mg/L) in waste water, respectively. The effect of parameters such as, pH, adsorbent concentration, agitation times, initial ion concentration, on the adsorption of V(IV) are presented in Fig. 1, 2, 3, 4, respectively.

III-I. Adsorption isotherms

Adsorption isotherm can be generated based on numerous theoretical models where langmuir and freundlich models are the most commonly used. The Longmuir model takes the following form:

$$Ce/qe=1/Q0b+Ce/Q0 \quad (2)$$

Where Ce is the equilibrium concentration (mg/L), qe the amount of metal ion adsorbed at specified equilibrium (mg/g), Q0 and b are the Langmuir constants related to adsorption capacity and energy of adsorption.

The Freundlich equation [3] is an empirical equation based on adsorption on a heterogeneous surface. The equation is commonly represented by $qe=K_fC^{1/ne}$ (3), where K_f and 1/nare the Freundlich constants characteristics of the system, indicating the adsorption capacity and the adsorption intensity, respectively.

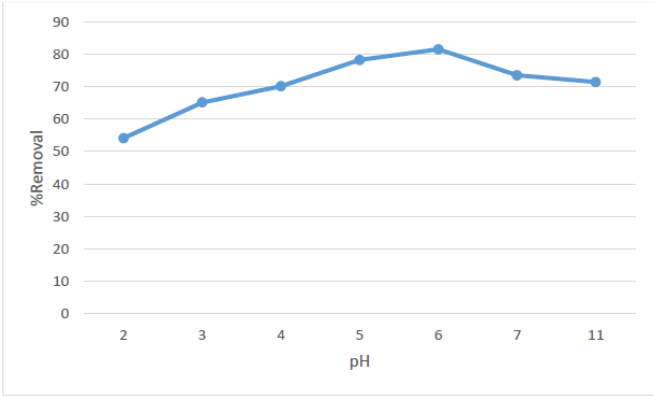

Fig 1. The effect of pH on removal of V(IV).

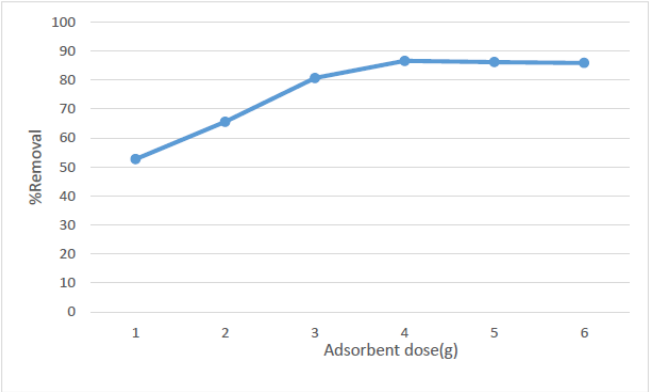

Fig 2. The effect of adsorbent dose on removal of V(IV).

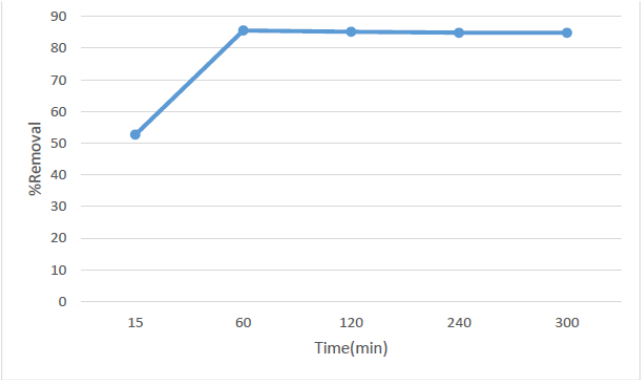

Fig 3. The effect of agitation times on removal of V(IV).

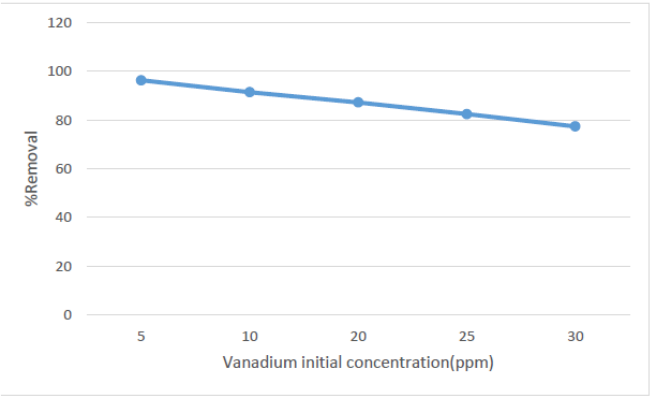

Fig 4 . The effect of V(IV) initial concentration on removal of V(IV).

IV. CONCLUSION

Generally speaking the nano composite adsorbent (chitson/MgO) exhibited an effective role in the removal of V(IV) from aqueous solution. Our studies showed that adsorption maximum of V(IV) from solution is in pH=6, after 60 minutes with 4 gr adsorbent and initial concentration 5 ppm of V(IV) solution. Adsorption data fitted well with the Langmiur and Freundlich models, however Langmiur isotherm displayed a better fitting model than freundlich isotherm because of the higher correlation coefficient that the former exhibited. Thus it indicates that the adsorbent layer, adsorbs Vanadium ion in the form of monolayer coverage.

REFERENCES

[1] H. Sharififard, M.Nabavinia, M. Soleimani, Advances In Environmental Technology, 4, 215-227, **2016.**

[2] C. Diaz, G. Barvera, and C. O'Dwyer. Journal Of Nano Materials, 2015, 1-13, **2015**.

[3] O. S. Amuda, A. A. Giwa, I.A. Bello, Biochemical Engineering Journal, 36, 174-181, **2007**.

Electrochemical Evaluation of Antioxidant Activity and Herb-Herb Interaction of Iranian *Echium amoenum Fisch* and *Citrus aurantifulia* aqueous extracts

A. Amani*

Department of Chemistry, University of Nahavand, Nahavand, Iran.

E-mail address: amani.iran@gmail.com

Abstract. Electrochemical oxidation of *Echium amoenum Fisch* extract has been studied in the presence of *Citrus aurantifulia* aqueous extract in aqueous solution and biological pH, using cyclic voltammetry, and differential pulse voltammetry methods. The results revealed that the electrochemically generated compounds in *Echium amoenum Fisch* extract, participate in the chemical reaction with phenolic compounds in *Citrus aurantifulia* extract. Based on these results there is a herb-herb interaction between this two extract, that can be reduce the antioxidant activity of *Echium amoenum Fisch* extract. Also Antioxidant activity of this extract has been compared with the galic acid, salicilic acid and quercetin as standard antioxidants.

Keywords: Herb-Herb interaction, *Echium amoenum Fisch*, *Citrus aurantifulia*, Cyclic voltammetry, Antioxidant activity.

I. INTRODUCTION

Herbal products are of interest to many patients and health care practitioners since about 70% of population worldwide rely on herbal medicines for part of their primary health care [1]. In different regions and cultures, herbal products are used as single herb, combination of herbs, or combination of herb(s) and drug(s). When herbs are used in combination, the effects can be complicated as various interactions can occur among the individual components. The most desirable interactions are those which can result in additional therapeutic benefit. This is often the intended or expected outcome when using combination therapy. However, due to the presence of multiple components in the herbal products, the effects arising from herb-herb or herb-drug interactions are often unpredictable and complicated. Various types of pharmacokinetic and pharmacogenomic interactions from herb-drug combinations have been well described and documented in recent literature . On the other hand, medicinal plants are a potential source of antioxidants and reactive oxygen species (ROS) [1,2]. One of these plants is *Echium amoenum Fisch* that has been shown as a rich source of antioxidants, like rosmarinic acid (RA) and flavonoids (Fig. 1) [3,4].

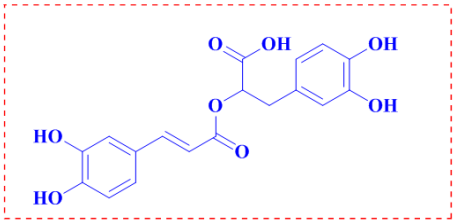

Fig 1: Chemical Structure of Rosmarinic Acid

In this work because of the electrochemical oxidation is very often parallel with the cytochrome P450 catalyzed oxidation in liver microsomes and with the aim of obtaining the information about of antioxidant capacity of *Echium amoenum Fisch* extract, we studied the anodic oxidation of this herb. then due to this medicinal herb usually consumed with *Citrus aurantifulia* extract, it was interesting to study the anodic oxidation of aqueous extract *of Echium amoenum Fisch* in the presence of *Citrus aurantifulia* extract**.** Finally the antioxidant activity of *Echium amoenum Fisch* extract has been compared with the galic acid, salicilic acid and quercetin as standard antioxidants.

II. METHODS

Apparatus and reagents

Reaction equipments is described in earlier paper [5]. All chemicals were reagent-grade materials from E. Merck. These chemicals were used without further purification.

Preparation of Echium amoenum Fisch and Citrus aurantifulia extract:

Echium amoenum Fisch and *Citrus aurantifulia* were purchased from a retail food store (Hamedan, Iran). Then, 1 gram of each herb weighed and 25 ml distilled water added it and then warmed up to 50°C. The mixture was passed through filter paper (Whatman filter paper number 1) and left to cooled. This extract was considered an aqueous extract of *Lemon verbena* leaves and *echium amoenum.*

RESULTS AND DISCUSSION

The cyclic voltammogram of 2mL *Echium amoenum Fisch* extract (**1**) in water (phosphate buffer, at the biological pH = 7.0, *c* = 0.2 mol/L) is shown in Figure 2 I, curve a.

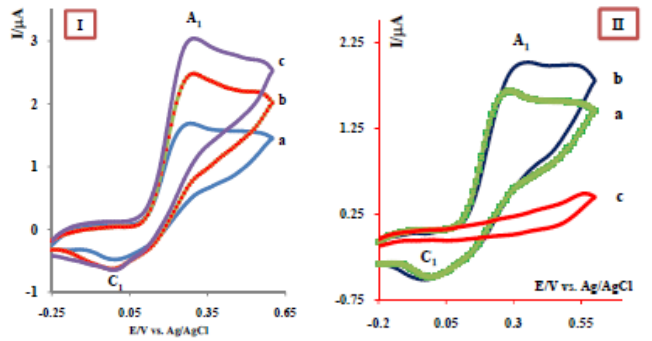

Fig. 2: (**I**) Cyclic voltammogram of *Echium amoenum Fisch* extract (a) 2mL, (b)3mL and (c)4 mL in the absence of *Citrus aurantifulia* extract (**II**) Cyclic voltammogram of *Echium amoenum Fisch* extract (2 mL), in the presence of *Citrus aurantifulia* extract (2 mL), at a glassy carbon electrode in a water (phosphate buffer, c = 0.2 mol/L, pH 7.0) Scan rate: 25 mV/s. T = 25 ± 1°C.

As can be seen, one anodic (A_1) and cathodic peaks C_1 were obtained. Anodic and cathodic peaks A_1 and C_1 are counterpart and are correspond to the transformation of rosmarinic Acid (Fig 1) to corresponding *o*-quinone and *vice versa* within a quasi-reversible process [5].

Electrochemical oxidation of *Echium amoenum Fisch* extract (**1**) carried out by varying concentration of extract (2, 3, 4 mL). The results indicate that the I_p^{A1} and I_p^{C1} is dependent on the concentration of extract and increases with increasing it (Figure 2, I. curves a,b,c). The oxidation of **1** in the presence of *Citrus aurantifulia* extract (**2**) was studied in some detail. Figure 2, II. curve b, shows the cyclic voltammogram obtained for 2 mL solution of **1** extract in the presence of 2 mL *Citrus aurantifulia* extract (**2**). As can be seen, the cathodic peak (C_1) decreased and anodic peak (A_1) increased. In this figure, curve c is the cyclic voltammogram of *Citrus aurantifulia* extract (**2**).

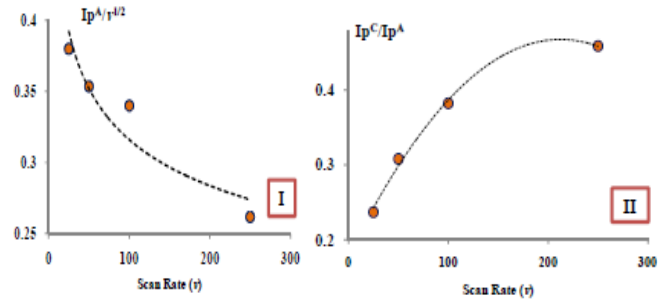

Fig. 3: (I) Normalized cyclic voltammograms of **1** in the presence of *Citrus aurantifulia* extrac in the various scan rates. (II) Variation of peak current ratio versus scan rate. other conditions such as Fig.2.

Normalized cyclic voltammograms are obtained by dividing the current of cyclic voltammograms by the square root of the scan rate ($I_p^{A1}/v^{1/2}$) [6,7]. Multiple files at different scan rates can be normalized and overlaid for obtaining more information. In Fig. 3, I the normalized voltammograms show that proportional to the decreasing of potential sweep rate the height of A_1 peak increases. At low scan rates the time scale and extent of reaction increase, oxidation of produced intermediate at the electrode surface cause an anodic peak current increase (A_1).

More studies were performed by varying the potential sweep rate in a solution of **1** in the presence of *Citrus aurantifulia* extract. Figure 3,II shows the effect of potential sweep rate on the cyclic voltammograms of 2mL *Echium amoenum Fisch* extract in the presence of 2 mL solution *Citrus aurantifulia* extract. The results indicate that the peak current ratio (Ip^{C1}/Ip^{A1}) strongly depends on the potential sweep rate and increases when the sweep rate increases (Figure 3,II).

According to the voltammetry results, it seems that the phenolic compounds in the *Echium amoenum Fisch extract*. such as rosmarinic acid oxidized at the surface electrode and entred in a chemical reaction with chemical compounds in *Citrus aurantifulia* extract. This reaction cause an increasing in the oxidation potential of **1** (E_p^{A1}) (Fig. 2,II, curve b). In an earlier paper it is reported a relationship between the oxidation potential measurement in cyclic voltammetry and ferric reducing antioxidant power. The increasing in the antioxidant activity caused a decrease in E_{pa} and observed an increased number on hydroxyl groups on the aromatic ring [8].

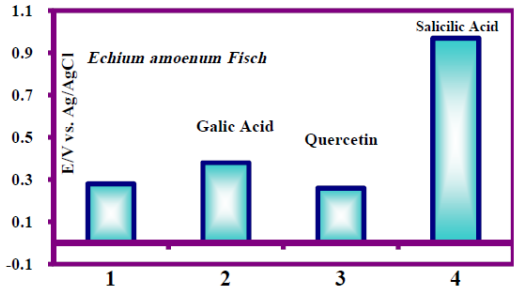

Fig. 4: Copmartion of E_p of *Echium amoenum Fisch* extract with the galic acid, salicilic acid and quercetin as standard antioxidants.

Electrochemical oxidation of galic acid, salicilic acid and quercetin has been performed in the same situation of *Echium amoenum Fisch* extract (**1**). The Oxidation potential (E_p) of *Echium amoenum Fisch* extract has been compared with E_p of the galic acid, salicilic acid and quercetin as standard antioxidants (Fig 4). Our results show that *Echium*

amoenum Fisch extract has a high antioxidant capacity in comparison of the galic acid, salicilic acid and quercetin.

III. CONCLUSION

The results of this study have shown a herb-herb interaction between *Echium amoenum Fisch* (**1**) and *Citrus aurantifulia* extract (**2**). This interaction reduces the antioxidant activity of *Echium amoenum Fisch* extract (**1**). Also our results show that in comparison of the galic acid, salicilic acid and quercetin as standard antioxidants, *Echium amoenum Fisch* extract has high antooxidant activity.

REFERENCES

[1] Ch. T. Che, Zh. J. Wang. M. S. Sum Chow, Ch. W. K. Lam, Molecules, 18, 5125-5141, **2013**.
[2] L. W. Chang, W. J. Yen, S. C. Huang, P. D. Duh, Food Chemistry, 78, 347-354, **2002**.
[3] C. Galli, A. Petroni, F. Visioli, European Journal of Pharmaceutical Sciences, 2, 67-68, **1994.**
[4] M. Mehrabani, M. R. Shams-Ardakani, A. Ghannadi, N. Ghassemi Dehkordi, S. E. Sajjadi Jazi, Iranian Journal of Pharmaceutical Research, 2, 111-115, **2005.**
[5] D. Nematollahi, A. Amani, J. Electroanal. Chem. 681, 11**, 2012**.
[6] A.J. Bard, L.R. Faulker, Electrochemical Methods, second ed., Wiley, New York, **2001**.
[7] R.S. Nicholson, I. Shain, Anal. Chem. 36, 706, **1964**.
[8] S. Chatterjee, Z. Niaz, S. Gautam, S. Adhikari b,P. S. Variyar, A. Sharma, Food Chemistry, 101, 515-523, **2007.**

Interaction of Superparamagnetic Iron Oxide Nanoparticles with Bovine Alpha-Lactalbumin

Marzieh Moeeni **, *Fakhrossadat Mohammadi*** *

444 prof. Sobouti Blvd., Department of Chemistry, Institute for Advanced Studies in Basic Sciences (IASBS), Gava Zang, Zanjan 45137-66731, Iran
Email: f.mohammadi@iasbs.ac.ir

Abstract: In recent years numerous studies have focused on the understanding of the interactions between proteins and nanoparticles (NPs). In this work we focus on the interaction of bovine α-lactalbumin (BLA), the second important whey protein, with magnetic nanoparticles (MP). The adsorbed BLA on the magnetic nanoparticles surface leads to a well-organized layer (protein corona) preserved its biological identity. The range of physico-chemical approaches including, zeta potential analysis, UV-vis spectroscopy, steady state fluorescence, CD spectroscopy and molecular docking studies were employed for investigating the MP-BLA corona.

Keywords*:* Alpha-Lactalbumin, magnetic nanoparticles protein corona, steady state fluorescence

I. INTRODUCTION

The increased use of nanomaterials for biomedical applications necessitates an improved understanding of their behavior in biological environments. This is in particular relevant as upon injection of nanostructures into the bloodstream, nanomaterials interact with different serum proteins resulting in the formation of protein corona (PC). Most importantly, the decoration of nanomaterials with proteins endows them with new properties which can significantly affect their biological pathways The physicochemical properties of nanoparticles, including material composition, size, shape, surface charge, surface functionalization etc. have to be taken into account in the understanding of protein corona formation [1]. Most of these considerations are also valid for superparamagnetic iron oxide nanoparticles (SPIONs) widely used for biomedical applications [2,3]. BLA is a major component of milk proteins and possess immunologic defense as well as antitumor and bactericidal activities. This small protein (14.2 kDa), homologues to the lysozyme family in sequence, stabilizes itself against the action of temperature and various denaturing factors upon binding the calcium cation (Ca^{2+}). BLA has also been widely used as model system as its high surface hydrophobicity has shown to be a key factor in modulating protein-nanoparticle interactions [4].

Π. METHODS

Bovine α-lactalbumin (BLA), iron(II) chloride tetarahydrate ($FeCl_2.4H_2O$), iron(III) chloride hexahydrate ($FeCl_3.6H_2O$), ammonium hydroxide (NH_4OH) was purchased from Sigma-Aldrich and used as received. Absorption spectra were recorded using SAFAS UV/Vis spectrophotometer (Société Anonyme de Fabrication d'Appareillages Scientifiques, Monaco) in quartz cuvettes with an optical path of 10 mm. Size and zeta-potential measurements carried out by Zetasizer Nano-ZS (Malvern Instruments Inc. Worcestershire, UK). Nanomaterials were diluted to 1 nM and measured in Milli-Q water. The intrinsic fluorescence spectra of BLA were recorded by Varian Cary Eclipse fluorescence spectrophotometer. For FRET investigation emission and adsorption spectrum of the solution containing 1.5 µM protein and 400 µl magnetic particle (0.5 mg/ml) was recorded. Aviv spectropolarimeter model 215 (proterion Corp., USA) was used for recording the circular dichroism spectra by using 1 mm path length cell. CDNN software as an artificial intelligence program based on the neural network, was used to estimate the secondary structure content of the protein. The results were expressed in molar ellipticity (deg cm^2 $dmol^{-1}$). Molecular docking was carried out using software Hex.8.8**.** Discovery studio visualizer (DSV) was used for visualizing the docked structures. The distances between bound ligands and the tryptophan residues were calculated with Pymol method.

II. RESULTS AND DISCUSSION

A. Figures and Tables

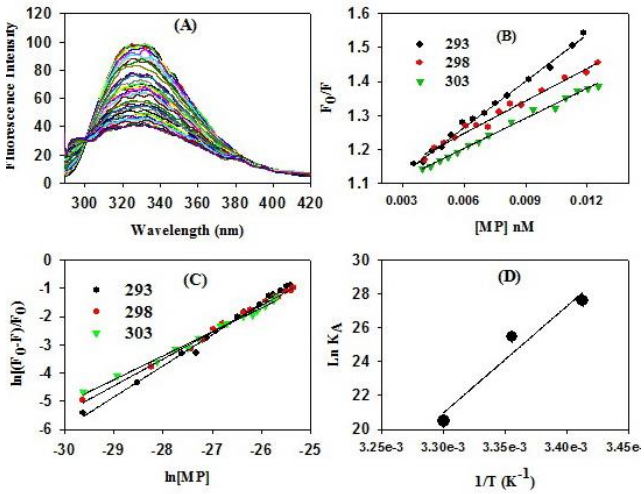

Fig.1: Determination of interaction strength between BLA and magnetic particles (A) Fluorescence quenching of BLA (2.5μM) by magnetic particles (MP) upon excitation at λ_{ex} = 280 nm in the absence and presence of increasing concentration of particles (0-0.015 nM); (B) The Stern-Volmer plots for magnetic particles at different temperatures; (C) plots of ln (F_0 - F / F) versus [particles] of BLA quenched by magnetic particles; (D) van't Hoff plot

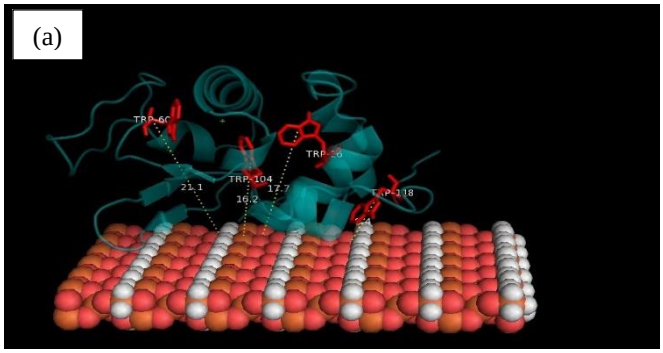

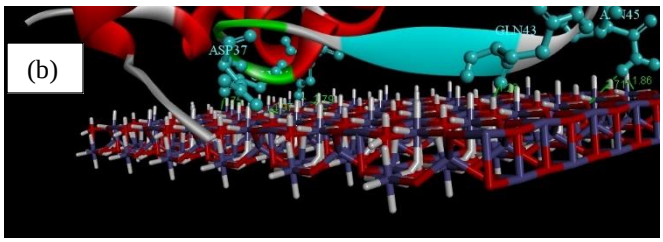

Fig.2. a) Representation of the interface interactive amino acids of BLA and the MP-Sheet and the hydrogen bindings (in green color) which contributed in the binding site, b) The calculated distances between MP-sheet and four tryptophans in BLA rendered by pymol

Table 1: Change in Stern-Volmer quenching constant (K_{SV}), the number of binding sites n, and binding constant (K_A) between magnetic particles and BLA = 2.5 μM at different temperatures

T/K	K_{SV}/ M^{-1}	n	K_A/M^{-1}
298	(3.01±0.07) × 10^{10}	0.58 ± 0.02	(8.29 ± 3.81) × 10^5
303	(1.97±0.05) × 10^{10}	0.64 ± 0.03	(2.01 ± 1.50) × 10^6
308	(2.71±0.07) × 10^{10}	0.69 ± 0.01	(1.14 ± 3.33) × 10^7

Table 2: Förster's theory: determination of Förster critical distance R_0, the distance between the donor and acceptor r, *J* a factor describing the overlapping between the emission spectrum of the donor and the absorption spectrum

Förste parameter	R_0(nm)	*r* (nm)	$J(\lambda)$ (M^{-1} cm^{-1})	*E*
MP-BLA	4.5-5.4	4.9-5.9	2.51 × 10^{-13}	0.3776

B. Equations

$$\frac{F_0}{F} = 1 + K_{SV}[Q] = 1 + k_q\tau_0[Q] \quad (1)$$

$$\ln\left(\frac{F-F_0}{F}\right) = LnK_A + nln[MP] \quad (2)$$

$$lnK = \frac{-\Delta H^{\circ}}{RT} + \frac{\Delta S^{\circ}}{R} \quad (3)$$

$$\Delta G^0 = \Delta H^0 - T\Delta S^0 \quad (4)$$

$$q_e = \frac{(C_0 - C_e)V}{W} \quad (5)$$

$$\frac{1}{q_e} = \frac{1}{q_{max}} + \frac{1}{q_{max}K_L c_e} \quad (6)$$

$$R_L = \frac{1}{1+(1+K_L C_0)} \quad (7)$$

$$E = 1 - \frac{F}{F_0} = \frac{R_0^6}{R_0^6 + r^6} \quad (8)$$

$$R_0^6 = 8.79 \times 10^{-25}[\kappa^2 n^{-4} \phi J(\lambda)] \quad (9)$$

$$J(\lambda) = \frac{\int_0^\infty F_D(\lambda)\varepsilon_A(\lambda)\lambda^4 \, d\lambda}{\int_0^\infty F_D(\lambda) d\lambda} \quad (10)$$

IV. CONCLUSION

The strong binding affinities between magnetic nanoparticles (MP) and bovine alpha lactalbumin (BLA) was concluded from the zeta potential analysis, UV-vis spectroscopy, steady state fluorescence. This considerable affinity could be related to hydrogen bonding resulted from the docking studies and thermodynamic parameters. The involved amino acid of BLA in the process of binding to magnetic particles was identified by docking calculation and the Trp-118 evaluated as key fluorophore**.** A non-radiative energy transfers with high probability between these particles and BLA was confirmed because of the 2-7 nm distances between MP-sheet and four tryptophans in BLA calculated by FRET experiment and pymol calculations. The determined R_L values are greater than 0 but less than 1 indicating that under the Langmuir isotherm model adsorption of BLA onto the particles is favorable. No altering in the major roles of BLA in transport of the drugs/ bioactive compounds is expected because of the no conformal change of the protein in the process of binding to the magnetic nanoparticles. This important characteristic in addition to extremely strong binding affinity and low cell toxicity make these particles new model nanostructures for nanomedicine orientated applications**.**

REFERENCES

[1] Mahmoudi, M.; Lynch, I.; Ejtehadi, M. R.; Monopoli, M. P.; Bombelli, F. B.; Laurent, S., Protein-Nanoparticle Interactions: Opportunities and Challenges. *Chem Rev* **2011**, *111*, 5610-37

[2] Ashby, J.; Pan, S.; Zhong, W., Size and Surface Functionalization of Iron Oxide Nanoparticles Influence the Composition and Dynamic Nature of Their Protein Corona. *ACS Appl Mater Interfaces* **2014**, *6*, 15412-15419

[3] Liu, S.; Han, Y.; Qiao, R.; Zeng, J.; Jia, Q.; Wang, Y.; Gao, M., Investigations on the Interactions between Plasma Proteins and Magnetic Iron Oxide Nanoparticles with Different Surface Modifications. *J. Phys. Chem. C* **2010**, *114*, 21270-21276.

[4] Permyakov, E. A.; Berliner, L. J., A-Lactalbumin: Structure and Function. *FEBS Letters* **2000**, *473*, 269-274.

Effect of different concentrations of 1-Butyl-3-methylimidazolium bromide on activity and structure of Chloroperoxidase: Molecular Dynamics Simulation

***Maryam Ghorbani .S*[a]*, *Mohammad Reza Housaindokht*[b,c], *Mohammad Reza Bozorgmehr*[c][d]**

[a]*International Campus, Ferdowsi University of Mashhad, Mashhad, Iran*

[b]*Department of Chemistry, Faculty of Science, Ferdowsi University of Mashhad, Mashhad, Iran*

[c]*Research and Technology Center of Biomolecules, Faculty of Science, Ferdowsi University of Mashhad, Mashhad, Iran*

[d]*Department of Chemistry, Mashhad Branch, Islamic Azad University, Mashhad, Iran*

**Email: ma_gh817@mail.um.ac.ir*

Abstract*:* The present study aimed to assess the effects of different concentrations of 1-Butyl-3-methylimidazolium bromide (BMIMBr) on the structure and activity of Chloroperoxidase (CPO) enzyme through the simulation of the CPO enzyme in the presence of two different concentrations of BMIMBr. The Root Mean Square Fluctuation (RMSF) diagrams indicated that the presence of BMIMBr caused changes in the location of compounds such as nitrates, halogens, and organic compounds. The second structure of the protein was examined; as a result, it is less effective in low concentrations of ionic liquids.

Keywords: Chloroperoxidase, MD Simulation, RMSF, Activity, Ionic Liquid.

I. INTRODUCTION

Chloroperoxidase (CPO) is a hemoprotein peroxidase glycoside enzyme with the molecular weight of 42 kDa and is obtained from caldariomyces fumago [1]. The maximum activity of CPO occurs at the pH of three, and most of its reactions occur within the pH range of 3-6 depending on the substrate. This enzyme belongs to the prosthetic group protoporphyrin with the pI range of 3.2-4 [2]. Recently, ionic liquids (ILs) have been investigated as alternative solvents for non-conventional biocatalysis. Remarkable results have been obtained for lipase catalysis in ILs with, in some cases, enhancement of activity and stereoselectivity. A few examples have also been reported for activity of peroxidases in pure ILs or homogeneous ILs/water mixtures; however, the behavior of CPO has never been investigated in these non-conventional media [3]. The modeling methods in molecular dynamics are a combination of complex techniques, which could be used to address chemical-physical problems using computers [4]. In fact, model building is an imitation of the real system over time, which could be applied to address the questions regarding the real system [5].

II. METHODS

The molecular dynamics simulations were carried out by GROMACS 5.1.2 [6]. The topological parameters of the atoms and SPC model of water were used in a cubic box for all the systems using the GROMOS96 force field. The simulation was performed for CPO and system in the presence of BMIMBr 2% and 30% in 100 nanoseconds. The root-mean-square deviation (RMSD) and root-mean-square fluctuations (RMSF) were performed using g_rms and g_rmsf tools. The minimum energy of each system was obtained by Gibbs energy diagram relative to the simulation time range. The obtained value represented a particular stage in the simulation, in which the energy of each system is minimum. By considering the calculated time step and g_rmsf and trjconv programs in the pdb file in GROMACS, the most plausible structures were obtained from the simulation.

III. RESULTS AND DISCUSSION

The RMSD diagram of the performed simulations is shown in Fig. 1. The obtained results confirmed that the simulation time range was adequate for the investigation of the effects of various factors on the CPO structure.

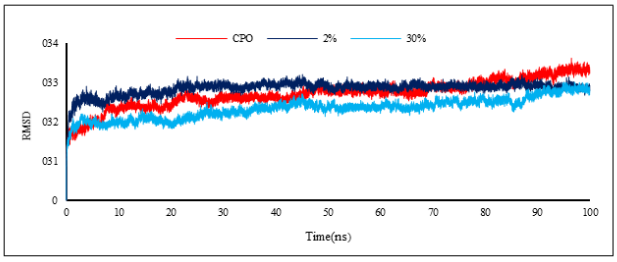

Fig. 1: Time-variant RMSD Diagrams of CPO and different concentrations of BMIMBr

Fig. 2 shows the RMSF diagrams of each system relative to the CPO, and the important locations in structure are specified with different colors.

The variations in the diagrams indicated that the presence of ILs caused changes in the location of compounds such as nitrates, halogens, and organic compounds, which in turn decreased the flexibility to the CPO structure.

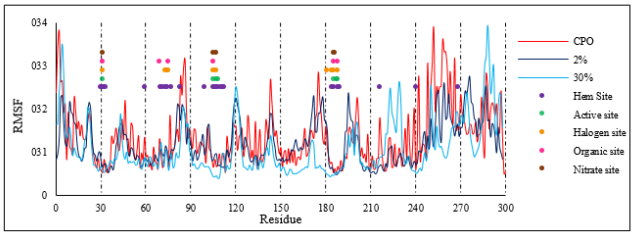

Fig. 2**:** RMSF diagrams Relative to residues (Important locations specified with different colors).

The pdb structure of the most plausible formations was compared using the PyMOL software. The optimized structures of all the systems were aligned with the halo structure, and the changed areas are shown in Fig.3. As shown in Fig. 3, the secondary structure has more variations in the presence of higher ILs.

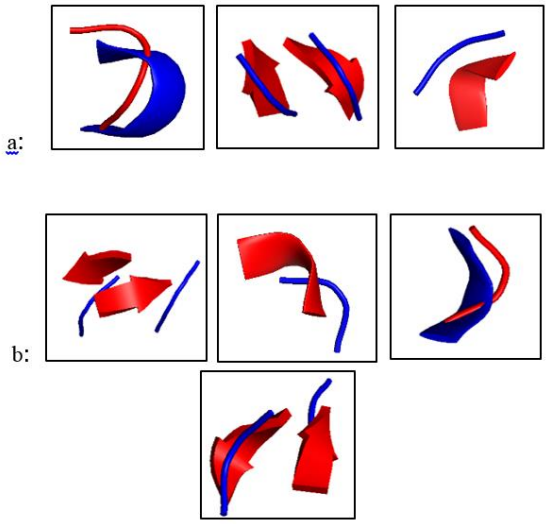

Fig. 3: Comparison of some changed areas of the CPO structure with structure in the peresence of BMIMBr a: 2%, b: 30%(CPO shown in red and structure in the presence of ILs shown in blue).

IV. CONCLUSION

According to the performed simulations, the presence of ILs caused changes in the macromolecule structure. For instance, flexibility has changed. As a result in the presence of low-concentration ILs, the oxidation efficiency of the enzyme has been increased. On the other hand, the ILs could be changed the activity and structure of the enzyme.

REFERENCES

[1] S.C.Myneni, J. Science, vol 295, pp. 1039–41, **2002.**
[2] J.Terner and T. L. Poulos, J. Structure, vol. 3, pp.1367-1377, **1995**.
[3] C.Sanfilippo, N.D. Antona and G.Nicolosi, J. Biotechnology Letters, vol. 26, pp. 1815–1819, **2004.**
[4] A.Satoh,, Elsevier, London , **2010**.
[5] M.C. Childers and V. Dagget, J. Molecular Systems Design & Engineering, vol. 2, pp. 9-33, **2017**.
[6] B. Hess, c. Kutzner, D. Vander Spoel, E. Lindahl, J. Chemical Theory and Computation, vol. 2, pp. 435–447, **2008**.

Thermal stability improvement of tyrosinase in the presence of spermine

Amir Tajik [a], ***Hassan Faridnouri*** [b*]

a: MSc student of Biochemistry, School of Biology, Damghan University, Damghan 36715-364, Iran. amirtajik71@yahoo.com

b: Assist. Prof. in Biophysics, School of Biology, Damghan University, Damghan 36715-364, Iran. faridnouri@du.ac.ir

Abstract: In this research, thermal stability changes of tyrosinase (Tyr) in the presence of different concentrations of spermine (Sp) was studied using different spectroscopic methods. Thermal scan investigations in relation to T_m changes indicated that the thermal stability of the enzyme in the presence of Sp significantly was increased. The calculated thermodynamic parameters also indicated of increasing free energy of Tyr in the presence of Sp, which confirmed the stabilization effect of this polyamine on Tyr. According to the information obtained in this work, it can be concluded that Sp polyamine is an appropriate option for the stabilization of the Tyr, especially at low concentrations.

Keywords: Tyrosinase, Spermine, Activity, Thrmal stability, Spectrophotometry

I. INTRODUCTION

The short lifetimes of enzymes and their sensibility to environmental changes is one of their characteristics. Therfore, enzymes in free form usually have poor stability towards pH, heat or other factors and so, it is difficult to recover them and reuse [1]. Sp is one of the natural metabolites of the human body. It was introduced for the first time as one of the compounds in the sperm. These kinds of components have positive charge, therefore, their interaction with negative charge of the macromolecules such as proteins and enzymes for regulating the function and stabilizing the structure have been reported [2]. Tyr is a copper carrier enzyme which is found in high level in microorganisms, plants, animals and fungi, which is responsible for the biosynthesis of melanin and polyphenolic compounds [3]. Despite extensive studies on the inhibition of Tyr, there are little studies about the conditions which led to increase its sustainability. While this topic is important for the use of Tyr as the biosensors in order to detect and measure phenolic derivatives such as L-DOPA. In this research, thermal stability changes of Tyr in the presence of various amount of Sp was studied using UV-Vis spectrophotometry.

II. METHODS

The Sp thermal stability effect on Tyr was investigated by monitoring absorbance intensities of free and Sp-Tyr complex with UV–Visible spectrophotometer in the presence and absence of 0.1, 0.3, 0.5 and 1 mM of Sp at temperatures range from 300-390 K according to the two state equilibrium model N ↔ U. Quartz cells were used for all studies which including 0.1 mg/cm^3 Tyr and different concentrations of Sp with scan rate 1 ºC/min. Then absorption data vs. temperature were plotted and the thermodynamic profile was predicted by the two-state model, the temperature in which ΔG^o was zero (melting temperature, T_m), was determined as the transition midpoint of the melting curve.

III. RESULTS AND DISCUSSION

The recovery amount of the Tyr native conformation in the absence and presence of Sp different concentration was investigated using thermal stability studies over a temperature range of 300 to 390 K. Assuming the simple mechanism of the two- state model denaturing for Tyr as a small and spherical molecule, the thermal denatured fraction of the enzyme (F_u) could be obtained by the Eq. 1 [4]:

$$F_u = \frac{(Y - Y_F)}{Y_U - Y_F} \qquad \text{Eq. 1}$$

where Y_F, Y_u and Y are the absoebance intensities of the native, denatured state and the observed parameter of Tyr at the specific concentration of Sp, respectively. The sigmoidal curves of the denatured fraction of Tyr in the presence of different concentrations of Sp are displayed in Fig. 1. As shown, increasing in the Sp concentrations led to right shifting the curves into the higher temperatures. ΔG_u° for Tyr at different concentrations of Sp at any temperature T (K), was calculated from the Eqs. 2 and 3 [4, 5]:

$$K = \frac{F_u}{1 - F_u} = \frac{Y_f - Y}{Y - Y_u} \qquad \text{Eq. 2}$$

$$\Delta G^0 = G^0{}_U - G^0{}_F = -RT \ln K = -RT \ln \frac{[U]}{[F]} \qquad \text{Eq. 3}$$

The summation of F_n (fraction of the native state) and F_u (fraction of the denatured state) is equal to total enzyme components in systems at temperature T (K). Using Eq. 2, the value of the equilibrium constant (K) is calculated at any temperature and then by replacing it in Eq. 3, Gibbs free energy (ΔG_u°) is obtained. The plot of free energy changes of Tyr during denaturing vs. absolute temperature, in the absence or presence of different concentrations of Sp is shown in Fig.

2. The midpoint of each graph represented the melting point (T_m). By using the Eq. 4, the values thermodynamic parameters at T_m (ΔS°_m and ΔH°_m) are calculated which demonestrated in Table 1. According to Table 1 and Fig. 2, in a concentration-dependent manner, an increasing in Sp concentration led to T_m increasing from 318 to 338 which indicates that thermal stability has been promoted 20° C. In the other hand, $\Delta G_{(25^\circ)}$ has been increased from 16 to 34.8 kcal/mol at 1 mM Sp which indicates improvement of enzyme stability. Also ΔS°_m and ΔH°_m of Tyr were induced by Sp. The increasing in ΔH°_m induced by Sp could be associated to the increment in intramolecular hydrogen bonds of Tyr [5, 6].

These results showed that Sp could have a favorable interaction with Tyr and stabilized its folded structure. Similar results were reported on the stabilization of protein due to the favorable interaction with polyamines [7, 8] and the results of this research are in good agreement with the results of other literature reviews.

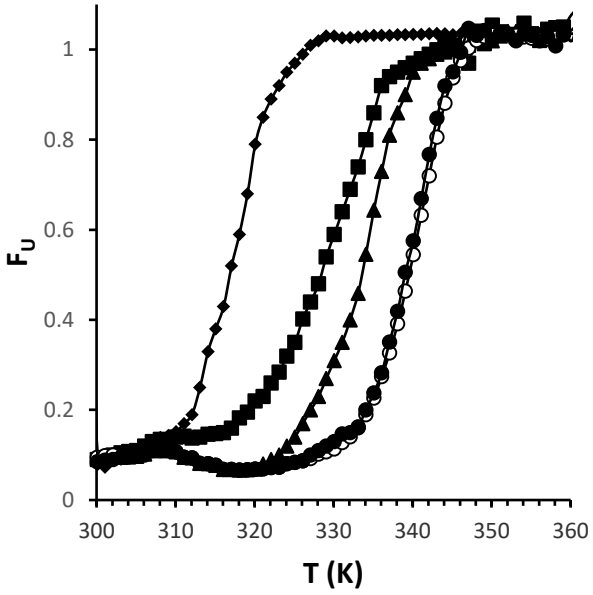

Fig.1: Fraction of the denatured changes of Tyr induced by different concentrations of Sp (0, 0.1, 0.3, 0.5 and 1 mM) from left to right.

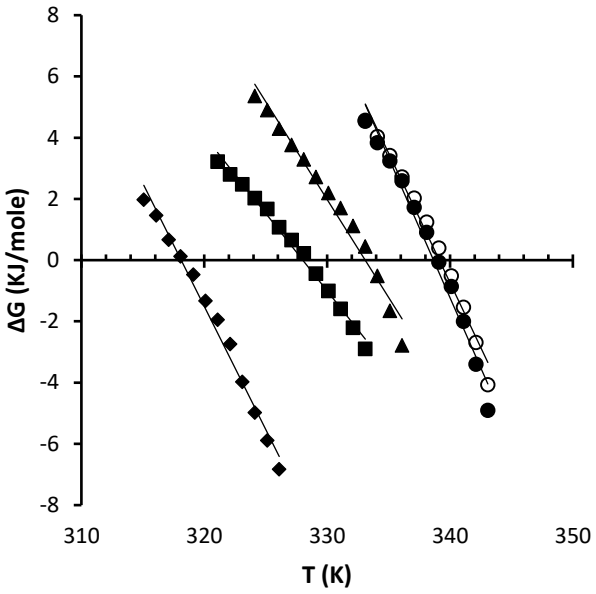

Fig 2: Free energy changes of the denaturing of Tyr induced by different concentrations of Sp (0, 0.1, 0.3, 0.5 and 1 mM) from left to right.

Table1: T_m, $\Delta S°_m$ and $\Delta H°_m$ changes of Tyr at different concentrations of Sp.

[spm](mM)	0	0.1	0.3	0.5	1
ΔS	0.803	0.506	0.558	0.846	0.914
ΔH™	255.48	166.18	186.268	287.19	309.85
ΔG™	0.131	0.218	0.454	0.4	0.916
T_m	318	328	333	339	338
$\Delta G_{(25°)}$	16.177	20.02	22.5	37.2	34.8
ΔH_{vh}	1.436	1.77	2.28	6.16	5.95

IV. CONCLUSION

To conclude, utilization of Sp as a co-solvent improves the stability of Tyr. Therefore, thermodynamic parameters which obtained in this study, suggested that hydrogen and van der Waals interactions between the enzyme and polyamine has changed the enzyme's micro-environment and thereby made it more stable. Since protein stability is affected by its native conformation, any factor that maintains it in native form can be considered as a stabilizing agent, provided that enzyme activity does not undergo major changes. Sp has not only stabilized Tyr in this study but also improved its catalytic activity. However, data related to the activity evaluation section was not provided here. Therefore, the present results

revealed that Sp could act as a stabilizer of structure and an enhancer of the activity of Tyr.

REFERENCES

[1] Xu, J., Sun, J., Wang, Y., Sheng, J., Wang, F., & Sun, M. (). Application of iron magnetic nanoparticles in protein immobilization. Molecules, **2014**, Vol. 19(8), pp. 11465-11486J.

[2] Kudou M, Shiraki K, Fujiwara S, Imanaka T, Takagi M. Prevention of thermal inactivation and aggregation of lysozyme by polyamines. Eur J Biochem **2003**; Vol. 270, pp. 4547-54.

[3] Robb, D. A. Tyrosinase. In *Copper Proteins and Copper Enzymes*; Lontie, R., Ed.; CRC Press: Boca Raton, FL, **1984**; Vol. II, pp 207-240.

[4] A. Saboury, A. Moosavi-Movahedi, Derivation of the thermodynamic parameters involved in the elucidation of protein thermal profiles, Biochemical education, **1995**, Vol. 23(3), pp. 164-167.

[5] A. Rani, P. Venkatesu, Insights into the interactions between enzyme and co-solvents: stability and activity of stem bromelain, International journal of biological macromolecules, **2015**, Vol. 73, pp. 189-201.

[6] G. De Sanctis, A. Maranesi, T. Ferri, A. Poscia, F. Ascoli, R. Santucci, Influence of glycerol on the structure and redox properties of horse heart cytochrome c. A circular dichroism and electrochemical study, Journal of protein chemistry, **1996**, Vol. 15(7), pp. 599-606.

[7] M. Kudou, K. Shiraki, S. Fujiwara, T. Imanaka, M. Takagi, Prevention of thermal inactivation and aggregation of lysozyme by polyamines, European Journal of Biochemistry, **2003**, Vol. 270(22), pp. 4547-4554.

[8] H. Hamada, R. Takahashi, T. Noguchi, K. Shiraki, Differences in the Effects of Solution Additives on Heat- and Refolding-Induced Aggregation, Biotechnology progress, **2008**, Vol. 24(2), pp. 436- 443.

Selective sensing of Fe^{3+} and Al^{3+} over mixed metal ions using functionalized microporous MOF as a new fluorescent probe

***Hossein Shayegan*[a], *Hooman Taherkhani*[b], *Yeganeh Davoudabadi Farahani*[a] *Vahid Safarifard*[a,*] *and Mohammad Ali Rezvani*[b]**

[a] *Department of Chemistry, Iran University of Science and Technology, Tehran 16846-13114, Iran.*
[b] *Department of Chemistry, Faculty of Science, University of Zanjan, 451561319, Zanjan, Iran.*

Email: vsafarifard@iust.ac.ir

Abstract*:* Metal-organic frameworks are a class of attractive materials for fluorescent sensing. In this research, a two-fold interpenetration pillared-layer amine/imine-functionalized MOF known as TMU-16-NH_2, [$Zn_2(NH_2$-BDC$)_2$(4-bpdh)]·3DMF, have been synthesized via a mixed ligand approach using amino-1,4-benzenedicarboxylate (NH_2-BDC) and 2,5-bis(4-pyridyl)-3,4-diaza-2,4-hexadiene (4-bpdh) under solvothermal condition. Sensor TMU-16-NH_2 exhibits Al^{3+}-selective TURN-ON and Fe^{3+}-selective TURN-OFF type fluorescence emission responses, for which the electrostatic interaction between Fe^{3+} and Al^{3+} ions and the inner surface of the micropores may play a critical role.

Keywords: Metal-organic frameworks; fluorescence; Sensing; Fe^{3+}; Al^{3+}

I. INTRODUCTION

Metal ions are required for the proper function of all cells within every living organism, and disruptions in localizations and concentrations of metal ion pools are a major contributor to aging and disease [1]. Recently, fluorescent sensors based on MOFs have been regarded as one of the most promising candidates for detecting metal ions owing to their high efficiency, low cost, and portability. MOFs, as indicated by the name, are crystalline solids constructed via self-assembly of single metal cations or metal clusters and organic ligands having multiple binding sites, forming one, two, or three dimensional extended coordination networks. The intrinsic porosities of the luminescent MOFs enable them to reversibly adsorb and release guest molecules and to provide a platform for specific luminescent recognition of targets due to the host-guest interactions [2]. As reported in several papers, a new sensor design with differential responses towards multiple ions gets more and more attention because of cost-effective, analytical time reduction and create effective practical applications [3].

Here, we prepared two organic ligands 2,5-bis(4-pyridyl)-3,4-diaza-2,4-hexadiene (4-bpdh) and amino-1,4-benzenedicarboxylate (NH_2-BDC) and employed it to react with Zn(II) salt to construct crystalline solid luminescent materials. The fluorescence studies show that TMU-16-NH_2 can sense Fe^{3+} and Al^{3+} through fluorescence quenching and enhancement, respectively. More importantly, this MOF can realize fast detection for Fe^{3+} and Al^{3+} with a response time of less than 1 min, as well as shows low detection limits of 0.7 μM and 0.09 μM, respectively.

II. METHODS

Starting reagents for the synthesis were purchased and used without further purification from commercial suppliers (Sigma-Aldrich, Merck and others). $Zn(NO_3)_3·6H_2O$ and a Briefly, $Zn(NO_3)_2·6H_2O$ (0.297 g, 1 mmol), 4-bpdh mino-1,4-benzenedicarboxylic acid (NH_2-BDC) were used to synthesize TMU-16-NH_2. (0.119 g, 0.5 mmol), NH_2-BDC (0.181 g, 1 mmol) were dissolved in 15 ml DMF.

The luminescence properties of TMU-16-NH_2 dispersed in DMF were investigated at room temperature. To a 1 cm × 1 cm quartz cell, a TMU-16-NH_2 suspension (250 mg L^{-1}, 4 mL), and certain amounts (20 μL) of selected analytes were sequentially added. The fluorescence experiments were performed at room temperature on a Shimadzu RF-6000 fluorescence spectrometer (kyoto, Japan) with a photomultiplier voltage of 700 V, scan speed of 60,000 nm min^{-1}, excitation slit width of 900 nm, emission slit width of 200-800 nm, and a 380 nm optical filter.

III. RESULTS AND DISCUSSION

The pore surface of TMU-16-NH_2 is decorated with pendant amine and imine functional groups. Two of the 3D frameworks interpenetrate in TMU-16-NH_2, reducing the pore size. A 1D channel occurs in the direction of the rectangular diagonal of the paddle-wheel clusters (Fig. 1) [4].

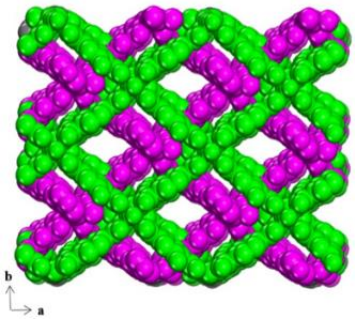

Figure 1. Representations of the two-fold interpenetration TMU-16-NH_2 which contain 1D channels of 3 Å, viewed along the rectangular diagonal of the paddle-wheel clusters.

To examine the potential of TMU-16-NH_2 for sensing of metal ions, the as-synthesized samples (1 mg) were ground and immersed in DMF solutions containing different metal ions (Zn^{2+}, Pb^{2+}, Co^{2+}, Cu^{2+}, Cd^{2+}, Al^{3+}, Fe^{3+}, As^{3+}, Mn^{2+} and Ni^{2+}) to form a metal-ion-incorporated MOF suspension. The emission spectra show that the various metal ions display markedly different effects on the luminescence of the MOF, particularly for Fe^{3+} ion and Al^{3+} ion, whose varying extents could be easily distinguished .

To better understand the fluorescence response of TMU-16-NH_2 to Fe^{3+} and Al^{3+}, concentration-dependent luminescence measurements were also carried out. As demonstrated in Figure 2a and b, the emission intensity of the TMU-16-NH_2 suspension at 440 nm was quenched steadily with increasing Fe^{3+} concentration and enhanced accordingly with increasing Al^{3+} concentration.

The fluorescence quenching and enhancing follow the Stern–Völmer (SV) equation: $I_0/I=1 + K_{SV}[M]$, where I_0 and I correspond to the luminescence intensity for TMU-16-NH_2 in absence and presence of metal cations, respectively, [M] is the metal concentration, and K_{SV} is the Stern – Völmer constant. The K_{SV} values are calculated via luminescent data. An exceptionally high K_{SV} value of 21600 M^{-1} was obtained for Fe^{3+}, while K_{SV} for Al^{3+} was 1435 M^{-1}. Based on the slope of the calibration curve (K) values and the standard deviations (S_b) from ten repeated fluorescent measurements of blank solutions, the detection limits ($3S_b/K$) of TMU-16-NH_2 towards Fe^{3+} ion in DMF were calculated to be 0.7 μM (corresponding to 40 ppb) and 0.09 μM (2.4 ppb) for Al^{3+}. This is also comparable to or better than some previously reported Fe^{3+} and Al^{3+} fluorescent sensors [5, 6].

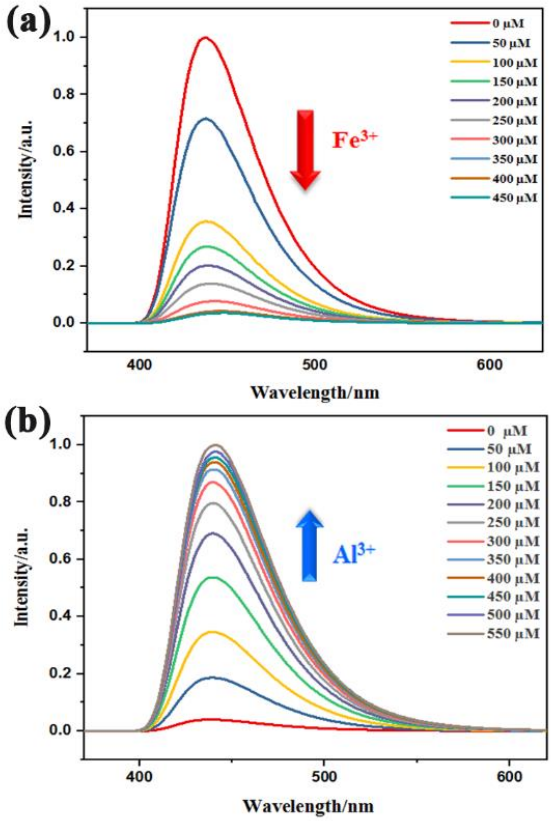

Figure 2. The luminescence spectra of TMU-16-NH_2 with different concentration of (a) Fe^{3+} and (b) Al^{3+} ions.

According to the reported literature, porous MOFs with Lewis basic sites, such as amine, pyridyl, amide and anionic sulfonate sites, can have significant interactions with guest metal ions [7]. We therefore suggest that the quenching/enhancing might be related to the interaction between the Fe^{3+}/Al^{3+} ions and pendant amine and imine functional groups in TMU-16-NH_2.

IV. CONCLUSION

In this work, we have reported the synthesis and metal ions sensing properties of amine/imine-functionalized microporous TMU-16-NH_2 MOF. TMU-16-NH_2 could be employed as potential multifunctional luminescent material for sensing of Fe^{3+} and Al^{3+} ions with high selectivity and considerable sensitivity and fast response time. The limit of detection of this luminescent probe for Fe^{3+}/Al^{3+} in DMF medium was found to be 0.7 µM and 0.09 µM respectively, which is comparable to the recommended maximum contaminant level or to the value mentioned in the guidelines

of WHO for Fe^{3+} (0.3mg/L, 5.4 μM) and Al^{3+} (0.2 mg/L, 7.4 μM) in drinking water.

REFERENCES

[1] D.W. Domaille, E.L. Que, C.J. Chang, Nature chemical biology, vol. 4, pp. 168. **2008**.
[2] X. Luo, X. Zhang, Y. Duan, X. Wang, J. Zhao, Dalton Transactions, vol. 46, pp. 6303-6311, **2017**.
[3] L. Wenfeng, M. Hengchang, M. Yuan, Q. Chunxuan, Z. Zhonwei, Y. Zengming, C. Haiying, RSC Advances, vol.5, pp. 6869-6878, **2015**.
[4] V. Safarifard, A. Morsali, CrystEngComm, vol. 16, pp. 8660-8663, **2014**.
[5] S. Chen, Z. Shi, L. Qin, H. Jia, H. Zheng, Crystal Growth & Design, vol. 17, pp. 67-72, **2016**.
[6] W.-M. Chen, X.-L. Meng, G.-L. Zhuang, Z. Wang, M. Kurmoo, Q.-Q. Zhao, X.-P. Wang, B. Shan, C.-H. Tung, D. Sun, Journal of Materials Chemistry A, vol. 5, pp. 13079-13085, **201**7.
[7] J.-R. Li, R.J. Kuppler, H.-C. Zhou, Chemical Society Reviews, vol. 38, pp. 1477-1504, **2009**.

Inclusion Complexes between (α-, β- and γ-) cyclodextrins as a nanocarriers with serotonin: Molecular Docking and Molecular Dynamics simulation

F. Fateminasab*[a], *A.K. Bordbar*[a]

[a] *Department of Chemistry, University of Isfahan, Isfahan, 8174673441, Iran*

[b] *Institute of biochemistry and biophysics, University of Tehran, Tehran*

Email: ftmfatemi61@gmail.com

Abstract*:* Molecular docking results predicted three, three, and two hydrogen bond between SER and α-CD, β-CD, and γ-CD, respectively. The molecular dynamics simulations confirmed the formation of stable inclusion complex of β-CD: SER. While, inclusion complex (IC) of α-CD: SER is unstable and SER comes out of cavity in the initial times of the MD. Finally, in case of γ-CD: SER, there is conformational change in γ-CD observed during the complexation process. The RMSD, RDF and H-bonding analyses represent the following order for the stability of complexes: β-CD: SER> γ-CD: SER> α-CD: SER. The results of MD represent the lack of hydrogen bond in α-CD: SER and the small number of hydrogen bonds in β- and γ-CD: SER that are in agreement with molecular docking results.

Keywords: Cyclodectrin, Serotonin, Molecular docking, Molecular dynamics.

I. INTRODUCTION

Serotonin (SER) AS A chemical neurotransmitter is an active molecule primarily found in various tissues AND the brain' human body, remarkable hormonal activities and as in various cognitive and behavioral functions including sleep, mood, pain, addiction, locomotion, anxiety, aggression, and learning. Specially, the insufficiency of SER is related with the risk of dementia, disease of Alzheimer's, various mental disorders, such as schizophrenia, suicidal behavior, infantile autism, eating disorders, disorder of obsessive-compulsive, and insomnia [1]. Cyclodextrins (CDs) are family of cyclic oligosaccharides that have truncated cone structure. Native CDs, containing of linked 6,7 and 8 D-glucopyranose units by α-(1→4) glycosidic bonds, are named as α-, β or γ-cyclodextrins (abbreviated as α-, β- or γ-CD), in that order. [2]

II. METHODS

Docking calculations was achieved by the AutoDock 4.2.5 software. The initial structures of CDs were extracted from the webserver (http://upjv.q4md forcefieldtools.org/REDDB/projects/F-85/).

The consequential structures were subjected to the MD simulation by the module of PMEMD in AMBER 12 package of MD. The GAFF was applied to parameterize the guest molecule SER. For analysis, the PTRAJ and CPPTRAJ modules of AMBER 12 program were used to evaluate the RMSD, the (O4-O5) distance in glucose units in CDs, RMSF, RDF and H-bonding.

III. RESULTS AND DISCUSSION

This section must be included experimental or computational data, figures, tables and equations. The number of figures, tables and equations throughout the text must be brought orderly.

A. Molecular docking

Molecular docking was employed to study α-, β- and γ-CD ICes. (Fig. 1 and Table 1)

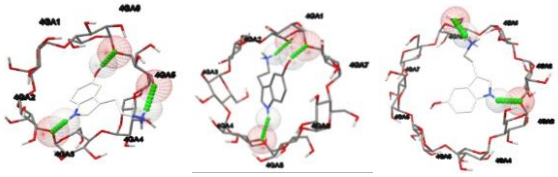

Fig.1: Molecular docking of ICes between α -, β or γ-CDs: SER

Table1: the binding free energies of ICes between of α-, β or γ-CDs with SER

CDs: SER	*ΔG°* (kcal/mol)
α-CD: SER	-6.15
β-CD: SER	-5.91
γ-CD: SER	-5.30

B. Molecular dynamics simulation

MD simulation methods provide valuable insight into the structure, dynamics, and interactions of biological macromolecules. MD runs for the native CDs were performed only in water solution. The comparison of the RMSD, distance O4-O5 in CDs behavior (Table 2-a,b) lead us to conclude that SER forms more stable inclusion complex with β-CD than with α- and γ-CD that does not totally agree with docking results.

Table2: a) RMSD (Å) of CDs in free and complex state with SER, b) (O4-O5) of CDs distance in free and complex states with SER

a) RMSD (Å)			
α-CD: SER	1.114 ±0.213	**free α-CD**	0.798 ± 0.259
β-CD: SER	1.112± 0.208	**free β-CD**	0.848±0.247
γ-CD: SER	1.559± 0.329	**free γ-CD**	1.043±0.336
b) Distance			
α-CD: SER	1.408 ±	**free α-CD**	1.346 ± 0.113
β-CD: SER	1.243± 0.107	**free β-CD**	1.247 ± 0.112
γ-CD: SER	1.151 ±	**free γ-CD**	1.168 ± 0.112

IV. CONCLUSION

We predicted the presence of three, three and two H-bonds in α-, β- and γ-CDs-SER ICes from the molecular docking methods. The simulations of MD corroborated stable β-CD: SER IC formation, even though, the α-CD: SER IC was unstable so that SER came out of the cavity in the initial times of MD. In addition, the major change in γ-CD conformation for the duration of the MD simulation of γ-CD: SER IC could be associated to the unfitting size of its hole for SER. The MD analysis results via various parameters, i.e. RMSD, RDF and distance, led to the same conclusion. The β-CD: SER IC is more stable than α- and γ-CDs: SER ICes. Therefore, β-CD is the best choice for encapsulation of SER among the others.

REFERENCES

[1] Lesch KP, Waider J. Serotonin in the Modulation of Neural Plasticity and Networks: Implications for Neurodevelopmental Disorders. Neuron. vol 76, pp. 175-191, **2012.**

[2] Astray G, Gonzalez-Barreiro C, Mejuto JC, Rial-Otero R, Simal-Gándara J. A Review on the Use of Cyclodextrins in Foods. Food Hydrocoll. vol 23, pp. 1631-1640, **2009.**

Spectroscopic Study of the Interaction of Trans_Aco Base (curcuminato) Exo Zirconium IV Hydrate and Curcumin with DNA

M.Biuki, H. Dezhampanah*
Department of Chemistry, Faculty of Science, University of Guilan, P.O. Box: 19141, Rasht, Iran,
Email: ***h.dpanah@guilan.ac.ir***

ABSTRACT: An assessment of the interactions between drugs and DNA to design more effective anticancer drugs and better understanding of biological processes, such as gene translation and transcription of the DNA sequence, is important. Binding interaction of novel six-coordinate complex of zirconium with curcumin ligand (trans-[ZrO(curcumin)2(H2O)].H2O) and curcumin with calf thymus (CT-DNA) were investigated using UV–Vis absorption spectroscopy and fluorescence spectrophotometry. The appearance of hypochromicity effect and the blue shift in UV-Vis spectrum of complex and curcumin were due to the interaction with CT-DNA. The binding constants (K) were determined from the changes in the optical absorption spectra at various CT-DNA concentrations. The values of K were 8.50×104 M-1 and 2.25×104 M-1 for complex and curcumin, respectively, at 25 ºC. The UV–Vis and fluorescence results suggested that complex and curcumin prefer to bind on the minor groove of CT-DNA Accordingly, the constant hybridization equilibrium of drug composition and DNA has been estimated and is consistent with the amounts and evidence available, which indicates a strong association for the drug with these two strands..

Keywords: CT-DNA, Curcumin, fluorescence spectroscopy;

I. INTRODUCTION

DNA is central to the biological activities of all living cells [1]. (DNA) or(Dena) The term Deoxyribo nucleic acid is a type of nucleic acid that contains genetic instructions that are used to function and develop biological organisms of living organisms and viruses. The main role of the DNA molecule is the long-term storage of genetic information and instructions. Experiments like Griffith experiment and Yuri experiment were revolutionary experiments and the beginning of DNA identification and study as a genome. Aliving organism has genetic material containing the coded information for its functioning that makes the DNA an obvious target of study for many researchers [2,3]. The drug-DNA interaction is an important area since it provides valuable information in the development of drugs and controlling gene expression [4-6]. DNA is also target molecule for many drugs including those under advanced clinical trials, especially anticancer drugs [7,8].
Curcumin or Di-frucloyl Methane is an active ingredient in turmeric and has anti-inflammatory properties;Curcumin is a potent antioxidant. Curcumin, possesses a variety of remarkable pharmacological activity including anti-inflammatory, anti carcinogenic, and anti-oxidant activity [9]
Scheme. 1. Chemical structure of (a) complex of curcumin and (b) curcumin. In this study, the interaction between Zirconium curcumin complex (trans-[ZrO(curcumin)2(H2O)].H2O) scheme 1 and CT-DNA was investigated by the application of UV–vis and fluorescence spectroscopic techniques.

II. METHODS

Calf thymus DNA and curcumin were purchased from Sigma Chemical Co. and was used without further purification. trans-[$ZrO(curcumin)_2(H_2O)$].H_2O was synthesized according to a method described by khorshidi in [10].The stock solution of Zr(IV) complex and curcumin were prepared in 5 mM phosphate buffer, pH 7.20 and stored in the dark at 5–10 ºC. To prepare the DNA stock solution, 2 mg of DNA was dissolved in 1 mL of phosphate buffer one day before experiment and stored at 4ºC.
The absorption spectra were recorded on a Cary 500 scan UV-vis-NIR spectrophotometer. The UV-vis titration experiments were made by addition of the CT-DNA stock solutions into a 1 mL cuvette containing the complex and curcumin solution of appropriate concentration.

III. RESULTS AND DISCUSSION

Figs. 1 and 2, show the UV–Vis absorbance spectra of complex of zirconium and curcumin upon increasing addition of CT-DNA. In both cases, a bathochromic shift of $\Delta\lambda \leq 10$ nm and moderate hypochromism (H ≤32%) in maximum band were observed, which represents the existence of interaction and groove binding, between CT-DNA and complex of Zirconium(IV) and curcumin [11,12].
The absorbance of complex and curcumin decreased with increasing concentration of CT-DNA for both figures.

Binding constants for the interaction of complex and curcumin with CT-DNA were determined by analysis of absorption spectrophotometric titrations data.

The values for apparent binding constants of Complex - DNA and curcumin - DNA at our experimental conditions were calculated to be 8.50×104 M-1 and 2.25×104M-1, respectively at the 25 °C. Comparison of these results has revealed that the affinity of complex of Zirconium to CT-DNA is greater than to curcumin.

The fluorescence quenching curve of ethidium bromide(EB) bound to DNA by zirconium complex are shown in Fig. 3.

In this case, the reduction in emission intensity could be due to displacement of EB from the interaction sites by this complex, and representing that binding constants of this complex to CT-DNA are comparable with binding constant of EB to DNA which is in the order of 106 M-1

The quenching plots illustrate that the quenching of EB bound to CT-DNA by the zirconium complex is in good agreement with the linear Stern–Volmer equation, which also proves that the porphyrins bind to CT-DNA (ksv=9.9335)

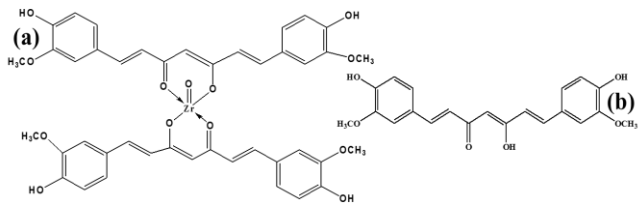

Scheme. 1. Chemical structure of (a) complex of curcumin and (b) curcumin

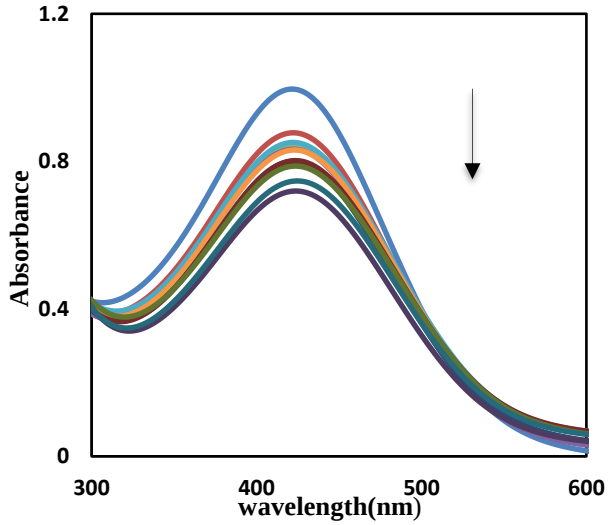

Fig2. UV-Vis spectra of the complex of curcumin (The arrow indicates the absorbance changes with increasing of the DNA).

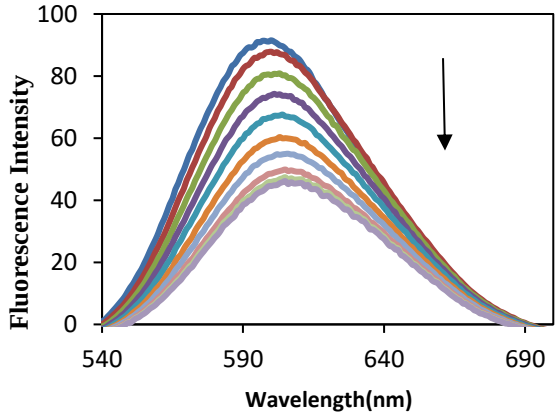

Fig3.steady state fluorescence spectra of DNA in absence and presence of varying concentration of complex

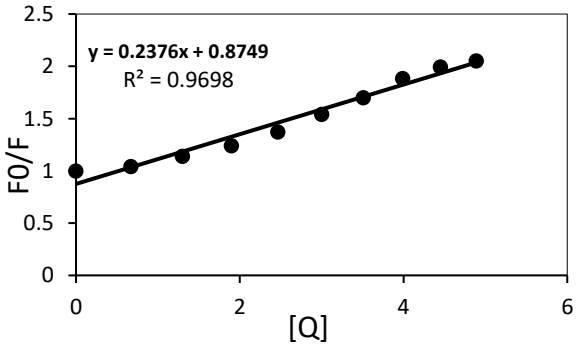

Fig4.The stern-volmer plots for the complex-DNA

IV.CONCLUSION

The existence of a moderate hypochromicity and shift of wavelength in the UV-vis spectra of the zirconium complex suggests a groove binding mode with no stake formation of zirconium complex on the CT-DNA surface.

The fluorescence quenching results showed the Stern-Volmer equation is linear and quenching is static.

Our study could provide more help in understanding the binding mechanism of zirconium curcumin complex curcumin and curcumin and related compounds with Ct-DNA and the pharmacological effects of curcumin as well as designing the structure of new and efficient drug molecules.

REFERENCES

[1] Wang AH, Quigley GJ, Kolpak FJ, Crawford JL, Van Boom JH, Van der Marel G, Rich A**. 1979**

[2] X.L. Li, Y.J. Hu, H. Wang, B.Q. Yu, H.L. Yue, Molecular spectroscopy evidence of berberine binding to

DNA: comparative binding and thermodynamic profile of intercalation, Biomacromolecules 13 (February (3)) **(2012)**
[3] M.L. Örberg, K. Schillén, T. Nylander, Dynamic light scattering and fluorescence study of the interaction between double-stranded DNA and poly (amido amine) dendrimers, Biomacromolecules 8 (May (5)) **(2007)**
[4] Y. Shi, C. Guo, Y. Sun, Z. Liu, F. Xu, Y. Zhang, Z. Wen, Z. Li, Interaction between DNA and microcystin-LR studied by spectra analysis and atomic force microscopy, Biomacromolecules 12 (February (3)) **(2011)**
[5] R.M. Elder, T. Emrick, A. Jayaraman, Understanding the effect of polylysine architecture on DNA binding using molecular dynamics simulations, Biomacromolecules 12 (September (11)) **(2011)**
[6] Y. Ding, L. Zhang, J. Xie, R. Guo, Binding characteristics and molecular mechanism of interaction between ionic liquid and DNA, J. Phys. Chem. B 114 (January (5)) (**2010)**
[7] G. Yunus, S. Srivastava, M. Kuddus, V.D. Gupta, Drug–DNA interaction: a theoretical study on the binding of thionine with DNAs of varying base composition, Curr. Appl. Phys. 13 (March (2)) **(2013)**
[8] A. Opar, Novel anticancer strategy targets DNA repair, Nat. Rev. Drug Discov. 8 (June (6)) **(2009)**
[9] N.R. Jana, P. Dikshit, A. Goswami, and N. Nukina, J. Biol. Chem. 279 pp. 11680–11685, **2004**.
[10]. N. Kiani, B. Heidari, M. Rassa, M. Kadkhodazadeh, B. Heidari, J. Basic Clin. Physiol. Pharmacol. 25, 367 **(2014)**
[11] Scott, J. E.; Metachromasia of Alcian blue, Astrablau and other cationic phthalocyanin dyes. Histochemie**., 1970.**
[12] Thamae, M.; Nyokong, T.; Cobalt(II) porphyrazine catalysed reduction of nitrite. J. Electroanal. Chem**., 1999**

Investigation of the interaction between quercetin and Jack bean urease by Isothermal Titration Calorimetry and Hill analysis

Morteza Vaezi [a] ***,Gholamreza Rezaei Behbehani*** [1]***

Department of Chemistry, Imam Khomeini International University, Qazvin,3414896818, Iran
Email: **** grb402003@yahoo.com***

Abstract:The aim of this investigation was to measure the influence of quercetin on urease activity.In this paper,the interaction of Jack Bean Urease (JBU) with quercetin was studied by isothermal titration calorimetry(ITC) at 298 K.The Hill equation was used to analysis the heats of interaction. Thermodynamic parameters, free energy (ΔG),enthalpy changes (ΔH) and entropy changes(ΔS) were calculated.

Keywords: urease , quercetin , inhibitory, Isothermal Titration Calorimetry.

I. INTRODUCTION

Urease is a nickel-dependent enzyme [1],is synthesized by plants, some bacteria, and fungi[2]. JBU was the first enzyme to be crystallized.Like urease, its substrate urea is also very important.Urea is one of the most important nitrogenous waste product of biological activities.In general,urea is short-lived and rapidly metabolized by microbial activity and forms urea in the form of ammonia and carbamate as a result of hydrolysis.Carbamate is unstable and spontaneously hydrolyzed to carbonic acid and ammonia[3].The reaction occurs as follows:

$$(NH_2)_2CO + H_2O \rightarrow CO_2 + 2NH_3 \quad (1)$$

$$NH_2COOH + H_2O \leftrightarrow NH_3 + H_2CO_3 \quad (2)$$

There are compounds that can inhibit the activity of urease enzyme and prevent the production of carbonic acid and ammonia.Urease inhibitors can block the hydrolysis of urea to ammonium and decrease ammonia production.Urease inhibitor is a very promising tool to control the damaging effects of ureolytic bacterial infections in humans.The inhibition of the enzymes by small organic molecules has fascinated the synthetic and medicinal chemists as a valuable strategy in drug discovery leading to the development of effective drugs[4].Therefore, finding a stable and non-toxic inhibitor to inhibit this enzyme is important to us and it can improve life quality of human.

Flavonoids are polyphenols of plant origin that are among the most important compounds in human diet due to their widespread distribution in foods and beverages[5].In this study we have attempted to investigate the effect of quercetin as a flavonoid on urease enzyme inhibition,in order to prevent the ammonia released also assess the conformational changes,stability as a result of its reaction, and the thermodynamic parameters of quercetin to the enzyme reaction has been considered using Hill Eq.Therefore, it is possible to conclude that quercetin could decrease the urease activity significantly, which is so important in medical science against a variety of diseases.

II. MATERIAL AND METHODS

Jack Bean Urease, quercetin and Tris buffer obtained from Sigma Chemical Co.The buffer solution used in the experiments was 40mmol$L^{-1}$and pH=7.The isothermal titration micro calorimetric experiments were performed with the four channel commercial micro calorimetric system. Quercetin solution(10mM)was injected by use of a Hamilton syringe into the calorimetric titration vessel, which contained1.8mL JBU(4μM).Injection of quercetin solution into the perfusion vessel was repeated 30 times,the first injection was 5μL and the remaining ones were 10μL.The calorimetric signal was measured by a digital voltmeter that was part of a computerized recording system.The heat of each Injection wase calculated by the Thermometric Digit am'3'software program.measurements were performed under constant temperature of 25.0±0.02ºC.The heat of dilution of the quercetin solution was measured as described above except JBU was excluded.The micro calorimeter was frequently calibrated electrically during the course of the study.The data best fit to the Hill equation(Eq.4)[6].

III.RESULTS AND DISCUSSION

Consider a biomolecule,with n binding sites for ligands that had to be occupied simultaneously.The binding of the ligands to the biomolecule can be represented by the chemical equilibrium expression:

$$P + nL \Leftrightarrow PL_n \qquad K_a = \frac{[PL_n]}{[P][L]^n} \qquad (3)$$

Where K_a (forward rate, or the rate of association of the protein-ligand complex).Assuming that $\frac{q}{q_{max}}$ is the fraction of the ligand binding sites on the biomolecule which are occupied by the ligand.It is reasonable to write the Eq.4.

n is The number of quercetin around urease,and K_a is association equilibrium constant for quercetin + urease, that were determined graphically(Fig2)on the basis of Eq.4 in high concentration of quercetin.If q and q_{max} are calculated per mole of urease,then the standard molar enthalpy of binding for each binding side, ΔH^o, will be $\Delta H^o = \frac{q_{max}}{n}$ [7],Gibbs free energy, ΔG^o ,and entropy, ΔS^o ,of the interaction can be obtained as Eq.5and 6,That have been summarized in Table1.

The values of n are more than one,which suggests that the binding of one molecule of quercetin to urease increases affinity of the other binding site on urease.The interaction is entropy-driven, indicating that the hydrophobic forces are dominant.Hydrophobic interactions are important for the folding of proteins.This is important in keeping a protein stable and biologically active,because it allow to the protein to decrease in surface are and reduce the undesirable interactions with water[7,8].Therefore the structure of urease folding and stabilized by quercetin.Also hydrophobic interaction plays a very important role in the formation of higher-order structure and phase transitions in biological systems[8,9].The large of values Ka indicate that quercetin is stroghly associated with JBU, In other words JBU has high affinity for binding to quercetin.The results show that quercetin caused inhibition of urease activity significantiy,as evidenced by larger association equilibrium constant.

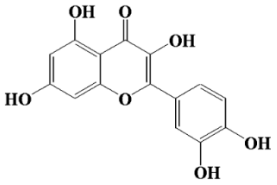

Fig. 1. Chemical structur of quercetin.

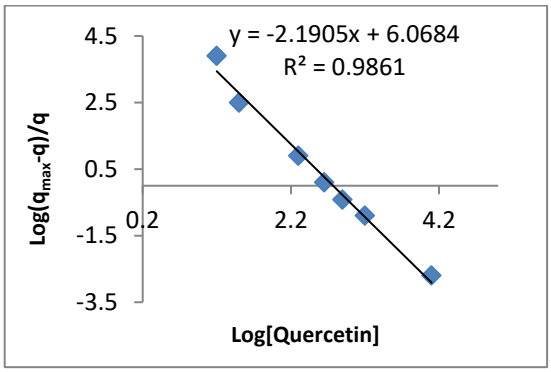

Fig2 :the fitting of heats of quercetin + JBU interactions (in the high concentration of quercetin)

Table1:Thermoynamic parameters for JBU+ quercetin interaction via Eq.4.

parameters	T=298K
Ka / M^{-1}	$1/17\times10^6$
n	2.2
ΔH^o/ kJ mol^{-1}	5.16
ΔG^o/ kJ mol^{-1}	-34.62
ΔS^o / kJ mol^{-1}	0.133

$$Log(\frac{q_{max}-q}{q}) = LogK_a - nLog[Quercetin] \qquad (4)$$

$$\Delta G^o = -RT\ln K_a \qquad (5)$$

$$\Delta G^o = \Delta H^o - T\Delta S^o \qquad (6)$$

IV. CONCLUSION

All parametrs of ΔG^o, ΔH^o and ΔS^o indicate that the process is spontaneous.endothermic and entropy-

driven.This issue shoes the hydrophobic interaction is more important force for the inhibition of urease aggregation.Also, the analysis of the value of n obtained from the Hill Eq indicate positively cooperative binding.and confirms the accuracy of the results obtained from the study of thermodynamic parameters.

REFERENCES

[1].Zambelli, B., Musiani, F., Benini, S., & Ciurli, S. (2011). Chemistry of Ni2+ in urease: sensing, trafficking, and catalysis. Accounts of chemical research, vol. 44, no. 7, p. 520-530.

[2]. Krajewska, B., (2009). Ureases I. Functional, catalytic and kinetic properties: A review. Journal of Molecular Catalysis B: Enzymatic, vol. 59,no 1-3, p. 9-21.

[3].Behbehani, G.R. and Saboury, A.A., (2007). A thermodynamic study on the binding of magnesium with human growth hormone. Journal of Thermal Analysis and Calorimetry,vol.89,no 3, p.857-861.

[4].Menteşe, E., Akyüz, G., Emirik, M., & Baltaş, N. (2019). Synthesis, in vitro urease inhibition and molecular docking studies of some novel quinazolin-4 (3H)-one derivatives containing triazole, thiadiazole and thiosemicarbazide functionalities. Bioorganic chemistry, vol. 83, p. 289-296.

[5].Pinheiro, P. F. and G. C. Justino (2012). Structural analysis of
flavonoids and related compounds-a review of spectroscopic
applications. Phytochemicals-a global perspective of their role in
nutrition and health, IntechOpen.

[6].Lolkema, J. S. and D.-J. Slotboom (2015). "The Hill analysis and co-ion–driven transporter kinetics."The Journal of general physiology 145(6): 565-574

[7].Rezaei Behbehani et al. (2017). "Application of the extended solvation theory to study the interaction of β-CD with interpolyme of PEO and PAA." Iranian Chemical Communication 5: 286-292.

[8].Saboury,A.A.:A review on the ligand binding studies by isothermal titration calorimetry.J.Iran.Chem.Soc.3,1–21 (2006)

[9] Atkins,Peter and Julio de Paula. Physical Chemistry for the Life
Sciences.Oxford, UK: Oxford University Press. 2006. 95.

Insights into the Binding of Cafaminol to Human Serum Albumin: Multi-Spectroscopic and Molecular Modeling Studies

D. Mohammad-Aghaie*, N. Parvizi, M. M. Alavianmehr and M. N. Soltani Rad

Department of Chemistry, Shiraz University of Technology, Shiraz, 71555-313, Iran.
E_mail address: d_aghaie@sutech.ac.ir

Abstract: In this study, the binding affinity of Cafaminol with human serum albumin (HSA) was investigated by fluorescence, UV and circular dichroism (CD) spectroscopies, along with molecular dynamics and Docking simulations. The Stern-Volmer plots were employed to specify the fluorescence quenching mechanism, while the simulation methods were utilized to deduce the approximate binding position of cafaminol on HSA. On the other hand, thermodynamic parameters, enthalpy and entropy changes, were determined using the Vant Hoff equation and analyzed to specify the main acting forces, between cafaminol and HSA. The overall results showed that cafaminol was bound to the domain IA of HSA, as a result of an enthalpy-driven process, mainly through the van der Waals and hydrogen bonding interactions. Static quenching mechanism was found to be responsible for the fluorescence quenching of HSA in the cafaminol presence, while the number of binding sites, and apparent binding constant were measured accordingly.

Keywords: Cafaminol, Docking, HSA, Molecular Dynamics Simulation, Spectroscopic methods.

I. INTRODUCTION

Human serum albumin (HSA) is the most abundant globular plasma protein, with a fundamental role in the transport and deposition of many endogenous and exogenous substances in blood. HSA, shown in Fig. 1, is a single-chain protein of 585 aminoacids and a molecular mass of 66.5 kDa. [1] This molecule has three specific interaction domains, I, II and III, while each of them are divided into sub-domains, A and B.

Cafaminol, also known as methylcoffanolamine, is a vasoconstrictor and anticatarrhal of the methylxanthine family, which is used as a nasal decongestant [2]. Fig. 2 shows the molecular structure of cafaminol, with the formula $C_{11}H_{17}N_5O_3$.

It is of great importance to determine the interaction of different drugs with HSA, not only to comprehend their transport and metabolism in the body, but also to shed light on their therapeutic effectiveness. It is well known that the binding mechanism has important pharmacokinetic and pharmacodynamics implications, and the degree of protein binding affects the absorption, distribution and excretion of the drugs. [3]

A wide variety of biophysical methods have been used for the analysis of the interactions between proteins and ligands, such as, fluorescence and UV/visible spectroscopies, fluorescence resonance energy transfer (FRET), nuclear magnetic resonance (NMR), besides computational methods and molecular modeling. This study aims to elucidate different aspects of cafaminol-HSA binding interactions, through several spectroscopic and simulation techniques.

Fluorescence quenching occurs due to the decrease in the quantum yield of fluorophore, induced by the quencher molecule. The inherent fluorescence of HSA comes mainly from tryptophan-214 and is very sensitive to the environment, around this amino acid residue. Here, cafaminol acts as a quencher for HSA molecule. Fluorescence quenching is classified into dynamic and static quenching. These two mechanisms are distinguished, based on their response to the temperature. To examine the mechanism of cafaminol induced quenching, the Stern-Volmer equation was employed.

The effect of cafaminol on the secondary structure of HSA was explored using the circular dichroism, while the UV/vis absorption was carried out to obtain more information on the drug binding to HSA.

On the other hand, nature of binding forces are detectable based on the analysis of thermodynamic parameters and molecular dynamics and docking simulations provide microscopic information on cafaminol-HSA interactions.

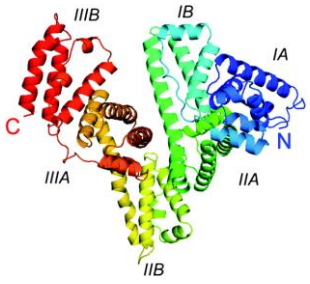

Fig. 1: The ribbon model of albumin, derived from X-ray crystallog- raphy, the subdivision of albumin into domains (I,

II, III) and subdomains (A and B) is indicated. C and N show the C-terminal and N-terminal ends, respectively.

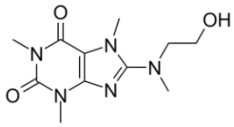

Fig. 2: Molecular structure of Cafaminol

II. METHODS

2.1. ***Fluorescence Spectroscopy*:** The steady-state fluorescence emission spectra of HSA were measured in the 300–450 nm range, at 289, 296, 303, and 310 K, with the wavelength at 295 nm. In each temperature, a 1 ml portion of 10 μmol L^{-1} HSA solution, was titrated manually by successive additions of stock solution of cafaminol, to span the drug concentration range, from 0 to 40 μmol L^{-1}.

Tabel 1: Stern-Volmer quenching constants (K_{SV}), binding constants (K_b), binding sites (n) and Thermodynamic parameters.

T(K)	$K_{SV}(\times10^3 M^{-1})$	n	$\log K_b(\times10^3 M^{-1})$	ΔG (kJ.mol^{-1})	ΔH (kJ.mol^{-1})	ΔS (J.mol^{-1}.K^{-1})	R^2
289	10.459	1.0957	4.454	-24.644	-105.878	-282.34	0.998
296	8.925	0.9863	3.887	-22.027			0.999
303	7.705	0.8957	3.413	-19.7601			0.992
310	6.705	0.8514	3.167	-18.7621			0.997

After each drug addition, the complex solution was left for 3 min, to reach equilibrium at the desired temperature, then fluorescence intensities were measured. Fig. 3 shows the fluorescence emission spectra of HSA at 289 K.

2.2. ***UV-visible Absorption Spectroscopy*:** UV-Visible absorbance spectra of HSA, were recorded both in absence and presence of cafaminol, in the range of 200-400 nm. HSA concentration was fixed at 20 μmol L^{-1}, while the cafaminol concentration was varied from 0 to 40 μmol L^{-1}.

2.3. ***Circular Dichroism (CD) Measurement:*** CD is an optical technique to monitor the protein's conformational changes. CD measurements were taken at constant 10 μmol L^{-1} HSA concentration, while cafaminol was added gradually to cover the concentration range of 0 to 74 μmol L^{-1}.

2.4. ***Molecular Dynamics Simulation:*** Initial structure of HSA, (PDB ID: 1AO6) modelled by GROMOS96-43a1 force field, was inserted in a cubic box of simple point charge (SPC) water molecules. The steepest descent algorithm was employed to run energy minimization, continued by two short position restrained MD simulations, in NVT and NPT ensembles, each for 100 ps. At the end, the system was subjected to a 20 ns MD simulation, at 310 K, and the trajectory was analyzed by the Gromacs package tools.

2.5 ***Docking:*** The structure of cafaminol was generated and energy minimized by Chemdraw ultra 8. It was then docked into the quasi-equilibrated HSA structure from MD simulation, using the AutoDock Vina.

III. RESULTS AND DISCUSSION

This paper is devoted to the study of mutual interactions, between cafaminol and HSA, through spectroscopic and simulation methods. Inspecting fluorescence spectra at

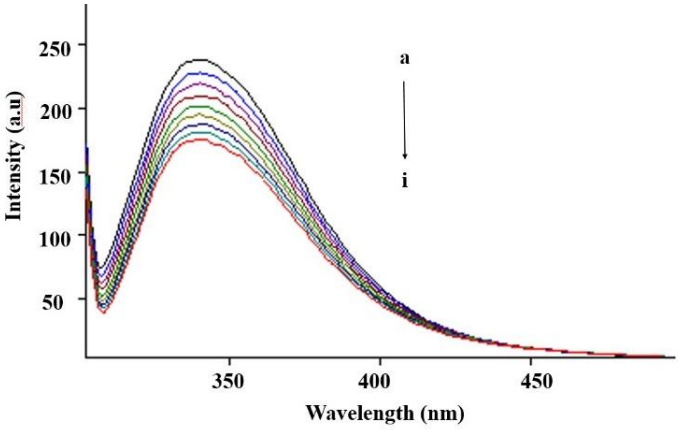

different temperatures, showed that the fluorescence intensity of HSA was reduced, due to adding increasing amounts of cafaminol. Analysis of Stern-Volmer plots, revealed the static quenching mechanism, to be responsible for fluorescence quenching. [4]

$$\frac{F_0}{F} = 1 + K_q\tau_0[Q] = 1 + K_{SV}[Q] \qquad (1)$$

F_0 and F are respectively the fluorescence intensities in the absence and presence of cafaminol (quencher). K_q is the biomolecular quenching constant, [Q] the concentration of quencher, and K_{sv}, the stern-volmer quenching constant. Eq. 2 gives the number of binding sites of a small molecule (cafaminol) on the macromolecule (HSA).

$$\log\frac{(F_0-F)}{F} = \log K_b + n\log[Q] \qquad (2)$$

The thermodynamic binding parameters were determined by the van't Hoff equation, to specify the main acting forces between cafaminol and HSA. All obtained results from Eqs.1, 2, and van't Hoff equation, are listed in Table 1. On the other hand, the microscopic aspects of the HSA-cafaminol

interactions, were studied by molecular dynamics and docking simulations.

Fig. 3: Conventional fluorescence spectra of HSA at 289 K. HSA: 10 μmol L^{-1}; Cafaminol (a-i): 0-40 μmol L^{-1}.

In total, it was determined that cafaminol binds to the domain IA of HSA, in an exothermic and enthalpy driven process. Both negative ΔH and ΔS values, indicate that van der Waals and hydrogen bonding interactions stabilize the cafaminol in HSA binding domain. This, in turn leads to the complex formation, and consequently the fluorescence quenching, via static mechanism.

By adding cafaminol to the solution, UV-Visible absorption spectra of HSA, showed obvious intensity increase, along with a slight red shift. These clues are enough to confirm both the complex formation between HSA and cafaminol, and the microenvironmental perturbations around the protein's chromophore, due to the cafaminol presence. On the other hand, CD analysis showed that the structure of HSA remains predominantly alpha-helical, even after cafaminol addition.

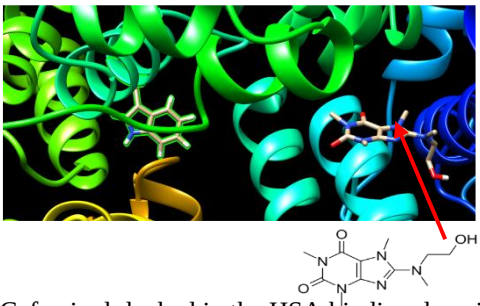

Fig. 4: Cafaminol docked in the HSA binding domain

REFERENCES

[1] Y. Wang and G. Zhang, *Luminescence*, vol. 30, pp. 198-206, **2015**.

[2] M. Rogowski, S. Chodynicki, *Wiad. Lek.*, vol. 38(20), pp. 1437–40, **1985**.

[3] N. Seedher and S. Bhatia, *Drug Metabol. Drug Interact.*, vol. 22, pp. 25-45, **2006**.

[4] X.Z. Feng, Z. Lin, L.J. Yang, C. Wang, C.L. Bai, Talanta, vol. 47, pp. 1223–1239, **1998**.

Biochemical Studies of A New Schiff Base Ligand and Its Complex Containing 2-Thiophenecarboxaldehyde

***BaharehNorouznezhad*, BitaShafaatian*, Maryam Noori**
School of Chemistry, Damghan University, Damghan 3671641167, Iran

Email:shafaatian@du.ac.ir

Abstract: A new Schiff base ligand containing 2-thiophenecarboxaldehyde and its zirconium complex was synthesized and their structure details were investigated by different spectroscopies. DNA interaction of the compounds has been investigated by the fluorescence and UV-Vis spectroscopies and intrinsic binding constants were calculated. In order to quantitatively compare the binding strength of bonds between compounds and DNA, the intrinsic binding constants (K_b and K_f) were calculated. The results suggest that interactions between the compounds and CT-DNA occur by intercalative binding modes. The positive values of enthalpy and entropy showed hydrophobic interaction.

Keywords: Schiff base, DNA interaction, zirconium complex, CT-DNA.

I. INTRODUCTION

During the last decade, great attention has been focoused on the area of Schiff bases and their due to the electron transfer pathways in biological systems [1]. Among of different Schiff base complexes, zirconium(IV) complexes have been shown to possess biochemistry.

DNA is the primary target for most anticancer and antiviral therapies according to the cell biology. When some kinds of metal complexes interact with DNA, they could induce the breakage of DNA strands by appropriate ways. Thus, the interaction of coordination complexes with DNA has been of interest due to their possible applications in cancer therapy and biochemistry. In the case of cancer genes, after DNA strand are cleaved by metal complexes, the DNA double strand break. Thus, in recent years, binding studies of Schiff base ligands and its metal complexes have become very important in the development of DNA molecule probes and chemotherapy [2]. Thus, the medicinal properties of Schiff base complexes are very important for improving their applications in the treatment of cancer.

II. METHODS

All chemicals used were analytical reagent grade and were used without further purification. Calf thymus DNA (CT-DNA) was purchased from Sigma–Aldrich. All the reactions were carried out in an argon atmosphere. Electronic absorption spectra of the compounds were recorded in H_2O solvent on an Analytik Jena Specord 205 spectrophotometer. Emission spectra for the Schiff base ligand and its zirconium complex were measured with an FP-6200 spectrofluorometer. All the experiments containing the compounds with DNA were investigated in 10 mM Tris-HCl buffer (pH = 7.4) including 50 mM NaCl. The solution of CT-DNA gave a ratio of UV absorbance at 260 and 280 nm more than 1.8, representing that DNA was sufficiently free from protein. Electronic absorption spectra experiments were carried out at 27 °C by keeping the compounds concentration constant (10.0 µM) while varying the DNA concentration from 0 to 18.0 µM and 0 to 22.0 µM for the Schiff base ligand and its zirconium complex, respectively. Absorbance values were recorded in the range of 260-400 nm after each successive addition of CT-DNA solution, followed by 10 minutes incubation time.

III. RESULTS AND DISCUSSION

The interaction of Schiff base ligands and their complexes with DNA is one of the most important for developing of antitumor compounds [3]. Electronic absorption and fluorescence spectroscopies are very important tools for studying the binding mode of DNA with the synthesized compounds (The structure of new Schiff base ligand was shown in Fig. 1). Binding of DNA via intercalation mode generally results in hypochromism and bathochromism effect because the process involves a strong stacking interaction between an aromatic chromophore and the DNA base pair [4]. On the other hand, the absorption intensity of a complex is also decreased (hypochromic effect) upon increasing the concentration of DNA due to the damage of the DNA double helix structure. The extent of the hypochromism is indicative intercalative binding modes.

The UV-Vis spectra of the Schiff base ligand and its zirconium(IV) complex in the absence and presence of DNA were shown in Figs. 2 and 3, respectively. In UV-Vis spectra of compounds showed intense absorption bands with maxima at 285 nm and 289 nm, which can be attributed to intra-ligand π-π* transitions. Upon addition of incremental amounts of CT-DNA, the absorption bands of the compounds exhibited hypochromic effect including red shift. These results provide significant support to the intercalative binding mode.

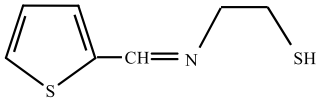

Fig.1: The structure of Schiff base ligand.

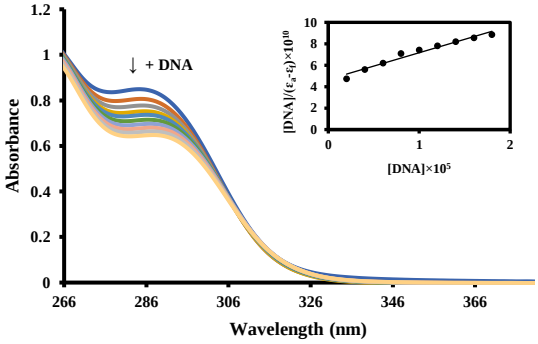

Fig.2: Changes in the UV–Vis spectra of the Schiff base ligand with increasing concentrations of DNA; [Schiff base] = 10 µM, [CT-DNA] = 0–18 µM. The arrow represents the absorbance changes by addition of different concentrations of DNA. Inset plot of $[DNA]/(\varepsilon_a - \varepsilon_f)$ *vs* [DNA].

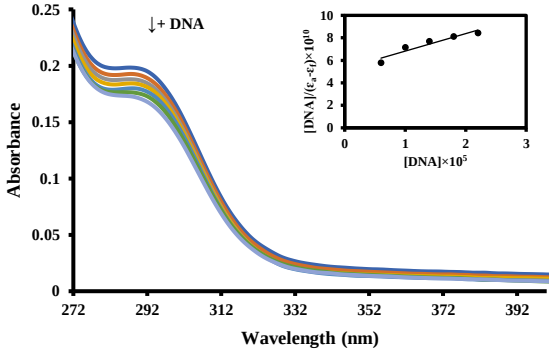

Fig.3: Changes in the UV–Vis spectra of the zirconium complex with increasing concentration of CT-DNA; [Zr complex] = 10 µM, [CT-DNA] = 0–22 µM. The arrow represents the absorbance changes by addition of DNA concentrations. Inset plot of $[DNA]/(\varepsilon_a - \varepsilon_f)$ vs [DNA].

In order to quantitatively compare the binding strength of bonds between the compounds and DNA, the intrinsic binding constants (K_b) were calculated by the Eq. 1.

$$[DNA]/(\varepsilon_a - \varepsilon_f) = [DNA]/(\varepsilon_b - \varepsilon_f) + 1/K_b(\varepsilon_b - \varepsilon_f) \quad (1)$$

where, [DNA] is the concentration of DNA in base pairs, ε_a is the apparent extinction coefficient obtained by calculating A/[complex], ε_f corresponds to the extinction coefficient of the compound in its free form and ε_b refers to the extinction coefficient of the complex in the fully bound form. In the plot of $[DNA]/(\varepsilon_a - \varepsilon_f)$ *vs* [DNA], K_b is given by the ratio of slope to intercept [5]. The binding constants for the Schiff base ligand and zirconium complex were obtained 5.34×10^4 and 2.96×10^4, respectively. For studying fluorescence spectra of interaction of the complounds with CT-DNA, a solution with constant concentration of the synthesized compounds were titrated with different values of DNA.
In this figure increasing emission intensity can be observed

upon addition of the solution of DNA in Tris-HCl buffer. These reactions were performed at 25.0 °C and pH = 7.4. Binding constants of the interaction (K_f) were calculated using the Eq. 2.

$$\log(F_0 - F)/F = logK_f + nlog[DNA] \quad (2)$$

Furthermore, the values of K_f were obtained 1.46×10^4 and 0.0035×10^4 for the ligand and zirconium complex, respectively. The thermodynamic parameters of interaction between CT-DNA and the new synthesized compounds were

given in Table 1. In order to calculate entropy and enthalpy changes the linear graphs of lnK *vs* 10^5 (1/T) were investigated and the ΔH and ΔS values at 17 °C, 27 °C and 37 °C were obtained using the slope and intercept of these graphs, respectively.

Table1: Thermodynamic parameters of DNA binding of Schiff base ligand and its zirconium complex

	T(K)	ΔG(kJ mol^{-1})	ΔH(kJ mol^{-1})	ΔS(kJ mol^{-1})
	290	-24.2		
Schiff base	300	-26.84	52.54	264.63
	310	-29.49		
	290	-22.32		
Zr complex	300	-25.22	61.94	290.56
	310	-28.13		

IV. CONCLUSION

DNA binding experiments show that the new synthesized compounds bind to CT-DNA through the intercalative mode. The obtained data from different spectroscopies showed that the interaction between the Schiff base ligand and CT-DNA was performed better than zirconium complex. Furthermore, the positive values of enthalpy and entropy showed hydrophobic interaction.

REFERENCES

[1] B. Z. J. Zhuang, H. Okawa, N. Matsumoto, H. Sakiyama, S. J. Kida, J. Chem. Soc., Dalton Trans., pp. 37-41, **2004**.
[2] P. Uma Maheswari, V. Rajendiran, M. Palani, avar, R. Thomas and G. U. Kulkarni, Inorg. Chim. Acta, vol. 359, pp. 4601-4612, **2006**.
[3] M. P. Heng, S. K. Sinniah, W. Y. Teoh, K. S. Sim, S. W. Ng, Y. K. Cheah, K. W. Tan, Spectrochim. Acta A, vol. 150, pp. 360-372, **2015**.
[4] M. N. Patel, C. R. Patel, H. N. Joshi, Spectrochim. Acta A, vol. 97, pp. 66-73, **2012**.
[5] F. Mohammadtabar, B. Shafaatian, A. Soleymanpour, S. A. Rezvani, B. Notash, Transition Met. Chem., vol. 41, pp. 475-484, **2016**.

Investigation of DNA Interaction with Two New Platinum(II) Complexes

Maryam Noori*, Bita Shafaatian
School of Chemistry, Damghan University, Damghan 3671641167, Iran

Email: shafaatian@du.ac.ir

Abstract: Two new Pt(II) complexes were synthesized and their structure details were investigated by different spectroscopies methods. Interaction of the Pt(II) complexes were investigated with calf thymus DNA (CT-DNA) by UV-Vis, photoluminescence and viscosity measurements. The binding constants containing K_b and K_f were calculated and the obtained data were compared with each other. The spectra of emission and absorption increased upon addition of DNA. Moreover, thermodynamic parameters of the interaction between Pt(II) complexes and DNA were calculated. The positive changes of enthalpy and entropy proved hydrophobic interaction.

Keywords: Platinum, DNA interaction, UV-Vis spectroscopy, photoluminescence, CT-DNA.

I. INTRODUCTION

Bioorganometallic chemistry is one of the most important fields between two different area, containing biochemistry and organometallic chemistry. Conjugation of organometallic complexes with biomolecules such as DNA and its application to living systems have drawn much more attention [1]. Organometallic complexes can be used as therapeutic drugs. Thus, the medicinal properties of these complexes are very important for improving their applications in the treatment of cancer, fungal, viral and parasitic infections [2]. Platinum is valuable precious metal ion in organometallic chemistry which its complexes have an important role in catalysis and biochemistry. Investigations on chemical and pharmaceutical properties of Pt complexes lead to synthesize hundreds of these compounds for studying their anti-tumor activity. These studies revealed that the kind of ligand, coordination number and geometry of the platinum center are important for designing of these complexes in order to improve their anti-cancer activity. Interaction studies of organoplatinum complexes with nucleobases especially DNA as a main target for these complexes have attracted much more attention. Platinum complexes such as cisplatin is used in the treatment of different cancers

II. METHODS

In order to investigation interaction of the Pt(II) complexes with DNA, buffer solution containing (10 mM Tris–HCl/50 mM NaCl, pH=7.4) was prepared. The mixture of DNA and complexes were allowed to equilibrate for 10 min. before recording UV-Vis spectra. The stock solution of CT-DNA was prepared in Tris buffer and stored at 4 °C. DNA concentration in stock solution was confirmed by absorbance in the range of 260-280 nm with molar absorption coefficient of A_{260} = 6600 L mol^{-1} cm^{-1}. The concentration of the complexes were kept constant (1.0×10^{-5} M), during the titration with DNA at different concentrations from 0 to 1.2×10^{-5} M ([Compound]/[DNA] : 0.0, 0.2, 0.4, 0.6, 0.8, 1.0, 1.2, 1.4, 1.6 and 1.8). The emission and absorbance spectra were saved during each injection of DNA solution after 10 minutes. Measurements of viscosity were performed in constant temperature (25 °C) using a viscometer (SCHOT AVS 450).

III. RESULTS AND DISCUSSION

In order to study the interaction of Pt(II) complexes (Fig. 1) with CT-DNA, UV-Vis spectroscopy technique was used [3]. The intensity of absorption decreased through adding of CT-DNA. These changes were depicted in Figs. 2 and 3. The most changes was observed at 230 and 262 nm for two Pt(II) complexes respectively, due to the intraligand π–π* transitions. Increasing injection of different values of DNA (0–18 μM), depicted decreasing absorbance intensity (hypochromic) and a little changes of the maximum wavelength (red shift) for these complexes during the reaction. This evidence revealed the mechanism of intercalative for CT-DNA interactions with Pt(II) complexes. For calculating the binding constant, K_b, of these complexes, the Eq. 1 was used:

$$[DNA]/(\varepsilon_a - \varepsilon_f) = [DNA]/(\varepsilon_b - \varepsilon_f) + 1/K_b(\varepsilon_b - \varepsilon_f) \quad (1)$$

In this equation, [DNA] represented the concentration of DNA in different injections, ε_a obtains by the ratio of A/[complex], ε_b is related to the extinction coefficient in the completely bound form and ε_f represents the extinction

coefficient of the free form of complex. K_b was obtained by drawing $[DNA]/(\varepsilon_a - \varepsilon_f)$ against [DNA] and calculating the ratio of slope to intercept. The binding constants (K_b) for **1** and **2** complexes were calculated 1.82×10^5 and 2.03×10^5, respectively.

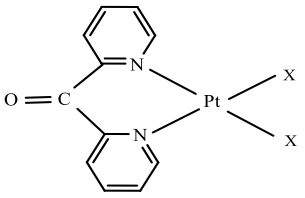

1) X = MeC_6H_4
2) X = Cl

Fig.1: The Structure of Pt(II) complexes.

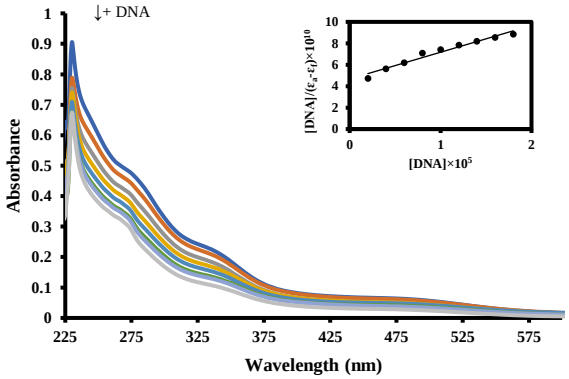

Fig.2: Changes in the UV–Vis spectra of complex **1** with increasing values of CT-DNA; [Complex **1**] = 10 µM, [CT-DNA] = 0–18 µM. The arrow represents the absorbance changes through adding of different concentrations of DNA. Inset: plot of $[DNA]/(\varepsilon_a - \varepsilon_f)$ *vs* [DNA].

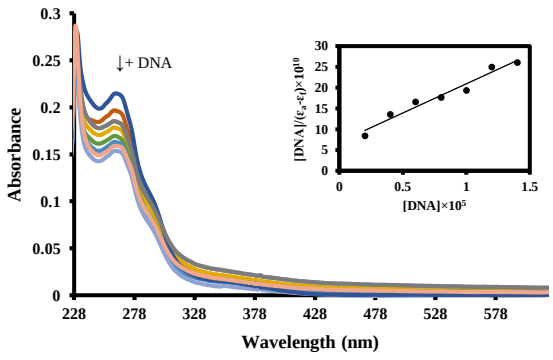

Fig.3: Changes in the UV–Vis spectra of complex **2** with increasing concentrations of CT-DNA; [Complex **2**] = 10 µM, [CT-DNA] = 0–16 µM. The arrow represents the absorbance changes through adding of different concentrations of DNA. Inset: plot of $[DNA]/(\varepsilon_a - \varepsilon_f)$ *vs* [DNA].

In order to investigation fluorescence spectra of interaction of these complexes with CT-DNA constant concentration of these Pt(II) complexes were titrated with different concentrations of DNA. Changes of fluorescence spectra were depicted in Fig. 4.

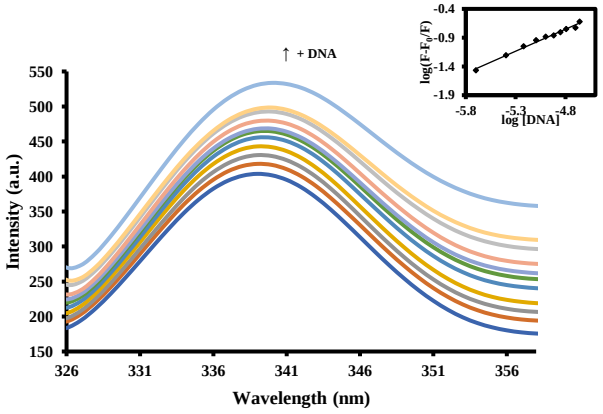

Fig.4: Changes in the emission spectra of complex **2** (λ_{exc} = 263) by increasing concentrations of CT-DNA; [Complex **2**]=10 µM, [CT-DNA] = 0–20 µM.

In this figure increasing emission intensity can be observed upon addition of the solution of DNA in Tris-HCl buffer. These reactions were performed at 25.0 °C and pH = 7.4. Binding constants of the interaction (K_f) were calculated using the Eq. 2.

$$\log(F - F_0)/F = logK_f + nlog[DNA] \qquad (2)$$

F_0 and F are due to the fluorescence intensities of the fluorophore in the absence and presence of different concentrations of DNA. The values of K_f for Pt(II) complexes were calculated 0.011×10^3 and 0.824×10^3, respectively. The thermodynamic parameters of interaction between DNA and the new synthesized compounds were given in Table 1.

In order to calculate entropy and enthalpy changes the linear graphs of lnK *vs* 10^5 (1/T) were developed and the ΔH and ΔS values at 17 °C, 27 °C and 37 °C were obtained using the slope and intercept of these graphs, respectively.

Table1: Thermodynamic parameters of DNA binding of complexes **1** and **2**

	T(K)	ΔG(kJ mol^{-1})	ΔH(kJ mol^{-1})	ΔS(kJ mol^{-1})

	T(K)	ΔG(kJ mol^{-1})	ΔH(kJ mol^{-1})	ΔS(kJ mol^{-1})
	290	-27.14		
Complex **1**	300	-29.73	47.97	259.87
	310	-32.32		
	290	-27.09		
Complex **2**	300	-29.81	51.79	272.36
	310	-32.53		

IV. CONCLUSION

DNA binding experiments show that the new Pt(II) complexes bind to CT-DNA through the intercalative mode. The obtained data from different spectroscopies showed that the interaction between the complex **2** with CT-DNA was performed better than complex **1**. Furthermore, the viscosity measurements confirmed the spectroscopies data. The intercalative mode causes to elongate the double helix of DNA and increase the viscosity of DNA is due to the increasing in separation of base pairs to embed the ligands between the bases.

REFERENCES

[1] M. Noori, B. Shafaatian, B. Notash, Inorg. Chim. Acta, vol. 485, pp. 1-8, **2019**.
[2] E. Wong, C. M. Giandomenico, Chem. Rev, vol. 99, pp. 2451-2466, **1999**.
[3] B. Shafaatian, A. Baharian, Phosphorus, Sulfur, and Silicon and the Related Elements, vol. 192, pp. 1102-1109, **2017**.

Exploring the Effect of Surface Functionalization of Superparamagnetic Iron Oxide Nanoparticles (Fe_3O_4) on the Interaction with BLG

Z.Kavianfar[a], F.mohammadi[b]*

Department of chemistry, Institute for Advanced Studies in Basic Sciences (IASBS), Zanjan, iran

Email: fmohammadi***@iasbs.ac.ir*** **,** ***zkavianfar@iasbs.ac.ir***

Abstract*:* Using different coatings on nanoparticles can help to satisfy some prerequisites including high magnetization, good stability, biocompatibility, and biodegradability. So, studying the interactions of coated nanoparticles with biological compounds is important. In this we examined the interaction of the super paramagnetic iron oxide nanoparticles (SPIONs) with β- lactoglobulin.

Keywords: nanoparticles, drug delivery, industry, SPIONs, protein corona, cellulose, dopamine, BLG, UV-Vis, fluorescence, surface functionalization, coating.

I. INTRODUCTION

Among the different models of nanoparticles, iron oxide superconducting nanoparticles are known as one of the most practical nanoparticles. After entering the nanoparticles into the body, blood is the first physiological environment that a nanomaterial faced with it. These proteins and also lipids adsorption layers that form on the surface of colloidal nanoparticles called protein corona. Parameters like size, shape composition, surface functional groups and surface charges of nanomaterial and the physiological environment characterize corona composition. Of course, the corona surface is not a fix layer, and its composition is determined by the kinetic rate of adsorption and desorption [1, 2].

BLG represents approximately half of the total protein in bovine whey, while human milk contains no BLG. Besides being a source of essential and branched chain amino acids, a retinol-binding protein has been identified within the BLG structure [3-6]. BLG has been described by nagaoka et al as a cholesterol-lowering agent [7]. BLG has been widely studied in the food industry because of its nutritional and functional effects on various biological processes [8]. In this study, we investigate the interaction of SPIONs in pure state and in superficially regulated conditions such as dopamine-stabilized Fe_3O_4 nanoparticles and Cellulose-stabilized Fe_3O_4 nanoparticles with β-lactoglobulin (BLG).

II. METHODS

The materials which were used in this project including β-lactoglobulin (BLG) were purchased from Sigma-Aldrich. The buffer solution was prepared by double distilled water. Also Fe_3O_4 nanoparticles, dopamine-stabilized Fe_3O_4 nanoparticles, Cellulose-stabilized Fe_3O_4 nanoparticles Have been purchased. BLG were weighed and dissolved in 0.05 M pH 7.4 phosphate buffer solution. The exact concentrations of BLG were determined using molecular absorption coefficient of ε_{278}=17600$M^{-1}cm^{-1}$. BLG (1−5μM) was added to a nanoparticles dispersion and incubated for 1 min at 25 °C. In fluorescence spectra, the excitation wavelength was adjusted at 295nm to selectively excite the tryptophan residues of BLG. Both the excitation and emission slit widths were adjusted at 5 nm. The BLG solution (3μM) was titrated sequentially by adding Fe_3O_4 nanoparticles dispersion, and the concentration of SPIONs was varied from 0 to 0.015nM. The UV/Vis spectrum was recorded at room temperature on a SAFAS UV/Vis spectrophotometer in quartz cuvettes with an optical path of 10 mm.

III. RESULTS AND DISCUSSION

Table 1. Effect of Temperature on the Stern−Volmer Quenching Constant (K_{SV}), Bimolecular Quenching Rate Constant (kq), Hill Coefficient (n), and Binding Constant (K_A) between protein/ligand.

Nps	T(K)	$K_{SV}(M^{-1})$	n	$K_A(M^{-1})$
SPIONs	298	(3.2±0.05) ×10 ^{10}	(1.2±0.01)	(2±1.1) ×10 ^{6}
	303	(3.8±0.06) ×10 ^{10}	(0.8±0.01)	(5.01±1.1)×10 ^{4}
	308	(4.7±0.05) ×10 ^{10}	(0.9±0.01)	(5±1.1)× 10 ^{3}
dopamine@SPIONs	298	(4±0.04) ×10 ^{10}	(1.04±0.02)	(3.2±1.2) ×10 ^{6}
	303	(4.3±0.04) ×10 ^{10}	(0.8±0.01)	(1±1.1) ×10 ^{5}
	308	(5.03±0.05) ×10 ^{10}	(1.2±0.02)	(5±1.17) ×10 ^{3}

cellulose @SPIONs.	298	(3.4±0.07) ×10 ^{10}	(1.2±0.03)	(1.6±1.3) ×10 ^{4}
	303	(3.45±0.07) ×10 ^{10}	(1±0.02)	(6.3±1.13)×10 ^{3}
	308	(3.5±0.06) ×10 ^{10}	(0.8±0.02)	(1±1.2) ×10 ^{3}

A. Figures and Tables

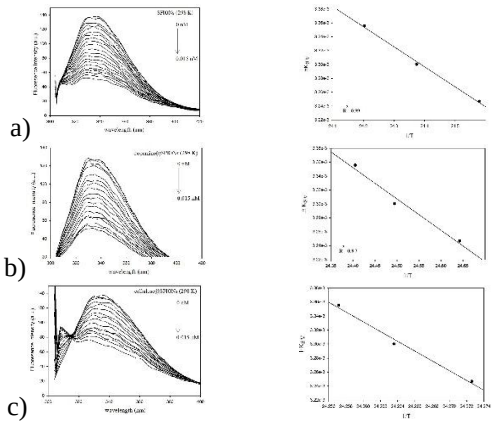

Fig.1: Fluorescence quenching of BLG (2.5μM) upon excitation at λ_{ex} = 295 nm in the absence and presence of increasing concentration of particles (0-0.015 nM) and van't Hoff plot a) SPIONs b) dopamine@SPIONs c) cellulose@SPIONs.

Table 2. Thermodynamic Parameters for Interaction of BLG with Fe Nanoparticles.

Nps	ΔH° (kJ.mol^{-1})	ΔS° (Jmol^{-1}K^{-1})	T(K)	ΔG° (kJmol^{-1})
SPIONs	31.085	305.42	298	-52.18
			303	-61.33
			308	-62.855
cellulose@SPIONs	1.175	210.32	298	-60.09
			303	-61.122
			308	-54.98
dopamine@SPIONs	2.305	205.65	298	-60.36
			303	-61.41
			308	-62.46

B. Equations

$$\frac{F_0}{F} = 1 + k_q \tau_0 [Q] = 1 + K_{SV}[Q] \quad (1)$$

$$ln \frac{F_0 - F}{F} = ln K_A + n \, ln \, Q \quad (2)$$

$$ln \, K = \frac{-\Delta H}{RT} + \frac{\Delta S}{R} \quad (3)$$

$$\Delta G = \Delta H - T\Delta S \quad (4)$$

$$E = 1 - \frac{F}{F_0} = \frac{R_0^6}{R_0^6 + r^6} \quad (5)$$

$$R_0^6 = 8.8 \times 10^{-28} K^2 N^{-4} \Phi J \quad (6)$$

$$J = \frac{\sum F(\lambda)\varepsilon(\lambda)\Delta\lambda}{\sum F(\lambda)\Delta\lambda} \quad (7)$$

II. CONCLUSION

In our experiments the fluorescence intensity of BLG gradually decreased with increasing the concentration of SPIONs thus, it indicates the formation of BLG ligand complex. Also according to Table 1, the n values at different temperatures are about 1; hence, it can be inferred that binding of BLG molecules on the nanoparticles occurs. According the views of Ross and Subramanian, amount of enthalpy (Table 2) cannot be mainly attributed to electrostatic interactions since for electrostatic interactions ΔH◦ is very small, almost zero but it can show the presence of hydrogen in the binding. It was more likely van der Waals and hydrogen bonds, electrostatic interactions were involved in its binding process. J, R_0, E, and r were calculated which indicated that the energy transfer from BLG to SPIONs and SPIONs to BLG occurred with high probability (K^2 is 2/3, N is 1.3598, and Φ is 0.08). Our results were as follows: For SPIONs: J = 3.7×10^{-14} cm^3.M^{-1}, R_0 = 2.5 nm, E = 0.0.46, and r = 2.6 nm. For cellulose@SPIONs: J = 2.2×10^{-14} cm^3.M^{-1}, R_0 = 1.8 nm, E = 0. 33, and r = 2 nm. For dopamine@SPIONs: J = 2.7×10^{-14} cm^3.M^{-1}, R_0 = 2.4 nm, E = 0.39, and r = 2.6 nm. It is expected that the results of this study could lead to more effective use of nanoparticles in the diagnosis and treatment of diseases, including the production of engineered drugs, and on the other hand, these improvements will reduce problems, such as undesirable drug and disintegration. Non-spontaneous impacts in the environment.

REFERENCES

[1] Vroman, l., et al. "interaction of high molecular weight kininogen, factor xii, and fibrinogen in plasma at interfaces." blood 55.1 (1980): 156-159.

[2] Rahman, masoud, et al. "nanoparticle and protein corona." protein-nanoparticle interactions. Springer, berlin, heidelberg, 2013. 21-44.

[3] Walzem, r. L., c. J. Dillard, and j. Bruce german. "whey components: millennia of evolution create functionalities for mammalian nutrition: what we know and what we may be overlooking." critical reviews in food science and nutrition42.4 (2002): 353-375.

[4] Keri marshall, n. D. "therapeutic applications of whey protein." alternative medicine review 9.2 (2004): 136-156.

[5] Guimont, c., et al. "biologically active factors in bovine milk and dairy byproducts: influence on cell culture." critical reviews in food science & nutrition 37.4 (1997): 393-410.

[6] Mullally, margaret m., hans meisel, and richard j. Fitzgerald. "synthetic peptides corresponding to a-lactalbumin and b-lactoglobulin sequences with angiotensin-1-converting enzyme inhibitory activity." biological chemistry-hoppe seyler377.4 (1996): 259-260.

[7] Nagaoka, s. "studies on regulation of choleserol metabolism induced by dietary food constituents or xenobiotics." j. Jpn. Soc. Nutr. Food sci. 49 (1996): 303-313.

[8] Perez, adrián a., et al. "β-lactoglobulin heat-induced aggregates as carriers of polyunsaturated fatty acids." food chemistry 158 (2014): 66-72.

Section:
Chemical Kinetics

Water splitting and oxygen evolution by $BiVO_4$ -Mn_3O_4 p-n heterojunction composite

A. Moradpour* .S. Rahman setayesh

Department of Sharif University of Technology, Tehran, IRAN

Email:setayesh@sharif.edu

Abstract: In this article, $BiVO_4$ and Mn_3O_4 were synthesized by hydrothermal method. A one-pot hydrothermal method was also used to synthesize $BiVO_4$-Mn_3O_4 p–n heterojunction composite. The reaction of oxygen production, the process of water oxidation in the presence of heterogeneous nanocatalysts such as Mn_3O_4, $BiVO_4$, $BiVO_4$-Mn_3O_4 have been investigated. The $BiVO_4$and Mn_3O_4 percentages were also analyzed and the optimum percentage was found to be 60:40. Characterization of these nanocatalysts was performed using XRD method. Also, repeatability and recycling of this nanocatalyst was investigated.

Keywords*:* Water oxidation, Nanocatalyst, $BiVO_4$, Mn_3O_4, Oxygen production

I. INTRODUCTION

Water splitting and oxygen production endless and inexpensive energy source for clean fuel production. In this way, hydrogen is produced without releasing carbon dioxide. In many cases, water oxidation is essential, for example in the development of oxygen in synthetic or natural photosynthesis. The process of producing oxygen at sea is carried out by plants or natural catalysts such as Mn[1]. In this method using a nanophotocatalyst (heterogeneous) and visible light can be considered as an easy solution for oxygen evolution. One of the most interesting ways to decompose water and produce oxygen and hydrogen from water is photocatalytic decomposition which can be considered as the cheapest option for hydrogen generation. It is considered as potentially rather supportable than all other existent ways (like electrolysis of water, steam reforming of fossil fuel, biomass conversion, etc). This process can be more interesting if the reaction is carried out in one step without applying photovoltaic. For the first time Fujishima and Honda's reported photochemical water splitting by TiO_2 in 1972 [2].

Over the past few decades, metal oxide, semiconductors and metals nitrides have been used as photocatalyst for the production of hydrogen or oxygen.

In this project, production of hydrogen from renewable sources occurs as well as oxygen. Therefore, the amount of O_2 produced from water splitting utilizing Mn_3O_4, $BiVO_4$ and $BiVO_4$-Mn_3O_4 composite was measured. The reasons for using this composite are non-toxicity, cheapness, abundance of raw materials, good accountability and high chemical stability.

II. METHODS

A. Synthesis of Mn_3O_4 and $BiVO_4$

For synthesis of Mn_3O_4, 0.002 mol of $KMnO_4$ was dissolved in 80 mL of water. After combining ethylene glycol and potassium permanganate, 2 mL of ethylene glycol was added. The suspension was stirred for 1h at ambient temperature. After this step, the solution was transferred to the autoclave. The suspension was then heated at 120°C for 4h. After cooling the reaction to room temperature, the resulting product was washed with water and dried at 60 °C [3]. In a typical synthesis of $BiVO_4$, 0.002 mol of Bi $(No_3)_3$ and 0.002 mol of NH_4VO_3 were dissolved in 40 mL of ethylene glycol and hot water, respectively. Then, the above NH_4VO_3 solution was slowly added into the $Bi(NO_3)_3$ solution under vigorous stirring for 30 min and then transferred to a 100 mL autoclave and heated at 100 °C for 12 h. The yellowish resultants obtained from the reaction were precipitated naturally and washed with pure ethanol and distilled water several times [4].

B. Synthesis of BiVO4- Mn_3O_4

BiVO4-Mn_3O_4 nanocatalyst was synthesized by hydrothermal method. 0.1 g of Mn3O4 and 0.3 or 0.7 mmoles of Bi $(No_3)_3$ were dissolved in 40 ml of ethylene glycol (solution a). The same amount of NH_4VO_3 as Bi $(No_3)_3$ was dissolved in 40 mL of hot water (solution b). After half an hour stirring, solution (b) was slowly added to the solution a. After stirring the suspension was transferred into autoclave and heated at 100 °C for 12 h. The autoclave was allowed to cool to room temperature. The precipitate was washed with excess water and ethanol several times. Finally, the synthesized products were dried at 60°C for 6 h. The obtained products were labeled as BMV3, and BMV7.

C. The experiment of water splitting

Photocatalytic testing of water splitting was done in a Pyrex cell with a capacity of 250 ml. Taking 0.1g of prepared BiVO4- Mn3O4 (60:40) as a non-homogeneous catalyst in 200 mL distilled water and a magnetic stirrer is used to ensure the catalyst was suspended. Five LED of 60 W were used as light sources. The amount of water oxygen by flowing argon gas through the water becomes zero. Oxygen meter was placed in solution and the amount of oxygen was measured at specified time.

III. RESULTS AND DISCUSSION

A. Figures and Tables

To show the crystalline phases of the catalyst synthesized by hydrothermal method the XRD method was used. Fig. 1 shows the corresponding XRD patterns of the different samples. The Blue curve (b) shows the XRD pattern of the as-prepared Mn_3O_4. The characteristic peaks of Mn_3O_4 were nearly found at 2θ =32.77, 38.5129, 58.8386, and 60.2792, which match well with JCPDS cards Nos. 80-0382 [5] which perfectly indexed $Mn_3O_4$with a tetragonal spinel structure.

The Red curve (a) can be well indexed to the monoclinic $BiVO_4$ (JCPDS #14-0688). This indicates that the ethylene glycol assisted solvothermal process can produce a well-crystallized high-purity product [6].

The green curve (c) represents the XRD pattern of the prepared $BiVO_4$-Mn_3O_4 composite. The XRD pattern confirmed the tetragonal Mn_3O_4 and monoclinic $BiVO_4$ exist in the prepared composite [7].

The amount of oxygen production at specified time was shown in Table 1. The experimental conditions were room temperature and the pH 7.

Table 1: Oxygen production at specified time interval

Run	1	2	3	4	5
μmol O_2 by BM (60:40)	36.3	47	51.875	53	53.75
μmol O_2 by BM (60:40) and Material sacrifice	37	48	51	51	51

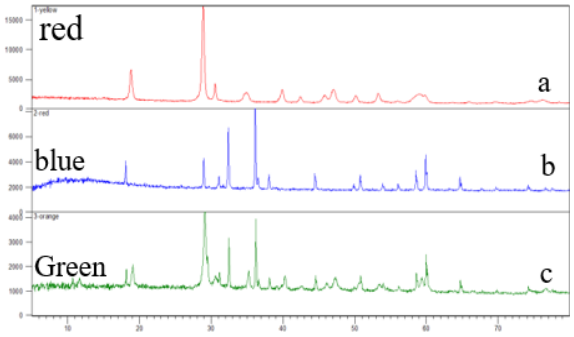

Angle 2θ

Fig 1: XRD templates of the prepared (a) BiVO4, (b) Mn3O4. (c)$BiVO_4$-Mn_3O_4 composite.

IV. CONCLUSION

The $BiVO_4$-Mn_3O_4 (60:40) was synthesized using a hydrothermal method. The XRD pattern confirmed the monoclinic $BiVO_4$ and tetragonal Mn_3O_4 exist in the prepared composite .The optimum time for the oxidation of water was found to be 5 hours. The production of oxygen by this catalyst is excellent and fast in comparison to others. Finally, 53 micromole of oxygen was produced. The reusability of the catalyst indicates the stability of the catalyst. The impact of the sacrificial substance was somewhat evident in the early but after the time passed, the material of sacrifice lost its effect. This is due to the silver surrounding the nanocatalyst, which prevents the reaction from occurring

REFERENCES

[1] G. Jingqi, Z. Duan, F. Zhang , S. Kelly, R. Si, M. Dupuis, J. Qianjun Chen3, Ch.Tang6 and C. Li, Nature Catalysis 1.11 .870, **2018.**

[2] A. Fujishima and K. Honda, Nature, 238, 37–38, **1972.**

[3] L, Jeong Woo .Chemistry of Materials, 24.6, 1158-1164, **2012**.

[4] L. Honglin.The Journal of Physical Chemistry, C 119.39.22681-22689,**2015**.

[5] Z. Wu, K. Yu, Y. Huang, C. Pan, Y. Xie, Chemistry Central Journal 1, 8,**2007.**

[6] L. Wang, Y. Li, Z. Han, L. Chen, B. Qian, X. Jiang, J. Pinto, G. Yang, Journal of Materials Chemistry A 1, 8385-8397,**2013.**

[7] R.Rahimi, A,Mehrehjedy, and S,Zargari., Environmental Progress & Sustainable Energy 36.5, 1439-1448,**2017.**

The studies of kinetic and atmospheric reaction mechanisms of pyrene in the presence of OH radicals

M. Nayebzadeh[a,]*, M. Vahedpour[a] and A. Shiroudi[b]

[a] Department of Chemistry, University of Zanjan, PO Box 45371-38791, Zanjan, Iran
[b] Young Researchers and Elite Club, East Tehran Branch, Islamic Azad University, Tehran, Iran

**E-mail: maryam.nayebzadeh@znu.ac.ir*

Abstract: Pyrene (Py) is a carcinogenic, colorless, solid polycyclic aromatic hydrocarbon (PAHs) which is the most plenteous hydrocarbon in the contaminated urban atmosphere and less volatile. For losing of Py from the environment, the initial reaction of pyrene by hyrdroxyl radical to form hydroxypyrene is the most important atmospheric reaction. The possible reaction mechanism explained by density functional theory (DFT) calculations. Calculations of reaction pathways and kinetics show that the main products are produced *via* OH-addition as well as the H-abstraction pathways. RRKM (Rice Ramsperger–Kassel–Marcus) theory was used to calculate the kinetic parameters such as rate constants for the beginning steps of Py with OH radicals. The atmospheric lifetime of gas-phase reactions between Py and OH radicals is evaluated about 5.5 days, according to the calculated $k_{overall}$ (overall rate constant) of 9.54×10^{-13} cm^3 molecule^{-1} s^{-1} at T=298 K and P=1 atm. The accessible experimental information show that we obtained the good results.

Keywords: Pyrene, atmospheric oxidation, OH radicals, rate constant, oxidation reaction mechanism

I. INTRODUCTION

The Polycyclic aromatic hydrocarbons (PAHs) which are results of pyrolitic process to form the byproducts of the combustion gas products, human activities and generated during various incomplete combustion of biomass, coal tar and fossil fuels from natural and agricultural fires [1,2] and especially the vehicle traffic. Py is not arranged as a human toxicity and carcinogen. However, beneath air conditions, Py can oxygenate under the photochemical reactions.

The carbon atoms in the pyrene molecule are marked up to explain the various reactions **1-6** *via* OH-addition and H-abstraction reactions. According to the studied pathways at 298 K for six products and the negative activation energy, we observed that OH-addition reaction pathway is more favored in compared with H-abstraction. Hence the P1–P3 are the main products.

DFT theoretically calculation could play an important role to study the oxidation reaction mechanism process by examining the kinetic and energetic the elementary reaction and radical intermediates [5, 6]. Thermodynamically data and also rate constant and the other kinetic parameters which are needed to modeling reaction pathways and transport of PAHs in the atmospheric zone [7]. Thus to calculate the rate constants for OH-addition pathways, we used RRKM theory [8] at T=298 K and a pressure of 1 bar.

II. METHODS

All the theoretical calculations have been performed by using the Gaussian 09 package of programs. By using GaussView program, we can visualize the molecular structures. The structural geometries of the intermediates, transition states, reactants and products of the stationary points optimized at the M06-2*x*/6-311G++ (2df, 2p) level of theory. Bond lengths, bond angles and the other structural information are agreed well with the available experimental data. Vibration analyses to find the structures of true minima with no imaginary frequency and to guarantee that the suitable products and reactant corresponding to the reaction the IRC (intrinsic reaction coordinate) were performed at the same theoretical level.

RRKM theory was carried out regarding the below equation to calculate kinetic rate constants of unimolecular reactions.

$$k(E) = \frac{W(E)}{h\rho(E)} \quad (1)$$

where, ρ(E) is the density of state of reactants, W(E) denotes the number of energy states of the transition state, and h represent plank's constant. Then the k(T) canonical rate constant is determined by using the regular below equation:

$$k(T) = \frac{1}{Q(T)} \int k(E)\rho(E)\exp(-\beta E)\,dE \quad (2)$$

Where β= ($k_B T$) $^{-1}$, k_B is the Boltzmann's constant, and Q (T) represent the partition function of reactants.

III. RESULTS AND DISCUSSION

The Py molecule has D_2h symmetry. ($C_{1, 3, 6, 8}$); ($C_{4, 5, 9, 10}$); ($C_{2, 7}$) are thus equivalent and just three Carbone atoms have different coordinates. Three reactions can be distinguished for OH-addition and H-abstraction of Py separately. The Gibbs activation energy ($\Delta G^{\dagger}$) are 6.94–10.75 and 10.71–11.48 kcal/mol, respectively, and also free Gibbs energies (ΔG) are −17.94 to −4.09 and –6.82 to –6.17 kcal/mol, respectively. Calculations show that both reaction pathways are exothermic. It is worth mention that all the Gibbs reaction energies and Gibbs activation energies were evaluated at T=298 K and P=1 bar.

The calculated results of reaction energies and its differences for the two reaction pathways (H-abstraction and OH-addition reactions) is shown in Fig 1 and tabulated in Table 1 that the thermodynamically favorable reactions **1**$_{OH}$-**3**$_{OH}$ to produce the P1–P3 complexes. Among the P1–P3, the P2 species result of OH react with C_1, which is most favorable product. so the pathway 2 is more exothermic than other ways due to the thermodynamic calculated data as ΔG = –17.94 kcal per mol and ΔH= –27.37 kcal per mol, and also the pathways reaction **1**$_{OH}$-**3**$_{OH}$ seems to be the rather strongly exothermic reactions chemically with reaction energies ranging from –12.79 to –23.83 kcal mol^{-1}, whereas H-abstraction pathway **4**$_{H}$-**6**$_{H}$ appears to be less exothermic with the reaction energies –4.03 to 4.73 kcal/mol and ΔH= –3.7 to –4.44 kcal/mol.

The determination of the kinetic rate constant is a main role in assuming the transport and estimating the reaction pathways of PAHs in the presence of atmosphere component. The overall rate constant calculated and resulted k =9.54×10^{-13} cm^3 per molecule per s and it is in agreement with experimental data [9–12]. The participation rate of rate constant of reaction of OH to C_2 atom in contrast with the other position are equal to 85.4%.

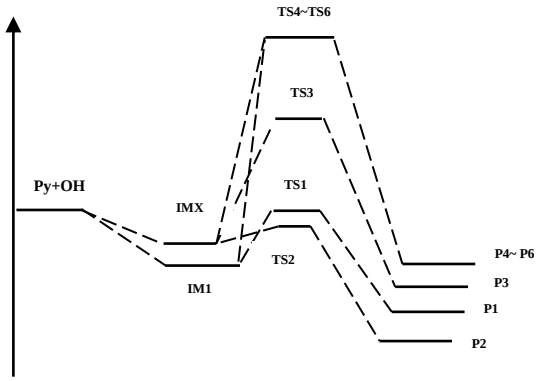

Fig.1: Energy diagram of PES of the OH-addition and H-abstraction reactions of pyrene

Table1: Results of kinetic parameters (in kcal/mol) of transition states, pre-reactive intermediate and products relative to the reactants along pathways **1**~**6**.

Species	Parameters					
	ΔE	$\Delta H°$	$\Delta G°$	$\Delta E^{\dagger}$	$\Delta H^{\dagger}$	$\Delta G^{\dagger}$
Py + OH$^{\bullet}$	0	0	0	-	-	-
IM1	–4.029	–4.059	2.92	-	-	-
IM$_{x(x=2,3)}$	–3.99	–3.95	2.57	-	-	-
OH-addition						
P1	–23.83	–24.68	–15.41	-	-	-
P2	–26.51	–27.37	–17.94	-	-	-
P3	–12.79	–13.62	–4.09	-	-	-
TS1	-	-	-	–0.98	–1.7	7.44
TS2	-	-	-	–1.32	–1.97	6.94
TS3	-	-	-	2.38	1.69	10.75
H-abstraction						
P4	–5.75	–5.47	–6.59	-	-	-
P5	–5.33	–5.06	–6.17	-	-	-
P6	–5.99	–5.71	–6.82	-	-	-
TS4	-	-	-	2.89	2.46	10.71
TS5	-	-	-	3.20	2.72	11.15
TS6	-	-	-	3.64	3.16	11.48

We used DFT calculations to allow the estimation of lifetime of the atmospheric reaction of Py in the presence of OH radicals. Hydroxyl radicals tropospheric concentrations (C_{OH}) in 12 hr daytime is 2.2×10^6 molecule cm^{-3} [13] typically. We can used the below equation to approximate the lifetime for pyrene in the atmosphere.

$$\tau = \frac{1}{k_{overall} \times C_{OH}} \qquad (3)$$

The lifetime (τ) of pyrene reaction initiated by hydroxyl radical is estimated about ~5.5 days.

IV. CONCLUSION

The reaction pathways and kinetics of pyrene initiated by OH radicals studied by means of DFT calculation at M06-2x/6-311++G (2df, 2p) level. By using RRKM method, the rate constants calculated. Two following main conclusions can be described in this work:

(1) The calculated energy and rate constants show that P2 species the producer of related the OH-addition reaction type will be favorable thermodynamically, and these processes

appear to be exergonic (ΔG < 0) and more exothermic reactions at temperature 298 K and pressure 1 bar.

(2) The RRKM overall rate constant for reactions of Py by OH radicals at environment temperature and pressure was 9.54×10^{-13} cm^3 $molecule^{-1}$ s^{-1}. To calculate the atmospheric reaction lifetime of pyrene, assume that the tropospheric 12 hr average daytime concentrations of OH radicals is 2.2×10^6 molecule per cm^3, the estimated lifetime of Py in troposphere is ~5.5 days so it suggests that Py in the atmospheric condition will be consumed by OH radicals as an atmospheric component and formed to the secondary contaminate products.

REFERENCES

[1] I. T. Salmeen, A. M Pero, R. Zator, D. Schuetzle, T. L Riley, Sci Technol, vol. 18, pp. 375–382, **1984**.
[2] D. Schuetzle, Environ Health Perspect, vol. 47, pp. 65–80, **1983**.
[3] W. C. Herndon, J. org. C/arm. vol. 46, pp. 2119-2125, **1981**.
[4] S. C. Dickerman, W. M. Feigenbaum, M. Fryd, N. Milstein, G. B. Vermont, 1. Zimmerman and J. F. W. McOmie, J. Am. Chem. Sot, vol. 95, pp. 4624-4632, **1973**.
[5] J. G. Calvert, R. Atkinson, K. H. Becker, R. M. Kamens, J. H. Seinfeld, T. J. Wallington, G. Yarwood, Oxford University Press, New York, **2002**.
[6] J. Zhao and R. Zhang, Adv. Quantum Chem, vol. 55, pp. 177–214, **2008**.
[7] A. Feilberg, R.M. Kamens, M.R. Strommen, T. Nielsen, Atmos. Environ, vol. 33 (8), pp. 1231–1243, **1999**.
[8] P.J. Robinson, K. A. Holbrook, Unimolecular Reactions. John Wiley & Sons. **1972**.
[9] Y. Bedjanian, M. L. Nguyen and G. Le Bras, Atmos. Environ, vol. 44, pp. 1754–1760, **2010**.
[10] W. Esteve, H. Budzinski and E. Villenave, Atmos. Environ, vol. 40, pp. 201–211, **2006**.
[11] Miet, H. Budzinski and E. Villenave, Polycyclic Aromat. Compd, vol. 29, pp. 267–281, **2009**.
[12] W. Esteve, H. Budzinski and E. Villenave, Atmos. Environ, vol. 38, pp. 6063–6072, **2004**.
[13] J. Arey, R. Atkinson, B. Zielinska, P. A. McElroy, Environ Sci Technol, vol. 23, pp. 321-327, **1989**.

Solvent Effects on the Reduction of Hydrogen Peroxide in the presence of Glutathione Peroxidase Mimic, Molecular Approach

Mohammad Tashakori **, *Mohammad Izadyar* , *Ramesh Kheirabadi***

Computational Chemistry Research Lab, Department of Chemistry, Faculty of Science, Ferdowsi University of Mashhad, Mashhad, Iran. Email: Izadyar@um.ac.ir

Abstract: The mechanism of reduction of the hydrogen peroxide by glutathione peroxidase mimic (GPx) were investigated by density functional theory (DFT) method at the M06-2X/6-31+G(d,p) level of theory. Thermodynamic and kinetic characteristics of the oxygen transfer from hydrogen peroxide molecule to selenium center in the GPx mimic were calculated for the related processes. Reduction reaction of H_2O_2 in the presence of GPx mimic was examined in different solvents, such as water, dimethyl sulfoxide (DMSO), methanol and chloroform. Based on the obtained results, the activation Gibbs energies of the reduction of H_2O_2 by GPx mimic in these solvents are 31.63 , 31.69 , 31.76 and 31.77 kcal.mol^{-1}, respectively. Also, the rate constants (k) of the hydrogen peroxide reduction in the presence of GPx mimic were calculated using the conventional transition state theory (TST), which are 6.47×10^6 , 6.45×10^6 , 6.44×10^6 and 6.41×10^6 s^{-1} , respectively. Finally, the GPx mimic due to structural stability and best performance in various solvents as a candidate, has widespread applications in the fields of green chemistry, medicine and food industry.

KEYWORDS: Density functional theory**,** GPx mimic, Hydrogen peroxide, Thermodynamic and the kinetic parameters, Solvent effect.

I. INTRODUCTION

Glutathione peroxidase (GPx) can reduc hydrogen peroxide (H_2O_2), which acts as an antioxidant and protect various living organism against oxidative stress [1]. A series of organoselenium compounds exhibited GPx-like antioxidant activity. GPx and other selenoproteins are used to prevent some diseases, such as cancer , Alzheimer and arthritis [2]. Due to the high signification of GPx, some small organoselenium compounds were designed and synthesied by the mimicking the active site structure of the GPx. The first favored GPx mimic was ebselen (2-phenyl-1,2-benzoisoselenazol-3-(2H)-one,1), which showed an important antioxidant activity in reduction of hydrogen peroxide in vivo. Ebselen represents the stimulating therapeutic properties, such as anti-inflammatory activities [3].

In this research, the comparison of different solvent effects on the reduction reaction hydrogen peroxidase have been performed to predict the reactivity of the new molecular structure containing both the Se−N covalent bond and amid group by the DFT method from the energetic point of view to characterize the transition state (TS) on the reaction pathway. For consideration the solvent effects on the reaction, four various solvents (water, DMSO, methanol, chloroform) were considered.

II.COMPUTATIONAL DETAILS

Density functional theory (DFT) was applied for geometery optimizations in Gaussian09[4] and M06-2X/6-31+G(d,p) level of theory. The Schlegel's synchronouss transit-guided quasi-Newton (STQN) method was used to locate the TSs. All the thermodynamic and the kinetic parameters were calculated for the oxygen transfer in the presence of water, methanol, DMSO and chloroform as solvents . The solvent effects were calculated by using the conductor-like polarizable continuum model (CPCM) [5]. Also, (k) rate constants in the reduction of H_2O_2 in the presence GPx mimic were estimated using the conventional transition state theory (TST) by equation 1 in various solvents.

$$k = \sigma\kappa\,(k_B T/h)\exp(-\Delta G^{\neq}/RT) \qquad (1)$$

σ represents the reaction path of degeneracy, κ is the number of equivalent reaction paths for tunneling correction, (k_B) is the Boltzmann's constant and (h) is the Planck's constant. R is the global gas constant and (T) is the temperature [6].

III. RESULTS AND DISCUSSION

The reaction pathway for the reduction hydrogen peroxide in the presence of GPx mimic is predicted by the DFT calculations, which were performed through a single-step hydrogen transfer via the SN2 mechanism. Selenoxide and water products are formed with oxygen atom transfer from H_2O_2 to the selenium center of the GPx mimic to reduce the hydrogen peroxide by O-O bond cleavage. Finally, the proton shuttle in the hydrogen peroxide occurrs to the

hydroxyl group, yielding the O···H bond that produce water molecule. The reduction reaction mechanism of H_2O_2 in the presence of the GPx mimic was employed for investigate of various solvent effects, such as water , DMSO , methanol and chloroform on the activation Gibbs energy and reaction kinetic (Fig 1).

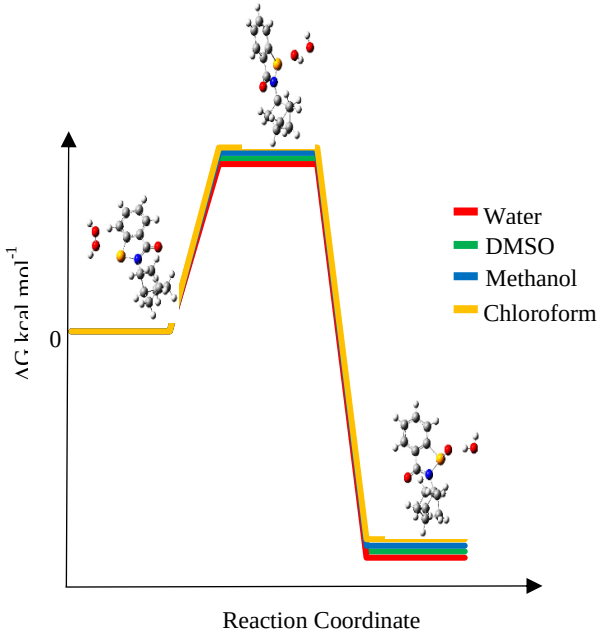

Fig.1 Energy diagram for oxidation of GPx mimic with the hydrogen peroxide in presence of different solvents

Based on the obtained results, the activation Gibbs energy showed that the reduction hydrogen peroxide by GPx mimic is the lowest value in the presence of water. Although, the Gibbs energy of the reduction of H_2O_2 by GPx mimic in the presence of chloroform solvent confirmed that selenoxide and water as the products are unstable (Table 1). Additionaly, based on the obtained results, the kinetic reduction reaction between H_2O_2 and GPx mimic indicated that chloroform is not a suitable solvent.

Table 1. The kinetic and thermodynamic parameters for the reaction between the GPx mimic and H_2O_2 in different solvents

Solvent	ΔG (kcal.mol^{-1})	$\Delta G^{\ddagger}$ (kcal.mol^{-1})	k (s^{-1})
Water	-40.86	31.63	6.47×10^{6}
Methanol	-40.59	31.76	6.45×10^{6}
DMSO	-40.68	31.69	6.44×10^{6}
Chloroform	-40.36	32.77	6.41×10^{6}

IV. CONCLUSIONS

A computational study was performed to evaluation the different solvent effects on the kinetic and on the reduction mechanism of hydrogen peroxide in the presence of GPx mimic. Based on the obtained results, water is the best solvent for the reduction hydrogen peroxide by GPx mimic, but whereas chloroform solvent indicated that not suitable. Finally, these results show that, the GPx mimic that contained selenium-organic frameworks (MOFs) is provieded the structural stability and excellent performance in various solvents.

REFERENCES

[1] G. Alfthan, M. Eurola, P. Ekholm, E.-R.Venäläinen, T. Root, K. Korkalainen and A. Aro. Journal of Trace Elements in Medicine and Biology, vol 31, pp 142–147, **2015**.
[2] J. K. Pearson & R. J. Boyd. The Journal of Physical Chemistry A, vol 112(5), pp 1013–1017, **2008**.
[3] C. Barkus, J.-M. N.Ferland, W. K. Adams, G. C. Churchill, P. J. Cowen, , D. M. Bannerman, T. Sharp. Journal of Psychopharmacology. vol 32 issue 9, pp 1018-1026, **2018**.
[4] M. J. Frisch, G. W. Trucks, H.B. Schlegel, G. E. Scuseria, M. A Robb, J. R. Cheeseman, G.V. Scalmani, B. M. Barone, G. A.Petersson, H. Nakatsuji, et al. Gaussian 09, revision A.02; Gaussian. Inc.: Wallingford, CT, **2009**.
[5] A. M. Mkadmh, R. Y. Morjan, J. Raftery, A. M. Awadallah & J. M. Gardiner. Arabian Journal of Chemistry. **2019**.
[6] M. Cui, W. Li, L. Wang, L. Gong, H. Tanga and D. Cao. J.Mater.Chem.C. vol 7,pp 3779-3786, **2019**.

Electro-Fenton-like process for treatment of aqueous solution of MO dye

R. Maghbool*[a], *P. Nazari*[a], *S. R. Setayesh*[a]
[a]*Department ofChemistry, Sharif University of Technology, Tehran, PO Box 11155-3516, Iran*
Email: setayesh@sharif.edu

Abstract*:* The $FeVO_4/CeO_2$nanocomposite was synthesized by hydrothermal method and characterized by XRD technique. The catalytic activity was examined by the degradation of methyl orange through electro-Fenton-like process. In this study, the influence of different parameters such as catalyst dosage, initial pH, and current intensity on the removal of dye was investigated. The optimum conditions were reported.At the optimum conditions methyl orange (MO) removal attained to 90% in 60 min. Based on the results,$FeVO_4/CeO_2$ can be introduced as a novel catalyst for electro-Fenton like process in wastewater treatment.

Keywords: cerium oxide,Electro-Fenton-like, iron vanadate, methyl orange

I. INTRODUCTION

Treatment of water which contains pollutants has been introduced as a crucial challenge in the environmental science. One of the efficient methods for solving this problem is the advanced oxidation process (AOP). Among the divers AOPs, electrochemical oxidation processes (EAOPs) that include electro-Fenton can be proposed as the promising methods for the degradation and mineralization of organic pollutants and dyes. One of the advantages of the electro-Fenton process is thein-situelectrogeneration of $H_2O_2$from the reduction of O_2 at the cathode surface (Eq. 1). Therefore, this process does not require H_2O_2 transportation and storage.

$O_2 + 2H^+ + 2e^- \rightarrow H_2O_2$(1)

The process continues by adding iron catalysts for generation of $^{\cdot}OH$product (Eq. 2).

$Fe^{2+} + H_2O_2 \rightarrow Fe^{3+} + {}^{\cdot}OH + OH^-$ (2)

The OH radicals have high oxidationpotential and they are appropriate for oxidizingof different dyes and organic pollutants. This beneficial property makes it as a first applicable oxidant in wastewater treatment. Deng and et al. have presentedthe TPP-assisted EF process as a promising technique for extending coking wastewater treatment at near-neutral pH with a high mineralization [1].In addition, the hydroxyl radical has the degradation power of bio-refractory organic pollutants. In the recent study,a bioelectrochemical platform (3D-EF-MFCs) combining two-chamber microbial fuel cells and three dimensional electro-Fenton technique were delicately designed and assembled to explore the decolorization, bio-genericity performance of the methyl orange, and the possible biotic-abiotic degradation mechanisms[2].

One of the choices for electro-Fenton process is synthesis of nanocomposites.

In this paper, $FeVO_4/CeO_2$ nanocomposite was synthesized by hydrothermal methodfor the first time and characterized. The catalytic activity of $FeVO_4/CeO_2$ analyzed through electro-Fenton-like degradation of methyl orange in wastewater.

II. METHODS

A. *Material*

Ammonium metavanadate, Iron (III) nitrate nona-hydrate, cerium (IV) sulfate, sodium hydroxide,hydrochloric acid, sodium sulfate, ethanol, sulfuric acid, methyl orange were all purchased from Merck (Darmstadt, Germany).

B. *Synthesis of CeO_2*

4g $Ce(SO_4)_2$was dissolved in 12.5 mLdouble distilled water (solution 1) and 2g NaOH was dissolved in 12.5 mLdouble distilled water (solution 2). Then solution 1 was added to solution 2 under stirring.Stirringwas continued until homogeneous gel was produced. The pH was adjusted to 11 by NaOH (1M) and HCl (1M). The solution was sealed in 100 mL-Teflon-lined stainless steel autoclave allowed toheat at 200˚Cfor 24 h.The precipitate was washed with double distilled water and ethanol and dried for 12h at 80˚C.

C. *Catalyst preparation*

1g of CeO_2wasdissolved in 50 mL double distilled water(solution1). Then 1.2 mmoL NH_4VO_3 and 1.2 mmoL$Fe(NO_3)_3.9H_2O$ were dissolved in 30 mL double distilled water at 80˚C. The mixed solution was added tosolution1and stirred for 3 h. The mixture transferred to Teflon-lined stainless steel autoclave and heated to 180˚C for 5h. The precipitate was washed with double distilled water and ethanol. Finally, the precipitate was dried at 60˚C.

D. *Experimental section*

The electro-fenton degradation of methyl orange was accomplished in an undivided cylindrical reactor, which equipped with two stainless steel plates (2×5 cm^2) as cathode and anode. The distance between of these electrodes was 3cm. The solution was saturated with O_2 by flowing pure

oxygen, 150 mL/min for 15 min prior to the electro-Fenton reaction. The electric current was supplied by a DC power supply. Na_2SO_4 was used as the supporting electrolyte. 100 mL solution containing of desired concentration of MO, the appropriate weight of the catalyst and 0.05M Na_2SO_4 were subjected to the reactor (a cylindrical glass with volume of 250 mL). The initial pH of the solution was adjusted by H_2SO_4 (0.1 M) or NaOH(0.1 M) solutions and the current was set at desired amount. At specified times 2mL of the solution was taken and then centrifuged. The absorption of the solution was measured by spectrophotometer (Unico, 4802 (Dayton, NJ, USA)).

III. RESULTS AND DISCUSSION

Fig 1 illustrates the XRD pattern of $FeVO_4/CeO_2$ nanocomposite.The peaks at 2θ= 28.5˚ and 34.0˚demonstrate that $FeVO_4$and CeO_2 were the phases,which are present in $FeVO_4/CeO_2$ catalyst[3]. This technique reveals that the nanocomposite has been synthesized successfully.

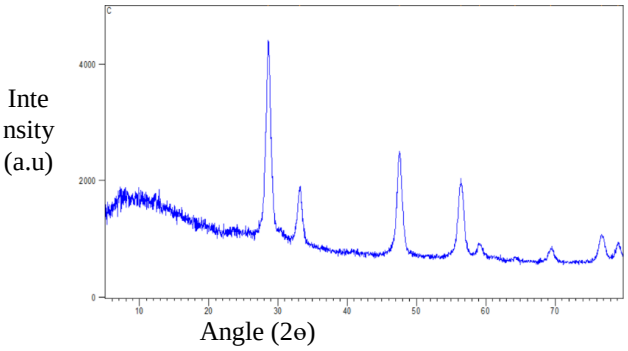

Fig.1: XRD pattern of $FeVO_4/CeO_2$powder.

The percentage of MO degradation was calculated by the following equation (Eq. 3):

$$\%MO\ degradation = \frac{C_0 - C_t}{C_0} * 100 (3)$$

WhereC_0 and C_t are the initial and final MO concentrations inElectro-Fenton reaction,respectively.

The maximum efficiency (90%)of electro-Fenton removal of MO at the initial pH of 3, the catalyst dosage of 0.1g, and current intensity of 200mA was achieved after 60 min treatment.

The possible pathway of pollutants degradation by the$FeVO_4/CeO_2$nanocomposite is presented by following equations:

$Fe^{3+} + H_2O_2 \leftrightarrow Fe\ldots OOH^{2+} + H^+$ (4)

$Fe\ldots OOH^{2+} \rightarrow HOO^{\cdot} + Fe^{2+}$(5)

$Fe^{2+} + H_2O_2 \rightarrow Fe^{3+} + {}^{\cdot}OH + OH^-$(6)

$V^{5+} + H_2O_2 \rightarrow V^{4+} + HO^{\cdot}{}_2 + H^+$(7)

$V^{4+} + H_2O_2 \rightarrow V^{5+} + {}^{\cdot}OH + OH^-$(8)

$RH + {}^{\cdot}OH \rightarrow CO_2 + H_2O$ (9) [4].

These reactions indicate that the presence of vanadium in the structure of nanocomposite, improves the catalytic activity of electro-Fenton catalyst via generation of hydroperoxyl and hydroxyl radicals.

IV. CONCLUSION

$FeVO_4/CeO_2$ was applied as a heterogeneous electro-Fenton-like catalyst for degradation of methyl orange. The optimum operating conditions of the system for maximum removal of MO were reported, which was 90% removal at 60 min. The results indicate that the synthesized nanocomposite can be introduced as a promising heterogeneous catalyst for wastewater treatment.

REFERENCES

[1] F. Deng, S. Qiu, Y. Zhu, X. Zhang, J. Yang, and F. Ma, Environmental Science and Pollution Research, vol. 26, pp.1-12, **2019**.

[2] T. Huang, L. Liu, J. Tao, L. Zhou, and S. Zhang Environmental Science and Pollution Research, vol.25, pp. 17989-18000, **2018**.

[3] Q. Nong, RSC Advances, vol. 5.35, pp. 27933-27939, **2015**.

[4] P. Xu, H. Xu, and Z. Shi, Separation and Purification Technology, vol. 194, pp. 457-461, **2018**.

Persulfate ions activated TiO_2/Carbon dots nanocomposite as a highly active photocatalyst for the degradation of Congo red under visible-light illumination

M. Sabri**, A. Habibi-Yangjeh
Department of Chemistry, Faculty of Science, University of Mohaghegh Ardabili, P.O. Box 179, Ardabil, Iran.
Email: minasabri@uma.ac.ir

Abstract*:* In this study, we synthesized TiO_2/Carbon dots nanocomposite and its photocatalytic performance was exceptionally improved under visible light in removal of Congo red using persulfate anions. The TiO_2/C-Dots (0.50 mL) photocatalyst had the greatest photocatalytic ability. In addition, the removal rate constant of Congo red by this photocatalyst in the existence of 1.48 mM of persulfate ions was 158×10^{-4} min^{-1}, which is almost 5.60, 3.91, and 1.46-folds premier than those of the pure TiO_2, TiO_2/persulfate, and TiO_2/C-Dots (0.50 mL) samples, respectively.

Keywords: Persulfate activation, Photocatalytic activity, TiO_2/Carbon dots, Visible-light-active photocatalyts.

I. INTRODUCTION

Currently, advanced oxidation processes (AOPs) have been widely studied to eliminate wastewater contaminants owing to the generation of highly reactive radicals. Among these AOPs, sulfate radical anion ($SO_4^{\bullet-}$) based AOPs have attracted attention due to their high selectivity and remarkable reactivity with the resistant pollutants [1,2]. The activation of pioneer peroxides such as persulfate and peroxymonosulfate via ultrasonic waves, heat, transition metals, UV radiation or heterogeneous photocatalysts, lead to produce $SO_4^{\bullet-}$ [3,4].

TiO_2 is one of the widely investigated semiconductors for photocatalytic applications, but due to the rapid photoexcited e^-/h^+ pairs recombination and limitation in visible-light harvesting as its inherent disadvantages, the researchers are interested to overcome these limitations [5,6]. For this purpose, an electron acceptor has been commonly utilized for accepting electrons from the conduction. Among the electron acceptors, persulfate, oxygen and hydrogen peroxide have been widely applied in photocatalytic degradation [7].

Carbon dots (C-Dots) have emerged recently and attracted remarkable attention over the past few years, owing to their unique properties such as high solubility, low toxicity, chemical inertness and reservoir capability. They have been applied to enhance photocatalytic ability of large band gap photocatalysts under visible light [8,9]. Particularly, C-Dots also have supreme upconversion photoluminescence characteristic, which means that C-Dots could be excited by long-wavelength light and the up converted emissions produced short wavelengths [10].

Hence in this work, we applied C-Dots for increase photocatalytic ability of TiO_2 under visible light, and fabricate TiO_2/C-Dots nanocomposite to activate persulfate ions in removal of Congo red pollutant.

II. METHODS

The TiO_2/C-Dots (0.50 mL) nocomposite was prepared using the procedure reported elsewhere [11]. Photocatalytic ability of the synthesized sample was studied by degradation of Congo red upon visible-light illumination. The concentration of Congo red was specified using the maximum wavelength at 496 nm. The visible light was reflected by a 50W LED lamp. The solution was mechanically stirred and repeatedly aerated by a pump to provide oxygen and complete mixing of the reaction solution. Before to irradiation, the suspensions were stirred in dark for 60 min to attain the adsorption–desorption equilibrium. After every 30 min illumination intervals, 4 mL aliquot of the mixture was sampled and centrifuged (8000 rpm, 7 min) to eliminate the photocatalyst. Additionally, all photocatalysis experiments were performed in the presence of 0.1 g of the photocatalysts added to 250 mL of Congo red solutions.

III. RESULTS AND DISCUSSION

The TiO_2/C-Dots (0.50 mL) nanocomposite exhibited the greatest photocatalytic ability. Figure 1 displays removal of Congo red over various photocatalysts under visible light. It can be shown that the kinetic constant of TiO_2/C-Dots (0.50 mL) nanocomposite with persulfate ions is about 5.60, 3.91, and 1.46-folds premier than those of the as-fabricated TiO_2, TiO_2/persulfate, and TiO_2/C-Dots nanocomposite, respectively. These outcomes revealed that the adding of C-Dots and persulfate ions into the TiO_2 photocatalyst is very impressive to ameliorate the photocatalytic ability. In the TiO_2/C-Dots nanocomposite, C-Dots with up conversion feature could be excited by long-wavelength lights and the up converted emissions produce short wavelengths. Therefore,

C-Dots produce needed short wavelengths for excitation of TiO_2 through conversion of long wavelengths [10]. The produced high-energetic photons excite TiO_2 particles to generate e^-/h^+ pairs. In addition, persulfate ions can generate hydroxyl and sulfate radicals through activation by conduction-bond electrons. So persulfate ions act as an electron acceptor in photocatalytic treatment. In fact, the existence of persulfate ions accelerates the photocatalytic removal of Congo red by the concurrent production of sulfate and hydroxyl radicals.

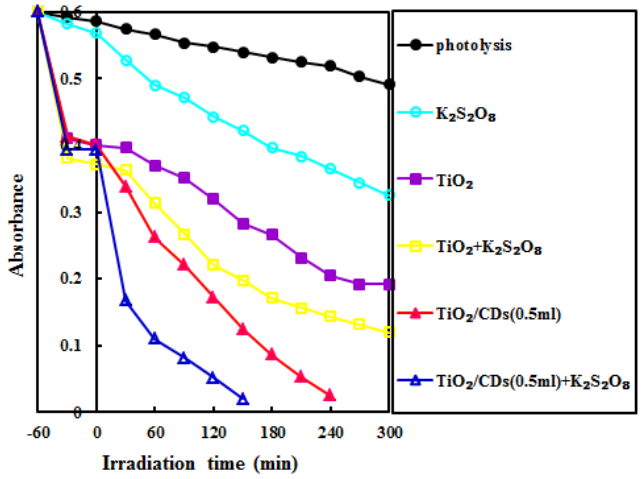

Fig.1: Photocatalytic degradation of Congo red on the TiO_2 and TiO_2/C-Dots nanocomposites under visible light.

IV. CONCLUSION

In this paper, we efficiently synthesized the TiO_2/C-Dots nanocomposite, as visible-light-driven photocatalyst, through a simple procedure, which was employed for photocatalytic removal of Congo red in the presence of persulfate ions. The addition of persulfate anions considerably enhanced photocatalytic performance of the nanocomposite. Photocatalytic ability of the TiO_2/C-Dots/persulfate system was about 5.60, 3.91, and 1.46-folds higher than those of the TiO_2, TiO_2/persulfate and TiO_2/C-Dots (0.50 mL) samples in removal of Congo red, respectively. This work displayed that the TiO_2/C-Dots (0.50 mL)/persulfate system under visible light is a cost effective and eco-friendly method to remove Congo red dye from water.

REFERENCES

[1] M. Gągol, A. Przyjazny, G. Boczkaj, Chemical Engineering Journal, vol. 338, pp. 599–627, **2018**.

[2] F. Ghanbari, and M. Moradi, Chemical Engineering Journal, vol. 310, pp. 41–62, **2017**.

[3] G. Matafonova, and V. Batoev, Water Research, vol. 132 pp. 177–189, **2018**.

[4] G. Zhen, X. Lu, H. Kato, Y. Zhao, and Y.-Y. Li, Renewable and Sustainable Energy Reviews, vol. 69, pp. 559–577, **2017**.

[5] S. Ghosh, and A.P. Das, Toxicological & Environmental Chemistry, vol. 97 pp. 491–514, **2015**.

[6] N.R. Khalid, A. Majid, M.B. Tahir, N.A. Niaz, and S. Khalid, Ceramics International, vol. 43, pp. 14552–14571, **2017**.

[7] M.A. Zazouli, F. Ghanbari, M. Yousefi, and S. Madihi-Bidgoli. Journal of Environmental Chemical Engineering, vol. 5 pp. 2459-2468, **2017**.

[8] Z. Zhang, S. Lin, W. Cui, X. Li, and Hong Li, Materials Letters, vol. 234, pp. 264−268, **2019**.

[9] Y. Zhang, L. Wang, M. Yang, J. Wang, and J. Shi, Applied Surface Science, vol. 466, pp. 515−524, **2019**.

[10] P. Chen, F. Wang, Z.-F. Chen, Q. Zhang, Y. Su, L. Shen, K. Yao, Y. Liu, Z. Cai, W. Lv, and G. Liu, Applied Catalysis B: Environmental, vol. 204, pp. 250–259, **2017**.

[11] S. Feizpoor, A. Habibi-Yangjeh, and K. Yubuta, Journal of Photochemistry and Photobiology A: Chemistry, vol. 367, pp. 94–104, **2018**.

Photofixation of Dinitrogen to Ammonia by ZnO Nanostructure Decorated with MnV_2O_6 under Ambient Conditions

Elham Vesali-Kermani**, Aziz Habibi-Yangjeh

Department of Chemistry, Faculty of Science, University of Mohaghegh Ardabili, P.O. Box 179, Ardabil, Iran.

Email: elhamvesali@uma.ac.ir

Abstract: Photofixation of nitrogen, the best successor to the Haber-Bosch method, is eco-friendly, mild, and low–cost process that needs more attempts to discover high stable photocatalysts. In this study, ZnO/MnV_2O_6 photocatalysts with different percentages of MnV_2O_6 (10%, 20%, and 30%) fabricated and their nitrogen fixation ability was explored under visible- light irradiation. The ZnO/MnV_2O_6 (10%) nanocomposite revealed the maximum ammonia production rate, which was 1.5-fold premier than the initial ZnO photocatalyst.

Keywords: ZnO; Nitrogen photofixation; Photocatalyst.

I. INTRODUCTION

Nitrogen photofixation, the reduction of atmospheric N_2 to ammonia, is the importantly catalytic reaction in chemistry and biology. As regards, N_2 is an inert molecule in chemistry because a triple bond in this molecule is very strong, both spurious and biological nitrogen reduction can be derived in the attendance of metal-based catalysts. The N_2 and H_2 gases transform into ammonia by the Haber–Bosch process on the iron-based surface catalysts under high temperature and pressure. This process is undesirable from the economics and environmental viewpoints. Hence, for the nitrogen reduction, we need to use a low energy and eco-friendly alternative process. These processes can be referred as nitrogen reduction. Ammonia can be generated in a mild condition utilizing photocatalysts under sunlight illumination. Among the various semiconductors, ZnO has been interested due to its more negative CB (-0.44 eV) than many metal oxides such as TiO_2 (-0.29 eV). Hence, ZnO could be a suitable choice for the nitrogen photofixation process. Janet et al. investigated ZnO capability in the nitrogen photoreduction process, in 2010. According to studies by the group, the zinc oxide structure in the presence of platinum nanoparticles produces more ammonia at a rate of 860 μmol g^{-1} h^{-1}, which indicates better photocatalytic activity of this nanocomposite. Despite the negative potential for the CB, use efficiency of this reaction over the pristine ZnO is not enough [1].
In this study, nitrogen photoreduction ability of ZnO/MnV_2O_6 nanocomposites with different percentage of MnV_2O_6 (10%, 20%, and 30%) was investigated. Among them, the optimal percentage, which produced the highest ammonia content, was 10%.

II. METHODS

A. Materials

Zinc nitrate ($Zn(NO_3)_2 \cdot 6H_2O$, extra pure), sodium hydroxide (NaOH), manganese (II) acetate ($Mn(CH_3CO_2)_2.2H_2O$, extra pure), ammonium metavanadate (NH_4VO_3, 99%), absolute ethanol (Merck) and distilled H_2O was applied for the experiments.

B. Instrument

The pH of solutions was adjusted by a Metrohm pH meter with a model of 691. The absorbance was provided by a UNICO model 2100 series spectrophotometer. Ultrasonic irradiation was provided by Bandelin ultrasound processor HD 3100 (12 mm diameter Ti horn, 75 W, 20 kHz). The light source in this study was 500W Xe lamp (Ushio Xenon Short Arc Lamp) by power density of 100 mW/cm^2, with a 420 nm cutoff filter to simulate visible light.

C. Preparation of the photocatalysts

The ZnO/MnV_2O_6 (10%) photocatalyst was prepared by using the refluxing method. In the first procedure, $Zn(NO_3)_2 \cdot 6H_2O$ (2.3 g) and 0.199 g $Mn(CH_3CO_2)_2.2H_2O$ were dissolved in 150 ml of H_2O and stirred for 30 min at 25 °C. After that, $NH_4VO_{3\,(aq)}$ (0.046 g at 20 mL of H_2O) was added by dropwise and the milky suspension was formed. Then, NaOH (5 M) was added to the system and stirred until pH reached to 10. After refluxing at 96 °C for 3 h, the fabricated brown suspension was centrifuge and washed (with water and ethanol) and dried at 60 °C for 24 h.

D. Nitrogen fixation under visible light

Nitrogen fixation tests were performed in a 50 mL cylindrical double-walled glassy photoreactor. For these experiments, 0.04 g of the ZnO/MnV_2O_6 was established to 0.04 L of water and dispersed using an ultrasound bath for 6 min. Then, 40 µL absolute ethanol (0.789 g/L), as a hole scavenger, added to the suspension. The suspension was continually stirred for one hour in the dark with air purging for balance the N_2 adsorption. After that, the Xe lamp was turned on, by gathering 1.5 mL of the provided suspension at any 30 min (for 3 h) and extenuating with water, the samples were centrifuged and the ammonia concentration of the supernatant was defined with Nesslerization method [2].

III. RESULTS AND DISCUSSION

Figure 1 displays the N_2 photofixation ability of the ZnO and ZnO/MnV_2O_6 nanocomposites with various percentages of MnV_2O_6 (10%, 20%, and 30%). The ammonia generation rates for the ZnO/MnV_2O_6 (10%) (1544.2 µmol $g^{-1}.h^{-1}$), ZnO/MnV_2O_6 (20%) (1353.8 µmol $g^{-1}.h^{-1}$), ZnO/MnV_2O_6 (30%) (1251.7 µmol $g^{-1}.h^{-1}$), and ZnO (1153.4 µmol $g^{-1}.h^{-1}$) were obtained. This result shows photofixation activity for the ZnO increases by adding MnV_2O_6 component (1.5-folds) and the ZnO/MnV_2O_6 nanocomposite with 10% of MnV_2O_6 shows the best activity.

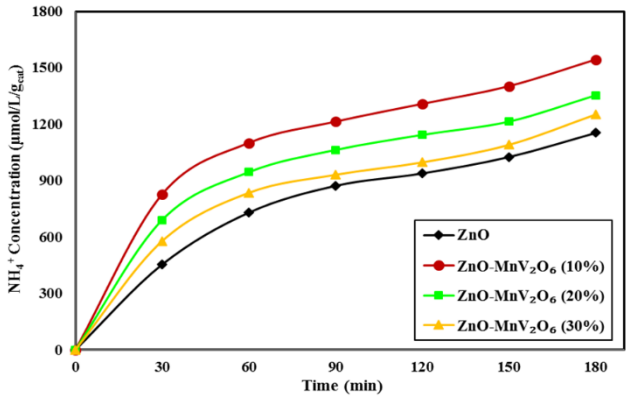

Fig. 1. NH_4^+ production rate over the pure ZnO and ZnO/MnV_2O_6 nanocomposites under visible light.

IV. CONCLUSION

In this study, the ZnO/MnV_2O_6 photocatalysts were synthesized by an easy one-path method in H_2O. These nanocomposites were used for the NH_4^+ production under visible-light irradiation. The ZnO/MnV_2O_6 (10%) nanocomposite revealed the maximum ammonia production rate, which was 1.5-fold premier than the initial ZnO photocatalyst. The combination of the ZnO and MnV_2O_6 improved photoactivity due to reducing the recombination rate of the photogenerated electrons and holes.

REFERENCES

[1] S. Wang, F. Ichihara, H. Pang, H. Chen, and J. Ye, Advanced Functional Materials, vol. 28(50), pp. 1803309, **2018**.

[2] H. Diarmand-Khalilabad, A. Habibi-Yangjeh, D. Seifzadeh, S. Asadzadeh-Khaneghah, and E. Vesali-Kermani, Ceramics International, vol. 45, pp. 2542-2555, **2019**.

High efficient photocatalytic degradation of Malachite green using visible-light-driven TiO_2/CDs/Polyaniline photocatalyst

S. Feizpoor**, A. Habibi-Yangjeh
Department of Chemistry, Faculty of Science, University of Mohaghegh Ardabili, P.O. Box 179, Ardabil, Iran,
Email: Solmazfeizpoor@uma.ac.ir

Abstract*:* The fabrication of photocatalysts with considerable photocatalytic performance can be the main purpose for the researchers as a substitute for the traditional wastewater treatment processes. In the present work, the TiO_2/CDs/Polyaniline (20%) nanocomposite as efficient visible-light-driven photocatalyst was fabricated using a facile method. Photocatalytic ability of the nanocomposite was evaluated by photocatalytic removal of Malachite green under visible-light illumination. The results demonstrated that the TiO_2/CDs/Polyaniline (20%) nanocomposite exhibited remarkably enhanced photocatalytic activity, which was approximately 32.7, 3.4, and 9.4 times higher than the pure TiO_2, TiO_2/CDs (0.5mL) and TiO_2/Polyaniline (20%) photocatalysts,

Keywords: TiO_2/CDs/Polyaniline (20%); TiO_2; Water pollutants; Visible-light-driven photocatalyst.

I. INTRODUCTION

The enhancement of polluted water quality is the most significant issue that human being faces [1]. Hence, finding effective strategies for the elimination of harmful contaminants from wastewater are very momentous. Heterogeneous photocatalysis has been gained increased attention, as one of the impressive strategies, to confront energy and environmental contamination crises [2].

Among semiconductors, titanium dioxide is believed to be the most appropriate semiconductor, due to its chemical stability, excellent biocompatibility, and high oxidation ability. In spite of the unique features of TiO_2, it possesses low photocatalytic efficiency in practical applications under solar energy, because it can only absorb UV light. Accordingly, to overcome this problem and boost the photo-response region of TiO_2, various methods have been offered, like dye photosensitization, doping of metals and nonmetals, and coupling TiO_2 with other semiconductors [3].

As one of the conducting polymers, polyaniline (PA) can be a prime candidate for visible-light photocatalysts, due to easy preparation, narrow band gap, high stability, good electrical conductivity, and reasonable visible-light responsive property [4]. Then, PA is utilized to develop the electronic conductivity and prevent the recombination of photogenerated charge carriers of TiO_2, which leads to enhance the photocatalytic efficiency [5]. To more pronounced transfer of charge carriers between two semiconductors, carbon dots (CDs) are used, as a low-price mediator [6].

The fabricated nanocomposites were fully characterized and the nanocomposites exhibited exceptional photocatalytic ability for degradation of Malachite green. Based on the results, the ternary photocatalyst can be considered as a beneficial photocatalyst for practical applications in wastewater treatments.

II. METHODS

Synthesis of photocatalysts

The TiO_2/CDs/PA (20%) nocomposite was prepared using the procedure reported by our research group [7].

Evaluation of photocatalytic activity

Photocatalytic reaction was carried out in a cylindrical glassy reactor upon LED lamp illumination (50W). 100 mg of the sample was added in 250 mL of Malachite green. Before starting the photocatalytic activity, the solution took place in the dark for 1h to get equilibrium of adsorption–desorption. After exposing to the visible light illumination, 3 mL of suspension was withdrawn from the reaction system at certain times. Eventually, the concentration of Malachite green was estimated by an UV-vis spectrophotometer at wavelength of 610 nm.

III. RESULTS AND DISCUSSION

The photocatalytic ability of the photocatalysts was appraised by the removal of Malachite green under visible-light (Fig. 1). Before the photocatalytic processes, the self-degradation of Malachite green under visible-light illumination was investigated. It can be realized that the Malachite green concentration has hardly altered in the absence of the photocatalyst upon visible-light irradiation. As envisaged, the TiO_2 demonstrated low photocatalytic ability, with only 38% Malachite green degradation, after 270 min illumination. In comparison to TiO_2, the TiO_2/CDs (0.5 mL) and TiO_2/PA

(20%) samples exhibit higher photodegradation ability and removal efficiency approaches 63.3 and 44.7%, respectively. The results obviously illustrated that the TiO_2/CDs/PA (20%) exhibited the best photocatalytic performance and the Malachite green was quite degraded after 120 min illumination.

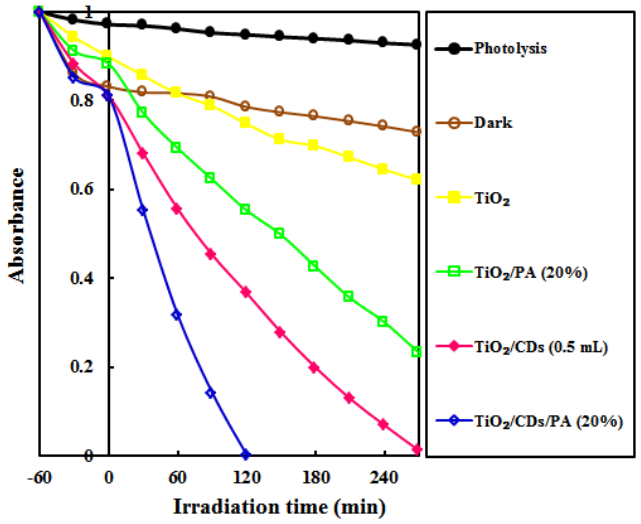

Fig.1: Photodegradation of Malachite green over the TiO_2, TiO_2/PA (20%), TiO_2/CDs (0.5 mL), and TiO_2/CDs/PA (20%) nanocomposites under visible-light irradiation.

IV. CONCLUSION

Briefly, ternary TiO_2/CDs/PA photocatalysts were synthesized by a facile method. The TiO_2/CDs/PA (20%) nanocomposite displayed the excellent photocatalytic performance for removal of Malachite green exceeding that of the pure TiO_2 and TiO_2/PA (20%) by a factor of 32.7 and 9.4, and the TiO_2/CDs (0.5 mL) by a factor of 3.4. This work would promote the potential of TiO_2-based semiconductors for removal of Malachite green.

REFERENCES

[1] Y. Zhang, B. Wu, H. Xu, H. Liu, M. Wang, Y. He, and B. Pan, NanoImpact, vol. 3, pp. 22–39, **2016**.
[2] C. Sushma, and S.G. Kumar, Chemical Papers, vol. 71, pp. 2023–2042, **2017**.
[3] S. Feizpoor, A. Habibi-Yangjeh, and S. Vadivel, Journal of Photochemistry and Photobiology A: Chemistry, vol. 341, pp. 57–68, **2017**.
[4] M.N. Rantho, M.J. Madito, and N. Manyala, Electrochimica Acta, vol. 262, pp. 82-96, **2018**.
[5] V. Eskizeybek, F. Sari, H. Gülce, A. Gülce, and A. Avci, Applied Catalysis B: Environmental, vol. 119, pp. 197-206, **2012**.
[6] S. Asadzadeh-Khaneghah, A. Habibi-Yangjeh, and M. Abedi, Separation and Purification Technology, vol. 199, pp. 64-77, **2018**.
[7] S. Feizpoor, A. Habibi-Yangjeh, and K. Yubuta, Journal of Photochemistry and Photobiology A: Chemistry, vol. 367, pp. 94–104, **2018**.

g-C_3N_4 nanosheet/Carbon dots/BiOBr Nanocomposite: An Impressive Photocatalyst for Degradation of Congo-Red Dye Under Visible-Light Illumination

S. Asadzadeh-Khaneghah*, A. Habibi-Yangjeh
Department of Chemistry, Faculty of Science, University of Mohaghegh Ardabili, P.O. Box 179, Ardabil, Iran,
E-mail: Soheila.asadzadeh@uma.ac.ir.

Abstract*:* In this report, g-C_3N_4 nanosheet/Carbon dots/BiOBr (signify as NCN/CDs/BiOBr) nanocomposite was successfully applied for the elimination Congo-Red as typical azo dye under visible-light irradiation. The results showed that photocatalytic performance of this material was significantly higher for the degradation of this dye. The ternary nanocomposite demonstrated the highest ability that is as much as 22.2, 6.4, and 3.6 times of the pure CN, NCN, and NCN/CDs in photodegradation of Congo-Red dye, respectively. This work highlights the potential application of extremely effective CDs anchored semiconductors in environment and related applications including waste water cleaning.

Keywords: Graphitic carbon nitride, Photocatalysis, Visible-light response, Congo-Red dye.

I. INTRODUCTION

Organic dyes have become one of the original sources of water pollution in the environment, because these compounds release chemically stable, carcinogenic, and toxic pollutants into the effluent [1]. So the removal of these water pollutants has become a burgeoning field of research. Among various pollutants, Congo-Red dye is a typical water-soluble anionic pollutant utilized in cellulose and cotton textile industries. This azo dye is dangerous for the aquatic environment even at low concentrations [2].

Semiconductor-based photocatalysis can be an efficient method for water remediation [3]. With the porpuse of impressive utilization of the solar irradiation in the photocatalytic processes, preparation of visible-light-driven photocatalysts have gained much more interests [4].

For this purpose, in this study, g-C_3N_4 (denoted as CN) was utilized as a base semiconductor with narrow band gap. Due to its shortcomings such as smaller specific surface area, it was changed to nanosheet of g-C_3N_4 (denoted as NCN). In addition, to further absorption of visible light and retardation of the e^-/h^+ pairs from recombination, Carbon dots (denoted as CDs) are deposited over the NCN [5]. Finally, with the aim of providing considerably boosted photocatalytic ability, we focused on integration of BiOBr, as a low band gap semiconductor with the NCN/CDs nanocomposite. The fabricated photocatalyst was subsequently characterized by different techniques and it was utilized for photocatalytic removal of Congo-Red dye under visible light. It was deemonstrated that by depositing both BiOBr and CDs particles on the NCN, photocatalytic activity was greatly increased. Hence, photodegradation of Congo-Red should be effective way to alleviate or solve pollution in the wastewater over the NCN/CDs/BiOBr nanocomposite.

II. METHODS

The NCN/CDs/BiOBr (20%) nocomposite was prepared using the procedure reported by our research group [5]. Also the photocatalytic ability of photocatalyst was evaluated at 25 ºC under visible light using a 50W LED lamp for Congo-Red dye with the concentration of 20 µg/L by recording the characteristic absorption peaks at 496 nm. Briefly, in the photocatalysis reaction, 250 mL aqueous solution including Cong-Red dye and 0.1 g of the nanocomposite was put in the reactor with an air bubbling system and for keep the suspension homogeneous a stirrer was embedded. Also, to reach equilibrium, the suspension was kept in dark condition and then the lamp was switched on to start the photocatalysis reaction. Finally, the remained concentration of the Congo-Red was analyzed after removing the nanocomposite by measuring the absorbances of Congo-Red at the mentioned wavelength.

III. RESULTS AND DISCUSSION

In order to observe the excellent visible-light photoability of the NCN/CDs/BiOBr (20%) nanocomposite in degradation of an anionic pollutant, photodegradation of Congo-Red dye was explored and the outcomes are demonstrated in Fig. 1.

In the photolysis experiment, only 9% of Congo-Red is photodegraded, denoting that elimination of Congo-Red is poor without any photocatalyst. Also ability of the optimum nanocomposite for removal of Congo-Red in dark condition was explored. As observed, in the dark condition, the process was reached to equilibrium after 60 min and then elimination of Congo-Red without light did not show any changes.

Interestingly, highly boosted rate constant was seen for the photodegradation reaction over the NCN/CDs/BiOBr (20%)

nanocomposite, which is 22.2, 6.4, and 3.6 times as high as the CN, NCN, and NCN/CDs photocatalysts. This improved photocatalytic ability of the NCN/CDs/BiOBr nanocomposite was related to the rapid segregation of generated e^-/h^+ pairs, because the CDs act as electron mediator among NCN and BiOBr semiconductors. Therefore, considerable activity in degradation of this stable organic contaminant was observed; indicating its ability to usage in the water remediation applications.

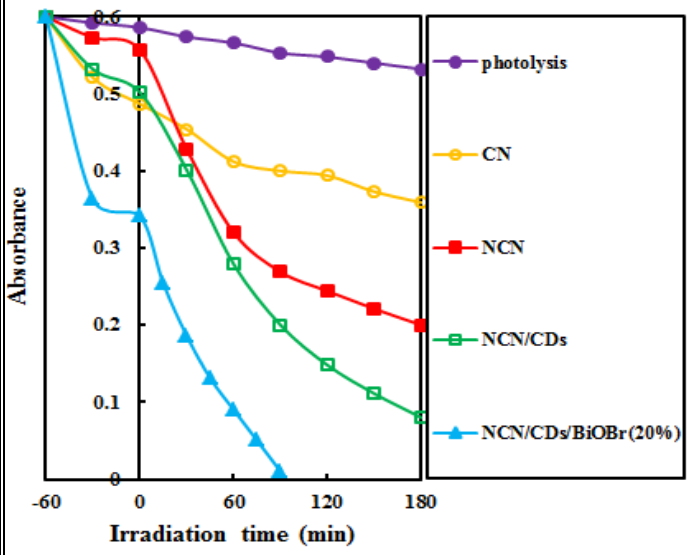

Fig.1: Photodegradation of RhB over the CN, NCN, NCN/CDs, and NCN/CDs/BiOBr photocatalysts.

IV. CONCLUSION

We synthesized the NCN/CDs/BiOBr (20%) composite through a facile refluxing approach and applied the nanocomposite to the photodegradation of Congo-Red. Also, the NCN/CDs/BiOBr (20%) photocatalyst exhibited the highest reaction rate ($k = 358.1\ min^{-1}$) and more than 99% Congo-Red was degraded after 90 min of irradiation, which can be attributed to the low recombination rate among generated e^-/h^+ pairs and impressive light harvesting ability in visible region.

REFERENCES

[1] M. Ge, J. Cai, J. Iocozzia, C. Cao, J. Huang, X. Zhang, J. Shen, S. Wang, S. Zhang, K.-Q. Zhang, Y. Lai, and Z. Lin, International Journal of Hydrogen Energy, vol. 42, pp. 8418-8449, **2017**.

[2] S.M.S. Arabi, R. Shakibaei Lalehloo, M.R. Talei Bavil Olyai, G.A.M. Ali, and H. Sadegh, Physica E: Low-dimensional Systems and Nanostructures, vol. 106, pp. 150-155, **2019**.

[3] S. Dong, J. Feng, M. Fan, Y. Pi, L. Hu, X. Han, M. Liu, J. Sun, and J. Sun, RSC Advances, vol. 5, pp. 14610–14630, **2015**.

[4] G. Mamba, and A.K. Mishra, Applied Catalysis B: Environmental, vol. 198, pp. 347–377, **2016**.

[5] S. Asadzadeh-Khaneghah, A. Habibi-Yangjeh, and K. Nakata, Journal of Colloid and Interface Science vol. 530, pp. 642-657, **2018**.

Kinetics of chemical equilibrium between adenine and its tautomers

Rahman Padash[a] ***and Shapour Ramazani***[a, *]
[a]*Department of Chemistry, Yasouj University, 75914 Yasouj, Iran.*
[*]*Corresponding author Email: ramazani@yu.ac.ir*

Abstract - In the present work, tautomeric reactions of amino−imino adenine isomer ($A_1 \rightarrow A_n$, n=2-16) are investigated in the gas phase by the mpwb95/6-31+g(d,p) level of theory. Some of these tautomers are reported for the first time. Four types of hydrogen abstraction involving (N–H→N, N–H→C, C–H→N and C–H→C) observed. rate constants and kinetic parameters (such as A, n and E_0) are calculated using the RRKM-TST theory.

Keywords: Kinetic, potential energy surface, rate coefficient, adenine, tautomer.

I. INTRODUCTION

One of the four DNA nucleobases is adenine (A), 6-amino derivative of purine, and is formed in base pairing, via two hydrogen bonds, with thymine and uracil in DNA and RNA, respectively. [1]. This base similar to other nucleoside bases (guanine, cytosine, thymine, and uracil), represents prototropic tautomerism [2, 3]. During this process all properties of adenine and its tautomers such as structure, acidity-basicity, hydrogen-bonding, redox properties, which are responsible for the structure of nucleic acids, were changed. Also, it could be effect on the replication, mutation, and degradation processes. Due to very low energy difference between some tautomers, these tautomers are converted to each other at room temperature. There are numerous tautomers for adenine [4-6] and have been investigated by theoretical and experimental methods [7, 8]. For example, Raczynska et al. [9] studied the favored and rare tautomers of neutral and redox adenine using quantum-chemical calculations. They reported tautomers for adenine in gas phase (A1, A3, A4, A5, A7, A8, A9, A11b, A13a, A14b, A15b, A18a, A19a, A20a, A21a, A22a) that are marked in this work as A16, A2, A12, A5, A8, A6, A1, A13, A7, A10, A14, A3, A4, A11 and A15 respectively. The results shown that there is a good correlation with those of the current work. Lower than room temperature, tunneling effect has a main role in the kinetics and dynamics of abstraction reactions. The high precision of tunneling calculations depends on the potential energy surface (PES) calculations [8]. With the increasing atomic mass, tunneling efficiency decreases. The reactions including heavier isotopes are slower and kinetic isotope effects (KIE) are more considerable. The PES and transition states of whole channels are presented for the first time. As well as, we suggest the mechanism of the titled reaction presented in Fig. 1, and endeavored to give a deeper grasp of the phenomena and to prepare useful instruction for experiments.

II. METHODS

In this study, the Gaussian 03 package [10] is used to perform all calculations in the gas phase.
Single-point calculations on the optimized mpwb95 geometries at the CCSD(T)/6-31g** level are carried out to obtain more accurate energies for the stationary. Frequency calculations have been carried out to determine the nature of stationary points at the mpwb95/6-31+g** level of theory.

III. RESULTS AND DISCUSSION

A. Potential energy surface

There are 14 reactions in the present paper. In this work, four types of hydrogen abstraction involving (N–H→N, N–H→C, C–H→N and C–H→C) are considered. H11, H12 and H14 are moved among the N1, N3, C4, C5, N7, C8, N9 and N10 to produce new geometries.
There are eight sites (N1, N3, C4, C5, N7, C8, N9 and N10) for hydrogen shifts (H11, H12 or H14) of A1, which product different rare tautomers. Five channels are considered for these processes. In these channels hydrogen (H11, H12 and H14) is moved from one atom to other one (N9–H14→N3), (N9–H14→C4), (N10–H12→N1), (N10–H11→C5) and (N9–H14→N1). In this work, there are seven structures with amino groups (–NH_2), and nine structures with imino groups (=NH). As well as, 21 transition states were recorded to connect these tautomers.

B. Comparison of tautomers and reactions

As seen in Fig. 1, the potential energy surface of channels 1 and 2 differ from the other reactions. So, we can divide the potential energy levels into two parts. In the first part, the stationary points have a few relative energies with respect to the reactant (A1). The reactions in this part are very important. In the next part, relative energy of the stationary points is high with respect to the reactant (A1), hence the investigation of kinetic and thermodynamic of these reactions is not really important. Because of the high activation energy of the (R3, R5–R8, R13 and R14) reactions, the probability

of these reactions is much lower than the rest. It is also shown that there are nine structures with imino group (=NH) and seven structures with amino group (–NH2). Using the PES, the energy ranking of the various adenine tautomers in the gas phase is as follows: A1<A8<A2<A14<A7<A3<A16<A11 <A6<A10<A5<A4<A15<A9<A13<A12.

The relative free energies of adenine and its tautomers and ΔG of all tautomers display that A1 is more stable than the other tautomers.

C. Rate constant calculation

The investigation of the PES is demonstrated that some of the reactions (such as R1, R8 and R14) are significant. R1, R8 and R14 reactions are two-step. In order to find the individual rate constants for R1, R8 and R14 reactions, which contain energized intermediates, the multichannel RRKM-TST [11] method are applied.

The assumption of strong collision and overestimates the rate of collisional stabilisation of the intermediates are two most important factors in the calculation of rate constants. The tunneling effect (Γ) is very important because of the hydrogen abstraction reaction. Γ is calculated by the simple expression suggested by Shavitt [12]. Fig. 2 show the Arrhenius plots of the obtained unimolecular rate constants from the RRKM theory. As represented in Fig. 2, the rate of unimolecular reaction R8 is more than the unimolecular reactions R1 and R14. Finally, the hydrogen 11, 12 and 14 were substituted with deuterium, and the primary kinetics of the isotope effect was examined. So, the rate constants of deuterium exchanged (k_1^D, k_8^D and k_{14}^D), and tunneling coefficient were calculated.

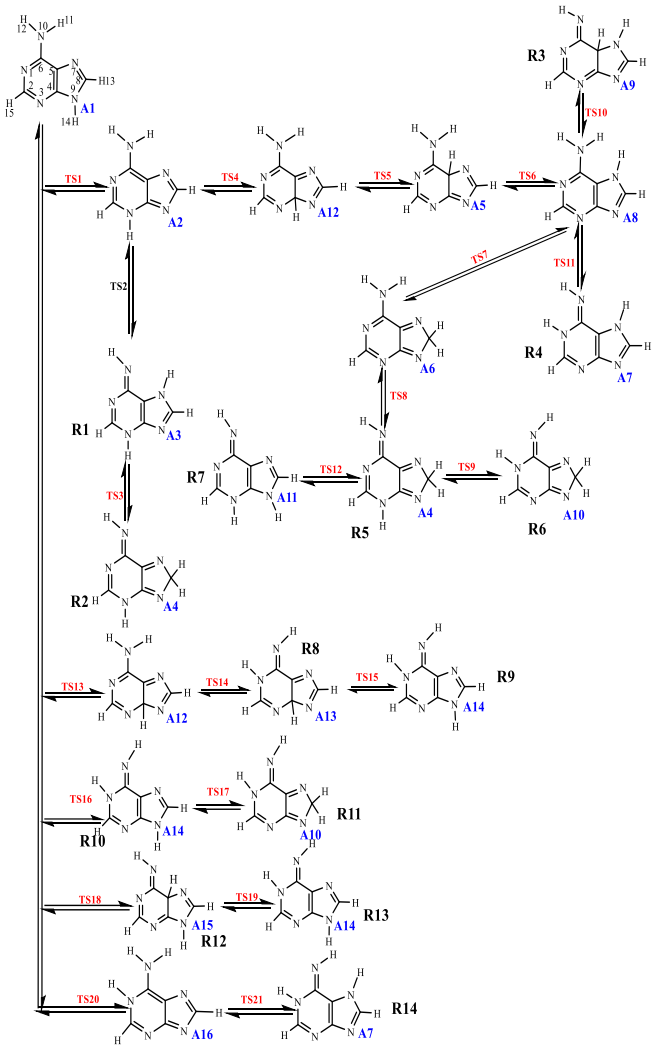

Fig.1. Isomerization diagram for tautomers of adenine.

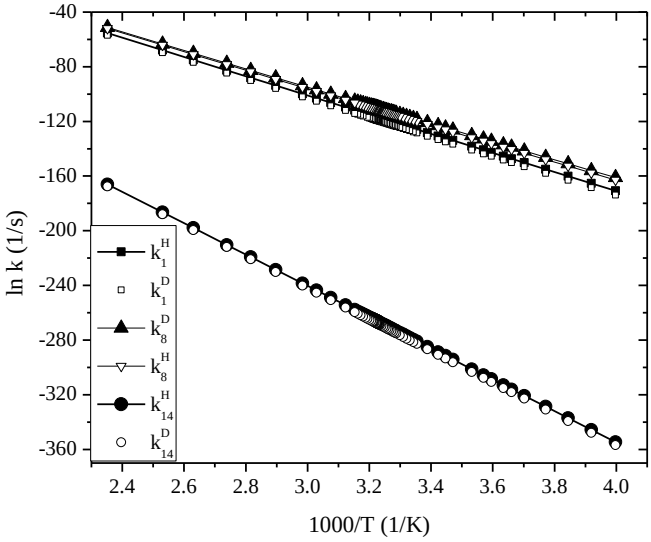

Fig.2. Arrhenius plot of the calculated rate constants

IV. CONCLUSION

In the current work, accurate set of structural parameters for adenine and its tautomers are obtained. The potential energy surfaces for the intermolecular proton transfer are determined. Using the PES, the energy ranking of the various adenine tautomers in the gas phase is A1< A8< A2< A14 < A7< A3< A16< A11< A6< A10< A5< A4< A15< A9< A13< A12. In addition, the rate constants and rate expressions for the R1, R8 and R14 reactions were reported.

REFERENCES

[1] A. W. Schwartz, C. Bakker, Science, vol. 245 ,pp. 1102-1104, **1989**.
[2] M. T. Chenon, R. J. Pugmire, D. M. Grant, R. P. Panzica, L. B. Townsend, Journal of the American Chemical Society, vol. 97, pp. 4636-4642, **1975**.
[3] T. A. Mohamed, I. A. Shabaan, W. M. Zoghaib, J. Husband, R. S. Farag, A. E. Alajhaz, Journal of Molecular Structure, vol. 938, pp. 263-276, **2009**.
[4] W. Saenger, Principles of nucleic acid structure, Springer Science & Business Media, **2013**.
[5] B. A. Cerda, C. Wesdemiotis, Journal of the American Chemical Society, vol. 118, pp. 11884-11892, **1996**.
[6] V. N. Potaman, V. N. Soyfer, Journal of Biomolecular Structure and Dynamics, vol. 11, pp. 1035-1040, **1994**.
[7] L. Tkeshelashvili, T. McBride, K. Spence and L. Loeb, Journal of Biological Chemistry, vol. 266, pp. 6401-6406, **1991**.
[8] A. Fernández-Ramos, D. G. Truhlar, J. C. Corchado, J. Espinosa-García, The Journal of Physical Chemistry A, vol. 106, pp. 4957-4960, **2002**.
[9] E. D. Raczyńska, M. Makowski, K. Zientara-Rytter, K. Kolczyńska, T. M. Stepniewsk, M. Hallmann, The Journal of Physical Chemistry A, vol. 117, pp. 1548-1559, **2013**.
[10] M. J. Frisch, G. W. Trucks, H. B. Schlegel, G. E. Scuseria, M. A. Robb, J. R. Cheeseman, J. A. Montgomery, T. Vreven, Gaussian03, (Gaussian, Inc.,Wallingford, CT, **2004**).
[11] M. R. Berman, M. C. Lin. The Journal of Physical Chemistry, vol. 87, pp. 3933–3942, **1983**.
[12] I. Shavitt, The Journal of Physical Chemistry, vol. 31, pp. 1359-1367, **1959**.

Adsorption study of Penicillin onto Single-Walled Carbon Nanotubes from Kinetics Perspective

A. Mehrizad

Department of Chemistry, Tabriz Branch, Islamic Azad University, Tabriz, Iran.

Email:mehrizad@iaut.ac.ir

Abstract: In this research, adsorption of penicillin by single-walled carbon nanotubes (SWCNTs) has been investigated from kinetics perspective. Three famous adsorption kinetics model, namely pseudo first order, pseudo second order, and Elovich models were employed to fit experimental data. Based on the results, adsorption of penicillin onto SWCNTs was well obeyed by pseudo second order model.

Keywords: Adsorption, Kinetics, Penicillin, Carbon nanotubes.

I. INTRODUCTION

Water is a precious environmental resource because it is used by nearly all living organisms; therefore, pollution of water resources may be a serious problem in all parts of the world. The pharmaceutical industry produces compounds that are toxic at trace concentrations if released to the environment in water or soil. Penicillin, selected as a model compound in the present study, is widely available in bulk drugs. It is recalcitrant and persistent towards biodegradation and is constituent intermediate of many pharmaceutical industrial effluents. The generation of penicillin containing aqueous wastes during formulation, distribution and field application of antibiotics is often unavoidable [1]. Hence, removal of penicillin from wastewater before its discharge is necessary in order to reduce this side effect on the environment and human health. In the last decade, various methods have been proposed to remove the penicillin [2-5]. The adsorption method appears to be the best strategy, especially for removal of the moderate and low concentration antibiotic compounds from effluent.

II. METHODS

In this research, the adsorption of penicillin onto single-walled carbon nanotubes (SWCNTs) was investigated by 250 mL of aqueous solution containing 10 mg/L penicillin in the range of 0-30 min. All of the experiments were done on a magnetic stirrer for a period of 30 min. Samples were withdrawn every 5 min, then filtered using filter paper. The remaining penicillin concentration was analyzed using a UV-Vis spectrophotometer (HACH-DR5000) at maximum wavelength of penicillin (λ_{max} = 255 nm).

The adsorption kinetics data were described according to the integrated rate equations of pseudo-first order, pseudo-second order and Elovich (1-3), respectively:

$$\ln(q_e - q_t) = -k_1 t + \ln q_e \quad (1)$$

$$t/q_t = 1/k_2 q_e^2 + t/q_e \quad (2)$$

$$q_t = \beta \ln(\alpha\beta) + \ln t \quad (3)$$

where q_e and q_t are the amount of penicillin adsorbed (mg/g) at equilibrium and time t (min). k_1 (1/min) and k_2 (g/mg.min)

are the pseudo-first and pseudo-second order rate constants, respectively. α is the initial adsorption rate (mg/g.min) and β is the desorption constant during each experiment (g/mg).

III. RESULTS AND DISCUSSION

The results of the kinetics parameters for penicillin adsorption by SWCNTs are listed in Table 1.

Table1: Kinetics parameters for penicillin adsorption onto SWCNTs

Kinetics model	Kinetics parameters and these values	
pseudo-first order	$q_{e,cal}$ (mg/g)	9.584
	k_1 (1/min)	0.107
	R^2	0.805
pseudo-second order	$q_{e,cal}$ (mg/g)	19.193
	k_2 [g/(mg.min)]	0.027
	R^2	0.995
Elovich	α [mg/(g.min)]	523.327
	β (g/mg)	1.764
	R^2	0.844

According to Table 1, the coefficient of determination, R^2, for the pseudo-second order adsorption model has a high value (>0.99), and its calculated equilibrium adsorption capacity ($q_{e,cal}$) is consist with experimental data ($q_{e,exp}$=18.445 mg/g). These facts suggest that the pseudo-second order adsorption mechanism is predominant.

IV. CONCLUSION

In this paper, adsorption of penicillin onto **s**ingle-**w**alled **c**arbon **n**anotubes from aqueous solutions was studied. Three famous adsorption kinetics model, namely pseudo first order, pseudo second order, and Elovich models were employed to fit experimental data. Based on the results, adsorption of penicillin onto SWCNTs was well obeyed by pseudo second order model.

REFERENCES

[1] Ania, C.O., Pelay o, J.G. & Bandosz, T. J. (2011). Reactive adsorption of penicillin on activated carbons. *Adsorption* 17, 421–429. DOI: 10.1007/s10450-010-9271-9.

[2] Choi, K.J., Kim, S.G. & Kim, S.H. (2008). Removal of antibiotics by coagulation and granular activated carbon Filtration. *J. Hazard. Mater.* 151, 38–43. DOI: 10.1016/j.jhazmat. 2007.05.059.

[3] Al-Ahmad, A., Daschner, F.D. & Kummerer, K. (1999). Biodegradability of cefotiam, ciprofl oxacin, meropenem, penicillin G, and sulfamethoxazole and inhibition of waste water bacteria. *Arch. Environ. Contam. Toxicol.* 37, 158–163. DOI*:* 10.1007/s002449900501.

[4] Zümriye, A. & Özlem, T. (2005). Application of biosorption for penicillin G removal: comparison with activated carbon. *Process Biochem.* 40, 831–847. DOI: 10.1016/j.procbio.2004.02.014.

[5] Chaubal, M.V., Payne, G.F., Reynolds, C.H. & Albright, R.L. (1995). Equilibria for the adsorption of antibiotics onto neutral polymeric sorbents: Experimental and modeling studies. *Biotechnol. Bioeng.* 47, 215–226. DOI: 10.1002/bit.260470213.

Equilibrium and Kinetic Study of 4-Nitrophenol Removal by Modified Silk Waste

Parvin Gharbani

Department of chemistry, Ahar Branch, Islamic Azad University, Ahar, Iran
Email: parvingharbani@yahoo.com, p-gharbani@iau-ahar.ac.

Abstract: In this research, silk waste was modified by H_2SO_4 and used as an adsorbent to remove of 4-nitrophenol from aqueous solutions. After preparing of adsorbent, the adsorption experiments were down in a batch system in an erlenmeyer flask under various conditions such as different initial concentrations of 4-nitrophenol (10, 20, 30, 40, 50 mg/L), pH (3, 7, 10), dosage of modified silk waste (0.5, 1, 1.5, 2, 2.5 g/50 mL), temperature (20, 30, 40 °C) and contact time. Data revealed that adsorption of 4-nitrophenol onto modified silk waste was reached equilibrium at 40 min. Also, results have shown that, the removal of 4-nitrophenol decreased with increasing of pH and initial concentration of 4-nitrophenol and increased by increasing of modified silk waste dosage. Also, obtained data confirmed that the increasing of temperature has negative effect on adsorption of 4-nitrophenol onto modified silk waste. Pseudo-first-order and pseudo-second-order equations were used to determine the kinetics of adsorption process. The analysis of kinetics models showed that the pseudo-second-order adsorption mechanism is predominant. Langmuir, Freundlich and Temkin isotherm models were studied. The results indicated the adsorption of 4-nitrophenol onto modified silk waste could be well fitted with the Langmuir isotherm model.

Keywords: Kinetic, 4-nitrophenol, Silk, Adsorption, Isotherm

I. INTRODUCTION

Phenols are highly important, well known and widely used compounds in different fields of the chemical industry. This group of compounds found its application in the Plastics and plasticizers, explosive, drugs, colors and detergents. Different substituted phenols are included among herbicides, insecticides, algaecides, bactericides, molluscicides, fungicides, etc. 4-nitrophenol is a toxic and hazardous compound and exhibits mutagenic and carcinogenic signs in humans and animals [1]. The removal of 4-nitrophenol from contaminated groundwater was studied by a heterogeneous nano-iron [2], catalytic ozonation [3], Iron silicate/ ozonation [4] and ozone [5]. Adsorption is a simple and cheap method to remove the pollutants. Various adsorbents were used to removal of 4-nitrophenol from aqueous solutions [6].

This study aims to investigate the modified silk waste efficiency to remove of 4-nitrophenol from aqueous solutions. In addition, the effect of contact time, initial 4-nitrophenol concentration, pH, modified silk waste dosage, and temperature were studied. Also, kinetic and equilibrium isotherms were analysed.

II. METHODS

All used chemicals were purchased from Merck compony. Experiments were done in a batch system in a 50 mL Erlenmeyer on the shaker. The efficiency of modified silk waste on removal of 4-nitrophenol was studied as a function of the initial 4-nitrophenol concentration, pH , modified silk waste dosage and different temperatures . The samples were shaken at 140 rpm, and a sampling was taken every 5 min. Then it was filtered and the 4-nitrophenol concentration was recorded by using a UV-Vis spectrophotometer (HACH-DR5000) at maximum absorption wavelength

III. RESULTS AND DISCUSSION

The results of 4-nitrophenol removal from aqueous solutions using modified silk waste are as following:
Decreasing of pH from 10 to 3 lead to increase of 4-nitrophenol removal from 55.06% to 67.70%.

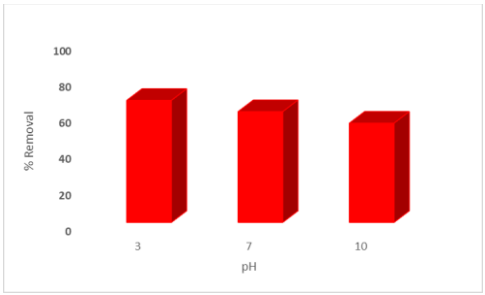

Fig. 1 Effect of pH

Varying the initial concentrations of 4-nitrophenol shows that increasing of initial concentrations due to low yield in 4-nitrophenol removal efficiency. As already known, there are limited vacant sites for adsorption; hence, by increasing 4-nitrophenol molecules, the sites were full and the adsorption was dropped [7].

Increasing the modified silk waste dosage leads to increasing adsorption of 4-nitrophenol. Raising adsorption by increasing the adsorbent dosage can be related to an increase in the surface area and the availability of more adsorption sites [8-9].

Results demonstrated that the temperature has a negative effect on removal of 4-nitrophenol.

Table 1 represents the Langmuir, Freundlich and Temkin isotherm constants. As shown earlier, the Langmuir isotherm is best fitted with the experimental data (R2=0.995), and it can be concluded that the Langmuir model is a suitable isotherm to describe the adsorption equilibrium of 4-nitrophenol onto modified silk waste.

Table 1: Constants of the linear form of the Langmuir, Freundlich and Temkin isotherms of 4-nitrophenol adsorption onto modified silk waste.

Langmuir			**Freundlich**			**Temkin**
qm	KL	R	Kf	n	R2	B1
KT	R2					
9.28	0.45	0.995	0.96	0.59	0.98	4.203
0.560	0.990					

Competing R^2 (Fig. 2) values show that the pseudo second-order adsorption model has a higher regression and adsorption of 4-nitrophenol onto modified silk waste obeyed pseudo second-order kinetics. In fact, adsorption rates of 4-nitrophenol onto modified silk waste can be more appropriately described by using the pseudo second-order rate, and it can be deduced that the adsorption rate was increased twice by increasing the 4-nitrophenol concentration.

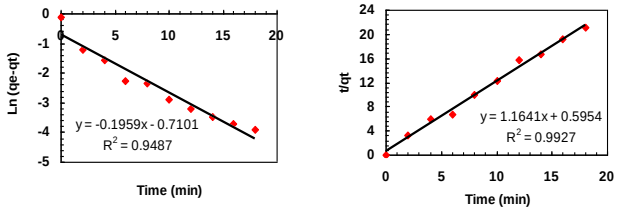

Fig. 2 Pseudo first order (left) and Pseudo second order (right) kinetic plot for adsorption of 4-nitrophenol onto modified silk waste.

IV. CONCLUSION

The results of 4-nitrophenol removal by modified silk waste confirm that adsorption depended on the 4-nitrophenol initial concentration, modified silk waste dosage, pH, and temperature. The maximum removal of 4-nitrophenol was about 69.59% at 50 mg/L of the 4-nitrophenol concentration at pH=3, T= 25°C, and 2 g/ 50 ml of adsorbent . Also, the adsorption followed the Langmuir isotherm and pseudo second-order kinetics. As a result, Modified silk waste can be applied as a performance adsorbent to remove 4-nitrophenol from aqueous solutions

REFERENCES

[1] H. Bao, J. Gao, Y. Liu and Y. Su, *Phys. Chem*., vol. 78, pp. 1137-1142, **2009** .

[2] B. Li and J. Zhu, *Chem. Eng. J*. vol. 255, pp. 225-231, **2014**.

[3] Z. Chen, Z.Z. Xu, Y. Ben, MM. Ye, X.H. Ma, J. Huan, and X. Ke,, vol. 28, pp. 2550, **2007**.

[4]Y. Liu, L. Liu, L and W.J. Gong, *Adv. Mat. Res.*, vol. 955, pp. 2162-2169, **2014**

[5]S. Li, Y. Zhu, X. Li, G. Wang and L. Ni, *Bull. Environ. Contam. Toxicol*., 87, pp. vol. 297-302, **2011**.

[6]O. Yavuz and A.H. Aydin, A.H. Pol. J. Environ. Stud, 51, 155. . **2006**

[7] U.R. Lakshmi, U.R., V.C. Srivastava, I.D. Mall and D.H. Lataye, J. Environ. Manage.,vol. 90, pp. 710-716, **2009.**

[8] A. Mehrizad, K. Zare,, H. Aghaie and S. Dastmalchi, Int. J. Environ. Sci. Tech. , vol. 9, pp. 355-361, **2012**

[9] T Akar, I. Tosun, Z. Kaynak, E. Kavas, G. Incirkus and S.T. Akar, J. Hazard. Mater. Vol. 171, pp. 865-871, **2009**

Collision Processes, Dynamic Parameters, Temperature Dependence of the Collisional Rate Coefficients of *NH + OH* and Deuterated Analogues on an Interpolated Potential Energy Surface

Raziyeh Sharafdini* and *Shapour Ramazani*

Department of Chemistry, Yasouj University, 7493475918 Yasouj, Iran

Email: ramazani@yu.ac.ir

Abstract: In this research, we report an interpolated potential energy surface (PES) from ab initio electronic energy of molecular fragments for NH + OH reaction and isotopic substitution. Classical trajectory simulations were performed on this surface to determine reaction probabilities and reaction cross sections for various channels. Nonlinear least squares fitting was applied to compute rate constants expressions and compute them as a function of the cross section.

Keywords: Cross section, Isotopic substitution, Potential energy surface (PES), Rate constant, Reaction probability

I. INTRODUCTION

Investigation of chemical reactions of nitrogen compounds in combustion chemistry is of great importance because nitrogen species derived from combustion reactions have an important role in air pollution. *NH and OH* radicals are two important reactive species in the combustion chemistry and in atmospheric processes. *NH* radical has a significant role in the oxidation of nitrogen combinations; for example in the reduction of NO in thermal NOx processes [1-3]. In this work, we investigate R1 to R4 reaction and isotope substituted analogues that as shown: $\cdot NH + \cdot OH \rightarrow$ products (R1), $\cdot ND + \cdot OH \rightarrow$ products (R2), $\cdot NH + \cdot OD \rightarrow$ products (R3), $\cdot ND + \cdot OD \rightarrow$ products (R18).

II. METHODS

Collins introduced a method (Growing program) to construct molecular PES with classical trajectory simulations. The Grow methodology was developed PES by a modified Shepard interpolation method [4,5].

$$E(\boldsymbol{Z}) = \sum_{i=1}^{N_{data}} w_i(\boldsymbol{Z}) T_i(\mathbf{Z}) \quad (1)$$

$$T_i(\boldsymbol{Z}) = V[\boldsymbol{Z}(i)] + \sum_{k=1}^{3N-6}[Z_k - Z_k(i)]\frac{\partial V}{\partial Z_k} + \frac{1}{2!}\sum_{k=1}^{3N-6}\sum_{j=1}^{3N-6}[Z_k - Z_k(i)] \times \left[Z_j - Z_j(i)\right]\frac{\partial^2 V}{\partial Z_k \partial Z_j} + \cdots \quad (2)$$

where $T_i(\mathbf{Z})$ is second order Taylor expansion for energy around each data point and the weights $w_i(\boldsymbol{Z})$ is a function of distance coordinates Z with regard to the data point configuration $\boldsymbol{Z}(i)$. Gaussian 03 program was used to optimize stationary points at MP2/6-311++G(d,p) and single point calculations were carried out at CCSD(T)/6-311++G(d,p).

III. RESULTS AND DISCUSSION

Figure 1 illustrates the total reaction probability as a function of the data set size. As it was seen, the final PES was interpolated over a data set of 1800 points. The velocity of molecules during collision has a great effect on the reaction rate reaction so that cross section were increased with increasing the translational energy (Fig. 2). A significant recent theoretical development is direct methods for evaluating rate constant. According to the collision theory, the reaction rate constant can be calculated as a function of reaction cross section, $\sigma(E)$, at temperature T by:

$$k(T) = a\left(\frac{8}{\pi\mu}\right)^{1/2}\Gamma(\gamma+2)(k_B T)^{\gamma+1/2} \quad (3)$$

for all reactions, nonlinear least-squares fitting was used to evaluate cross section expressions and rate constants $k(T)$ reported in Table 1 and Fig. 3.

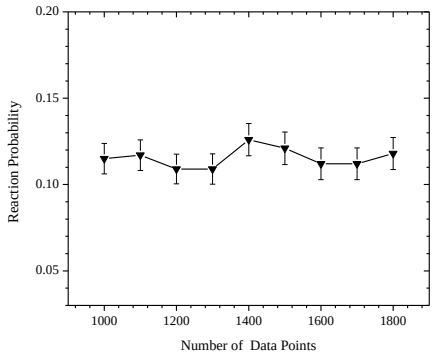

Fig. 1. The calculated reaction probability was presented as a function of the size of data points for (R1) reaction. The initial relative translational energy was 39.40 kJ mol^{-1}.

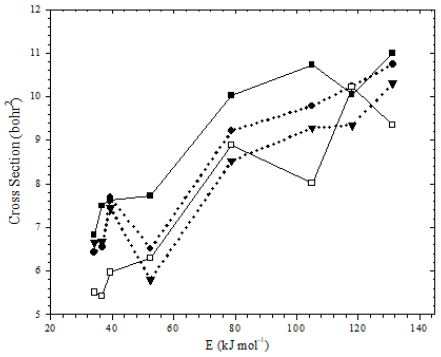

Fig. 2. The total reaction cross section was determined as a function of relative translation energy for (R1) reaction (—■—), (R2) reaction (…●…), (R3) reaction (…▼…) and (R4) reaction (—□—).

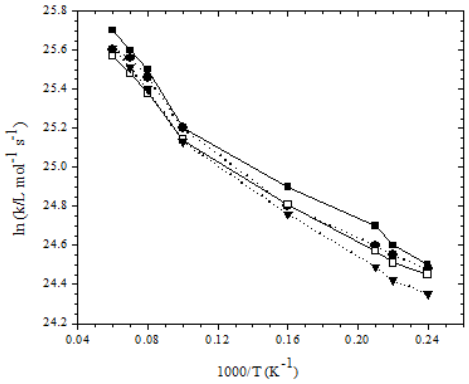

Fig. 3. Arrhenius plot of the calculated total rate constant for R1 reaction (—■—), R2 reaction (…●…), R3 reaction (—□—), R4 reaction (…▼…).

IV. CONCLUSION

An interpolated potential energy surface from *ab initio* electronic energy of molecular fragments for *NH + OH* reaction and deuterated analogs is reported. This surface was used to determine reaction cross sections as a function of translation energy of fragments. Also, the valuation rate constant reported.

Table 1. The fitted parameters using $\sigma(E) = a\,E^{\gamma}$ for the (R1) to (R4) reactions in which E_{tr}= 36.76-131.30 kJ mol^{-1}.

	a	γ	$\Gamma(\gamma+2)$	$k\,(T)(lit.mol^{-1}.s^{-1})$
(R1)	1.90	0.36	1.20	$3.5\times10^{7}\times T^{0.8628}$
(R2)	1.73	0.37	1.20	$3.0\times10^{7}\times T^{0.8728}$
(R3)	2.0	0.33	1.19	$4.2\times10^{7}\times T^{0.8278}$
(R4)	1.19	0.43	1.27	$1.6\times10^{7}\times T^{0.9318}$

REFERENCES

[1] J. A. Miller and R. J. Kee, J. Annu. Rev. Phys. Chem. 41, 345**, 1990.**
[2] J. A. Miller and C. T. Bowman, J. Prog. Energ. Combust. Sci. 15, 287, **1989**.
[3] S. P. Walch, J. Chem. Phys. 99, 3804, **1993.**
[4] M. A. Collins, Theor. Chem. Acc. 108, 313, **2002**.
[5] K. C. Thompson, M. J. T. Jordan, and M. A. Collins, J. Chem. Phys. 108, 8302, **1998**.

Theoretical Dynamics Study of Cytosine Tautomerism in the Gas Phase and Interaction of Na^+ With Its Tautomers

Raziyeh Sharafdini* and Shapour Ramazani

Department of Chemistry, Yasouj University, Yasouj, Iran

Email: ramazani@yu.ac.ir

Abstract: The present study is an investigation of theoretical dynamics of cytosine tautomerism in the gas phase. MP2/6-311G(d,p) calculation have been carried out to investigate twenty two cytosine tautomers so that some of them have been reported for the first time. C_3 and C_{20} are the most stable tautomers in gas phase. Interaction of cytosine tautomers with Na^+ metal cation have been studied using MP2/6-31G(d,p). Three types of interaction of metal cations with cytosine tautomers have been investigated. The interaction between metal cation with both nitrogen and oxygen in which the lone pair of nitrogen is located close to the lone pair of oxygen. The second type of interaction is metal cation with a lone pair of nitrogen or oxygen. Third, the interaction between metal cation with two nitrogens.

Keywords*:* cytosine, gas phase, Interaction, metal cation, stabilization energies, tautomerism.

I. INTRODUCTION

Cytosine is one of the most common bases of DNA. Importantly, cytosine exists in various tautomeric forms in an equilibrium and the equilibrium is strongly sensitive to the interaction of these molecules with their environment. The effect of environment on tautomeric equilibria can shift equilibrium constants very much. Tautomerism is relevant to the behavior of nucleic acids and amino acids in which tautomers may be have biological role in base mispairing and mutagenesis. Mispairing may lead to a point mutation eventuall. Interactions of nucleic acid bases with metal cations influenced properties of normal structure of DNA and mutations may occur in the pairing of cytosine with other bases and tuatomeris of cytosine [1-3].

II. METHODS

Gaussian 03 program was used to optimize stationary points at MP2/6-311G(d,p) //CCSD(T)/6-311G(d,p). Also, all complexes formed in interaction between cytosine tautomers with Na^+ metal cation were optimized at MP2/6-31g(d) level in the gas phase and their frequency calculations were calculated at mpwb95/6-31g(d) level so that all the harmonic frequencies were specified to be real.

III. RESULTS AND DISCUSSION

All 20 reactions under review include hydrogen abstraction. Actually, three types of hydrogen abstractions are observed (N–H→O, N–H→C, N–H→N) so that N–H→C hydrogen abstractions in cytosine tautomers have been reported for the first time. relative stability order of cytosine tautomers in the gas phase are C_3, C_{20} > C_6 > C_1 > C_2 > C_{17} > C_4 > C_5 > C_{10} > C_{18} > C_7 > C_{16} > C_9 > C_{19} > C_{21}> C_{12} > C_{11} > C_8 > C_{14} > C_{22} > C_{15} > C_{13}. C_3 and C_6 (enol form) are more stable than C_1 (keto form) about 7.16 and 4.39 kJ/mol. The most stable tautomers are shown in Fig. 1 and Table 1.

In present work, we prepared 41 complexes to study interaction of Na^+ cation with tautomers of cytosine in the gas phase at the MP2/6-31g(d) level to investigate the stability of complex in which some of them have been studied for the first time. Different structures for desired interactions studied so that there is one interaction between Na^+ with both C=O group and nitrogen ($[C_1Na^+]_1$) and it is the most stable complex (Fig. 2).

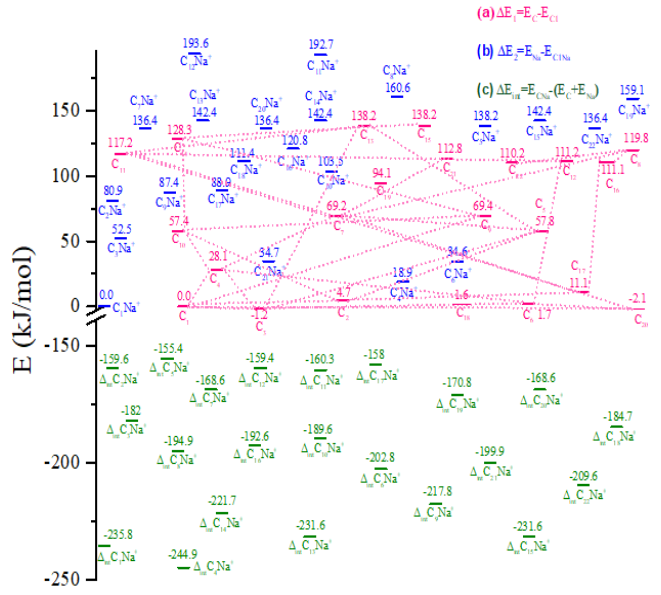

Fig. 1. Isomerisation diagram for cytosine tautomers.

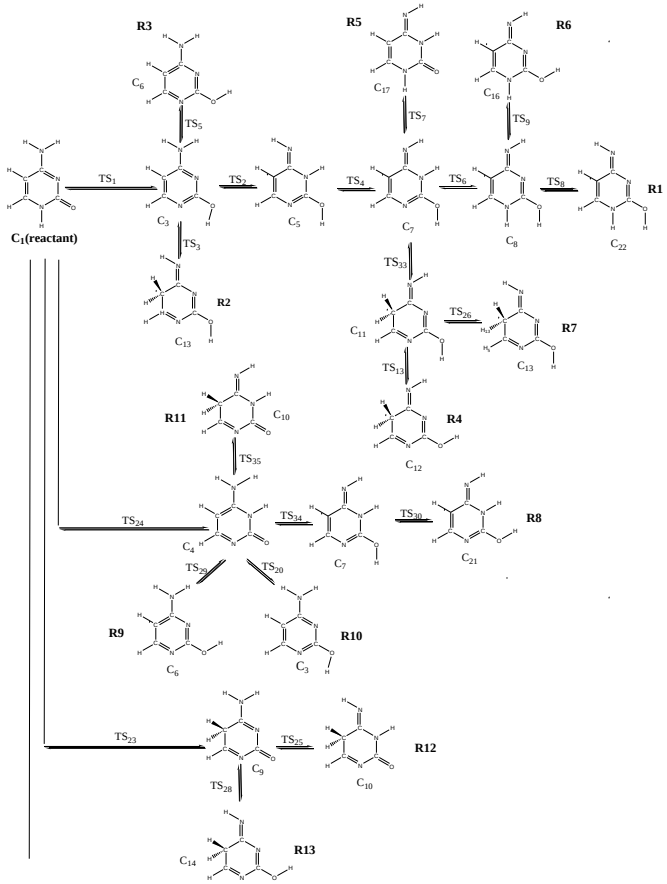

Fig 2. Relative energies of cytosine tautomers and their complexes with Na^+ cation for at MP2/6-31G(d) level.

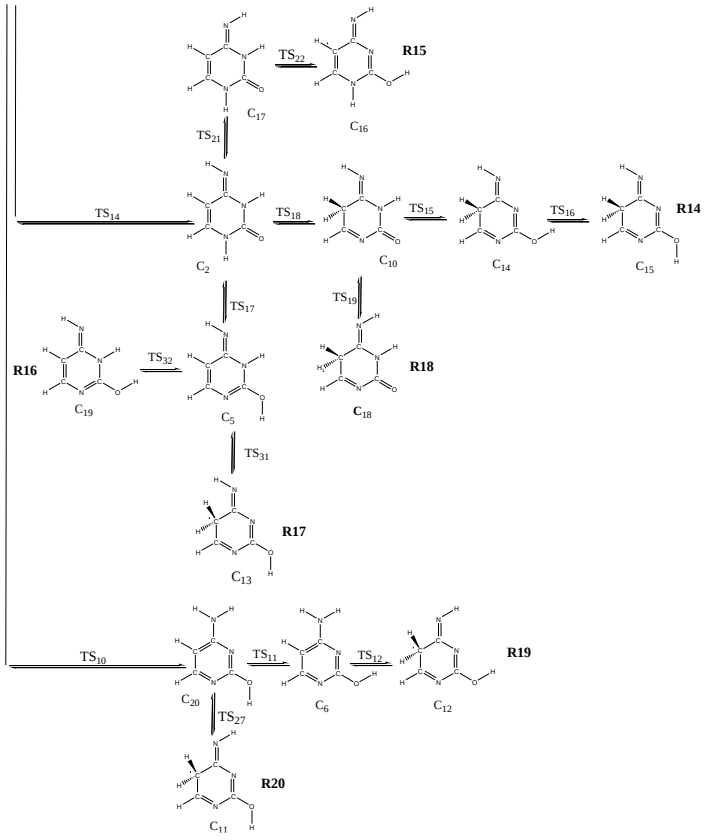

Table 1. Calculated relative energies of optimized structures

at different levels in kJ/mol in gas phase.

Isomer	MP2	CCSD(T)	ZPE
C_1	0.00	0.00	266.39
C_2	3.39	0.38	267.06
C_3	-8.91	-7.16	267.04
C_4	28.36	27.93	265.40
C_5	48.24	44.59	266.69
C_6	-6.04	-4.39	266.85
C_7	59.92	55.84	265.94
C_8	107.99	100.40	264.67
C_9	77.70	67.55	262.20
C_{10}	65.46	53.16	263.53
C_{11}	116.67	99.98	263.41
C_{12}	110.96	95.04	263.84
C_{13}	136.76	120.47	263.14
C_{14}	127.64	112.15	263.67
C_{15}	136.76	120.46	263.14
C_{16}	135.03	62.75	265.80
C_{17}	10.24	6.80	266.63
C_{18}	68.41	55.80	263.05
C_{19}	83.19	79.09	264.98
C_{20}	-8.90	-7.16	267.04
C_{21}	98.62	91.11	263.89
C_{22}	125.93	118.37	264.09

.

IV. CONCLUSION

In the present study, we investigated 22 tautomers of cytosine so that 8 tautomers have been studied for the first time which is corresponding to hydrogen transfer from nitrogen to carbon. Our investigations have been done in gas phase. The relative stability order of cytosine tautomers in the gas phase are C3, $C_{20} > C_6 > C_1 > C_2 > C_{17} > C_4 > C_5 > C_{10} > C_{18} > C_7 > C_{16} > C_9 > C_{19} > C_{21} > C_{12} > C_{11} > C_8 > C_{14} > C_{22} > C_{15} > C_{13}$. $\Delta E_3 = E_{[CNa^+]} - \left(E_{[C]} + E_{Na^+}\right)$ so that all complexes are more stable than interaction cytosine and tautomers with Na^+ cation because ΔE_3 is negative and corresponding to it, interaction between Na^+ cation and lone pairs of N1 and O10 or N3 and O10 make stable complexes.

REFERENCES

[1] S. A. Trygubenko, T. V. Bogdan, M. Rueda, M. Orozco, F. J. Luque, J. Sponer, P. Slavcek and P. Hobza, Phys. Chem. Chem. Phys. 4, 4192, **2002**.

[2] L. Antonov, Tautomerism: Methods and Theories (1st ed.). Weinheim: Wiley-VCH (2013).

[3] M. Kabelac, P. Hobza, J. Phys. Chem. B 110, 14515, **2006**.

Isotherm and Kinetic Studies on the Bi(III) Extraction from Hydrochloric Acid Media by a Polymer Inclusion Membrane Containing Trioctylamine

***N. Ghaderi*[a], *L. Dolatyari*[b], *D. Kazemi*[a], *M. R. Yaftian*[a]*, *H. Shayani Jam*[a]**
[a]*Department of Chemistry, The University of Zanjan, Zanjan, 45371-38791, Iran.*
[b]*Department of Chemistry, Zanjan Branch, Islamic Azad University, Zanjan, Iran.*
Email: yaftian@znu.ac.ir

Abstract*:* Polymer inclusion membranes (PIMs) containing cellulose triacetate (CTA) as the polymer matrix, trioctylamine (TOA) as extractant, and tributhyl phosphate (TBP) as the plasticizer were fabricated and characterized. The prepared membrane was used for the extraction of Bi(III) from hydrochloric acid medium. The optimized PIM composition was CTA (40%w/w), TOA (25% w/w) and TBP (35% w/w). Sorption isotherm experiments were carried out and modeling of the data was realized by applying the Langmuir, Freundlich, and Dubinin Radushkevich (D-R) isotherm models. The sorption kinetic was well described by the pseudo-second order model. The kinetic and isotherm experiments confirm that the extraction process of Bi(III) into the optimal CAT/TOA/TBP PIM is a chemisorption process.

Keywords: Bi(III), Extraction, Isotherm, Kinetic, Polymer Inclusion Membrane.

I. INTRODUCTION

Membrane-based separation methods are proposed as alternatives to the solvent extraction-based processes, which are used extensively in many industries [1]. This stems from the fact that membrane systems have selectivity, flexibility and enrichment properties like traditional solvent extraction but do not need large volumes of volatile, toxic and flammable solvents [2]. Main types of liquid membrane techniques include bulk liquid membranes (BLM), emulsion liquid membranes (ELM), supported liquid membranes (SLM), and polymer inclusion membranes (PIMs). Among these methods PIMs are the most recent and are proved to be extremely attractive for application to a wide range of separation problems. PIMs are thin and flexible films that are formed by casting an organic solution containing an extractant, a base polymer and, if necessary, a plasticizer [3].

This communication concerns on the isotherm and kinetic studies of the extraction process of Bi(III) from acid chloride medium by a newly development PIM including cellulose triacetate (CTA) base polymer, tri-*n*-octylamine (TOA) as extractant and tributyl phosphate (TBP) as plasticizer. The Langmuir, Freundlich and Dubinin Radushkevich isotherm models have been examined for describing the equilibrium data. In order to study the kinetic of the process, pseudo-first order, pseudo-second order, Elovich and intra-particle diffusion equations were applied.

II. METHODS

The PIMs were prepared by dissolving the membrane components in dichloromethane. This solution poured into a petri dish and allowed the solvent to evaporate. The physicochemical properties of the PIMs were investigated by measuring their weight, thickness, water contact angle, strain strength, FT–IR, TGA, FESEM and AFM analyses. Extraction experiments were performed by immersing a round disk of the PIM in a hydrochloric acid solution containing Bi(III). For the back-extraction step, the loaded PIM was immersed in a sodium carbonate solution (2 M). The analysis of metals was done by an atomic absorption spectrometer.

III. RESULTS AND DISCUSSION

It was found that the membrane including 40 wt% of CTA, 25 wt% TOA and 35 wt% of TBP were transparent, flexible and homogenous. The average mass and thickness of these PIMs were 0.0618±0.008 g and 0.062±0.009 μm, respectively. The FESEM image of the optimal composition PIM showed a uniform and homogenous surface and appear dense with no obvious porosity. The AFM image revealed the roughness of the membrane surface increases with addition of the extractant (TOA) to the blank membrane. The strain-stress curves indicated that elastic behavior of the studied PIM is more than the CTA blank film. The optimized PIM was able to efficiently extract Bi(III) in 60 min from hydrochloric acid solution. It was suggested that the presence of hydrochloric acid promoted the formation of $BiCl_5^{2-}$, which was the main species extracted via an ion pair mechanism with protonated TOA. The loaded PIMs could be quantitatively back-extracted with 2 M Na_2CO_3. The

developed PIM was stable for four extraction/back-extraction cycles.

The extraction data were fitted to different sorption isotherms such as Langmuir, Freundlich, and Dubinin Radushkevich (D-R) isotherm models [1,4]. The results showed that the fittings the Langmuir model describe suitably the experimental data (Fig. 1a). The calculated value of the isotherm parameter "separation factor" ($0<R_L<1$) indicated that the extraction process is favorable. According to this model maximum capacity of the developed PIM was found to be 73.5 mg bismuth/g PIM which was close to that obtain from experimental data (73 mg bismuth/g PIM).

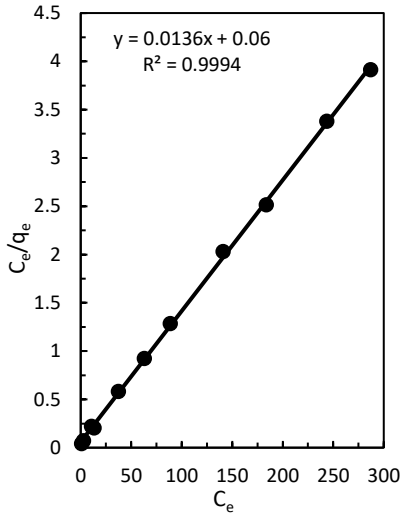

(a)

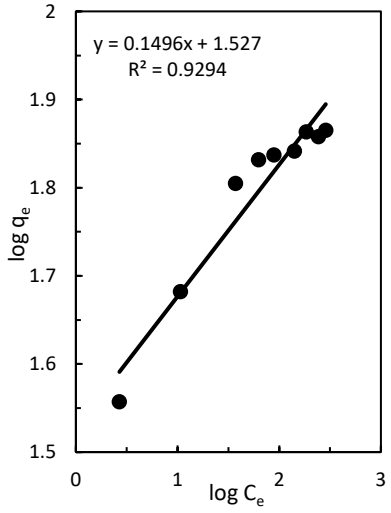

(b)

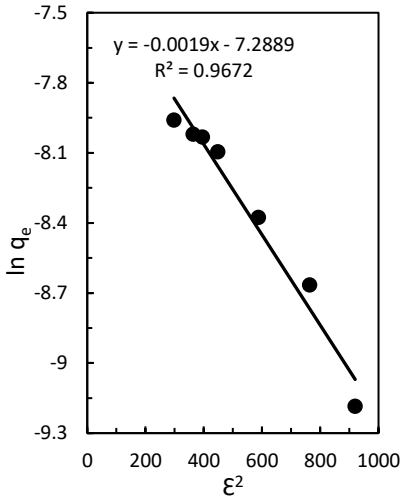

(c)

Fig.1. Adsorption isotherms fitting using a) Langmuir model, (b) Freundlich model, and c) D-R model in Bi(III) extraction by using CTA/TOA/TBP membrane.

The Freundlich constant parameter "1/n" that was lower than 1, and the value of energy "E" (kJ/mol), calculating from D-R model, was >8, revealing a favorable sorption process with chemical nature (Figs. 1b and 1c).

In order to investigate the controlling mechanism of the studied sorption process, four different kinetic models: pseudo-first order, pseudo-second order, Elovich and intra-particle diffusion model were tested [4,5]. The evaluated R^2 values (0.9969) obtained from the least squares lines allow considering the best fitting of the experimental data with those predicted by the pseudo-second order kinetic model. The comparison of the evaluated adsorption capacity based on the application of the pseudo-second order equation (17.2 mg bismuth/g PIM) and that found experimentally (14.5 mg bismuth/g PIM) reconfirms also the validity of this conclusion. This kinetic model suggests that chemisorption is the rate-limiting step.

IV. CONCLUSION

CTA/TOA/TBP PIM was fabricated and the AFM and FESEM images showed its heterogeneous structure and almost uniform distribution of the extractant in the PIM. The batch uptake results indicated that the PIM with the composition 40% w/w CTA, 25% w/w TOA and 35% w/w TBP can efficiently extract the Bi(III) ions in 60 min from aqueous hydrochloric acid solution. The analyses of the extraction data were well fitted by the pseudo-second order

model and Langmuir sorption isotherm model. Both of these models confirmed that the process followed a chemisorption mechanism.

REFERENCES

[1] B. N. Mahanty, P. K. Mohapatra, D. R. Raut, D. K. Das, P. G. Behere, and Md Afzal, Ind. Eng. Chem. Res., vol. 12, pp. 3237-3246, **2015.**

[2] M. I. G. S. Almeida, R. W. Cattrall, and S. D. Kolev, Anal. Chim. Acta, vol. 987, pp. 1-14, **2017**.

[3] M.R. Yaftian, M. I. G. S. Almeida, R. W. Cattrall, and S. D. Kolev, J. Membr. Sci., vol. 545, pp. 57-65, **2018**.

[4] L. Dolatyari, M.R. Yaftian, and S. Rostamnia, J. Environ. Manage, vol. 169, pp. 8–17, **2016**.

[5] C.V. Gherasim, G. Bourceanu, and D. Timpu. Chem. Eng. J., vol. 172, pp. 817-827, **2011**.

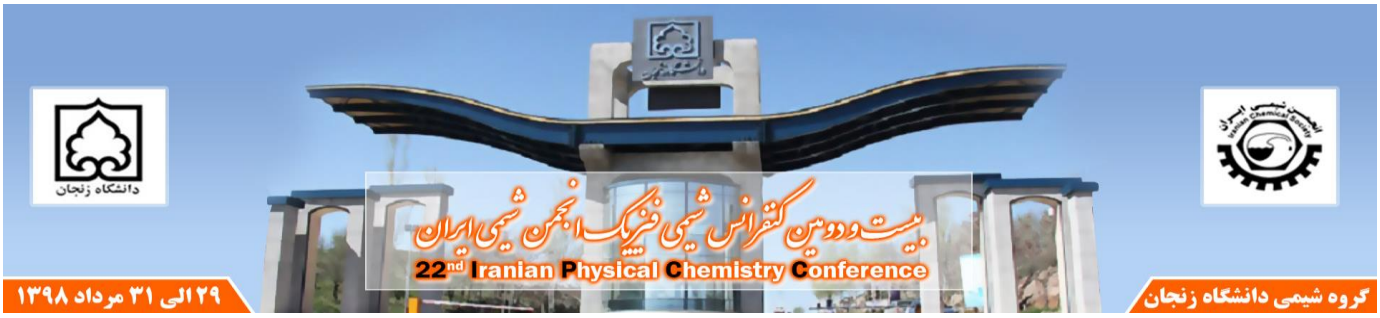

Dynamic and Kinetic Parameters of NH + H_2 Reaction on an Interpolated Potential Energy Surface

Rahman Padash [a] ***and Shapour Ramazani*** [a, *]
[a] *Department of Chemistry, Yasouj University, 75914 Yasouj, Iran.*
[*] *Corresponding author Email: ramazani@yu.ac.ir*

Abstract - Collision of NH radical with H_2 molecule was studied on an interpolated potential energy surface using ab-initio calculation. The classical trajectory was studied on this surface to determine the reaction probability. Reaction probability was used to calculate others observable properties like rate constant and cross section. Nonlinear least-squares ftting was also used to calculate the rate constants expressions.

Keywords: Reaction dynamics, Cross section, Reaction probability, Imidogen radical

I. INTRODUCTION

Due to severe environmental contamination caused by the ignition of nitrogenous compounds, the dynamics of these compounds in combustion have been the subject of intense experimental and theoretical research. The ammonia pyrolysis reaction has a significant role in combustion because of containing radical reactions. In a study, Imidogen radical NH was produced in its ground electronic state ($X^3\Sigma$) by thermal dissociation of ammonia [1, 2].

Imidogen radical NH plays a significant role in combustion processes. For example, NH radical is an important intermediate in producing NO and nitrogen atom, and also combustion reactions in the air [3]. As well as, the imidogen radical NH is one of the major components discovered in interstellar clouds, stars, and blazing stars [1, 2]. Another importance of NH reactions is in reburning processes [4] and techniques; e.g., thermal de-NO_x reactions for NO reduction in the combustion process [5]. Although imidogen radicals in the ground state are very reactive species, their reaction rate when reacting with stable molecules such as H_2, H_2O and CO_2 is very slow (particularly at low temperatures) [2, 6]. The reaction $NH(X^3\Sigma^-) + H_2\ (X^1\Sigma) \rightarrow NH_2(X^2B) + H(^2S)$, where $\Delta H^0_{298} = 50 \pm 2$ kJ mol^{-1}, has been widely investigated both experimentally and computationally [7]. Rohrig and Wagner [2] reported $k=(1.0 \times 10^{14})\exp(-20.1 \text{ kcal mol}^{-1}/RT)$ cm^{3}mol^{-1}s^{-1} as rate expression for this reaction in the temperature range 1100-1800 K. They inferred that this reaction is fast. The reaction was also studied by Fontijn et al. in a high-temperature photochemical reactor using laser-induced fluorescence from NH to display its concentration [8, 9]. The results of this group were in good agreement with those of Rohrig and Wagner.

In this article, the reaction of NH with H_2 is investigated. In this regard, NH_3, NH_2, and N^- are generated. Accordingly, the first step in this process is producing molecular potential energy surfaces by an interpolation method developed over the last several years [10-13]. This potential energy surface is applied to calculate the reaction probability of overall reaction and each product. The cross section and rate constant are also determined from the reaction probability.

II. METHODS

In this study, the Gaussian 03 package [14] is used to perform all calculations in the gas phase. Single-point calculations on the optimized mpwb95 geometries at the CCSD(T)/ 6-311++G(d,p) level are carried out to obtain more accurate energies for the stationary points. Frequency calculations have been carried out to determine the nature of stationary points at the same level of theory. The simulations of PES were carried out with the GROW Model. The details of GROW program have been designated by Collins et al. [10-13].

III. RESULTS AND DISCUSSION

A. Ab initio calculations and discussion

The relative energies diagram for all species at CCSD(T)/6-311++G is supplied in Fig. 1. In this reaction, depending on the orientation of the target and incident particles, three channels are reported, in which NH_3, NH_2+H, and H_3^++N^- are produced, respectively. Hydrogen molecule from attacking the NH radical can abstract hydrogen of NH to produce the trihydrogen cation and nitrogen atom. H_3^+ is one of the most abundant ions in the universe. It is stable in the interstellar medium due to the low temperature and low density of interstellar space. In this collision, one of the hydrogens react with NH to form the NH_2. From the collision of hydrogen radical and NH_2, ammonia is generated which is the most stable species in this research. The relative energy of NH_2+H, H_3^+ + N^- , and NH_3 compared to NH + H_2 are -129.5, 1231.2, and -552.8 kJ mol^{-1}, respectively.

B. Classical dynamics calculations

Classical dynamics simulations were performed for the sampling of molecular configurations during the construction of the PES, and also for the calculation of the reaction cross sections. The trajectories were calculated with a velocity-Verlet integration algorithm using a time step size of 1.0×10^{-17}s, starting with a fragment-to-fragment center of mass separation of 10.6 Å and an impact parameter of 0. The relative translational energies between the reactants particle were in a range of 0.26-52.51 kJ mol^{-1}. A total of 1744 data points sampled from batches trajectories were added to the initial data set of 96 points. The final PES was interpolated over a data set of 1840 points. The maximum impact parameter, b_{max}, to calculate the reaction probability and reaction cross sections was 4.5 Bohr. Batches of 1500 trajectories for the reactions between species were run at several sizes of the interpolation data set in order to determine the convergence of the reaction probability with respect to the size of the data set. Next, these batches of 1500 trajectories were calculated for the final data set of 1840 points in order to determine the reaction probability, cross sections, and rate constant for the reactive collisions. Most importantly, the reaction probability for the reaction studied in this article are reasonably well converged as a function of the size of the data set. This convergence is illustrated in Fig. 2, where the reaction probability for the collisions between reactants is presented as a function of the data set size in 26.25 kJ mol^{-1}. The reaction probability as a function of impact parameter in 26.25 kJ mol^{-1} is presented in Fig. 3, and illustrated an increase in the impact parameter leads to a subsequent decrease in the reaction probability.

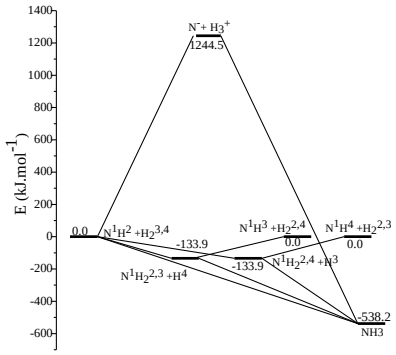

Fig.1. Relative energies of stationary points.

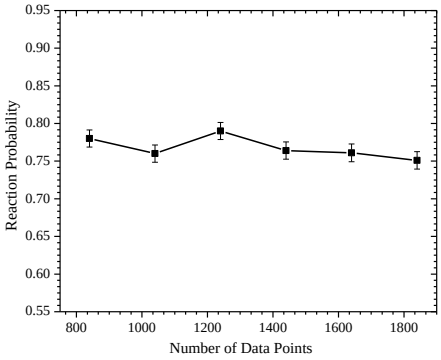

Fig. 2. The calculated reaction probability with respect to the number of date point.

C. Rate constant calculation

Clearly, a precise fit of the calculated total reaction cross sections, due to the sudden alteration of the cross sections with vibrational energy near dissociation, is very difficult to obtain using a two-dimensional excitation function. Thus, we instead chose to numerically calculate the rate constant. The reaction rate coefficient can be computed as a function of reaction cross section $\sigma_R(E)$ at temperature T. According to the collision theory, we have:

$$k(T)=a\left(\frac{8}{\pi\mu}\right)^{1/2}\Gamma(\gamma+2)(k_BT)^{\gamma+1/2} \qquad (1)$$

where $\Gamma(x)$ is the gamma function. Nonlinear least squares fitting parameters for main reaction are obtained, and finally, the fitted rate coefficient expressions were calculated as follow:

$$k(T) = 1.57\times10^{+10}\ T^{0.557}\ \text{L mol}^{-1}\ \text{s}^{-1}.$$

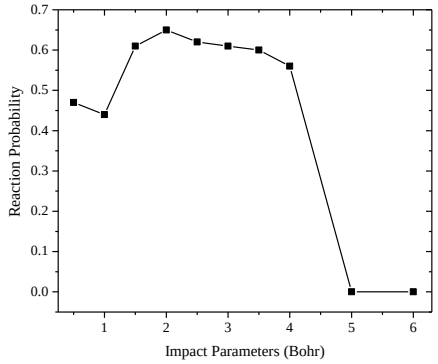

Fig. 3. Reaction probability was shown as a function of impact parameter.

IV. CONCLUSION

An interpolated potential energy surface from *ab initio* electronic energy of molecular fragments was used in order to describe the dynamics and kinetics of NH + H_2. Reaction probabilities and reaction cross sections as a function of translation energy of fragments and impact parameters for this reaction were determined. Reaction probabilityy in small impact parameter is greater than the large impact parameter.

REFERENCES

[1] X. Li-Jin, W. Xue-Bin, Y. Ji-Min and K. Fan-Ao, Chinese Journal of Chemistry, vol. 16, pp. 336-345, **1998**.
[2] M. Röhrig and H. G. Wagner, Chap. Chapter, vol. 25, pp. 975 -981, **1994**.
[3] J. A. Miller and C. T. Bowman, Progress in energy and combustion science, vol. 15, pp. 287-338, **1989**.
[4] L. D. Smoot, S. Hill and H. Xu, Progress in energy and combustion science, vol. 24, pp. 385-408, **1998**.
[5] R. K. Lyon, Science Technology, vol. 21, pp. 231-236, **1987**.
[6] R. Brownsword, T. Laurent, D. Maity, R. Vatsa and H. R. Volpp, Research on chemical intermediates,vol. 31, pp. 193-203, **2005**.
[7] M. W. Chase, American Chemical Society. vol. 9 **1998**, Washington, DC, .
[8] A. Fontijn, S. M. Shamsuddin, P. Marshall and W. R. Anderson, Chemical Physics Process Combustion, vol. 1, **2003**.
[9] A. Fontijn, S. M. Shamsuddin, P. Marshall and W. R. Anderson, Abstracts Work-in-Progress Posters; 30th International Symposium on Combustion; The Combustion Institute: Pittsburgh, PA **2004**.
[10]M. A. Collins, Theoretical Chemistry Accounts: Theory, Computation, and Modeling, vol. 108, pp. 313-324, **2002**.
[11]J. Ischtwan and M. A. Collins, The Journal of chemical physics, vol. 100, pp. 8080-8088, **1994**.
[12]K. C. Thompson, M. J. Jordan and M. A. Collins, The Journal of chemical physics, vol. 108, pp. 8302-8316, **1998**.
[13]R. P. Bettens and M. A. Collins, The Journal of chemical physics, vol. 111, pp. 816-826, **1999**.
[14]M. Frisch, G. Trucks, H. Schlegel, G. Scuseria, M. Robb, J. Cheeseman, J. Montgomery Jr, T. Vreven, K. Kudin and J. Burant, Inc., Pittsburgh, PA, **2003**.

Kinetic and Isotherm Modeling Studies of the V(V) Extraction from Sulfate Solution Using an Aliquat® 336/PVDF-*Co*-HFP Polymer Inclusion Membrane

***S. Bahrami*[a], *M. Cheraghi*[a], *L. Dolatyari*[b], *M. R. Yaftian*[a]*, *H. Shayani Jam*[a], *S. D. Kolev*[c]**
[a]*Department of Chemistry, The University of Zanjan, Zanjan, 45371-38791, Iran.*
[b]*Department of Chemistry, Zanjan Branch, Islamic Azad University, Zanjan, Iran.*
[c]*School of Chemistry, The University of Melbourne, Victoria 3010, Australia*
Email: yaftian@znu.ac.ir

Abstract*:* A polymer inclusion membrane (PIM) composed of poly(vinylidenefluoride-*co*-hexafluoropropylene) (PVDF-HFP) base polymer, tricaprylmethylammonium chloride (Aliquat® 336) extractant, and dibutyl phthalate (DBP) plasticizer with the 50/40/10 wt% ratio was prepared and characterized. This PIM was able to efficiently extract vanadium(V) from sulfate solutions adjusted to pH 2.5. The fabricated membrane was further used for the kinetic and isotherm studies. The process kinetic was well described by the pseudo-second order model. The adsorption isotherm was best fitted by the Langmuir equation, and the calculated maximum sorption capacity of V(VI) into the studied PIM was found to be 61 mg vanadium(V)/g PIM. The kinetic and isotherm experiments confirm that the sorption process of V(V) into the optimal plasticized PVDF-HFP based PIM is taken place via a chemisorption mechanism.

Keywords: Extraction, Isotherm, Kinetic, Polymer Inclusion Membrane, V(V).

I. INTRODUCTION

In recent years, membrane-based processes have attracted considerable attention as a valuable technology for many industries. These technologies are introduced as alternative for commonly used solvent extraction process because they eliminate the need for the toxic and flammable diluents required in solvent extraction systems while retaining the selectivity associated with the extractant [1]. Liquid membranes can be found in different forms i.e., bulk (BLMs), emulsion (ELMs) and supported (SLM) liquid membrane that they present poor stability and flux and complexity in operation. Polymer inclusion membranes (PIMs) a relatively recently developed liquid membranes, are known to be simple and more stable than another LMs techniques [2]. PIMs entrap an extractant within a polymer matrix, often with the addition of a plasticizer or modifier to improve their extraction characteristics [3].

This communication is devoted to the kinetic and isotherm study of the V(V) extraction from sulfate solution by a PIM composed of poly(vinylidenefluoride-*co*-hexafluoropropylene (PVDF-HFP) base polymer, tricaprylmethylammonium chloride (Aliquat® 336) extractant, and dibutyl phthalate (DBP) plasticizer. These data aimed to establish the controlling mechanism of the extraction process. In order to study the kinetics of the process, four most commonly models included pseudo-first order, pseudo-second order, Elovich and intra-particle diffusion equations were tested. The Langmuir, Freundlich and Dubinin Radushkevich (D-R) isotherm models have been applied for describing the equilibrium data.

II. METHODS

The PIMs were prepared by continuous magnetically stirring of determined amounts of PVDF-HFP, Aliquat® 336 and DBP with tetrahydrofuran (THF), until homogeneous solutions were obtained. The solution was then poured into a homemade teflon casting knife, placed on a glass plate. The glass plate was covered with an aluminium tray to allow slow evaporation of THF. The obtained thin PIMs were completely clear, homogeneous, and flexible. The prepared membranes were characterized using chemical techniques such as FTIR, TGA, FESEM, AFM, EDS, contact angle and mechanical properties by using strain strength. Extraction experiments were performed by immersing a 3.5 cm diameter round disk, with average mass of 0.057±0.005 g and average thickness of 46±6 µm, in a sulfate solution containing V(V) adjusted to the desired pH. The analysis of metals was done spectrophotometrically with the complexing reagent xylenol orange or by the flame atomic absorption spectrometer.

III. RESULTS AND DISCUSSION

A variety of PVDF-HFP-based PIMs containing Aliquat® 336 and various plasticizers/modifiers including 2-nitrophenyloctyl ether (NPOE), tributyl phosphate (TBP), dibutyl phthalate (DBP) and tris(2-ethylhexyl)phosphate (TEHP) were prepared. The successful PIMs; i.e. those were transparent, homogeneous, flexible and mechanically stable, were examined in the extraction of V(V) from sulfate solutions (0.2 mol L^{-1}) adjusted to pH 2.5. The most suitable, in terms of physical and mechanical properties and the

amount of V(V) extracted, PIM with the composition of 50/40/10 wt% with respect to the base polymer, Aliquat® 336 and DBP selected as optimum composition of membrane. The AFM image of the optimum PIM showed the roughness of the membrane surface decreases with addition of the extractant to the blank film and energy dispersive X-ray spectroscopy (EDS) revealed a uniform distribution of extractant within a base polymer. The strain-stress curves indicated that the addition of extractant and plasticizer increase significantly the flexibility of the membrane with a maximum elongation at around 505%.

The influence of pH, extraction time, sulfate ion concentration and initial metal ions concentration on the extraction of V(V) was studied.

In order to assess the controlling mechanism of the process, the concordance between the time dependency experimental data and four kinetic models: pseudo-first order, pseudo-second order, Elovich and intra-particle diffusion model was tested [4,5]. The values of R^2 showed a good agreement between the experimental data with those predicted by the pseudo-second order kinetic model (Fig. 1a). This point was also confirmed by comparing the predicted value of q_e (33.0 mg vanadium(V)/g PIM) by the pseudo-second order model with that found experimentally (31.7 mg vanadium(V)/g PIM). This kinetic model suggests that the rate determining step of this process is the chemisorption.

The experimental data obtained from experimental initial metal concentration were used to study the adsorption isotherms for obtaining more information about the solute interaction with the membrane. To this end, three most commonly isotherm models, namely Langmuir, Freundlich, and Dubinin Radushkevich (D-R), were examined [4,5].

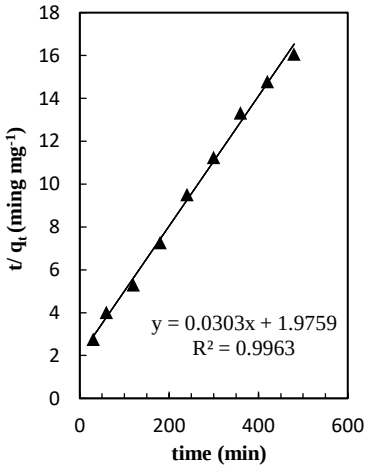

(a)

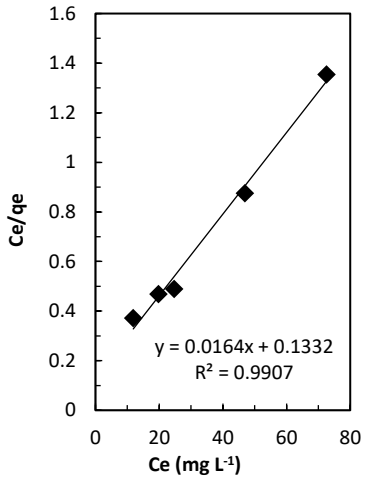

(b)

Fig.1. (a) Adsorption kinetic fitting using pseudo-second order model, (b) adsorption isotherm fitting using Langmuir model in V(V) extraction by using PVDF-HFP/Aliquat® 336/DBP PIM.

The results showed that the experimental data for the adsorption of the vanadium(V) ions onto the studied PIM were well described by Langmuir isotherm model (Fig. 1b). The proximity of the calculated maximum adsorption capacity value (61 mg vanadium(V)/g PIM) with that found experimentally (56 mg vanadium(V)/g PIM) showed also the applicability of this model for interpretation of the adsorption equilibria. The separation factor value ($0<R_L<1$) calculated by Langmuir isotherm indicated that the process is favorable. The 1/n value (a parameter appeared in the mathematical description of the Freundlich model) was evaluated to be lower than 1. This revealed that the adsorption process of vanadium(V) ions by the studied PIM was favorable and chemisorption. Moreover, the E value calculated based on the D-R model (>8 kJ/mol) revealed a chemisorption mechanism for the process. This agreed with the results obtained by using Freundlich isotherm and kinetic data.

IV. CONCLUSION

The extraction of V(V) ions from aqueous solutions by using a plasticized PIM containing a 50%w/w PVDF-HFP polymer matrix, 40% w/w Aliquat® 336 and 10% w/w DBP was investigated. AFM image and EDS indicated its heterogeneous structure and almost uniform distribution of the extractant in the PIM. It is found that the V(V) extraction process is influenced by polymeric sorbent composition, pH,

time of extraction process and initial metal ion concentration in the aqueous solution. The kinetic study showed that the V(V) sorption into the optimal membrane is a chemisorption process which is best fitted by the pseudo-second order model. The extraction system was best described by the Langmuir isotherm model and also it was indicated that the V(V) chemisorption on the studied PIM is favorable.

REFERENCES

[1] A. M. St John, R. W. Cattrall, S. D. Kolev, J. Membr. Sci., vol. 364, pp. 354–361, **2010**.
[2] A. Casadellà, O. Schaetzle, K. Nijmeijer, and K. Loos, Polymers, vol. 8, pp. 76-90, **2016**.
[3] M. R. Yaftian, M. I. G. S. Almeida, R. W. Cattrall, and S. D. Kolev, J. Membr. Sci., vol. 545, pp. 57-65, **2018**.
[4] Z. Dousti, L. Dolatyari, M.R. Yaftian, and S. Rostamnia, Separ. Sci. Technol., **2018.**
[5] C. V. Gherasim and G. Bourceanu,. Chem. Eng. J., vol. 220, pp. 24-34, **2013**.

Investigation of the kinetics and isotherms of the uptake of Bi(III) by a poly(vinyl chloride) inclusion membrane containing di-(2-ethylhexyl)phosphoric acid

***D. Kazemi*[a], *H. R. Sharafi*[a], *M. R. Yaftian*[a]*, *S. D. Kolev*[b]**
[a]*Department of Chemistry, The University of Zanjan, Zanjan 45371-38791, Iran.*
[b]*School of Chemistry, The University of Melbourne, VIC 3010, Australia.*
Email: yaftian@znu.ac.ir

Abstract*:* The present communication aims to describe the kinetics and isotherms of the extraction of bismuth(III) from sulfate solutions by a plasticizer-free polymer inclusion membrane composed of 50 %w/w polyvinyl chloride (PVC) as the base polymer and 50% w/w di-(2-ethylhexyl)phosphoric acid (DEHPA) as the carrier. The isotherms of the process are also studied by applying Langmuir, Freundlich and, Dubinin–Radushkevich (D–R) models. The analysis of the data showed that Langmuir isotherm can suitably describe the experimental data. The interpretation of the process kinetics was done by fitting the experimental data to the different kinetic models (i.e., pseudo-first order, pseudo-second order, intra-particle diffusion, power function, and Elovich models). Among these models, the pseudo-second order model described well the experimental data.The kinetic and isotherm studies revealed that the sorption of Bi(III) by the optimized membrane is a chemisorption process.

Keywords: Bismuth, DEHPA, Isotherm, Kinetic, Polymer inclusion membrane.

I. INTRODUCTION

Among the most commonly used methods for the extraction of metal ions, solvent extraction (SX) is a technique that can be easily performed in industrial level processes, but it suffers from using large volumes of volatile, flammable and toxic organic diluents [1]. Polymer inclusion membrane (PIM) based techniques, which is relatively a novel type of liquid membrane methods, has been introduced as a green alternative to the traditional SX process because it does not need to diluents and it is utilized a very little amount of extractant [2].

PIMs are the thin, flexible and transparent film. They are typically prepared by casting a solution of all membrane components; a polymer matrix, an extractant/carrier and often a plasticizer [3]. PIMs can be used in the extraction and transport of metal ions, organic compounds, drugs, and other analytes.

This communication is devoted to the kinetic and isotherm studies of the extraction process of Bi(III) from sulfate medium by a non-plasticized PIM containing polyvinyl chloride (PVC) base polymer and di-(2-ethylhexyl)phosphoric acid (DEHPA) extractant.

The isotherm study was realized by testing three most commonly used isotherm models, namely Langmuir, Freundlich and Dubinin Radushkevich (D-R). To investigate the kinetics of the extraction process, pseudo-first order, pseudo-second order, Elovich, power function ,and intra-particle diffusion model kinetic models were employed.

II. METHODS

In order to prepare the membranes, polyvinyl chloride (PVC) and di-(2-ethylhexyl)phosphoric acid (DEHPA) extractant were dissolved in tetrahydrofuran (THF) and magnetically stirred at 40 °C. The homogeneous solution was then poured into a petri dish of 76 mm in diameter. Petri dish was covered with filter paper and also a flat glass plate to allow slow evaporation of THF during 24 h. The physicochemical properties of the prepared membranes were investigated by measuring their thickness, weight, water contact angle, strain stress, FT–IR, TGA, FESEM, and AFM analyses. Circular membrane segments (3.5 cm in diameter) were cut from the casted PIM for using in bismuth(III) extraction experiments. The analysis of bismuth(III) was done by an atomic absorption spectrometer.

III. RESULTS AND DISCUSSION

The optimized membrane, including 50 wt% PVC and 50 wt% DEHPA was transparent, flexible, homogenous ,and mechanically stable. The average mass and thickness of these PIMs were 0.0618±0.008 g and 0.066±0.009 μm, respectively. FT–IR spectra of the optimized PIM signified the constituents are present in the membrane with no significant interaction between the membrane onstituents. The strain-stress curves showed that flexibility and elastic behavior of the PVC/DEHPA membrane is more than extractant free PVC film. The FESEM images from the surface and cross-section of the studied PIM showed a uniform and homogenous surface and appeared dense with no obvious porosity. The AFM image of the fabricated PIM

indicated that addition of extractant (DEHPA) to the PVC blank film increase roughness of the PIM surface.

The developed PIM was applied in the Bi(III) extraction experiments. It is found that this membrane could efficiently extract Bi(III) from sulfate solutions at low pH (1.3) via a proton exchange mechanism. A quantitative stripping of the extracted ions from the loaded PIM was achieved by using 2 mol/L sulfuric acid solution.

The isotherm studies were realized by analyzing the experimental data by applying Langmuir, Freundlich ,and Dubinin Radushkevich (D-R) isotherm equations [4,5]. The results are presented in Table 1. The correlation coefficients (R^2) indicated that the experimental extraction data were more suitably interpreted by the Langmuir model. The estimated maximum adsorption capacity of the studied PIM (q_m) based on this isotherm model was 51.5 mg Bi(III) per gram of PIM, which was close to that obtained from experimental data (50 mg Bi(III)/g PIM).

Table 1. Extraction isotherms parameters for Bi(III) sorption by the PVC/DEHPA polymervinclusion membrane.

Langmuir				**Freundlich**			**D-R**			
q_m (mg/ g)	b (L/ mg)	R_L	R^2	K_f ((mg /g) (mg /L)^n)	1/n	R^2	q_m (mmol/ g)	β (mol^2/.k J^2)	E (Kj/ mol)	R^2
51.54	0.17	0.14	0.998	19.92	0.19	0.743	1.93	0.003	12.9	0.996

Furthermore, the separation factor, R_L, calculated by the Langmuir isotherm revealed that the adsorption process is favorable. The evaluated value of E calculated based on the D–R model was higher than 8 (kJ/mol), indicating that the chemisorption for the processes nature. This was in consistent with the predicted 1/n values (<1) by Freundlich model.

In order to assess the controlling mechanism of the process, the concordance between the time dependency experimental data and five kinetic models: pseudo-first order, pseudo-second order, Elovich, power function ,and intra-particle diffusion model was tested [4,5].

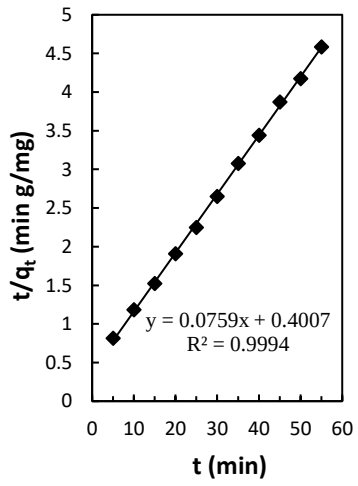

(a)

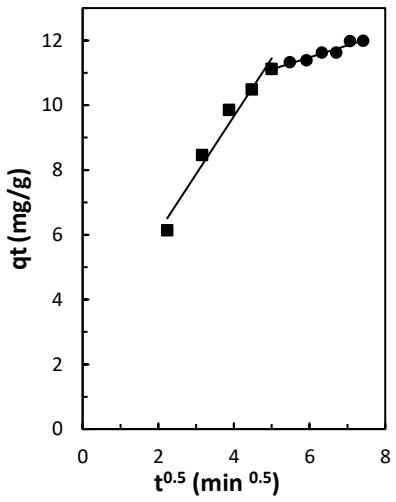

(b)

Figure. 1. Application of (a) pseudo-second order and (b) intra-particle diffusion models on the experimental data.

The evaluated correlation coefficients (R^2) values obtained from the least squares lines revealed that the extraction data were well fitted by the pseudo–second order model (Fig. 1a).

The estimated adsorption capacity, q_e, based on this model was 13.2 mg bismuth/g PIM, and that found experimentally was 12.1 mg bismuth/g PIM. This model suggested that chemisorption is the rate determining step. Intra–particle diffusion model's diagram (Fig. 1b) showed two linear regions. In fact, the two linear segments observed in this analysis showed that the extraction of Bi(III) ions, initially occurred on readily available surface, and then diffusion of the ions through the active sites within the membrane can occurre with slow kinetic.

IV. CONCLUSION

The non-plasticized PVC/DEHPA PIM with the composition 50% w/w PVC and 50% w/w DEHPA was fabricated. AFM and FESEM images illustrated the almost uniform distribution of the DEHPA in the surface of the membrane, as well as the heterogeneous structure of the PIM. This PIM can quantitatively extract Bi(III) ions from aqueous sulfate solution. The isotherms studies showed that the extraction process was well described by the Langmuir isotherm model and also indicated that the Bi(III) chemisorption on the prepared PIM is favorable. Pseudo-second order kinetic equation described suitably the experimental data which approved the nature of the chemical process in the Bi(III) extraction, as it was suggested by the isotherm studies.

REFERENCES

[1] A. M. St John, R. W. Cattrall, S. D. Kolev, J. Membr. Sci., vol. 364, pp. 354–361, **2010**.

[2] N. Yang, H. Sun. Bismuth: environmental pollution and health effects. Encyclopedia of environmental health. **2011**.

[3] M. I. G. S. Almeida, R. W. Cattrall, and S. D. Kolev, Anal. Chim. Acta., vol. 987, pp. 1-14, **2017**.

[4] B. N. Mohanty, P. K. Mohapatra, D. R. Raut, D. K. Das, P. G. Behere, and Md Afzal, Ind. Eng. Chem. Res., vol. 12, pp. 3237-3246, **2015.**

[5] L. Dolatyari, M.R. Yaftian, and S. Rostamnia, J. Environ. Manage, vol. 169, p.p. 8–17, **2016**.

P(AA)-Co(II) Based Catalyst for Kinetic Studies in Methyl Orange Degradation

Somayeh Rezheh*,[a] *Massomeh Ghorbanloo*[a]

[a] *Department of Chemistry, Faculty of Science, University of Zanjan, 45371-38791 Zanjan, Iran*
e-mail: m_ghorbanloo@yahoo.com

Abstract: Poly(acrylic acid), P(AA), hydrogel was synthesized by a very simple and easy method of free radical polymerization under mild reaction conditions. Synthesized hydrogel was used as support for in situ metal ion complex preparation by using $CoCl_2.6H_2O$ in H_2O. The p(AA)-Co(II)/H_2O_2 catalyst was used in the degradation of methyl orange (MO). In the presence of 30 mM H_2O_2, 100% of MO was removed in 35 min. The kinetics of the reaction was pseudo-first-order.

Keywords: *Hydrogel-metal ion complexes; azo compound degradation; kinetic study*.

1. INTRODUCTION

Until now, heterogeneous catalytic systems for degradation of synthetic dyes or other organic compounds by hydrogen peroxide has been explained with silica-supported complexes of Cu, Ni and Co [1] or metals embedded in polymeric matrix [2]. But the use of these processes for industrial effluents is limit, because of the requirements of visible light for photo–catalysis, unsuitable pH–dependence of activity or the need to perform the catalysis limits the use of these processes for industrial effluents. [3]. But, in this study we used a simple method for remove of methyl orange, in comparison to the other instruments. Herein, the degradation of MO by p(AA)-Co(II) complex were investigated. Different parameters on MO degradation rate were also studied.

2. Experimental

2.1. Preparation of p(AA)-Co(II) hydrogels

In the synthesis of p(AA) hydrogels, 5 mL acrylic acid (AA), and 0.055 g N,N′-methylenebisacrylamide (MBA) were mixed with 4 mL water and to this solution a APS solution of 0.165 g ammonium persulfate (APS) was added. After the washing procedure, hydrogels were dried to a constant weight. For in situ loading of metal nanoparticles within p(AA) hydrogel, first cobalt ions were loaded into hydrogel network by dispersing 0.1 g of the dried p(AA) hydrogel in 50 mL, 500 ppm aqueous solution of cobalt chloride for 24 h at room temperature, as shown in Scheme 1.

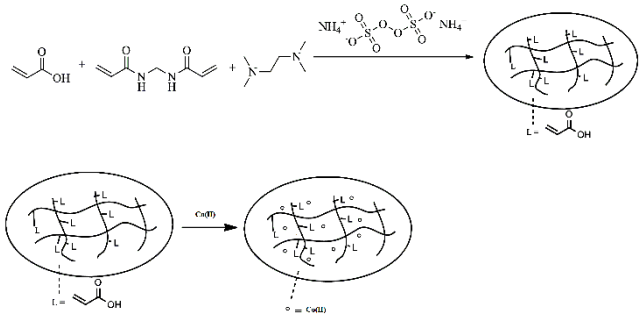

Scheme 1 Representation of p(AA)-Co(II) preparation

2.2. Methyl Orange Degradation by p(AA)-Co(II) hydrogel complex

The MO degradation studies were carried out by using 100 mg of p(AA)-Co(II) complex that was suspended in 100 mL 42 μM MO with 63 mM H_2O_2 solution. The degradation of MO was monitored as a function of time at 464 nm, and the degrading percent were determined from the previously constructed calibration curve at this wavelength.

3. RESULTS AND DISCUSSION

3.1. Synthesis and Characterization

The FT-IR spectra of AA and p(AA) hydrogel indicate the O–H stretching band in 3530 cm^{-1} region and the C–H stretching at 2935 and 2865 cm^{-1} regions, respectively. Also the bands at 1739 and 1462 cm^{-1} are assigned to C=O and COO^- stretching band of acrylic acid, respectively. In addition, the NH band of MBA is overlapped by OH peak at about 3200 cm^{-1}so the related peak is disordered.

3.2. Methyl Orange Degradation

The progress of the degradation reaction in the presence of p(AA)-Co(II) hydrogel composite was followed by UV–Vis spectrophotometer. The degradation reaction kinetics of MO was studied with the decrease of peak intensity at 462 nm. As illustrated in Fig. 1, the UV–Vis spectra for the degradation of MO measured at every 5 min after the addition of p(AA)-Co(II) hydrogel catalyst to reaction medium in order to follow the progress of the degradation reaction. It is important to mention that the degradation reaction does not take place in the absence of catalyst and this peak at 462 nm remained unchanged without the addition of p(AA)-Co(II) hydrogel catalyst.

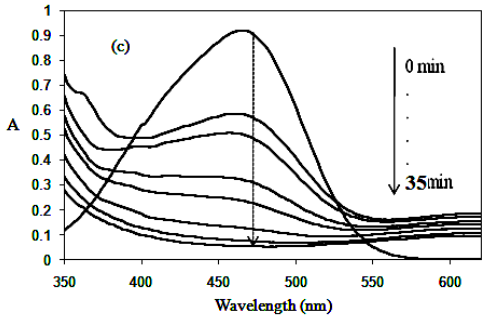

Fig. 1. UV–Vis spectra of degradation of methyl orange

To determine the effect of the concentration of H_2O_2, three different concentration of H_2O_2, 16 to 64 mM was used in MO degradation. The MO degradation rate was increased by the increase of H_2O_2 concentration from 16 to 64 mM. The increase in the H_2O_2 concentration resulted in an increase in the reaction activity, as expected, due to an increase of $^{\bullet}OH$ that place active role in the degradation of MO. The effect of MO concentration was also investigated. The initial concentration of MO has significant effect on the MO adsorption. When the amount of MO increased from 10 to 30 µM as shown in Fig. 2, the degradation time increased, the percentage degradation of the MO decreases corresponding to an increase in initial methyl orange concentration.

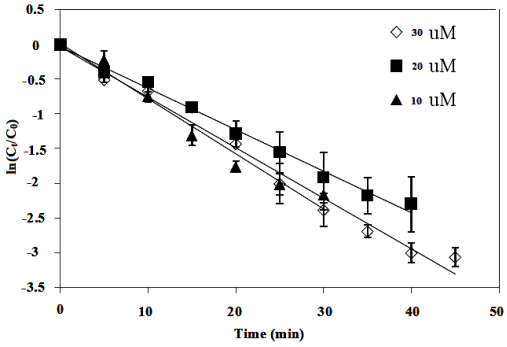

Fig.2 Effect of MO concentration on degradation of MO

The effect of catalyst amount on the degradation of MO was also studied. The activity of this heterogeneous catalyst for MO degradation was independent from catalysts as the increase in the amounts of catalyst from 50 mg to 150 mg did not change the amounts of MO residue in solution. This behavior could be attributed to the fact that 50 mg of catalyst is enough to provide catalytic sites for the available amount of reactants. To determine the effect of temperature, the degradation reactions of MO were carried out at four different temperatures; 30-60 °C, and the degradation rate constants were calculated for each temperature. As shown in Fig. 3, it was observed that the degradation rate is increased with increasing reaction temperature. It is obvious as expected, the higher the reaction temperature the lower the time for MO degradation under same reaction condition of increasing reaction temperature. As higher temperatures provide more energy for the reactant molecules to overcome the reaction activation energy barrier; faster dye degradation with higher reaction temperatures is reasonable.

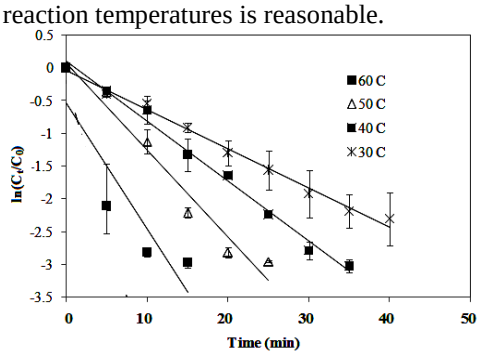

Fig. 3. The relationship between $\ln(C_t/C_0)$ with time at different temperature

To investigate the reaction kinetics, $\ln (C_t/C_0)$ versus time at different reaction temperatures was constructed. As can be seen the linear correlation of $\ln (C_t/C_0)$ versus time plot is the proof for the pseudo-first-order rate kinetics. The pseudo-first-order rate constants (k) and correlation coefficients (R^2) for MO degradation are 0.03 min^{-1}, 0.045 min^{-1} and 0.066 min^{-1} at 30 °C, 40 °C and 60 °C, respectively. Additionally, the activation parameters at different temperatures for MO degradation reaction were calculated by applying well-known Arrhenius equation and constructing the graph of ln$k$–1/T.The activation energy for degradation of MO was found as 32.69 kJ mol^{-1}.

4. Conclusions

Synthesis of p(AA) hydrogel was accomplished by a very simple and easy method of free radical polymerization and Co ions were prepared by using $CoCl_2$. A chemically stable p(AA)-Co (II) was used in the catalytic degradation of MO from aqueous media. Kinetic studies suggest that the degradation process of MO can be described by the pseudo-first-order kinetic model. Reuse of the catalysts can be achieved, without significant loss of catalytic activity.

REFERENCES

[1] A.H. Gemeay, I.A. Mansour, R.G. El Sharkawy, A.B. Zaki, J. Mol. Catal. A: Chem. 193, 109–120, 2003

[2] J. Jose, M. John, M.G. Gigimol, B. Mathew, J. Appl. Polym. Sci. 90, 895–904, 2003

[3] R.C. Wu, J.H. Qu, Water. Environ. Res. 76, 2637–2642, 2004

Starch-poly(acrylic acid)-Cu(II) Based Catalyst for Kinetic Studies in Epinephrine Oxidation

Somayeh Rezheh*, Zahra Mohammadi, Massomeh Ghorbanloo

[a] *Department of Chemistry, Faculty of Science, University of Zanjan, 45371-38791 Zanjan, Iran Email: e-mail: m_ghorbanloo@yahoo.com*

Abstract

Starch-poly (acrylic acid) hydrogel was synthesized via free radical polymerization reaction technique under mild conditions. Synthesized hydrogel was used as template for in situ metal ion complexes preparation by using $CuCl_2.6H_2O$ in H_2O. Starch-poly (acrylic acid)-Cu^{II} heterogeneous catalyst system comprised of copper ions embedded within hydrogel matrices has been employed for the oxidation of epinephrine in aqueous media. The epinephrine was partially oxidized to adrenochrome by St-p(AA)-Cu(II)/H_2O_2 hydrogel composite system. About 43.0% of epinephrine was conversion to adrenochrome in less than 30 min. The kinetics of the processes was pseudo-first-order kinetic model. EP oxidation reaction provides mild activation energies, 48.56 kj.mol^{-1}.

Keywords*:* Hydrogel-metal ion complex; Epinephrine Oxidation; kinetic study.

1. INTRODUCTION

Epinephrine (EP) is a important catecholamine neurotransmitter in the central nervous system and biological body fluids [1]. Many life phenomena are related to the concentration of EP in blood. Medically, EP has been used as a ordinary emergency healthcare medicine. The decrease of catecholamine level leads to diseases, an easy fast and sensitive method is essential for its determination [2]. Catalytic oxidation methods are faster, cheaper, safer analysis and high sensitivity in comparison with other methods. However, between reported compounds, modifiable polymeric particles with tunable functional groups and sizes such as starch-acrylic acid particles attract much attention owing to their superior properties [3].

2. Experimental

The Starch and Acrylic Acid were purchased from Aldrich. Epinephrine, and hydrogen peroxide (H_2O_2, 30%, Merck) was used as an oxidizing agents.

2.1. Synthesis of St-p(AA)-Cu$^{(II)}$

St-p(AA) hydrogel was prepared according to previous literatures Yan. *et al*. 12.25 g acrylic acid was partially neutralized with sodium hydroxide solution in an ice bath. A suspension of 1.00 g starch was added to acrylic acid solution and then was stirred for 15 min. 0.05 g of MBA and 1 mL ammonium persulfate was added to mixture and polymerization was completed in water bath. Then the sample was oven-dried in an air-circulating oven at 70 ºC for 24 h. For in situ fabrication of metal ions within St-p(AA) hydrogel, copper ions were loaded into hydrogel network by dispersing 0.1 g of the dried St-p(AA) hydrogel in 50 mL, 500 ppm aqueous solution of $CuCl_2$ for 24 h.

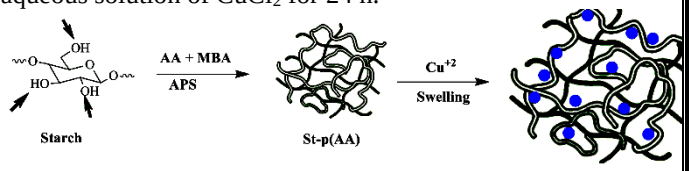

Scheme 1. Schematic representation for the Cu complex formation within St-p(AA) hydrogel

2.2. Epinephrine Oxidation by St-p(AA)-Cu(II) hydrogel comlex

The oxidation of epinephrine was carried using 40 mg of St-p(AA)-Cu(II) hydrogel complex which was suspended in 20 mL of 2 mM epinephrine and 46 mM H_2O_2 solution. Then the change in the absorbance of the solution was monitored as a function of time at 502 nm.

3. Results and Discussion

3.1. Characterization

The FT-IR spectra for Starch, acrylic acid, (AA), and Starch-p(AA) hydrogel are presented in Fig. 1-a, b and c, respectively. The FT-IR spectrum of starch displays the O–H stretching absorption in the region of 3400 cm^{-1} and the C–H stretching at 2935 and 2892 cm^{-1}. A triplet peak of starch for the C–O–C stretching appears in 1170, 1100, and 1000 cm^{-1}. In the spectrum of St-p(AA), two peaks at 2929 and 2860 cm^{-1} correspond to the C–H symmetric and asymmetric stretching of starch and MBA.

3.2. Epinephrine Oxidation to Adrenochrome using St-p(AA)-Cu(II)/H_2O_2

The progress of the oxidation reaction in the presence of hydrogel containing copper ions was followed by UV–Vis. The oxidation reaction kinetics of EP was investigated

consequently as an increase of peak intensity at 502 nm. As illustrated in Fig. 1, the UV–Vis spectra for the oxidation of EP measured at every 4 min after the addition of St-p(AA)-Cu(II) hydrogel composite catalyst to reaction medium in order to follow the progress of the oxidation reaction. In the absence of a catalyst, the oxidation of epinephrine by H_2O_2 was practically negligible.

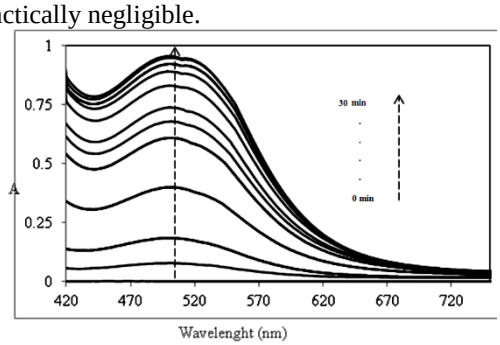

Fig. 1 The change in the absorbance of Epinephrine (EP) with time catalyzed by St-p(AA)-Cu(II).

The effect of catalyst amount on the oxidation of EP was investigated. The activity of St-p(AA)-Cu(II) heterogeneous catalyst system for EP oxidation increases with increasing catalyst amount from 20 mg to 40 mg, but further increase in the amount of catalyst, the conversion of EP oxidation was decreased. The effect of EP concentration in the oxidation reaction catalyzed by catalyst system was also investigated. The amount of EP increased from 1 to 4 mM, and the calculated percentage of EP conversion decreased from 98 to 22%. This phenomenon can be explained as same as initial concentration effect in EP degradation. A temperature range of 30–60 °C was studied due to investigate the effect of this parameter on EP oxidation catalyzed by St-p(AA)-Cu(II) catalyst system. The oxidation of EP is increased with increasing reaction temperature from 30 to 50 °C, and at higher temperatures the oxidation rate constants were also increased, and this increase is slowed at higher temperatures as the rate constants changed less at the reaction temperatures of 50, 60 ºC.

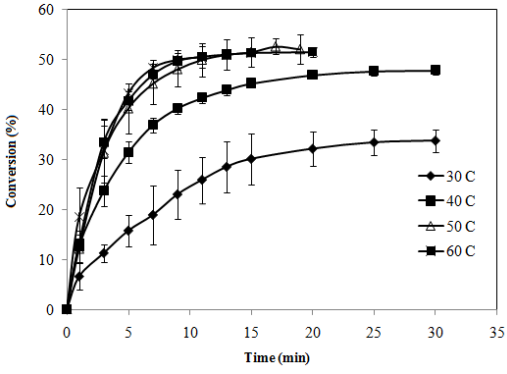

Fig. 2 Epinephrine conversion at different temperature catalyzed by PEI-Co(II) catalyst systems.

Again, to determine the reaction kinetics for EP oxidation by PEI-Cu(II), the $\ln(C_t/C_0)$ versus time plot was constructed, and good linear correlation of $\ln(C_t/C_0)$ versus time plot confirmed the pseudo-first-order rate kinetics. The pseudo-first-order rate constants (k) are 0.032, 0.075, 0.086 and 0.093 min^{-1} at 30- 60 °C, respectively. As expected, the k values were increased as the reaction temperatures were increased. The kinetic measurements have revealed that EP oxidation catalyzed by St-p(AA)-Cu(II) catalyst systems the pseudo-first-order kinetics. Additionally, the activation parameters for EP oxidation from the reaction carried out at different temperatures were calculated. The activation energy for oxidation of EP catalyzed by St-p(AA)-Cu(II) was found as 48.56 kJ mol^{-1}.

4. Conclusions

Synthesis of St-p(AA) hydrogel was accomplished by a very simple and easy method of free radical polymerization and Cu ions were prepared by using $CuCl_2$. A chemically stable St-p(AA)-Cu(II) was synthesized and used in the catalytic oxidation of epinephrine from aqueous media. Kinetic studies of EP catalyzed by St-p(AA)-Cu(II) suggest that the oxidation process can be described by the pseudo-first-order kinetic model. Reuse of the catalysts can be achieved, without significant loss of catalytic activity.

REFERENCES

[1] J.A. Ni, H.X. Ju, H.Y. Chen, D. Leech, Anal. Chim. Acta 378, 151–157, **1999**

[2] M. Taei, M. Jamshidi, J. Solid. State. Electrochem. 18, 673–683, **2014**

[3] S. Demirci, N. Sahiner, J. Mol. Liq. 194, 85–92, **2014**

Kinetic Study of Hydrogen Generation Reaction Over Co/Salep Nano Catalyst

M.H. Loghmani*, M. Jalali Rad
Department of Nanotechnology, University of Guilan, Rasht, Iran
Email: mhmdloghmani@guilan.ac.ir

Abstract*:* Salep-stabilized Cobalt nano catalyst has been synthesized with chemical reduction method. Kinetic studies on the hydrolysis reaction of $NaBH_4$ are investigated through three factors: (1) effect of $NaBH_4$ concentration, (2) effect of the catalyst dosage and (3) effect of solution temperatures. The activation energy (E_a) was achievement indicated that the compound of Co/Salep has the lowest agglomeration and the highest rate of hydrogen generation ($E_{a=}28.7$ kJmol^{-1}).

Keywords: hydrogen generation, hydrolysis of $NaBH_4$, Kinetic, nano catalyst, rate law

I. INTRODUCTION

Extraction of hydrogen gas from its compounds is necessary because hydrogen gas can be found rarely in its pure form. Fossil fuels, biomass and water electrolysis are the most resources for hydrogen generation. Sodium borohydride as a non-fossil energy sources has been suggested as a source for hydrogen gas under mild conditions. Among the certain catalysts, $NaBH_4$ can be hydrolyzed and hydrogen gas released. The hydrolysis of $NaBH_4$ is expressed as follows (1),

$$NaBH_4 + 2H_2O \rightarrow NaBO_2 + 4H_2 \uparrow \quad (1)$$

The reaction product (borax) is environmentally clean and can be recycled to the reactant $NaBH_4$. This reaction needs a catalyst. In the absence of a catalyst, sodium borohydride dissolves in deionized water without appreciable hydrogen production. It is found that, $NaBH_4$ solution hydrolyzed only when certain suitable catalysts are added. Noble metals such as Ru, Pt and Pd have been used as precious catalysts for hydrogen production over hydrolysis of $NaBH_4$. Their application as an industrial catalyst is limited because of their cost and availability. As known, it is necessary to stabilize metal nanoclusters in an aqueous solution because of aggregation and agglomeration phenomenon. These two phenomenon resulted in strongly interact of particles and subsequently larger particles can be formed. A large percentage of atoms in transition metal nanoclusters belong to surface so led to catalytic activity of them. Polymeric chains can improve properties of the nanoclusters such as the solubility, thermal stability and catalytic activity. Previously, we studied the effect of polymers and fatty acid long chain on size, morphology and catalytic activity of Co-La-Zr-B nano catalyst [1-3]. In addition, previously we studied the effect of polymers and surfactants as stabilizer agents on properties of Cu-Fe-B nano catalyst [4]. Salep is made from plant tubers from the orchidaceae family and is a good source of glucomannan, which is composed of linear chains consisting of glucose and mannose connected by β-(1→4) glycosidic bonds. The tubers are usually grow in eastern Mediterranean countries. In this work, in order to reduce particles aggregation and then enhance the catalytic activity of nano powder, Salep is used as a matrix in preparation processes. The catalytic activity of catalyst is tested for hydrogen generation through hydrolysis of alkaline sodium borohydride solution. In order to achieve a rate law equation, several parameters such as catalyst dosage, initial concentrations of $NaBH_4$ and temperature were considered. Arrhenius equation was used to calculate E_a of hydrogen generation reaction at different temperatures.

II. METHODS

The native salep powder purchased from a local market. Ethanol, sodium borohydride, cobalt(II) chloride.$6H_2O$, methylenebisacrylamide(MBA),methacrylicacid(MAA),potassium persulfate (KPS) and NaOH purchased from Merck. Appropriate amount of native salep powder was stirred in 500 ml of deionized water for 1 h at 318K followed by decantation to remove insoluble material. To precipitate of glucomannan the supernatant was mixed with absolute ethanol at a ratio of 1:1 (v/v). The wet gel was washed with absolute ethanol and acetone and then dried with a forced air dryer at 318K overnight. Next, glucomannan was dissolved in 500 ml deionizer water under stirring at 323K. After 20 min a homogenous solution was obtained. A solution of cobalt (II) ion (1mmol) was added to glucomannan solution. then, MAA as a monomer, MBA as a cross-linker agent and KPS as initiator were added. After solution was heated up to 353K. The solution condition. Finally, for reduction of cobalt ions a solution of $NaBH_4$ was added. The color of solution changed from pink to black indicating that cobalt ions were converted to cobalt. Over reduction of cobalt ions hydrogen gas released in the container. At the end of hydrogen release, the solution was added to ethanol. The black gel is formed in the ethanol. The obtained gel was dried in over at 50 ^oC overnight. Determining of rate law through hydrolysis of $NaBH_4$ aqueous solution was done as follows: A (5wt%) $NaBH_4$ aqueous

solution containing (2wt%) NaOH was added into a flask which was immersed in a water bath at 318 K. At this condition catalyst dosage was 50 mg. Hydrogen production was monitored via an inverted cylinder method. It involves a round bottom flask in which the reaction takes place and a cylinder filled with water and inverted in a tank of water. As the hydrogen gas is created, it will displace water from the cylinder. The volume of gas can be determined by the amount of water that was displaced by the gas. Kinetic study of hydrogen production via catalytic hydrolysis of $NaBH_4$ using Co/Salep catalyst was done over a series of experiments and the results are described in next section.

III. RESULTS AND DISCUSSION

In order to achieve a rate law equation, several parameters such as catalyst dosage, initial concentrations of $NaBH_4$ and temperature were considered. Activity of Co/Salep nano catalyst is higher than that of bare cobalt catalyst. Probably, it is attributed to the specific surface of Salep stabilized cobalt catalyst. Because of larger surface area and more active positions for hydrolysis of sodium borohydride solution by Salep stabilized cobalt powder; it is a faster, easier and significant reaction. The effect of sodium borohydride concentration on hydrogen evolution rate was studied with changing initial concentrations of $NaBH_4$ 1.25-10wt% and 2wt% NaOH while keeping the catalyst dosage constant at 50 mg Co/Salep at 318 K temperature. The volume of hydrogen gas versus time is plotted and results are shown in Fig.1(a). The volume of hydrogen generated versus time plots depending on the substrate concentrations at constant catalyst concentration. The slope (0.17) of the straight line is nearly zero indicating that the hydrolysis reaction is independent with respect to the initial concentration of $NaBH_4$. Fig.1(b) shows the plot of the volume of hydrogen gas generated from the hydrolysis of sodium borohydride solution versus time in the presence of different amounts of Co/Salep catalyst at 318K. It is clear that the hydrogen generation rate increases with the catalyst dosage increasing from 12.5, 25 and 50 mg. The hydrolysis of sodium borohydride is first order with respect to the Co/Salep catalyst dosage. As seen, the slope (1.03) of the inset diagram of Fig.1(b) is nearly 1. Finally, the rate law of the catalytic hydrolysis of $NaBH_4$ can be shown as equation (2),

$$\frac{-4d[NaBH_4]}{dt} = \frac{d[H_2]}{dt} = k[Co/Salep] \qquad (2)$$

Then, the hydrolysis of $NaBH_4$ catalyzed by Co/Salep was carried out at the temperatures of 298, 308 and 318K starting with the constant initial amounts of sodium borohydride 5wt% and 50 mg Co/Salep. The plot of the hydrogen generation at various temperatures is shown in Fig.1(c). As seen, hydrogen gas evolution increases with the temperature increasing in the range of 298-318 K. Langmuir–Hinshelwood mechanism of hydrolysis of sodium borohydride is proposed by Andrieux et al. [5].

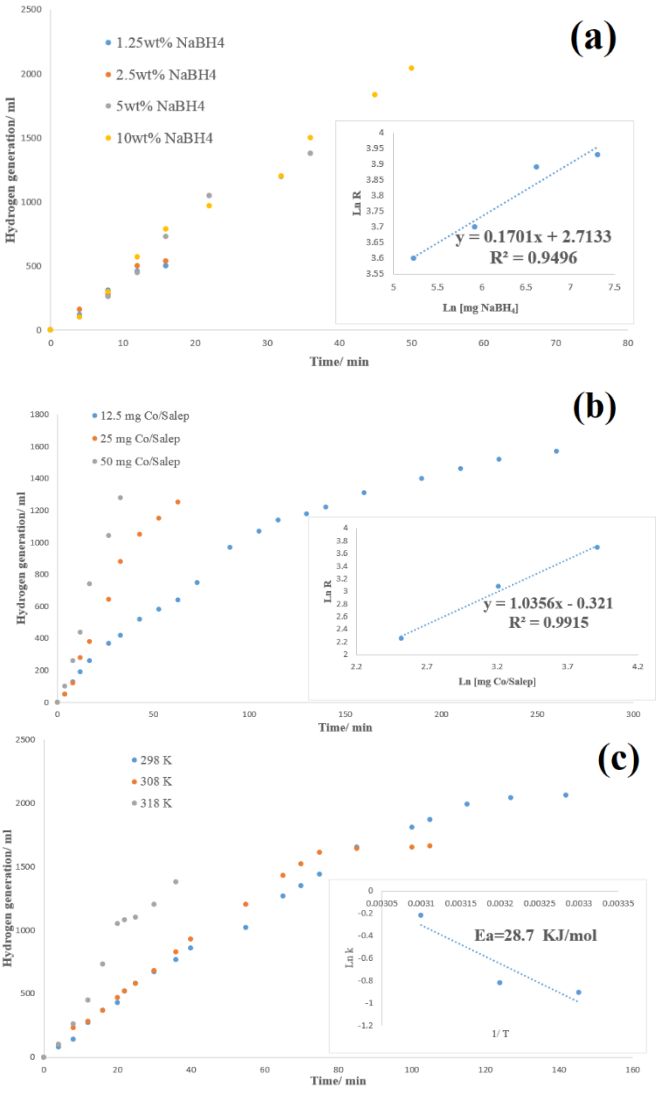

Figure1. Effect of (a) sodium borohydride concentrations, (b) dose of catalyst and (c) temperature on hydrogen generation rate

IV. CONCLUSION

In this work, a simple chemical reduction method was used to prepare Co/Salep catalysts. Effect of initial concentration of

NaBH4, catalyst dosage and temperature are discussed in this work. A kinetic study confirms that the catalytic activity of Co/Salep through hydrolysis of sodium borohydride aqueous solution is zero order with respect to $NaBH_4$ concentration and is first order with respect to catalyst dosage. The activation energy of the sodium borohydride aqueous solution hydrolysis over Co/Salep nano catalyst is obtained as 28.7 kJ mol^{-1} by Arrhenius equation.

REFERENCES

[1] M.H. Loghmani and A. Fallah Shojaei, Journal of Alloys and compounds, 580, pp. 61-66, **2013**

[2] M.H. Loghmani and A. Fallah Shojaei, International Journal of Hydrogen Energy, 38, pp. 10470-10478, **2013**

[3] M.H. Loghmani and A. Fallah Shojaei, Energy, 68, pp. 152-159, **2014**

[4] M.H. Loghmani, A. Fallah Shojaei and M. Khakzad, Energy, 126, pp. 830-840, **2017**

[5] J. Andrieux, U.B. Demirci and P. Miele, International Journal of Hydrogen Energy, 170, pp.13-19, **2011**

Theoretical study on the Potential energy surface of Numan rotation of N-Nitrosopiperazine

H. Arjmandfar

Department of chemistry, University of Zanjan, Zanjan, P. O. Box: 45195-313, Iran
Email:h110arj@yahoo.com

Abstract: To our knowledge, in large molecules Newman rotations effect on the energy barrier of reactions. A Newman rotation of the N-Nitrosopiperazine molecule has been investigated with the DFT-B3LYP method in connection with suitable triple zeta basis set. There are two barriers for NO group oration in the N-Nitrosopiperazine molecule. The computed energies for these barriers are 23.3 and 26.4 kcal mol^{-1}.

Keywords: Newman rotation, DFT-B3LYP, N-Nitrosopiperazine

I. INTRODUCTION

Piperazine (PZ) is a cyclic secondary diamine. In concentration about 5 mol dm^{-3}, aqueous piperazine is being recognized as a solvent. PZ has some applications such as (1) in CO2 absorption it acts faster than monoethanolamine (MEA). In comparison with 7 ml MEA, it has almost twice capacity. (2) Oxidative degradation by PZ is superior to MEA.[1]

PZ is a precursor of Nitrosamines. They are a class of harmful and carcinogenic compounds. [2]

II. METHODS

All electronic structure of title rotation is executed by the Gaussian 09 program [3]. Density functional theory by means of B3LYP [4] method is used for the description of electronic structures of all species. Pople triple zeta basis set, 6-311+g(d,p), is used for N, O and H atoms. Frequency calculations of transition states (TSs) and minimum geometries (G) show each TS has one imaginary frequency and each G has no imaginary frequency.

III. RESULTS AND DISCUSSION

A. Figures and Tables

Figure 1 includes the Potential energy surface which is drawn at B3LYP/6-311+g(d,p) level. Figure 2 show important bond lengths of N-Nitrosopiperazine. All absolute, zero points (ZPE) and relative energies are in Table 1.

B. PES description

The proposed PES is begun from a G1 structure. The relative energy of G1 manually has been chosen zero. So, the energy of other species has been computed relative to the G1. G1 and G2 are minimum structures in our PES. The differences between them relate to the orientation of the NO group. Also, the relative energy of G2 is zero. The proposed PES has been constituted of two transition states. The first transition state causes that G1 covert to G2 with the energy barrier of 23.30 kcal mol^{-1}. By the second transition state, TS2, G2 transformation to G1 happens. The energy barrier of TS2 about 3.14 kcal mol^{-1} is higher than TS1 barrier energy. From a geometrical point of view, the N-N bond of TS1 (1.507 Å) relative to the corresponding bond in G (1.333 Å) is elongated. Also, this elongation has been seen in TS2. The N- N bond in G2 and TS2 are 1.333 Å and 1.516 Å, respectively. The reason of high energy barrier of TS2 in comparison with TS1 is related to the differences of the N-N bond in TS1 and TS2.

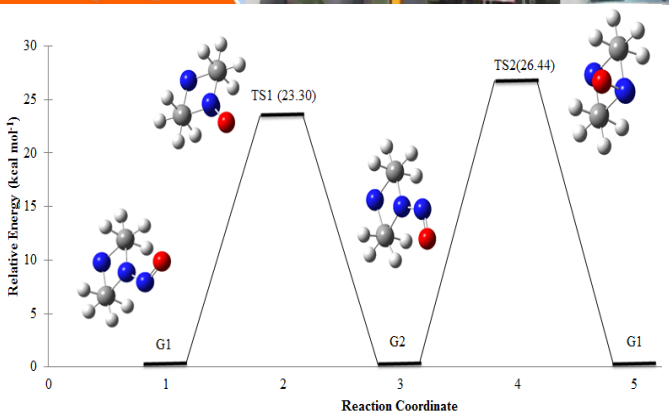

Fig.1 Potential energy surface for Newman rotation of N-Nitrosopiperazine at B3LYP/6-311+G(d,p) level of theory.

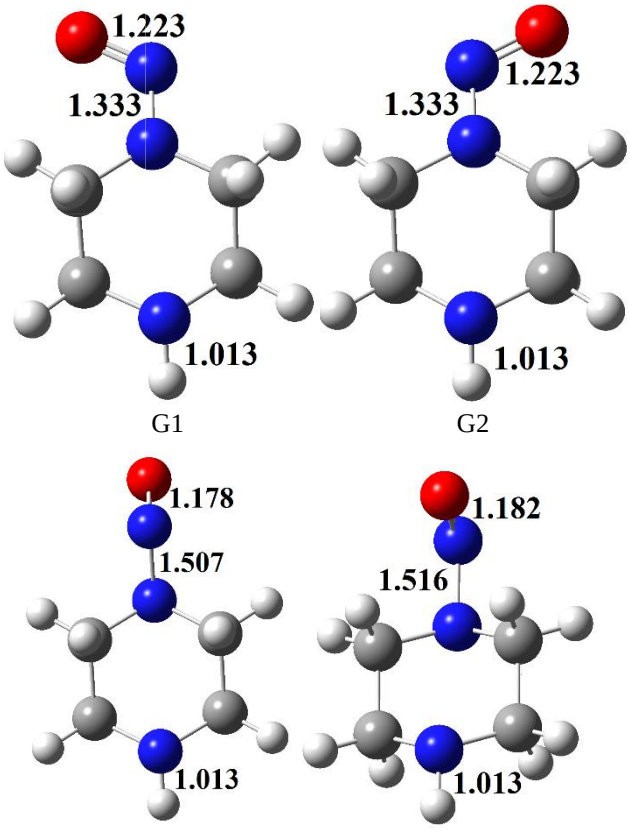

G1 G2

TS1 TS2

Fig.2 important bond lengths of N-Nitrosopiperazine.

Table1: the electronic, ZPE and relative energies of N-Nitrosopiperazine at B3LYP/6-311+G(d,p) level.

Species	Energies		
	Electronic	ZPE	Relative
G1= G2	-397.3568	0.1443	0.00
TS1	-397.3181	0.1427	23.29
TS2	-397.3128	0.1424	26.44

The electronic and ZPE energies are in Hartree
The relative energies are in kcal mol^{-1}.

IV. CONCLUSION

The PES of Newman rotations of N-Nitrosopiperazine is discussed by the DFT-B3LYP method. Two transition states for a Newman rotation is proposed. The second barrier energy due to the longer N-N bond has higher barrier energy. Relative energies of G1 and G2 are similar to the value of 0.00 kcal mol^{-1}.

REFERENCES

[1] G. Rochelle, E.Chen, S. Freeman, D.Van Wagener, Q. Xu, Chem. Eng. J. vol.171, pp.725−733, **2011**.

[2] P. T. Nielsen, L. Li, G. T. Rochelle, Presented at GHGT-11, Kyoto, Japan, published in Energy Procedia, **2013**.

[3] Lee C.; Yang W.; and Parr R.G., *Phys. Rev. B*, vol.37, pp.785-789, **1988**.

[4] Frisch M.; Trucks G.; Schlegel H.; Scuseria G.; Robb M.; Cheeseman J.; Scalmani G.; Barone V.; Mennucci B.; Petersson G., Revision A, 2, **2009**.

The Potential Energy surface of Numan Rotation of N,N'-dinitrosopiperazine: A Theoretical study

H. Arjmandfar

Department of chemistry, University of Zanjan, Zanjan, P. O. Box: 45195-313, Iran
Email:h110arj@yahoo.com

Abstract: Newman rotations of large molecules are important relative to small molecules because the energy barrier of large molecules reactions due to their rotations can be changed. One Newman rotations for N,N'-dinitrosopiperazine molecule with two barriers is studied. The PES of NO rotation of N,N'-dinitrosopiperazinee is evaluated by DFT-B3LYP method in connection with the Pople 6-311+g(d,p) basis set. During NO rotation There are two barriers with the barrier energies of 24.72 and 28.69 kcal mol^{-1} in N,N'-dinitrosopiperazine molecule.

Keywords*:* NO rotation, DFT-B3LYP, N,N'-dinitrosopiperazine

I. INTRODUCTION

In human saliva and gastric juice, Piperazine (PZ) is quickly nitrosated and yields N-mononitrosopiperazine (MNPZ) and N,N'-dinitrosopiperazine (DNPZ) under in vitro conditions [l]. Also, ingested piperazine nitrosation with nitrite has been demonstrated. Recently, MNPZ is found in human urine and human stomach after ingestion of piperazine by Bellander et al. [2]. The carcinogenic tests show DNPZ, and possibly MNPZ, are dangerous for laboratory animals [3].

II. METHODS

Gaussian 09 program is used for the electronic structure and N,N'-dinitrosopiperazine rotation description [4]. The B3LYP method [5] is implemented for investigation of the electronic structures of all species. For electronic structure calculation of N, O and H atoms suitable triple zeta basis set, Pople 6-311+g(d,p) basis set, is used. Frequency calculations are carried out at the same level. It is used for verifying nature of transition states (TSs) and minimum geometries (G). The results show TS1 and TS2 have one imaginary frequency and G1 and G2 have no imaginary frequency.

III. RESULTS AND DISCUSSION

A. Figures and Tables

In Figure 1, Potential energy surface (PES) of N,N'-dinitrosopiperazine is depicted at B3LYP/6-311+g(d,p) level of theory. Figure 2 shows the critical bond lengths of N,N'-dinitrosopiperazine

All calculated energies at B3LYP/6-311+g (d, p) level, such as absolute, zero points (ZPE) and relative are collected in Table 1.

B. PES description

The starting point of the PES is G1 with zero relative energy similar to N-nitrosopiperazine (N-PZ) study. The energies of G2, TS1, and TS2 have been calculated relative to G1. TS1 and TS2 (maximum structures) are connected to G1 and G2 minimum structures in the proposed PES. The relative energy of G2 is 0.1 kcal mol^{-1} higher than the corresponding structure in comparison with the N- PZ study. The origin of the differences is related to NO group orientations. Two transition states have proposed for PES. TS1 converts the G1 conformer to G2 conformer and TS2 transforms G2 to G1. The energy barriers of mentioned conversions are 24.72 and 28.69 kcal mol^{-1}, respectively. The corresponding transformations in N-PZ work were 23.30 and 26.44 kcal mol^{-1}, respectively. From a geometrical point of view, the bond lengths of N-N for TS1 and TS2 are 1.518 Å and 1.505 Å, respectively. Similar bond lengths in G1 and G2 are the same as the value of 1.339 Å. The difference of barrier energy of TS2 in comparison with TS1 may be related to overlapped orbits of nitrogen atoms in the geometries of the mentioned transition states.

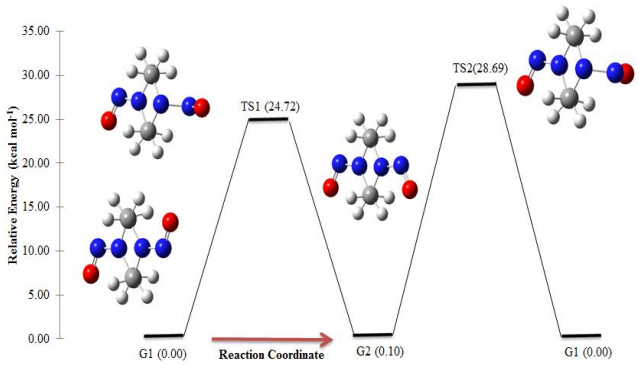

Fig. 1Potential energy surface for Newman rotation of N,N'-dinitrosopiperazine at B3LYP/6-311+G(d,p) level of theory.

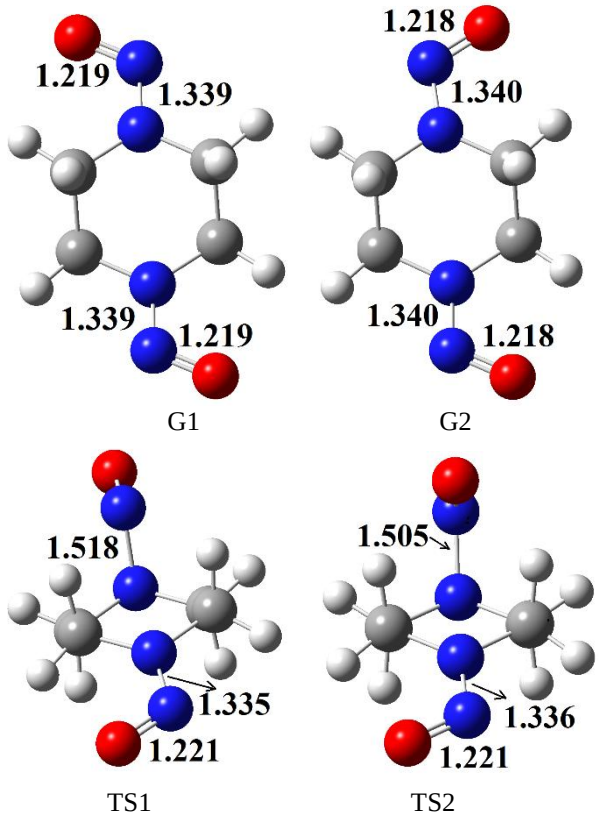

G1 G2

TS1 TS2

Fig.2 critical bond lengths of N,N'-dinitrosopiperazine

Table1: all of the computed energies for N,N'-dinitrosopiperazine at B3LYP/6-311+G(d,p) level.

Species	Energies		
	Electronic	ZPE	Relative
G1	-526.6968	0.1408	0.00
G2	-526.6967	0.1409	0.10
TS1	-526.6557	0.1391	24.72
TS2	-526.6492	0.1390	28.69

The electronic and ZPE energies are in Hartree
The relative energies are in kcal mol^{-1}.

IV. CONCLUSION

The DFT-B3LYP/6-311+g(d,p) level for (Newman rotation) PES of N,N'-dinitrosopiperazine is used. For N,N'-dinitrosopiperazine the proposed transition states have higher energy than N-nitrosopiperazine. The higher barrier energy of TS2 is related to overlapped orbitals of the N-N bond. The relative energy of G2 is 0.10 kcal mol^{-1} higher than the G2 in N-nitrosopiperazine study.

REFERENCES

[1] G.S. Rao, and D.A. McLennon, J. Anal. Toxicol., vol.1, pp. 43, **1975**
[2] B.T.D. Bellander, L.E. Hagmar, and B. G. Osterdahl, Lancet, vol.ii 372,**1981**
[3] H. Garcia, L. Keefer, W. Lijinski and C.E.M.Wenyon, Z. Krebsforsch., vol. 74,pp. 179,**1970**
[4] Lee C.; Yang W.; and Parr R.G., *Phys. Rev. B*, vol.37, pp.785-789, **1988**.
[5] Frisch M.; Trucks G.; Schlegel H.; Scuseria G.; Robb M.; Cheeseman J.; Scalmani G.; Barone V.; Mennucci B.; Petersson G., Revision A, 2, **2009**.

One-Pot Synthesis of Succinimide-3-Carboxamide Derivatives Using Microwave and Mechanistic insights and Kinetics analysis by Computational Method

***M. A. Kazemian*[a]*, S.M.R. Hosseini-Tabatabaei[a], Z.Shirdel[a]**

Department of Chemistry, Islamic Azad University, Zahedan Branch, Zahedan, , P.O. Box 98135-978, Iran

Email:kazemean@yahoo.com

Abstract: In the present work one-pot, four-component condensation of meldrum's acid and acetone with tert-butyl isocyanides in the presence primary amines under microwave irradiation which provided 1-tert-butyl-4,4-dimethyl-2,5-dioxopyrrolidine-3-carboxamides in short time with high yields have been investigated. Also, multiple mechanisms have been studied theoretically for comparing formation of the amidosuccinimide with triamide products from intermediate 9 using ab initio molecular orbital theory in gas phase. The potential energy profile was constructed at the HF/6-311G (d, p) level of theory. Among four speculative proposed path only the pathway A (intramolecular reaction to formation amidosuccinimide product) was recognized as a desirable mechanism. Theoretical kinetics data involving k and activation parametres were calculated for each step of the paths.

Keywords: Meldrum's acid; tert-butyl isocyanides; Mechanism; Theoretical and kinetics investigation; Two dimensional scanning.

I. INTRODUCTION

Multi-component reactions (MCRs), a type of reaction in which three or more compounds connect together by covalent bonds to produce a complex molecule that contains the main structure of all the starting materials. During the last few decades the field of IMCR research has experienced a steadfast growth with the discovery and development of new variations of the classical Passerini and Ugi IMCR.[1] Ugi four-component reaction (U-4CR). [2] and Passerini three component reaction (P-3CR)[3] are among the most important IMCRs. For the reaction of isocyanides with carboxylic acids in the presence of imines and aldehydes U-4CR and P-3CR are the describe ways, respectively. Microwave-assisted rapid organic reactions constitute an emerging technology that make experimentally and industrially important organic syntheses more effective and more ecofriendly than conventional reactions [4]. The latter synthesis used a procedure first described by yavari et al. [5] in which they synthesized a series of mixture of triamide and amidosuccinimide derivatives via isopropylidene meldrum's acid with tert-butyl isocyanide in the presence of two equivalents of primary amines in CH_2Cl_2. In the present work, we achieved a novel one-pot, one product, four-component condensation of acetone, meldrum's acid, tert-Butyl isocyanide in the presence of one equivalents of primary amines under microwave irradiation as a new efficient method to produce amidosuccinimide derivatives. In recent years, computational approaches have been developed and these have been important in kinetics and mechanistic investigations [6-9].

Here in, for the first time we describe theoretical studies of kinetics and a full mechanistic investigation for the reaction between acetone, meldrum's acid, tert-Butyl isocyanide in the presence of primary amines, in the gas phase.

II. METHODS

All geometries of the reactants, product, intermediates and transition states involved in the reaction were optimized at the HF/3-21G(d, p) level of theory in the gas phase. The vibrational frequencies were obtained for the verification of the optimized geometries at HF/3-21G(d, p) and HF/6-311G(d, p) levels. The intrinsic reaction coordinate (IRC) pathway from the transition states was performed to confirm the connection between reactants, transition states, and the products of each step. The activation energies (Ea) and the rate constants were computed using Eqs. All calculations were performed with the GAMESS program.

III. RESULTS AND DISCUSSION

A. Theoretical studies

To gain an insight into the mechanism, a theoretical kinetic investigation for comparison intramolecular reaction of intermediate 9 which lead to product 5 along with the reaction between intermediate 9 and aniline to form triamide product that did not get in this work was performed using computational methods. To achieve this, the proposed four mechanisms have been investigated theoretically.

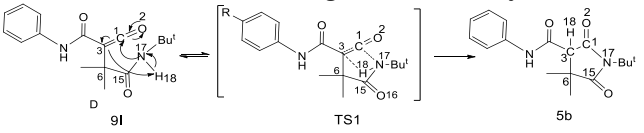

Fig.1: The pathway A for the generation of product (5b).

In pathway A (Fig. 1), intermediate 9 and aniline react through the concerted and intramolecular reaction and the reaction passes through TS_1 which involving a four-membered ring (between N_{17}, H_{18}, C_1, C_3 atoms) for formation of 5b. To obtain the energy profile, in each step of scanning N_{17}

approached to C_1 (0.1Å) after each time, H_{18} go to the near of C_3 step by step until a peak obtained (two dimensional scanning). After each scan, the result of this step was represented in a diagram. Then, we approached again N_{17} to C_1 step by step and repeated this large range. These results were represented in a separate diagram and the energy of all high energy points (TS) in each step was drawn versus to the N_{17}-C_1 bond length changes, see Fig. 2.

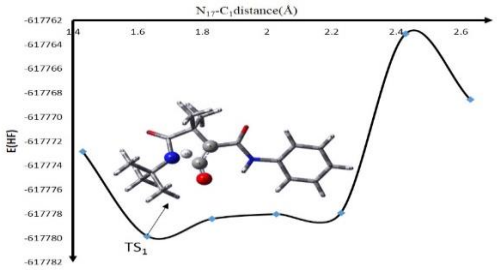

Fig.2: The two dimensional scanning of the obtained TS_1 structure

The TS_1 energy at the HF/3-21G level in the gas phase is 45.71 and 86.31kcal/mol higher than the energy of the intermediate 9 and product (5b), respectively. Imaginary frequency (863.62cm^{-1}) implies that TS1 is a transition state. Hence, this process is endothermic (Δr=-40.60kcal/mol) compared to the reactants. The activation energy for this path of the reaction is 45.71 kcal/mol. Also the single-point energy of the TS_1 at the 6-311G(d,p) level in the gas phase is 40.28 kcal mol^{-1}, and 86.51 kcal mol^{-1} higher than the energy of the intermediate 9 and 5b, respectively.

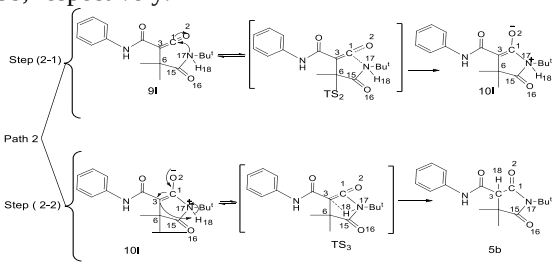

Fig.3: The pathway B for the generation of product (5b)

The first step of the pathway B, the concerted reaction occurs with the C_1-N_{17} bond formation through intramolecular reaction of intermediate 9 for the generation dipole intermediate ion (10I). The second transition state (TS_2, see Fig. 3) has a forming C_1-N_{17} bond distance of 1.93Å. Herein, TS_2 showed one imaginary frequency at 167.28cm^{-1}. The structure and potential energy profile of TS_2 is shown in Fig.4.

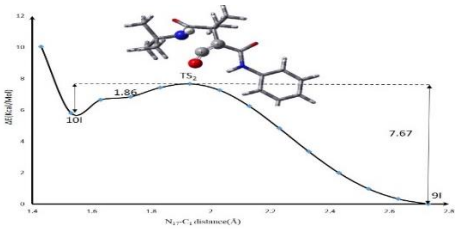

Fig.4: The potential energy profile for step1 of pathway B at the HF/3-21G level in the gas phase

The TS_2 energy at the HF/3-21G level in the gas phase is 7.67 and 1.86 kcal/mol higher than the energy of the reactant and 10I, respectively (see Fig.4). Hence, this process is endothermic (Δr=5.81kcal/mol) compared to the reactants.

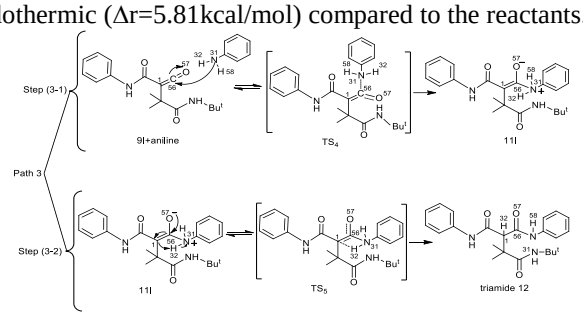

Fig. 5. The possible pathway C of the proposed theoretical mechanism for the generation of triamide 12

In the first step of the pathway C, the concerted reaction occurs with the C56-N31 bond formation between intermediate 9 and aniline for the generation of dipole intermediate ion (intermediate11) (TS_4, see Fig. 5). Has a C_{56}-N_{31} forming bond distance of 1.72Å. Herein, TS_4 showed one imaginary frequency 140.14 cm^{-1}. The structure and potential energy profile of TS4 is shown in Fig.6.

In pathway D (Fig.8), compound 9I and aniline react through the concerted reaction and the reaction passes through TS_6 which involving a four-membered ring (between N_{31}, H_{32}, C_1, C_{56} atoms) for formation of triamide 12. The TS_5 energy at the HF/3-21level in the gas phase is 33.10and 89.53 kcal/mol higher than the energy of the 11I and product triamide12, respectively (see Fig.7).

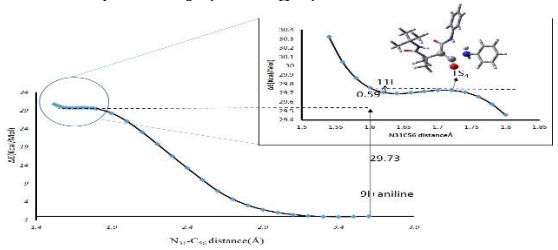

Fig. 6. The potential energy profile for step1of pathway C

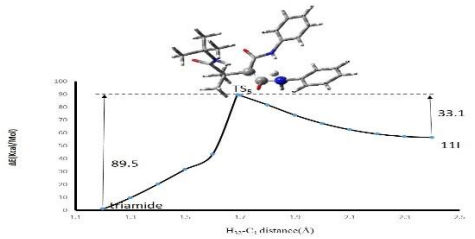

Fig. 7. The potential energy profile for step2 of pathway C

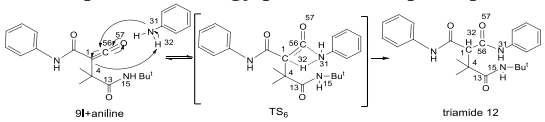

Fig. 8. The possible pathway D of the proposed theoretical mechanism for the reaction between intermediate 9 and aniline for formation of triamide 12

Activation parameters involving $\Delta H^{\ddagger}$, $\Delta G^{\ddagger}$ and $\Delta S^{\ddagger}$ for each path of the desirable theoretical mechanism at 298.15K, are reported in Table 8. The kinetic data involving activation energies, the rate constant (k) and pre-exponential factor using Eyring equation are reported in Table 1.

Table1: The activation parameters involving ΔH‡,ΔG‡, and ΔS‡ for each step of the desirable mechanism at 298.15K

Pathway A	**$\Delta H^{\ddagger}_{\text{Pathway A}}$**	**42.16**	**$\Delta G^{\ddagger}_{\text{Path1}}$**	**44.52**	**$\Delta S^{\ddagger}_{\text{Pathway A}}$**	**-7.91**
Pathway A	$\Delta H^{\ddagger}_{\text{Path}-1}$	83.39	$\Delta G^{\ddagger}_{\text{Path}-1}$	82.31	$\Delta S^{\ddagger\neq}_{\text{Path}-1}$	**3.64**
Pathway B	$\Delta H^{\ddagger}_{a}$	7.14	$\Delta G^{\ddagger}_{\text{a}}$	10.24	$\Delta S^{\ddagger}_{a}$	**-10.42**
Step (2-1)	$\Delta H^{\ddagger}_{-a}$	0.43	$\Delta G^{\ddagger\neq}_{-a}$	0.47	$\Delta S^{\ddagger}_{-a}$	**-0.13**
Pathway B	$\Delta H^{\ddagger}_{b}$	43.87	$\Delta G^{\ddagger}_{\text{b}}$	45.38	$\Delta S^{\ddagger}_{b}$	**-5.06**
Step (2-2)	$\Delta H^{\ddagger}_{-b}$	78.50	$\Delta G^{\ddagger\neq}_{-b}$	77.70	$\Delta S^{\ddagger}_{-b}$	**2.70**
Pathway C	$\Delta H^{\ddagger}_{c}$	30.10	$\Delta G^{\ddagger}_{c}$	35.62	$\Delta S^{\ddagger}_{c}$	**-18.51**
Step (3-1)	$\Delta H^{\ddagger}_{-c}$	-0.82	$\Delta G^{\ddagger\neq}_{-c}$	-0.24	$\Delta S^{\ddagger}_{-c}$	**-1.93**
Pathway C	$\Delta H^{\ddagger}_{d}$	30.73	$\Delta G^{\ddagger}_{\text{d}}$	30.70	$\Delta S^{\ddagger}_{d}$	**0.09**
Step (3-2)	$\Delta H^{\ddagger}_{-d}$	86.10	$\Delta G^{\ddagger\neq}_{-d}$	87.27	$\Delta S^{\ddagger}_{-d}$	**-0.92**
Pathway D	$\Delta H^{\ddagger}_{\text{Pathway D}}$	62.50	$\Delta G^{\ddagger}_{\text{Pathway D}}$	68.78	$\Delta S^{\ddagger}_{\text{Pathway D}}$	**-21.08**
Pathway D	$\Delta H^{\ddagger}_{\text{Pathway D}}$	88.77	$\Delta G^{\ddagger}_{\text{Pathway D}}$	91.61	$\Delta S^{\ddagger}_{\text{Pathway D}}$	**-9.52**

IV. CONCLUSION

The computed rate constants and activation energies with respect to the frequency calculations demonstrate that this pathway A is a rate-determining step which has a forward Ea=45.71kcal mol^{-1} and $k_{\text{pathwayA}}=3.57\times10^{-17}(s^{-1})$. Based on quantum mechanical calculations, only the first speculative mechanism (pathway A) as a desirable reaction mechanism.

REFERENCES

[1] B. H. Rotstein, S. Zaretsky, V. Rai, A. K. Yudin, Chem. Rev. vol. 114, pp. 8323-8326, **2014**.
[2] I. Ugi, B. Werner, A. Domling, Molecules vol. 8, pp.53-56, **2003.**
[3] M. Passerini, Gazz. Chimi. Italian. Vol. 51, pp. 126-132, **1921**.
[4] R. S. Varma, Green Chem. Vol. 1, pp. 132, **1999**.
[5] I. Yavari, A. Habibi, M.R. Hosseini-Tabatabaei, H.R. Bijanzadeh, Monatsh. Chemie, vol 134, pp. 1651, **2003**.
[6] M. Dehdab, M. Shahraki, S.M. Habibi-Khorassani. Amino Acids, vol. 54, pp.1450-1455, **2015**.
[7] M.A. Kazemian, S.M. Habibi-Khorassani, A. Ebrahimi, M.T. Maghsoodlou, P. Mohammadzadeh-Jahani, M. Ghahramaninezhad. J Mol Model, vol 18, pp.5075-5088, **2012**.
[8] M.A. Kazemian, S.M. Habibi-Khorassani, M.T. Maghsoodlou, A. Ebrahimi, J Mol Model, vol. 20, pp. 2103-2114, **2014.**

The gas phase reaction of $CH_2CH_2OH + NH_2$: A computational study

H. Zarepour [a], ***H. Douroudgari****[a], ***M. Vahedpour***[a]
Department of Chemistry, University of Zanjan, PO Box 38791-45371, Zanjan, Iran
E-mail: Douroudgari@Znu.ac.ir

Abstract: In the atmosphere, the reactions of CH_2CH_2OH with active compounds can play an important role in the fate of it. Theoretical investigations on the mechanism of the $CH_2CH_2OH + NH_2$ reaction carried out in the gas phase. The quantum mechanics methods are used for thermodynamic and mechanism consideration of the title reaction. The rate of the reaction is calculated in the atmospheric conditions. Finally, the exit channel adducts are investigated thermodynamically.

Keywords: CH_2CH_2OH, Mechanism, Thermodynamic

I. INTRODUCTION

In the hybrid fuels, including ethanol– gasoline can be used by combustion engines. The fuels contain up to 15% ethanol. Also, they may have 85% ethanol and15% gasoline [1]. Today, agricultural crops and residues used in the production of bioethanol. By surveying the literature, we find that sugar crops have 60% contribution and the contribution of other crops is 33% in the world ethanol production. The chemical synthesis by industrial activity has just 7% contribution. [2-3]. So, It mainly released to the atmosphere by mentioned activities.

II. METHODOLOGY

The B3LYP method in combination with a double zeta basis set, 6-31g(d, p), is used in the optimization of the geometries of the stationary points. In the reaction path, the stationary points are reactants, complex reactant, transition state, post reactive complex, and products which denoted by R, CR, TS, CP, and P, respectively. The frequencies of all species harmonically are calculated at the same level for characterizing the origin of the stationary point. In addition, the potential energy surface (PES) is computed by a more accurate method. So, the CCSD(T) method with the 6-31g(d, p) basis set is used on the obtained geometries of the B3LYP/6-31g(d, p) level.

III. RESULTS AND DISCUSSION

A. *Figures and Tables*

Figure 1 shows the presented PES at CCSD(T). Table 1 includes the computed energies at B3LYP and CCSD(T) methods. Table 2 involves the thermodynamic parameters for obtaining products.

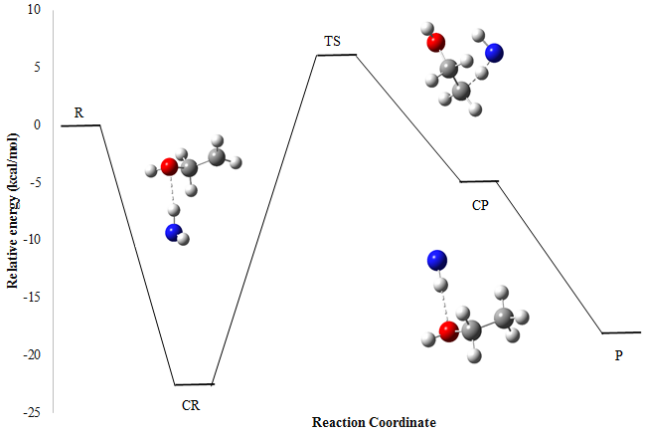

Fig.1: the potential energy surface of the $CH_2CH_2OH + NH_2$ at CCSD(T)/6-31g(d, p) of theory.

Table1: : Computed energies at B3LYP and CCSD(T) Methods.

species	E(Hartree)	Δ*E*(kcal/mol)
R	-209.6760	0.00
CR	-209.7120	-22.57
TS	-209.6662	6.12
CP	-209.6838	-4.88
p	-209.7047	-18.02

Table2:Thermodynamic parameters (in kcal/mol) of the product at B3LYP Method

species	ΔE°	ΔH°	ΔG°	ΔS°
R	0.00	0.00	0.00	0
CR	-2.52	-3.11	3.98	-7.09
TS	1.73	1.13	12.16	-11.02
CP	-2.52	-3.11	3.98	-7.09
p	-10.09	-10.09	-7.87	-2.21

B. Reaction mechanism

For the reaction of CH_3CH_2OH with ^3NH, the mechanism is investigated in the doublet state. At the beginning of the reaction the pre-reactive complex, CR, is observed(see Fig.1). The CR complex is more stable than free reactants with the relative energy of -22.57 kcal mol^{-1}. The conversion of CR to CP is needed to overcome the predicted TS. The TS has 28.69 kcal mol^{-1} barrier energy. The TS structure involves the hydrogen migration from NH_2 fragment to CH_2CH_2OH fragment. IRC calculation show TS is connected to two minimums. The post reactive complex, CP, is another minimum with the relative energy of -4.88 kcal mol^{-1}. Finally, ^3NH and CH_3CH_2OH adducts are released in the exit channel from CP. On the Thermodynamic point of view, the obtained adducts have favorable Gibbs free energy and enthalpy with the values of -7.87 and 10.09, respectively.

IV. CONCLUSION

We investigated the degradation of ethanol in the atmosphere The reaction mechanism of $CH_2CH_2OH + NH_2$ is explored by using DFT and ab initio methods. Also, thermodynamic of the reaction is considered.

REFERENCES

[1] Y. Sun and J. Cheng, Bioresour. Technol., 83, pp.1–11, **2002**.

[2] D. Pimentel and T. W. Patzek, Natural Resources Research, 14, pp.65–76, **2005**.

[3] T. W. Patzek, Natural Resources Research, 15, pp.255–270, **2007**.

The reaction of $CH_2OH + NH_2$ in the gas phase

H. Zarepour [a], ***H. Douroudgari*** [a]*, ***M. Vahedpour*** [a]
Department of Chemistry, University of Zanjan, PO Box 38791-45371, Zanjan, Iran
E-mail: Douroudgari@gmail.com

Abstract: Hydrogen abstraction of methanol by active atmospheric species plays a critical role in the degradation of it. Reaction of the H-addition to CH_2OH by NH_2 in the gas phase is investigated mechanistically based on the quantum mechanics methods. Finally, obtained adduct in the exit channel is considered thermodynamically.

Keywords: CH_3OH, ^3NH, Gas phase

I. INTRODUCTION

Methanol is a toxic compound. Its toxicity is confirmed when a human has consumed it. Methanol causes human poisoning [1,2]. The important metabolic adduct of methanol is formic acid. Formic acid leads to physical harms such as various neurological sequelae, acidosis, death in severe cases, and potential blindness [2–4]. So, its degradation in the atmosphere is important. In this work, we proceed the pathway of methanol degradation using computational chemistry.

II. METHODS

The popular DFT, B3LYP, is used for full optimization of reactants (R), complex reactant, (CR), transition state (TS), post reactive complex, (CP) and products (P). Double zeta basis set, 6-31g(d, p) is used with B3LYP method. Harmonic frequencies are computed for all species at B3LYP/6-31g(d, p) level of theory. In addition, the CCSD(T) method is carried out on the potential energy surface (PES) of the reaction at B3LYP/6-31g(d,p) level for reaching precise energies. The same basis set is implemented for CCSD(T) method.

III. RESULTS AND DISCUSSION

This section must be included experimental or computational data, figures, tables, and equations. The number of figures, tables, and equations throughout the text must be brought orderly.

A. Figures and Tables

The PES of the reaction at the CCSD(T) method is plotted in figure 1. The computed energies at CCSD(T) methods are collected in table 1. Thermodynamic parameters of the product are listed in table 2.

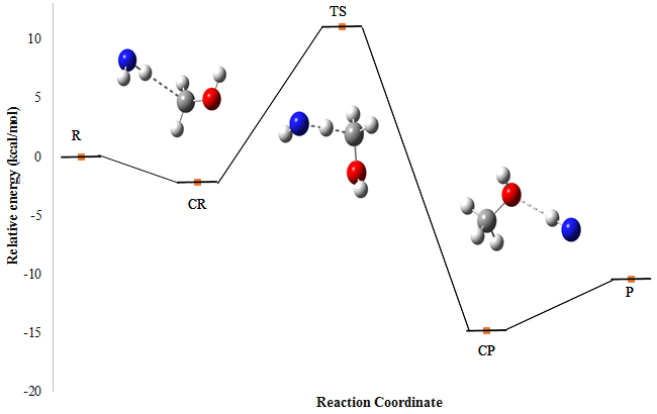

Fig.1: the potentiall energy surface of thye reaction at CCSD(T)/6-31g(d,p)//B3LYP/6-316-31g(d,p)level.

Table1: Computed energies at CCSD(T) Methods.

Species	E(Hartree)	ΔE(kcal/mol)
R	-170.48	0.00
CR	-170.49	-2.21
TS	-170.47	11.04
CP	-170.51	-14.83
p	-170.5	-10.47

Table2: Thermodynamic parameters (in kcal/mol) of the product at B3LYP Method.

Species	ΔE°	ΔH°	ΔG°	ΔS°
R	0.00	0.00	0.00	0.00
CR	-0.96	-1.55	4.72	-6.27
TS	4.95	4.35	13.78	-9.43

Species	ΔE°	ΔH°	ΔG°	ΔS°
CP	-5.69	-6.28	1.44	-7.72
p	-2.91	-2.91	-1.37	-1.54

B. Reaction mechanism

The reaction mechanism is explored in the triplet state. As shown in the Fig.1 the reaction is started with the formation of CR. The relative energy of CR is -2.21 kcal mol^{-1}. After Cr, the reaction continues with surmounting the bare energy of the TS. The barrier height of the TS is 13.25 kcal mol^{-1}. From a geometrical point of view, in the structure of the TS NH_2 moiety give a hydrogen atom to CH_2OH fragment. After TS, the post-reactive complex is created by the relative energy of -14.83 kcal mol^{-1}. In the final step, CP released to final adducts. Thermodynamically, the ^3NH and CH_3OH adducts have the favorable Gibbs free energy and enthalpy of the reaction with the values of -1.37 and -2.91 kcal mol^{-1}, respectively.

IV. CONCLUSION

We investigated the degradation of methanol in the atmosphere. The reaction mechanism of CH_2OH + NH_2 is explored by using DFT and ab initio methods. The obtained product is investigated thermodynamically.

REFERENCES

[1] E. Bogen, Calif Med, 65, pp.230-234, **1946**.

[2] PE. Hantson, Bull Mem Acad R Med 756 Belg, 161, pp.425-434, **2006**.

[3] JT. Eells, MM. Salzman, MF. Lewandowski, TG. Murray, Toxicol Appl Pharmacol, 140, pp.58-69, **1996**.

[4] J. Liesivuori, H. Savolainen, Pharmacol Toxicol, 762, pp.157-163, **1991**.

The atmospheric reaction of HS + HOCl: mechanistic and thermodynamic viewpoints

Kh. Seydi [a], ***H. Douroudgari*** [a]*, ***M. Vahedpour*** [a]
Department of Chemistry, University of Zanjan, PO Box 38791-45371, Zanjan, Iran
E-mail: Douroudgari@zunu.ac.ir

Abstract: Hydrogen abstraction reactions are a key reaction in both combustion and atmospheric chemistry. The atmospheric reaction of HOCl plus SH is investigated Theoretically based on DFT-MN12l and CCSD(T) methods. The energetic parameters of all stationary points through in the path are computed.

Keywords: HOCl, Atmospheric reaction, Thermodynamic

I. INTRODUCTION

The HOCl is named hypochlorous acid. It is a temporary source for Cl and ClO (generally ClOx) copmounds in the atmosphere and stratosphere [1-4]. The HOx and the ClOx cycles are coupled with the ozone depletion cycle by the HOCl photolysis reaction [5]. So, degradation of HOCl in the atmosphere is important .

II. METHODOLOGY

The Gaussian 09 program is used for electronic structure calculation of all stationary points. Optimization of all stationary points carried out by the density functional method, MN12l method, the suitable double zeta basis set, 6-31+G(d,p), accompanied by MN12l method. We used instead of reactants, complex reactant, transition state, post reactive complex, and products from their abbreviations such as R, CR, TS, CP, and P, respectively. To confirm the origin of each stationary point, we used frequencies of it. So, the harmonic frequencies of all stationary points are computed at MN12l/6-31+G(d,p) level. After that, the potential energy surface (PES) of the reaction contained by the CCSD(T)/6-31G(d,p) level.

III. RESULTS AND DISCUSSION

A. Figures and Tables

The CCSD(T) method is used for the plotted PES and is shown in Figure 1 shows. All of the computed energies at the mentioned methods are collected in Table 1. The thermodynamic parameters of ClO and H2S adducts are listed in Table 2.

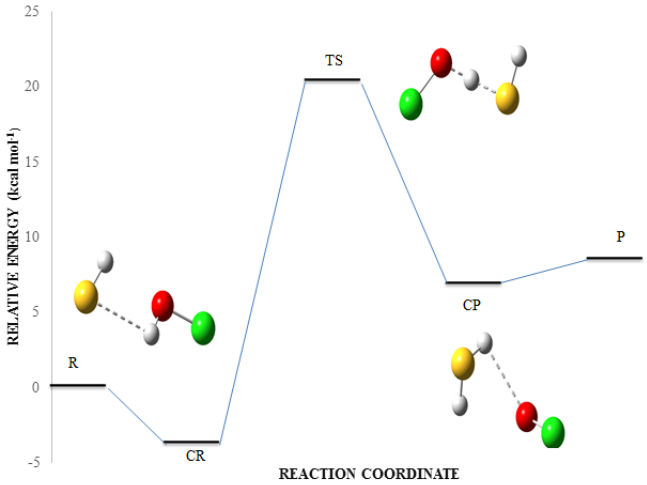

Fig.1: the potential energy surface of the HS + HOCl at CCSD(T)/6-31G(d,p) level of theory.

Table1: The calculated energies at CCSD(T)/6-31G(d,p)// MN12l/6-31+G(d,p) level.

Species	E (Hartree)	ΔE (kcal/mol)
R	-933.4023	0.00
CR	-933.4083	-3.77
TS	-933.3698	20.34
CP	-933.3914	6.83
p	-933.3888	8.44

Table2: Thermodynamic parameters (in kacl/mol) of the product at MN12l/6-31+G(d,p) level.

Species	ΔE°	ΔH°	ΔG°	ΔS°
R	0	0	0	0.00
CR	-2.36	-1.97	-1.97	-6.82
TS	11.57	11.20	11.20	-8.76
CP	3.96	4.36	4.36	-6.68
p	5.80	5.78	6.37	0.30

B. Reaction mechanism

In the doublet state, just the H-abstraction mechanism for title reaction is studied. As seen in Fig.1, The pre-reactive complex, CR, is the starting step of the reaction. It contains a Van der Waals interaction among HOCl and HS fragments. So, the relative stability of the CR complex is -3.77 kcal mol^{-1}. The predicted TS is connected from CR to CP with the barrier energy of 24.11 kcal mol^{-1}. From a geometrical point of view, the TS structure includes the hydrogen shifting from HOCl moiety to SH moiety. The two minimums, CR and CP, of the TS, are confirmed by IRC calculation. The product complex, CP, has the relative energy of 6.83 kcal mol^{-1}. The final stage of the reaction is ClO and H_2S releasing from CP complex. The product formation is investigated thermodynamically. It shows the P (ClO+ H_2S) adduct have negative Gibbs free energy and enthalpy.

IV. CONCLUSION

We explored the hydrogen abstraction reaction mechanism of the HOCl + SH reaction in the atmospheric conditions. The DFT (MN12l) and ab initio (CCSD(T) methods are used for derivation of the results. Also, key parameters of the thermodynamic (ΔG^o, ΔH^o, and ΔS^o) for all species are derived from the investigated reaction.

REFERENCES

[1] Y. L. Yung, J. P. Pinto, R. T.Watson, S. P .Sander, J. Atmos. Sci., 37, pp.339–353, **1980**.

[2] G. Poulet, M. Pirre, F. Maguin, R. Ramaroson, G. Lebras, Geophys. Res. Lett., 19, pp.2305–2308, **1992**.

[3] R. R. Garcia, S. J. Solomon, Geophys. Res., 99, pp.12937–12951, **1994**.

[4] S. C. Wofsy, , M. B. Can. McElroy, J. Chem., 52, pp.1582–1591, **1974**.

[5] S. Solomon, R. R. Garcia, F. S. Rowland, D. Wuebbles, J. Nature, 321, pp.755–758, **1986**.

The atmospheric reaction of HS + HOCl: mechanistic and thermodynamic viewpoints

Kh. Seydi [a], ***H. Douroudgari*** [a]*, ***M. Vahedpour*** [a]
Department of Chemistry, University of Zanjan, PO Box 38791-45371, Zanjan, Iran
E-mail: Douroudgari@zunu.ac.ir

Abstract: Hydrogen abstraction reactions are a key reaction in both combustion and atmospheric chemistry. The atmospheric reaction of HOCl plus SH is investigated Theoretically based on DFT-MN12l and CCSD(T) methods. The energetic parameters of all stationary points through in the path are computed.

Keywords: HOCl, Atmospheric reaction, Thermodynamic

I. INTRODUCTION

The HOCl is named hypochlorous acid. It is a temporary source for Cl and ClO (generally ClOx) copmounds in the atmosphere and stratosphere [1-4]. The HOx and the ClOx cycles are coupled with the ozone depletion cycle by the HOCl photolysis reaction [5]. So, degradation of HOCl in the atmosphere is important .

II. Methodology

The Gaussian 09 program is used for electronic structure calculation of all stationary points. Optimization of all stationary points carried out by the density functional method, MN12l method, the suitable double zeta basis set, 6-31+G(d,p), accompanied by MN12l method. We used instead of reactants, complex reactant, transition state, post reactive complex, and products from their abbreviations such as R, CR, TS, CP, and P, respectively. To confirm the origin of each stationary point, we used frequencies of it. So, the harmonic frequencies of all stationary points are computed at MN12l/6-31+G(d,p) level. After that, the potential energy surface (PES) of the reaction contained by the CCSD(T)/6-31G(d,p) level.

III. RESULTS AND DISCUSSION

A. Figures and Tables

The CCSD(T) method is used for the plotted PES and is shown in Figure 1 shows. All of the computed energies at the mentioned methods are collected in Table 1. The thermodynamic parameters of ClO and H2S adducts are listed in Table 2.

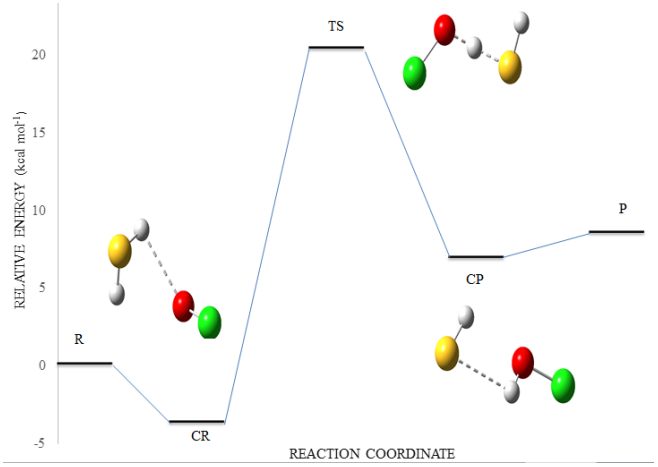

Fig.1: the potential energy surface of the HS + HOCl at CCSD(T)/6-31G(d,p) level of theory.

Table1: The calculated energies at CCSD(T)/6-31G(d,p)// MN12l/6-31+G(d,p) level.

Species	E (Hartree)	ΔE (kcal/mol)
R	-933.4023	0.00
CR	-933.4083	-3.77
TS	-933.3698	20.34
CP	-933.3914	6.83
p	-933.3888	8.44

Table2: Thermodynamic parameters (in kacl/mol) of the product at MN12l/6-31+G(d,p) level.

Species	ΔE°	ΔH°	ΔG°	ΔS°
R	0	0	0	0.00
CR	-2.36	-1.97	-1.97	-6.82
TS	11.57	11.20	11.20	-8.76
CP	3.96	4.36	4.36	-6.68
p	5.80	5.78	6.37	0.30

B. Reaction mechanism

In the doublet state, just the H-abstraction mechanism for title reaction is studied. As seen in Fig.1, The pre-reactive complex, CR, is the starting step of the reaction. It contains a Van der Waals interaction among HOCl and HS fragments. So, the relative stability of the CR complex is -3.77 kcal mol^{-1}. The predicted TS is connected from CR to CP with the barrier energy of 24.11 kcal mol^{-1}. From a geometrical point of view, the TS structure includes the hydrogen shifting from HOCl moiety to SH moiety. The two minimums, CR and CP, of the TS, are confirmed by IRC calculation. The product complex, CP, has the relative energy of 6.83 kcal mol^{-1}. The final stage of the reaction is ClO and H_2S releasing from CP complex. The product formation is investigated thermodynamically. It shows the P (ClO+ H_2S) adduct have negative Gibbs free energy and enthalpy.

IV. CONCLUSION

We explored the hydrogen abstraction reaction mechanism of the HOCl + SH reaction in the atmospheric conditions. The DFT (MN12l) and ab initio (CCSD(T) methods are used for derivation of the results. Also, key parameters of the thermodynamic (ΔG^o, ΔH^o, and ΔS^o) for all species are derived from the investigated reaction.

REFERENCES

[1] Y. L. Yung, J. P. Pinto, R. T.Watson, S. P .Sander, J. Atmos. Sci., 37, pp.339–353, **1980**.
[2] G. Poulet, M. Pirre, F. Maguin, R. Ramaroson, G. Lebras, Geophys. Res. Lett., 19, pp.2305–2308, **1992**.
[3] R. R. Garcia, S. J. Solomon, Geophys. Res., 99, pp.12937–12951, **1994**.
[4] S. C. Wofsy, , M. B. Can. McElroy, J. Chem., 52, pp.1582–1591, **1974**.
[5] S. Solomon, R. R. Garcia, F. S. Rowland, D. Wuebbles, J. Nature, 321, pp.755–758, **1986**.

Kinetic Studies of Oxidative Addition Reaction of Ethyl Iodide for Synthesizing New Pt(IV) Complex

Maryam Noori*, Bita Shafaatian
School of Chemistry, Damghan University, Damghan 3671641167, Iran

Email: shafaatian@du.ac.ir

Abstract: A New complex of organoplatinum(IV) containing chelated ligand and N_2 donor atoms was synthesized by the reaction of [(*p*-$MeC_6H_4)_2PtN_2$] with an excess of EtI. In this complex EtI as a reagent was coordinated to Pt(II) and formed a new complex of Pt(IV). The complex have been found to possess octahedral geometry and the molar conductivity values in $(CH_3)_2CO$ implied the presence of non-electrolyte complexes. The synthesized complex has been characterized by different spectroscopies. Moreovere, oxidative addition reaction of EtI with Pt(II) complex in different temperatures was investigated and calculation of k_{obs}, k_2, E_a, entropy and enthalpy of activation were calculated using curve fitting by Microsoft Excell solver.

Keywords: activation parameters, oxidative addition, platinum complex, rate constants

I. INTRODUCTION

Platinum has been an important element in organometallic chemistry because it forms a wide range of organometallic compounds that are kinetically inert to enable them to be isolated and characterized. The square-planar complexes of platinum(II) and palladium(II) are of increasing importance since the discovery of the anti-tumor property of *cis*-dichlorodiammineplatinum(II) [1]. Also, platinum complexes are relatively easily oxidized or reduced in two-electron processes between the three main oxidation states, so that oxidative-addition and reductive-elimination reactions are facile. Furthermore, since the predominant geometry for the +2 oxidation state is square planar and for the +4 oxidation state is octahedral, oxidative addition accompanied by the addition of two fragments to the Pt(II) and reductive elimination accompanied by loss of two fragments from Pt(IV) are both particularly favorable. Oxidative addition reactions in platinum complexes were investigated by the addition of a molecule X-Y to a square planar d^8 Pt(II) complex to give an octahedral d^6 Pt(IV) complex represents one of the classic example of such reactions [2].

II. METHODS

All reactions were carried out in an Argon atmosphere and dry solvents. Chemical reagents were provided from Sigma Aldrich and were used without further purifications.

Electronic absorption spectra of the compounds were recorded in $(CH_3)_2CO$ solvent on an Analytik Jena Specord 205 spectrophotometer and excess of EtI were used during investigation of oxidative addition reaction. Infrared spectra were measured as KBr disks on Perkin-Elmer spectrum RXI FT-IR spectrophotometer. Conductivities were measured at room temperature in $(CH_3)_2CO$ solution (3×10^{-4} M) using a 712 conductometer (Metrohm). Microsoft Excell solver were applied in order to calculate k_{obs}, k_2 and activation parameters.

III. RESULTS AND DISCUSSION

The platinum(II) complex exhibited a lower-energy band at substantially longer wavelengths in compare to the absorption of the bidentate chelating ligand, which arise from metal to ligand charge-transfer (MLCT) transitions. The bands observed in Pt(II) and Pt(IV) complexes at 461 and 445 nm, respectively, were due to the MLCT (the transition of Pt d-orbitals to the π^* orbital of the bidentate ligand) [3]. The intensity of MLCT band in higher oxidation number of Pt complex is very weak due to the lower tendency of the Pt(IV) for the MLCT transitions.

Oxidative addition reaction of Et-I to lower valence electron-rich metallic center (Pt(II)) under mild conditions represents the most important and synthetically useful transformation [4]. The oxidative addition of ethyl iodide with square-planar complex of Pt is often a key step in catalytic reactions in order to gain insights about the intrinsic properties of the reaction constituents [5,6]. The orange color of Pt(II) complex make it possible to monitor the oxidative addition reaction through UV/Vis spectroscopy. In $(CH_3)_2CO$ the complex reacted with an excess of ethyl iodide and a yellow solution of Pt(IV) complex was formed (Fig. 1). Using an excess of ethyl iodide made the reaction suitably followed as pseudo-first-order reaction. Formation of the Pt(IV) complex was followed by monitoring the decay

of MLCT band in the visible spectrum of Pt(II) complex at λ = 461 nm. The absorbance at λ = 461 nm was recorded at different time intervals (60 s) until the completion of reaction. This change in the color is one of the most important evidence for the formation of Pt(IV) complex due to the oxidative addition reaction of ethyl iodide.

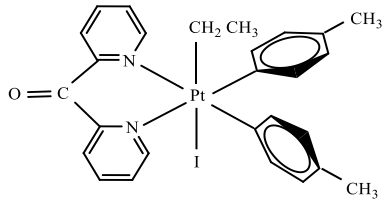

Fig.1: Structure of the [(*p*-$MeC_6H_4)_2PtCH_2CH_3IN_2$].

The change of orange color of the starting Pt complex to yellow color at different time intervals was shown in Fig. 2.

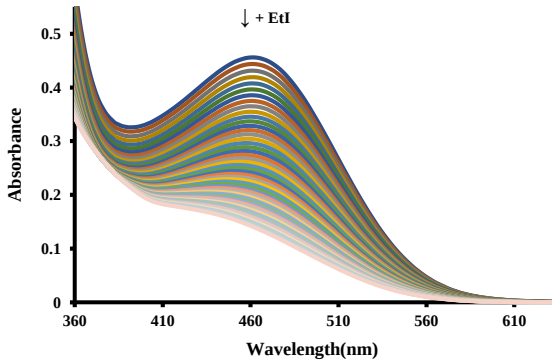

Fig.2: Changes in the absorption spectrum during the reaction of Pt(II) (3 mL, 3×10^{-4} M) with CH_3CH_2I in $(CH_3)_2CO$ at T = 25 °C, successive spectra recorded at intervals of 60 s.

The pseudo-first-order rate constants (k_{obs}) can be obtained with curve fitting by using Microsoft Excell solver [3]. A typical of curve fitting plots in acetone was shown in Fig. 3. Graphs of these k_{obs} against the concentrations of ethyl iodide gave straight line plots passing through the origin, showing a first-order dependence of the rate on the concentration of the Et-I (Fig. 4). The k_2 can be obtained from the slopes of these figures. The activation parameters were obtained from the measurements of k_2 at different temperatures, and the data were given in Table 1.

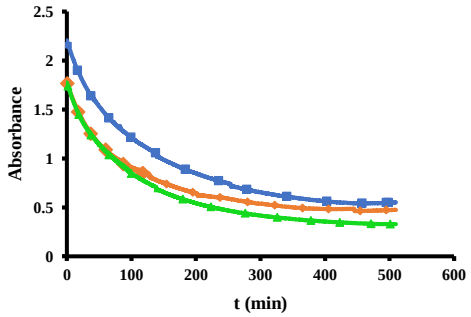

Fig.3: Curve fitting of absorbance *vs* time for the reaction of Pt(II) with CH_3CH_2I in $(CH_3)_2CO$ at T = 35 °C.

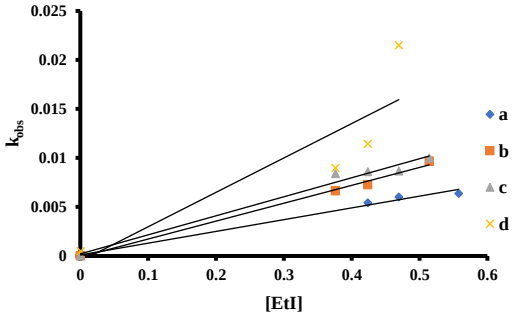

Fig.4: Graphs of first-order rate constants (k_{obs}/s^{-1}) for the reaction of Pt(II) with EtI in $(CH_3)_2CO$ at different temperatures *vs* [EtI], a = 20 °C, b = 25 °C, c = 30 °C and d = 35 °C.

According to the table 1, the rates of oxidative addition reaction of Et-I was increased with increasing of temperature.

Table 1: Activation parameters and rate constants in acetone

		k_2
Temperature	20 °	0.0104
	25 °	0.0226
	30 °	0.0404
	35 °	0.1334
$\Delta H^{\#}$ (kJ mol^{-1})	126.29	
$\Delta S^{\#}$ (J mol^{-1}K^{-1})	147.70	
E_a (kJ mol^{-1})	128.78	

Equations

The activation energy, E_a, was obtained from the Eq. 1.

$$\ln k_2 = \ln A - E_a/RT \quad (1)$$

Furthermore, $\Delta H^{\#}$ and $\Delta S^{\#}$ were obtained from the Eq. 2 (Eyring).

$$\ln(k_2/T) = \ln(k'/h) + \Delta S^{\neq}/R - \Delta H^{\neq}/RT \quad (2)$$

IV. CONCLUSION

kinetic studies due to the reaction of ethyl iodide with the Pt complex was occurred at 20 °C, 25 °C, 30 °C and 35 °C. The rate constants containing k_{obs}, k_2, E_a, enthalpy and entropy of activation parameters were calculated. The obtained data showed that the rates of oxidative addition reaction of Et-I with Pt(II) complex was increased with increasing of temperature.

REFERENCES

[1] B. Rosenberg, L. Van Camp, E. B. Grinley, A. J. Thomson, J. Biol. Chem. vol. 242, pp. 1347-1352, **1967**.
[2] F. R. Hartly, The Chemistry of Platinum and Palladium, Applied Science, London, **1973**.
[3] B. Shafaatian, B. Heidari, J. Organomet. Chem. vol. 280, pp. 34-42, **2015**.
[4] B. Shafaatian. H, Ghaedrahmat, Int. J. Chem. Kint. pp. 215-221, **2018**.
[5] J. K. Jawad, R. J. Puddephatt, J. Chem. Soc. Dalton Trans., pp. 1466-1469, **1977**.
[6] A. Capape, M. Crespo, J. Granell, M. Font-Bardía, X. Solans, Dalton Trans., pp. 2030-2039, **2007.**

Section:

Chemical Thermodynamics

Computational Modeling of Glutathione Peroxidase Mimic in Hydrogen Peroxide Reduction at Various Temperatures.

Mohammad Tashakori **, *Mohammad Izadyar*, Ramesh Kheirabadi***

Computational Chemistry Research Lab, Department of Chemistry, Faculty of Science, Ferdowsi University of Mashhad, Mashhad, Iran

**Email: Izadyar@um.ac.ir*

Abstract: The development of enzyme mimics has been rapidly increased, recently. Herein, the studies on the mechanism of oxidation reaction of GPx mimic in the presence of hydrogen peroxide were evaluated by using the 6-31+G(d,p) basis set and the density functional theory method at the M06-2X level of theory. All thermodynamic and kinetic parameters of oxygen atom transfer in H_2O_2 to the selenium center of the GPx mimic was calculated. The oxidation reaction of GPx mimic by H_2O_2 was investigated at 298,308,318 and 328K. The obtained results indicate that the activation Gibbs energies of the reduction of H_2O_2 at the mentioned temperatures are 31.63, 31.64, 31.68 and 31.72 kcal.mol^{-1}, respectively. Also, the rate constants of the reduction mechanism of H_2O_2 in the presence of GPx mimic are 6.5×10^6, 6.7×10^6, 6.9×10^6 and 7.1×10^6 s^{-1}, respectively. Finally, the proposed GPx mimic containing selenium-organic framework shows an acceptable thermal and structural stability.

keywords: Density functional theory**,** GPx mimic, Hydrogen peroxide, Thermodynamic and the kinetic parameters, Thermal effect.

I. INTRODUCTION

The enzymatic activity of glutathione peroxidase (GPx) is given by selenium, which has a vital role in the reduction of hydroperoxides [1]. The selenium metabolism shows a supplement enzymatic activity to control or direct the reduction of inflammation, cancer and arthritis diseases. Some selenium-containing enzymes are used as a nucleophilic and reducing GSH/H_2O_2 [2]. Glutathione peroxidase controls the oxidative stress and prevents cellular damage and apoptosis [3]. The first enzyme mimic, ebselen(2-phenyl-1,2-benzisoselenazol-3(2H)-one), was used to inhibit reactive oxygen/nitrogen species (ROS/RNS) in the cells, membranes and lipids [4].

In this study, the comparison of different temperatures on the oxidation reaction to predict the reactivity of the new molecular structure containing both Se−N covalent bond and amid group are reported by the DFT method from the energetic point of view to characterize the transition state (TS) on the reaction pathway. For consideration of the thermal effect on the reaction, different temperatures were applied.

II.COMPUTATIONAL DETAILS

All the geometry optimizations were performed by Gaussian 09[5]. The TS structures were calculated via the quasi-Newton method (STQN). All thermodynamic and the kinetic parameters were obtained by M06-2X/6-31+G (d,p) level of theory [6]. All the analyses were considered in the solvent (water) by the conductor-like polarizable model (CPCM). Also, the rate constant in the reduction of hydrogen peroxide was obtained by equation 1 at different temperatures.

$$k = \sigma\kappa\,(k_B T/h)\exp(-\Delta G^{\neq}/RT) \qquad (1)$$

where σ represents the reaction path of degeneracy, κ is the number of equivalent reaction paths for tunneling correction, (k_B) is the Boltzmann's constant and (h) is the Planck's constant. R is the global gas constant and (T) is temperature [7].

III. RESULTS AND DISCUSSION

The interaction of GPx mimic with hydrogen peroxide was kinetically modeled according to Fig. 1. The oxidation reaction of GPx mimic occurs through a one-step oxygen transfer mechanism. The oxygen atom in H_2O_2 is transferred to the selenium center of the GPx mimic to reduce the hydrogen peroxide by cleavage of O-O bond to facilitate the reaction proceeding through the S=O bond

formation in the selenoxide. Additionally, the proton shuttle immediately occurs to the hydroxyl group, yielding the O···H bond that produces water molecule. The reduction rates of hydrogen peroxidase were evaluated at different temperatures to estimate the thermal effects on thermodynamic and kinetic parameters, as shown in Fig. 1.

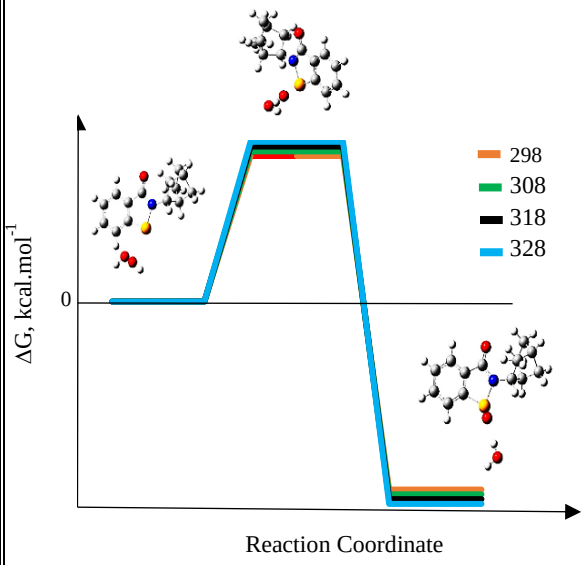

Figure1: Energy diagram for the oxidation of GPx mimic with the hydrogen peroxide at various temperatures

Based on Fig 1, related barriers are not significantly affected by the versions temperatures. On the basis of the activation parameters, temperature increasing did not obviously modify the reaction kinetic but increases the oxidation rate of GPx mimic in the presence of hydrogen peroxide. In the oxidation mechanism of GPx mimic, the highest energy barrier was found at 328K, whereas the lowest energy barriers were found at 298 K. Nevertheless, the activation energy of the oxidation mechanism of GPx mimic at 308 K, and 318 K are the same and considerably lower than that 328 K. Kinetic and thermodynamic parameters at different temperatures were calculated and reported in Table 1. Based on calculations, the most suitable values of the Gibbs energy and k are related to 328 K.

Based on Table 1, the reduction rate increases slightly in the reduction of H_2O_2 to 6.5×10^6, 6.7×10^6, 6.9×10^6 and $7.1\times10^6 s^{-1}$ respectively, at different temperatures. The obtained results at higher temperatures shows the stability of the GPx mimic.

Table 1. The kinetic and thermodynamic parameters for the reaction between the GPx mimic and H_2O_2 at various temperatures

T (K)	ΔG (kcal.mol^{-1})	$\Delta G^{\ddagger}$ (kcal.mol^{-1})	k (s^{-1})
298	-40.86	31.63	6.5×10^6
308	-40.90	31.64	6.7×10^6
318	-40.94	31.68	6.9×10^6
328	-40.98	31.72	7.1×10^6

IV. CONCLUSIONS

In summary, the GPx mimic was introduced as a selenium-containing molecule which provided high-efficiency active center to reduce the H_2O_2. The thermodynamic and the kinetic parameters as activation Gibbs energies and rate constant were calculated at different temperatures. Based on the results, higher temperature shows the stability of the GPx mimic.

REFERENCES

[1] X. Ren, L. Zou, J. Lu & A. Holmgren. Free Radical Biology and Medicine. vol. 127, pp 238-247,**2018**.

[2] D. Tanini, B. Lupori, P. Lo Nostro & A. Capperucci. Phosphorus, Sulfur, and Silicon and the Related Elements, pp 1–4, **2019**.

[3] M. Kim, Y. S. Min & U. D. Sohn. Archives of Pharmacal Research. vol 41, Issue 10, pp 1019–1031,**2018**.

[4] H. Ungati, V. Govindaraj, M. Narayanan & G. Mugesh. Angewandte Chemie, pp 1-9, **2019**.

[5] M. J. Frisch, G. W. Trucks, H.B. Schlegel, G. E. Scuseria, M. A Robb, J. R. Cheeseman, G.V. Scalmani, B.

M. Barone, G. A.Petersson, H. Nakatsuji, et al. Gaussian 09, revision A.02; Gaussian. Inc.: Wallingford, CT, **2009**.
[6] H. Liu, Y. Fang, S-Y. Wang & S-J. Ji. Organic Letters, 20(4),pp 930–933, **2018**.
[7] M. Cui, W. Li, L. Wang, L. Gong, H. Tanga and D. Cao. J.Mater.Chem.C. vol 7,pp 3779-3786, **2019**.

Conductometric Study of 1-Propyl-3-methylimidazolium Bromide Ionic Liquid in Water and Ethylene Carbonate Mixtures

Tayyebe Nosrati Fallahkar*, *Bahram Ghalami-Choobar*

Department of Chemistry, Faculty of Science, University of Guilan, P.O. Box: 19141, Rasht, Iran

**Email: B-Ghalami@guilan.ac.ir*

Abstract: In this work, we reported the electrical conductivity measurements for 1-Propyl-3-methylimidazolium Bromide, [PrMIm]Br, in ternary mixtures of [PrMIm]Br + ethylene carbonate + H_2O at T=(298.2, 308.2 and 318.2) K and P=0.1MPa. Conductometric measurements were carried out for [PrMIm]Br ionic liquid in ethylene carbonate + water solvent mixture in various composition 10, 20 and 30 mass% of ethylene carbonate (EC) in the ionic strength ranging from 0.0029 to 0.2500 mol.kg^{-1}. The Fuoss-Onsager conductivity equation was used to obtain the limiting molar conductivity ($\Lambda_\circ$) and ion association constant (K_A) for under investigation system. Also, the values of critical micelle concentration (cmc) and the degree of ionization (α) were deduced from conductivity data and used to obtain the corresponding standard thermodynamic functions of micellization process including Gibbs free energy ($\Delta G_m°$), enthalpy ($\Delta H_m°$) and entropy ($\Delta S_m°$).

Keywords: Conductivity, 1-Propyl-3-methylimidazolium Bromide, Association constant, Ethylene carbonate, Fuoss-Onsager equation

I. INTRODUCTION

During the last decade, ionic liquids (ILs) have involved extensive attention in many fields due to their special physical and chemical characteristics such as trivial vapor pressure, high thermal and chemical strength, widespread liquid range and strong solubility capacity [1]. Ethylene carbonate is a typical dipolar aprotic solvent, and almost iso-dielectric with water. This compound is notable for industrial use because large dipole moment, large dielectric constant, high boiling point and its capability to dissolve considerable amount of inorganic salts [2]. Since mixtures of ionic liquids with polar organic solvent (e. g., ethylene carbonate, and dimethyl carbonate) are widely used in the electric vehicle due to much improved properties including higher ionic conductivity and lower flammability [3], there is an immense need for determination and generating of thermodynamic and transport data of such solutions. This paper reports the conductometric and aggregation properties of 1-propyl-3-methylimidazolium bromide, [PrMIm]Br in various composition of EC-water mixed solvent systems from 10 to 30 mass% of EC in the ionic strength ranging from 0.0029 to 0.2500 mol. Kg^{-1} at T=(298.2, 308.2 and 318.2) K.

II. METHODS

Preparation of ionic liquid, [PrMIm]Br was performed based on a general standard procedure according to the literature [4, 5]. EC, N-methylimidazole, ethyl acetate and 1-bromopropane were supplied by Merck and were 99% mass fraction purity. Measurements of solution conductivity were made by means of a digital multimeter (Martini instrument Mi180) with fluctuations of 0.01%. The system of multimeter was equipped with a personal computer to collect data. The Mi 5200 software and Microsoft Excel software were utilized to collect and calculate data. Before and after the conductometric measurements, the calibration of conductivity meter with a cell constant of 1.361 cm^{-1} was done by an aqueous KCl (0.01M) solution. Also, all data were always corrected with the contribution of the solvent. The samples were stirred before measurements to minimize the concentration gradients. All measurements were made in a double-walled glass vessel, and the test solutions were equilibrated at T= (298.2, 308.2 and 318.2) using a model GFL circulation water bath with an uncertainty ± 0.1 K. The preparation of the stock electrolyte solutions was performed by weighting the ionic liquid and EC using an analytical balance (A&D HR 200) with precision 0.1 mg. also we applied double-distilled water with a conductivity of less than 2.0 μs.cm^{-1} to prepare the test solutions.

III. RESULTS AND DISCUSSION

Experimental conductance data for the ternary system [PrMIm]Br + EC + H_2O were measured and the molar conductivities Λ, were determined from the experimental specific conductivities. The plot of molar conductivity values Λ for [PrMIm]Br against the molal concentration, m_{IL}, monotonically decreases as shown in Figure 1. This indicates that an addition in the molal concentration of the ionic liquid enhances the ion pair formation process, relaxation effect and aggregation of the ionic liquid in the co-solvent, accordingly with arise in the microscopic viscosity of the mixture, the movement of the charge carriers decreases [6, 7]. The values of limiting molar conductivity and association constant were

obtained by an iterative solution of Fuoss-onsager equation (Eq 1) [8]. The obtained values of K_A and $\Lambda_\circ$ are recorded in Table 1. The graph of specific conductivity versus [PrMIm]Br concentration consists of two linear regions. The x-intersection point of these two linear regimes was taken as critical micelle concentration (cmc). In the other hand, the ratio of slopes corresponds to the degree of micelle ionization (α). The cmc and α value in the temperature range 298.2 to 318.2 K are summarized in Tables 1 and 2. To realize the micellization behavior of investigated system the standard thermodynamic functions such as Gibbs free energy, ΔG_m° , enthalpy, ΔH_m° and entropy of micellization, ΔS_m° have been calculated using the equations 2 to 4 [9] and are given in Table 2. An inspection of data from Table 2 reveals the spontaneous and endothermic nature of micellization process.

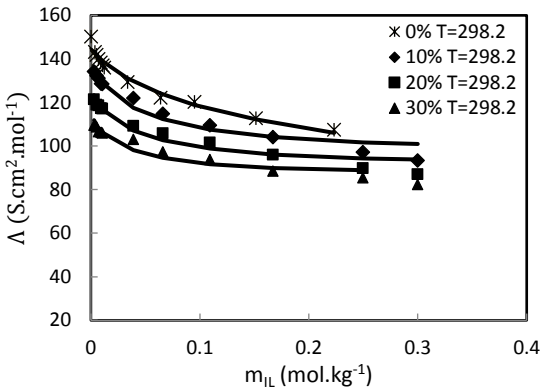

Fig 1: Molar conductivity of [PrMIm]Br versus the molal concentration (m_{IL}) of ionic liquid in various composition from 0 to 30% mass of the co-solvent at T = 298.2 K and P = 0.1 MPa. Solid lines depict Fuoss-onsager equation.

Table 1: Ion association constant (K_A), limiting molar conductivity ($\Lambda_\circ$) and critical micelle concentration (cmc) at different temperatures and P = 0.1MPa

T/K	K_A(dm³.mol⁻¹)	$\Lambda_\circ$(S.cm².mol⁻¹)	m_{cmc}(mol.kg⁻¹)×10²
$w_{EC}/w_{mixture}$ = 10%			
298.2	2.02	146.08	13.82
308.2	3.73	153.26	12.32
318.2	6.01	158.59	11.37
w_{EC}/w_{mixtur} = 20%			
298.2	1.61	132.14	13.61
308.2	3.65	138.90	11.87
318.2	5.58	145.36	11.02
w_{EC}/w_{mixtur} = 30%			
298.2	1.29	119.78	13.04
308.2	2.90	127.18	11.77
318.2	4.98	133.03	10.82

Table 2: Degree of dissociation (α) and the corresponding values of various thermodynamic functions (ΔG_m^0, ΔH_m^0 and ΔS_m^0) at different temperatures and P = 0.1MPa

T/K	α×10²	ΔG_m^0 (kJ.mol⁻¹)	ΔH_m^0 (kJ.mol⁻¹)	ΔS_m^0 (J.mol⁻¹.K⁻¹)
$w_{EC}/w_{mixture}$ = 10%				
298.2	76.19	-1.06	-1.77	-2.37
308.2	76.12	-1.13	3.98	16.59
318.2	74.71	-1.41	10.62	37.83
w_{EC}/w_{mixtur} = 20%				
298.2	77.79	-0.75	6.04	22.76
308.2	80.17	-1.00	8.60	31.14
318.2	77.60	-1.38	11.83	41.54
w_{EC}/w_{mixtur} = 30%				
298.2	83.76	-0.67	6.92	25.47
308.2	80.66	-0.97	8.01	29.14
318.2	79.09	-1.29	9.11	32.69

$$\Lambda = \Lambda_\circ - [(0.8204 + \frac{10^6}{(\varepsilon_r T)^{3/2}})\Lambda_\circ + 82.50/\eta(\varepsilon_r T)^{1/2}]C^{1/2}\gamma^{1/2} + (E_1'\Lambda_\circ - E_2')C\gamma\ln(6E_1'C\gamma) + LC\gamma - K_A C\gamma\Lambda\exp[-8.405\times10^6\frac{C^{1/2}\gamma^{1/2}}{(\varepsilon_r T)^{3/2}}] \quad (1)$$

$$\Delta G_m^\circ = (2-\alpha)RT\ln X_{cmc} \quad (2)$$

$$\Delta H_m^\circ = -RT^2[(2-\alpha)\frac{d\ln X_{cmc}}{dT} + \ln X_{cmc}\frac{d(1-\alpha)}{dT}] \quad (3)$$

$$\Delta S_m^\circ = \frac{\Delta H_m^\circ - \Delta G_m^\circ}{T} \quad (4)$$

IV. CONCLUSION

In this work, molar conductivities of [PrMIm]Br in the [PrMIm]Br + EC + water system were presented at T = (298.2, 308.2 and 318.2) K. Limiting molar conductivities, $\Lambda_\circ$ and ion association constants, K_A were derived by employing Fuoss-Onsager relation. The $\Lambda_\circ$ and K_A values decrease as the EC content in the mixed solvent increases. These are related to the strong ion-solvent interactions,

decrease in mobility of ions solvated, more viscose medium and reduction of ion pairing process in the rich-EC region.

Values of Gibbs free energy, enthalpy and entropy of micellization were assessed at different temperatures. The resulting values of these thermodynamic functions demonstrate that the nature of micellization is spontaneous, exothermic and entropy-driven.

REFERENCES

[1] B. Ghalami-Choobar, M. Azizpour, H. Ghanadzadeh Gilani and N. Chaibakhsh, Fluid Phase Equilib, vol. 436, pp. 1-12, **2017**.
[2] A. Arslanargin, A. Powers, T. L. Beck and S. W. Rick, J. Phys. Chem. B, vol. 120, pp. 1497-1508, **2016**.
[3] M. L. P. Le, N. A. Tran, H. P. K. Ngo, T. G. Nguyen and V. M. Tran, J. Solution Chem, vol. 44, pp. 2332- 2343, **2015**.
[4] M. Khoshalhan-Rastekenari, B. Ghalami-Choobar, Phys. Chem. Res, vol. 6, pp. 741-758, **2018**.
[5] H. Shekaari, M. T. Zafarani-Moattar, A. Kazempour and Z. Ghasedi-Khajeh, J. Chem. Eng. Data, vol. 60, pp. 1750-1755, **2015**.
[6] A. K. Srivastava, R. A. Samant and S. D. Patankar, J. Chem. Eng. Data, vol. 41, pp. 431-435, **1996**.
[7] H. Shekaari, S. S. Mousavi, Fluid Phase Equilib, vol. 286, pp. 120-126, **2009**.
[8] B. Ghalami-Choobar, T. Nosrati Fallahkar, Fluid Phase Equilib, vol. 496, pp. 42-60, **2019**.
[9] A. Pal, A. Pillania, J. Mol. Liq, vol. 212, pp. 818-824, **2015**.

Measurement the Sound Speeds, Densities and Refractive Indices of Biodiesel Components and Their Alcoholic Mixtures with 2Methyl1butanol, 2Butanol and 1,2Butandiol

M.M. Alavianmehr, H. Ghazipour, H. Ghazipour*

Department of Chemistry, Shiraz University of Technology, Shiraz 71555-313, Iran

Email: halehgh@gmail.com, alavianmehr@sutech.ac.ir

Abstract*:* Sound speeds, densities and refractive indices for two biodiesel components (methyl caprate and ethyl myristate) and their mixtures with 2- methyl -1- butanol, 2-butanol and 1,2butandiol were measured at temperatures ranging from 293.15 K to 338.15 K at 5K intervals and atmospheric pressure for the entire composition range. The experimental densities and sound speeds were employed to calculate excess molar volume, V_m^E, excess thermal expansion coefficient, α_p^E, infinite partial molar volumes, V_i^∞, and excess partial molar volumes at infinite dilution $V_i^{E,\infty}$. The magnitude and sign of these quantities have been employed to examine the power of intermolecular forces in mixtures.

Keywords: Biodiesel, Density, Methylesters, Refractive index, Speed of sound.

I. INTRODUCTION

Biodiesel is comprised of mono alkyl (methyl or ethyl) esters acquired from fatty acids from renewable vegetable oils or animal fats. [1,2] fatty acids coming from several sources have different chain lengths. babassu oil and coconut oil have saturated acids such as capric acid and myristic acid. [3,4] Biodiesels are produced by the transestrification of vegetable oils (triglycerides) with methanol or ethanol form fatty acid methyl (or ethyl) esters. Extensive use of fossil fuels caused decrease in the fossil fuels sources. Therefore, biofuels can be appraised for future energy sources. However, thermodynamic properties of this class of fluids are scarce. Biodiesels can be used in purification processes and synthesis routes, as substitutes for traditional materials.

II. METHODS

Methyl caprate, Ethyl myristate, 2 methyl 1butanol, 2butanol and 1,2butandiol were used in this study. Refractive indices were measured using Anton paar Abbemat 200. Densities and sound speeds were measured using an Anton Paar densitometer (DSA 5000).

III. RESULTS AND DISCUSSION

After preparation of solutions, the density measurements were performed for every binary mixture containing methyl caprate with 2methyl1butanol, 2butanol and 1,2butandiol and ethyl myristate with 2methyl1butanol, 2butanol and 1,2butandiol at temperatures from 293.15K to 338.15 K in 5K steps.

The excess molar volume V_m^E, for a binary mixture was calculated from density measurements according to the following expression:

$$V_m^E = \sum_{i=1}^{2} x_i M_i (\rho^{-1} - \rho_i^{-1}) \qquad (1)$$

here ρ is the density of the mixture, ρi , Mi and xi are the density, molar mass and mole fraction of component i, respectively. It can be seen that sign of values of excess molar volume for every mixtures are negative.

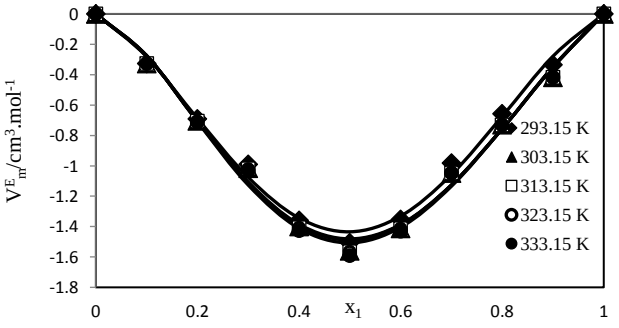

Fig.1: Excess molar volume of {Methyl caprate(1) + 2Butanol(2) } versus mole fraction.

Sound speed and density measurements were carried out in an extended range of temperature for all binary mixtures. These measurements are employed to compute isentropic (adiabatic) compressibility, ks, using the Newton – Laplace

equation.

$$K_s = \frac{1}{\rho u^2} \quad (2)$$

Here, ρ is the density and u is the sound speed of pure component or binary mixture. Change in isentropic compressibility, Δks, can be obtained from the following expression [5]:

$$\Delta K_s = K_s - \sum_{i=1}^{2} x_i K_{s,i} \quad (3)$$

Where ks,i and ks are the isentropic compressibility of component i and mixture, respectively.

Change in sound speed, Δu, can be calculated from the following equation [6]:

$$\Delta u = u - \sum_{i=1}^{n} x_i u_i \quad (4)$$

Here u_i and u are sound speed of component i and the mixture, respectively.

The sign of Δu and its variation in all systems investigated in this study are completely correspondent with excess molar volume variations and confirm our explanations about relation between intermolecular forces and V_m^E values. The calculated V_m^E , Δks and Δu values of all binary mixtures have been fitted to Redlich-kister polynomial equation.

IV. CONCLUSION

Speeds of sound, Densities and refractive indices of two biodiesel compound and their mixtures with 2- methyl -1-butanol, 2-butanol and 1,2butandiol were measured by means of Anton paar vibrating tube densitometer and Anton paar Abbemat 200 refractometer, respectively. Every mixtures presented non-ideal behavior. This nonideality can be elucidated by intermolecular interactions.

REFERENCES

[1] M. S. Graboski and R. L. McCormick, Progress in energy and combustion science, vol. 24, pp. 125-164, **1998.**

[2] A. Demirbas, Progress in energy and combustion science, vol. 31, pp. 466-487, **2005.**

[3] C. A. Nogueira Jr, F. X. Feitosa, F. A. Fernandes, R. S. Santiago and H. B. de Sant'Ana, Journal of Chemical & Engineering Data, vol. 55, pp. 5305-5310, **2010.**

[4] F. X. Feitosa, M. Rodrigues, C. B. Veloso, C. Cavalcante, M. C. Albuquerque and H. B. de Sant'Ana, Journal of Chemical and Engineering Data, vol. 55, pp. 3909-3914, **2010.**

[5] G. Douhéret, M. I. Davis, J. C. R. Reis and M. J. Blandamer, ChemPhysChem, vol. 2, pp. 148-161, **2001.**

[6] M. Moosavi, A. Motahari, A. Omrani and A. A. Rostami, Thermochimica acta, vol. 561, pp. 1-13, **2013.**

Thermodynamic Study of ($CaCl_2$ + N,N-Dimethylacetamide + H_2O) System Based on Potentiometric Measurements at T = 298.2 K

***F. Sayyadi-Kalashami*, B. Ghalami-Choobar*, T. Nasiri-Lohehsara**

Department of Chemistry, Faculty of Science, University of Guilan, Rasht, P.O. Box 19141, Iran
**E-mail: B-Ghalami@guilan.ac.ir*

Abstract*:* In this work, thermodynamic properties of ($CaCl_2$ + N,N-dimethylacetamide + H_2O) system were measured using the potentiometric technique. The potentiometric measurements were made on the galvanic cell of type: Ag-AgCl|$CaCl_2$ (m), DMA (w), H_2O (1 – w)|Ca-ISE in various mass fractions of N,N-dimethylacetamide in water (0, 0.10, 0.20, 0.30) in the molality ranging from 0.0100 to 4.000 mol.kg^{-1} at T = 298.2 K and P = 0.1 MPa. Thermodynamic properties were determined using the Pitzer ion-interaction model. Subsequently, adjustable parameters were determined and utilized to calculate the values of the mean activity coefficients, the osmotic coefficients, the excess Gibbs free energy and the solvent activity for the system under investigation.

Keywords: Activity coefficient, $CaCl_2$, Dimethylacetamide, Pitzer model, Potentiometric method.

I. INTRODUCTION

There is a growing interest in the determination of thermodynamic properties of electrolytes in multicomponent mixtures containing both electrolytes and nonelectrolytes. Electrolyte solutions are involved in several chemical, biological, biochemical, geological, and engineering processes. Therefore, the calculation of the thermodynamic properties of electrolyte mixtures poses an important challenge for many fields. Up to now, many works have been done concerning measurement of the thermodynamic properties of electrolyte solutions [1]. Hernandez-Luis et al. measured the activity coefficients of NaF in N-methylformamide + water and NaCl in formamide + water and PEG 4000 + water mixtures [2]. Hu et al. reported the thermodynamic properties of CsF/RbF in N,N-dimethylformamide /N,N-dimethylacetamide + H_2O mixtures [3]. Bagherinia et al. investigated the mean activity coefficients of $MgCl_2$ in pure water and (glucose + water) mixture solvent at T = 298.15 K [4]. Amides are widely used as solvents and reagents in organic synthesis and chemical analysis. It is well-known that, N,N-dimethylacetamide (DMA) is weakly ionized polar liquid with a dipole moment lower than that of water as well as a low dielectric constant. here is a great need to study aqueous mixtures containing amides in the interpretation of the behavior of complex molecules of biological and pharmaceutical interest [3]. In this research, the thermodynamic properties of the ($CaCl_2$ + N,N-dimethylacetamide + water) system were determined based on potentiometric technique. The Pitzer ion-interaction model was applied to explain the nonideal behavior of the electrolyte system. The adjustable parameters were evaluated for the system under investigation. Finally, the values of the solvent activity and the excess Gibbs free energy were calculated

II. METHODS

Data acquisition were performed using a digital multimeter (Martini instruments Mi180) whose resolution was 0.1 mV. The output of the multimeter was connected to a personal computer by the RS232 connector for data acquisition. The Mi 5200 software together with Microsoft Excel (Office 2007) software were used for data acquisition and calculations. The solutions were continuously stirred using a magnetic stirrer (Delta Model HM-101) at a slow constant rate to avoid concentration gradients in the test solutions. A Model GFL circulation water bath was used to control the temperature of the test solution at T = 298.2 K. The materials used were purchased from chemical companies. All primary stock solutions were prepared by using double-distilled water and DMA. The stock solution of electrolyte were prepared from calcium chloride and DMA by adding weighed amounts of solid, using an analytical balance (A&D HR 200) with a resolution of 0.1 mg, and double-distilled water whose specific conductance was less than 2.0×10^{-4} S·m^{-1}.

III. RESULTS AND DISCUSSION

The mean activity coefficients for $CaCl_2$ in DMA+water mixtures were determined from the emf measurements using the cell (A) according to Eq. (1).

Ag-AgCl|$CaCl_2$ (m), DMA (w), H_2O (1-w)|Ca-ISE (A)

$$E_A = E^0 + S\,log(\gamma_{\pm} I) \quad (1)$$

The emf of the cell (A) was measured at different series of electrolyte molalites in DMA+water mixtures through changing of electrolyte concentration with standard addition method. Table. 1 illustrates the values of measured emf and the obtained mean activity coefficients of the $CaCl_2$ electrolyte in 20% of DMA mass fraction in mixed solvent as a function of $CaCl_2$ molality. Fig. 1 indicates the variation of the $CaCl_2$ mean activity coefficient versus molality of electrolyte in different mass fraction of DMA in mixed solvents.

The Pitzer model was applied for the experimental data correlation and calculation of thermodynamic properties for under investigated system. According to the Pitzer, the mean molal activity coefficient ($\gamma_{\pm}$) for $CaCl_2$ in the mixed solvent is inscribed as Eqs. (2-4):

$$\ln \gamma_{\pm CaCl_2} = 2f^{\gamma} + \frac{4}{9} B^{\gamma}_{CaCl_2} I + \frac{2\sqrt{2}}{9} C^{\varphi}_{CaCl_2} I^2 \qquad (2)$$

Where

$$f^{\gamma} = -A_{\varphi}\left[\frac{\sqrt{I}}{1+b\sqrt{I}} + \frac{2}{b}\ln(1+b\sqrt{I})\right] \qquad (3)$$

$$B^{\gamma}_{CaCl_2} = 2\beta^{(0)}_{CaCl_2} + \frac{2\beta^{(1)}_{CaCl_2}}{a_1^2 I}\left[1 - \left(1 + a_1\sqrt{I} - \frac{a_1^2}{2} I\right)\exp(-a_1\sqrt{I})\right] \qquad (4)$$

A_{ϕ} denotes the Debye–Hückel (DH) parameter for the osmotic coefficients defined by Eq. (5):

$$A_{\varphi} = \frac{1.4006 \times 10^6 d_s^{1/2}}{(\varepsilon_r T)^{3/2}} kg^{1/2}.mol^{-1/2} \qquad (5)$$

Table 1: Ionic Strength of $CaCl_2$ electrolyte (I), mean activity coefficients ($\gamma_{\pm}$), and emf values for $CaCl_2$ in 20% mass fraction of DMA in mixed solvent.

I(mol.kg^{-1})	**E(mV)**	**$\gamma_{\pm CaCl2}$**
0.0132	-129.9	0.8934
0.0523	-82.8	0.7547
0.0973	-62.3	0.6874
0.2522	-30.0	0.6086
0.4988	-7.3	0.5514
0.7483	6.6	0.5254
1.0009	17.4	0.5184
1.2481	26.1	0.5199
1.5015	33.7	0.5254
1.7483	40.3	0.5346
1.9993	46.4	0.5469
2.5007	57.8	0.5861
2.9993	68.6	0.6450
3.5000	78.3	0.7092
4.0001	87.3	0.7820

The Pitzer parameters ($\beta^{(0)}$, $\beta^{(1)}$ and C^{ϕ}) together with E^0 and S were determined by using Eqs. (1) and (2) by an iteration minimization procedure employing the Microsoft Excel (solver) program. The obtained parameters were used to determine the thermodynamic properties.

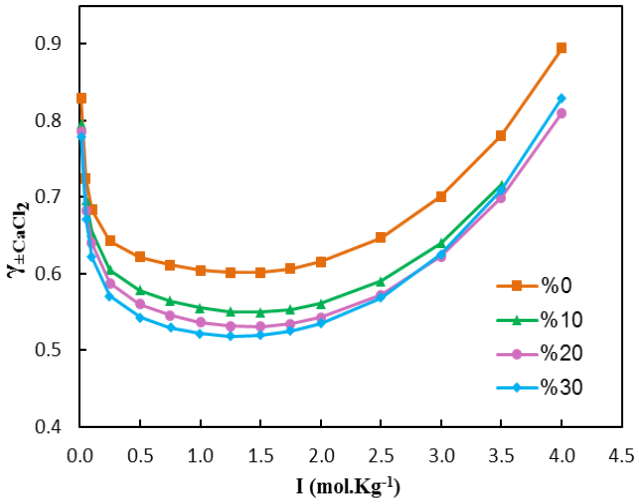

Fig.1: The mean activity coefficients of $CaCl_2$ versus molality of electrolyte in various DMA-water mixed solvent system at 298.2 K.

IV. CONCLUSION

The mean activity coefficients of $CaCl_2$ in the $CaCl_2$ + DMA + water mixture were made using a solvent polymeric ion-selective membrane electrode and Ag–AgCl electrodes at T= 298.2 K. The adjustable parameters ($\beta^{(0)}$, $\beta^{(1)}$ and C^{ϕ}) were determined for the whole data set. The obtained results show that the adjustable parameters have the explicit relation. It can be concluded that the Pitzer model satisfactorily describes the system under investigated. The obtained results show that the $CaCl_2$ mean activity coefficients decrease by

increasing mass fractions of DMA + water mixture. This is because the relative permittivity decreases when the mass fractions of DMA increase. Negative deviation to the ideal demonstrates that the ion−solvent interactions are stronger than the solute−solute interactions.

REFERENCES

[1] T. Nasiri-Lohehsara, B. Ghalami-Choobar, J. Chem. Eng. Data, vol. 63, pp. 2660-2670, **2018**.
[2] F. Hernandez-Luis, R. Rodriguez-Raposo, H. R. Galleguillos, J. W. Molares, Fluid Phase Equilib, vol. 425, pp. 451-464, **2016**.
[3] Y. Xu, S. Li, Q. Zhai, Y. Jiang, M. Hu, J. Chem. Thermodyn, vol. 77, pp. 71-76, **2014**.
[4] M. A. Bagherinia, A. Rouhi, J. Chem. Thermodyn, vol. 91, pp. 286-291, **2015**.

Investigation of changes effect of glycine / urea ratio on ΔCp during the process of synthesis of alumina nanopowder

Mostafa Rajabzadeh*[a], *Hossein Aghaie*[b]

Department of Chemistry, Science and Research Branch, Islamic Azad University, Tehran, Iran

**Email: hn_aghaie@yahoo.com*

Abstract: In this study, the preparation of alumina nanocrystal has been investigated by combustion synthesis method with the aim of studying its thermodynamic properties. Because of the combination of fuels and the relative ratio of fuel to oxidizing, it reduces the flame temperature and prevents the accumulation and growth of nanoparticles, a combination of two urea and glycine compounds was used to prepare nanopowders and improve properties such as porosity increase. The structure of the nanopowders has been studied by the X-ray diffraction, which confirms the structure of the aluminum oxide crystalline structure. Finally, the effect of fuel ratio on the thermodynamic properties of the powders was investigated.

Keywords: Aluminum oxide, Combustion Synthesis Nanocrystal, Thermodynamic, X-Ray diffraction

I. INTRODUCTION

Today, alumina (aluminum oxide) is used as a catalyst, absorbent and abrasive in various industries [1]. In this study, Aluminum oxide nanocrystal powders (Al_2O_3) was prepared using combustion synthesis method using urea and glycine as fuel [2]. Combustion synthesis is a particularly simple, safe and rapid fabrication process wherein the main advantages are energy and time savings [3]. The factors affecting on average size of the crystals were studied and their physical and thermodynamic properties were calculated and investigated. The main parameters influencing the reaction include type of the main fuel, fuel to oxidizer ratio, the amount of oxidizer in excess, ratio of fuels, pH of the solution and rate of calcination [4, 5]. In general, a good fuel should not react violently nor produce toxic gases, and must act as a complexing agent for metal cations [6]. The combination of fuel (urea and glycine) rather than just a fuel, improves the structural properties and increase the stability of the product. Also, the change in fuel/oxidizer ratio is effective on the thermodynamic properties of the DSC results.

II. METHODS

The raw materials used in this study include aluminum nitrate 9-hydrated, glycine and urea. All of the chemicals used by Merck Company were highly purified and were used in the same way as they were received without any additional purification. Initially, based on the stoichiometric coefficients, the mass of the aluminum nitrate, urea and glycine was weighed and transferred to the container, then the mixture was dissolved in the least amount of dionized water. The initial pH of the solution was adjusted by adding nitric acid and ammonia, and the solution was placed directly on the heater until it reached the combustion temperature. Finally, the produced powder were calcined by the furnace temperature 1100°C for 1 hour [7]. The X-ray diffraction patterns were recorded to confirm the formation of α-Al_2O_3 phase as well as to identify its structural properties before and after calcination by the Advanced D8 at a range of 10 to 60 degrees. The pattern of samples that were synthesized in two acidic and alkaline environments was studied before and after calcining to study the effect of the fuel ratio on the structural and thermodynamic properties of the particles.

III. RESULTS AND DISCUSSION

The crystalline powder has 2θ values are identical and diffraction peaks (012) (014) (110) (113) (024) (116) (018) (214) and (300) are attributed to the hexagonal phase [8].

A. Figures and Tables

As shown in Fig. 1, the thermal capacity values of the water evaporation process increased with increasing mole ratio of urea to glycine as fuel.

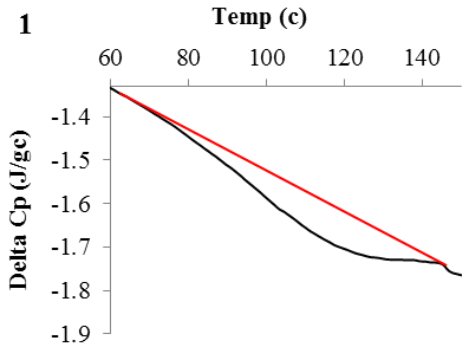

Fig.1: ΔCp versus temperature for samples 1.

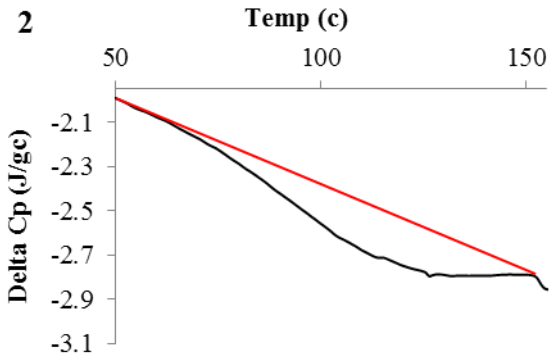

Fig.1: continue: ΔCp versus temperature for samples 2

ΔCp diagram is obtained by plotting the curve ΔH in terms of temperature. In samples 1 and 2, the ratio of urea to glycine is 2:2 and 3:1, respectively. It should be remembered that both samples 1 and 2 are synthesized in acidic environments. These charts were designed with Excel software.

Table1: ΔCp values for sample analysis

Samples	U:G	ΔCp (J/g°C)
1	2:2	0.772
2	3:1	0.839

It is observed that the thermal capacity of the water evaporation process has increased with increasing mole ratio of fuel to oxidizer.

B. Equations

Also, thermal capacity of the decomposition process was obtained using the following equations (Eq. 3).

$$H^{T} = H^{298} + \int_{298}^{T} \Delta C_p dT \qquad (1)$$

$$\Delta H = \int_{298}^{T} \Delta C_p dT \qquad (2)$$

$$C_p = \frac{\partial \Delta H}{\partial T} \qquad (3)$$

ΔCp is a specific heat capacity changes and its value is given in the Table1.

IV. CONCLUSION

Comparison of XRD graphs shows that the powders obtained from the combustion of fuel combinations (urea and glycine) have a higher crystallinity than those obtained from urea or glycine alone. It can be concluded that increasing the temperature of combustion increases the amount of crystallinity and formed metal is stable.

REFERENCES

1. Lide, D.R., *CRC handbook of chemistry and physics*. Vol. 85. 2004: CRC press.
2. Piticescu, R., et al., *Hydrothermal synthesis of zirconia nanomaterials.* Journal of the European Ceramic Society, 2001. **21**(10-11): p. 2057-2060.
3. Edrissi, M. and R. Norouzbeigi, *Synthesis and characterization of alumina nanopowders by combustion of nitrate-amino acid gels.* Materials Science-Poland, 2007. **25**(4): p. 1029-1040.
4. Aruna, S. and K. Rajam, *Mixture of fuels approach for the solution combustion synthesis of Al2O3–ZrO2 nanocomposite.* Materials research bulletin, 2004. **39**(2): p. 157-167.
5. Peng, T., et al., *Effect of acidity on the glycine–nitrate combustion synthesis of nanocrystalline alumina powder.* Materials research bulletin, 2006. **41**(9): p. 1638-1645.
6. Kingsley, J. and L. Pederson, *Combustion synthesis of perovskite LnCrO3 powders using ammonium dichromate.* Materials Letters, 1993. **18**(1-2): p. 89-96.
7. Ding, J., T. Tsuzuki, and P.G. McCormick, *Ultrafine alumina particles prepared by mechanochemical/thermal processing.* Journal of the American Ceramic Society, 1996. **79**(11): p. 2956-2958.
8. Patil, K., *Chemistry of nanocrystalline oxide materials: combustion synthesis, properties and applications*. 2008: World Scientific.

Volumetric and electromagnetic study of the binary mixtures nonelectrolyte solutions dibutylamine /1-heptanol at different temperatures

Fatemeh Parviz, Hossein Iloukhani, and Khatereh Khanlarzadeh
Department of Chemistry, Faculty of Chemistry, Bu-Ali Sina University, Hamedan, Iran
Email: 2001parviz@gmail.com

Abstract*:* In this research, volumetric and electromagnetic properties of the binary mixtures of dibutylamine and heptanol were studied. Also, thermo physical properties, including density, ρ and refractive index, n_D for binary mixtures of (dibutylamine + heptanol) were measured in the whole range of concentration. In this study of temperatures was (298.15 - 318.15) K with 10K intervals. These experimental data were used for calculating thermodynamic quantities, Such as, excess molar volumes, V_m^E, excess partial molar volume, $\bar{V}_{m,i}^E$, excess thermal expansion coefficient , α^E, isothermal coefficient of excess molar enthalpy, $(\partial H_m^E/\partial p)_{T,x}$, refractive index deviation, Δn_D. The excess molar volume, and refractive index deviation were correlated with the Redlich - Kister equation in this binary mixtures. The excess molar volume for mentioned mixtures was negative. Whereas the refractive index deviation is positive in the whole range of concentration and temperatures. the nature and power of intermolecular interactions have been recorded by obtained experimental result.

Keywords: Binary mixture, Excess molar properties, Redlich- Kister correlation, Density

I. INTRODUCTION

This rticle is a continuation of our earlier work relted to the Study of thermodynamic properties of binary mixture. In recent year, measurements of excess molar volumes and refractive index have been adequately employed in understanding the nature of molecular systems and physic-chemical behavior in liquid mixtures. The nonrectilinear behavior of the above- mentioned properties of liquid mixture whit changing mole or volume fractions is attributed to the difference in size of the molecules and strength of interactions. here, we have reported densities, ρ and refractive index, n_D, of the binary mixture of (dibutylamine + heptanol) at (298.15 - 318.15) K with 10K intervals and over the whole composition range for the liquid region and ambient pressure. The drived properties (excess molar volumes, V_m^E, excess partial molar volume, $\bar{V}_{m,i}^E$, excess thermal expansion coefficient , α^E , isothermal coefficient of excess molar enthalpy, $(\partial H_m^E/\partial p)_{T,x}$, refractive index deviation, Δn_D) in combinations whit other mixing properties provide valuable information for qualitatively analyzing the molecular interactions between molecules [1].

II. METHODS

All of chemical materials were purchased from Merck, Germany and were used without further purification. The purities of the components were verified by measuring the densities, and refractive indices which were in good agreement with the literature values. the compounds were degassed just before use. The densities of the pure components and their binary mixture were measured with an Anton Paar DMA 4500 Oscillating U-tube densitometer, and the uncertainties were estimated to be within ±1×10−2 kg m−3. The temperature in the cell was regulated to ±0.01K with a solid state thermostat Each mixture was immediately used, after it was mixed by shaking. All the weightings were performed on an electronic digital balance (AB 204-N Mettler) accurate to ±0.1 mg. The uncertainty in the mole fraction is estimated to be lower than ±1×10−4 [2].

III. RESULTS AND DISCUSSION

The excess molar volumes of binary mixture are negative within the entire composition range and become less negative with increasing temperature from (298.15 to 318.15) K. The obtained correlations were used to calculate the other thermodynamic functions such as thermal expansion coefficient, α, and its excess value, αE, excess partial molar volumes, $\bar{V}_{m,i}^E$ and isothermal coefficient of excess molar enthalpy $(\partial H_m^E/\partial p)_{T,x}$. Results of such calculations were used for interpreting intermolecular interactions that exist between molecules of the binary mixture,qualitatively.

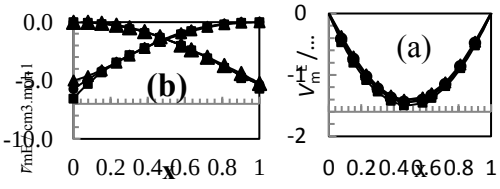

x	ρ	V_m^E	$\bar{V}_1^E$	$\bar{V}_2^E$	$10^3\alpha^E$	$(\partial H^E_m/\partial P)_{T,x}$
	g. cm^{-3}	cm^3. mol^{-1}	cm^3. mol$^-$	cm^3. mol^{-1}	(K^{-1})	J.MPa^{-1}.mol^{-1}
x dibutylamine + $(1-x)$ heptanol			T = 298.15 K			
0	0.81922		-6.547		0.000	0.000
0.0780	0.81612	-0.468	-5.287	-0.061	0.522	-2.451
0.1518	0.81264	-0.802	-4.314	-0.174	0.564	-2.796
0.2307	0.80859	-1.081	-3.467	-0.366	0.542	-2.838
0.3020	0.80469	-1.271	-2.828	-0.597	0.531	-2.886
0.3828	0.80004	-1.421	-2.214	-0.929	0.590	-3.244
0.4642	0.79508	-1.493	-1.678	-1.333	0.611	-3.399
0.5781	0.78768	-1.455	-1.041	-2.022	0.544	-3.112
0.6329	0.78393	-1.376	-0.778	-2.406	0.447	-2.636
0.7193	0.77786	-1.185	-0.440	-3.095	0.382	-2.279
0.8119	0.77116	-0.892	-0.188	-3.930	0.340	-1.995
0.9027	0.76444	-0.521	-0.058	-4.812	0.384	-2.120
1	0.75695			-5.707	0.000	0.000

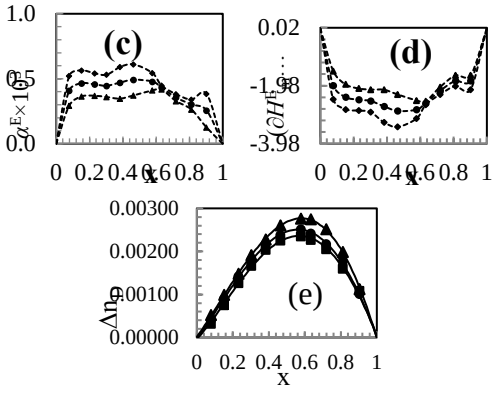

Fig. 1. a) V_m^E, b) $\bar{V}_{m.i}^E$ c) α^E, and d) $(\partial H_m^E/\partial P)_{T,x}$ e) Δn_D of binary mixture of {x_1 Dibutylamine+ x_2 + heptanol}, at temperatures (■)298.15 K, (●)308.15 K, and (▲)318.15 K. lines from Redlich- Kister correlation .

$$Y_m^E = x(1-x)\sum_{i=0}^{p} A_i(2x-1)^i$$

$$A_i = \sum_{j=0}^{q} B_{ij}T^j$$

IV. CONCLUSION

Results of these calculation have been used for discuss intermolecular interactions that exist between molecules of the binary mixture. interactions between unlike molecules are stronger than those exist between like molecules, as a consequence negative V_m^E will be observed, Other factors that affect the volume are molecular shape and size in the system [3-5]. The results showed small deviations from the behavior of ideal solution in these system and have been analyzed to discuss the nature and strength of intermolecular interactions [2-4].

REFERENCES

[1] H. Iloukhani, K. Khanlarzadeh, Thermochim. Acta, vol. 77, pp. 502, **2010**.
[2] F. Kermanpour, H. Z. Niakan, J. Chem. Thermodynamics, 48, pp. 129, **2012.**
[3] F. Kermanpour, H. Z. Niakan, J. Chem. Thermodynamics, vol . 10, pp. 54, **2012**.
[4] H. A. Zarei, F. Jalili, J. Chem. Thermodynamics, vol **.** 39, pp. 55, **2007**.
[5] O. Redlich, A.T. Kister, Ind. Eng. Chem, vol. 40, pp. 345, **1948**.

Solubility of Hydrogen Sulfide in 1-ethyl-3-methylimidazolium tris(pentafluoroethyl)trifluorophosphate ([C_2mim][eFAP])

F. Javanmardi**, F. Sabzi
Department of Chemical Engineering, Shiraz University of Technology, Shiraz 71555-313, Iran,
**Email: fatemehjavan6895@gmail.com*

Abstract*:* The solubility of hydrogen sulfide in the ionic liquid 1 – ethyl – 3-methylimidazolium tris (pentafluoroethyl) trifluorophosphate ([$\mathbf{C_2mim}$][**eFAP**]) was theoretically investigated at temperatures from 303 to 353 K and pressures up to about 2.0 MPa. The solubility values were correlated using Sanchez-Lacombe Equation of State (SL EoS). In overall, the results of the present model for binary systems comprising $\mathbf{H_2S}$ and ILs are in very good agreement with experiments.

Keywords: Ionic liquids, Solubility, Hydrogen Sulfide, Sanchez-Lacombe EoS.

I. INTRODUCTION

Many gas field processes and also hydrodesulfurization of crude oils contain sulfur compounds such as hydrogen sulfide along with methane and hydrocarbons [1]. For sweetening the gas, hydrogen sulfide needs to be separated. There are several methods for separation of acid gas from sour gas. The most common process for acid gas removal is alkanolamine based chemical absorption due to versatility, efficiency, and low solvent cost. But alkanolamine absorption is corrosive and volatile and needs high energy for regeneration process [2,3]. In comparison, ionic liquids as solvent can improve the safety, economics, and environmental sustainability. For this reason and in this study, the solubility of hydrogen sulfide in ionic liquid [C_2mim][eFAP] has been studied and sorption results have been predicted at several temperatures and pressures.

II. METHODS

Sanchez-Lacombe Equation of State (SL EoS), a thermodynamic model in terms of lattice fluid theory, is one of the equations of state for modelling phase behavior of polymer solutions. SL EoS describes the liquid phase as a crystalline lattice [4]. By using SL EoS we can predict the thermodynamic properties of multi component mixtures as well as pure fluids. The Sanchez-Lacombe equation of state is presented as follows:

$$\tilde{\rho}^2+\tilde{P}+\tilde{T}\left(\ln(1-\tilde{\rho})+\left(1-\frac{1}{r}\right)\tilde{\rho}\right)=0 \qquad (1)$$

where $\tilde{T}$, $\tilde{P}$, $\tilde{\rho}$ are the reduced temperature, pressure and density which are obtained with the help of PVT experimental data and application of the fminsearch method in the MATLAB program :

$$\tilde{T}=\frac{T}{T^*},\ \tilde{P}=\frac{P}{P^*},\ \tilde{\rho}=\frac{\rho}{\rho^*} \qquad (2)$$

The fugacity coefficients are expressed by the following relation:

$$\ln\varphi_i=-\ln Z+r_i^o\left[-\frac{2\tilde{\rho}}{\tilde{T}}-\ln(1-\tilde{\rho})\right]+\left(\frac{Z-1}{r}\right)\left[\frac{r_i^o}{v^*}\left(-v^*+v_i^*\right)\right] -\frac{\tilde{\rho}}{\tilde{T}}\left[\frac{v^*}{\varepsilon^*}2r_i\left(-P^*+\sum_{j=1}^{N}\phi_j P_{ij}^*\right)+\left[\frac{r_i^o}{v^*}\left(-v^*+v_i^*\right)\right]\right] \qquad (3)$$

III. RESULTS AND DISCUSSION

The experimental results [5] for the solubility of the hydrogen sulfide in [C_2mim][eFAP] at temperatures from 303.15 to 353.15 K and pressures up to 2.0 MPa were collected from references. Solubility of hydrogen sulfide in [C_2mim][eFAP] at different temperatures is drawn in Fig.1. The percent of absolute average relative deviation (AARD%) of calculated H_2S mole fraction in [C_2mim][eFAP] and interaction parameters (k_{ij}) are reported in Table1.

Table1: Binary interaction parameters and AARD%.

Temperature(K)	K_{ij}	AARD%
303.15	0.0452	0.52
313.15	0.0413	0.16
323.15	0.0410	0.41
333.15	0.0409	0.32
343.15	0.0407	0.17
353.15	0.0391	0.29

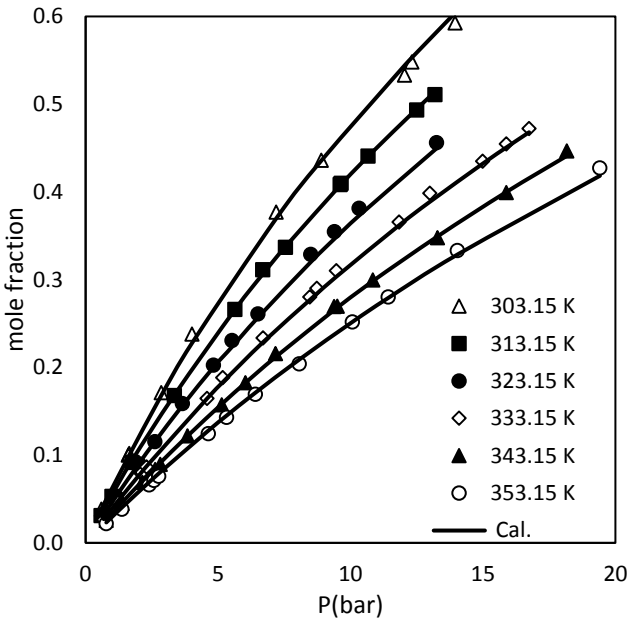

Fig.1: Solubility of hydrogen sulfide in [$\mathbf{C_2}$mim][eFAP] at different temperatures.

IV. CONCLUSION

In this work, we studied the use of SL EoS to quantitatively describe the solubility of hydrogen sulfide in ionic liquid 1-ethyl-3-methylimidazolium tris (penta fluoro ethyl) tri fluoro phosphate. The solubility of hydrogen sulfide in [C_2mim] [eFAP] can be accurately described using SL EoS with AARD percent ranging less than %0.5.

REFERENCES

[1] A.L. Kohl, R.B. Nielsen, Gas Purification, 5th Ed.; Gulf Publishing Company: Houston, TX, **1997.**
[2] S. Kumar, J. Cho, I. Moon, Journal of Greenhouse Gas Control, vol. 20, pp. 87-116, **2014**.
[3] F. Karadas, M. Atilhan, S. Aparicio, Energy Fuels 24, vol. 11, pp. 5817-5828, **2010**.
[4] A. Shojaei, M.R. Khorsand Movaghar, S.A. Mousavi Dehghani, The Canadian Journal of Chemical Engineering, vol. 93, pp. 1483-1489, **2015**.
[5] A. H. Jalili, M. Shokouhi, G. Maurer, M. Hosseini-Jenab, Journal of Chemical Thermodynamics, vol. 67, pp. 55-62, **2013.**

Dielectric study of 1,3- and 1,4-butanediol and Cyclopentanone

A. Akbarnia Dafrazi*[a], *A. Ghanadzadeh Gilani*[b]
[a]*Department of Chemistry, University campus 2, University of Guilan, Rasht, postal code: 4199613776, Iran.*
[b]*Department of Chemistry, Faculty of Science, University of Guilan, Rasht, postal code: 4199613776, Iran.*
Email: aggilani@guilan.ac.ir

Abstract: This investigation illustrates the role of electrostatic interactions and hydrogen bonding on the dielectric properties and mixtures structure. Relative permittivity was measured for the binary mixtures of 1,3-, 1,4-butanediol and Cyclopentanone over a wide concentrations range at T = 298.15 K. The experimental values were calculated by various approaches to obtain useful information about of intermolecular interaction and the structure of the mixture. This dielectric data are further applied to determine the Kirkwood correlation factor. Molecular interactions between the 1,3-, 1,4-butanediol –Cyclopentanone mixtures have been studied using Kirkwood correlation factor.

Keywords*:* Relative permittivity, 1,3-, 1,4-Butanediol, Cyclopentanone, Kirkwood correlation factor.

I. INTRODUCTION

The evaluation of dielectric permittivity is a useful factor to investigate molecular interactions in hydrogen-bonded liquids. The measured dielectric data provide the most important information about intermolecular interactions, self-association and structural rearrangements [1]. Evidence exhibit an electric dipole moment at molecules like diols. Diols are the most important organic materials in chemistry and biochemistry. Owing to the attendance of two –OH groups in a diol molecule, the solution of these compounds can be forcefully influenced by the intermolecular and intramolecular hydrogen bond formation. It also plays an important role in the physical properties of the molecules [2–4].

1,3-butanediol (1,3-BD) is the organic compound having structural formula $HOCH_2CH_2CHOHCH_3$ (Fig. 1a). This colorless liquid is derived from butane alcohol in which hydroxyl groups are attached to first and third carbon atoms of the chain. 1,3-BD is generally employed as a solvent for food seasoning factors and is a co-monomer employed in polyurethane and polyester resins.1,4-butanediol (1,4-BD) is also an organic compound with the structural formula $HOCH_2CH_2CH_2CH_2OH$ (Fig. 1b). It is employed industrially as a solvent and in the manufacture of several kinds of plastics, elastic fibers and the chain extender for polyurethanes [4].

Cyclopentanone (CPO) (Fig. 1c) is known as symmetrical five-membered cyclic ketone. It has a relatively little dielectric constant with a great dipole moment. This cyclic ketone is an important organic chemical, which has many applications in a diversity of chemical, pharmaceutical, and plastics industries [5].

In this paper, the dielectric properties of the binary system of 1,3-, 1,4-BD and CPO at 298.15 k have been investigated. The main aim of this investigation is to understand dielectric behavior and the molecular association of the 1,3-, 1,4-BD in a polar solvent. In the present work dielectric permittivity, Kirkwood correlation factor, excess permittivity has been determined and analyzed.

II. METHODS

All of the chemicals at this study for the dielectric study were supplied from Merck. The electrical capacitance measurement was done using a Wayne Kerr 6425.

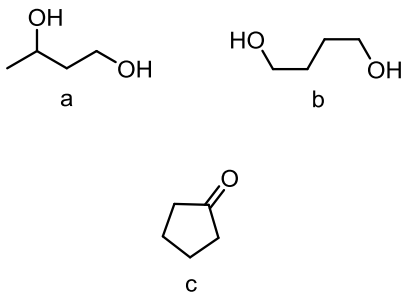

Fig. 1: a) 1,3-, b) 1,4-Butanediol and c) Cyclopentanone

III. RESULTS AND DISCUSSION

A. Experimental permittivity value

The plots of permittivity of BD–CPO mixtures against the mole fraction of CPO are shown in Fig. 2.

The plots exhibit the relative permittivity value increases towards the relative permittivity of BDs. This evidence explain the presence of the chemical structure of a molecule and intermolecular interactions factor. Therefore, the non-linear behavior of the permittivity displays intermolecular interaction between the unlike molecules and formation of their hetero structure. The hetero interaction is fundamentally related to the formation of donor-acceptor hydrogen bonding between the BDs and CPO molecules in these polar-polar mixed liquids.

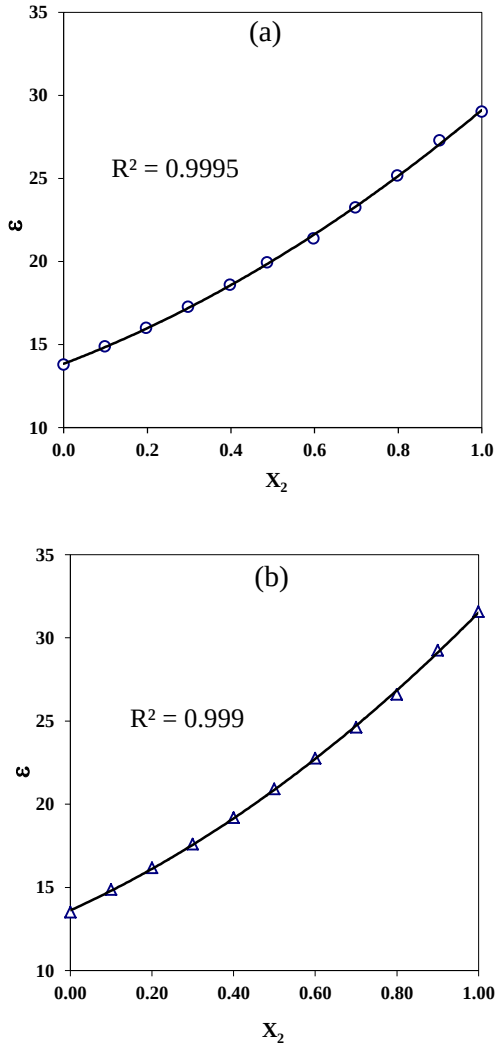

Fig. 2: the permittivity (ε_{12}) for (a) 1,3-BD and CPO mixtures and
(b) 1,4-BD and CPO mixtures at 298.15 k

B. *The Kirkwood correlation factor* (g_{eff})

Relative permittivity pertains to dipole moment 'μ' and volume number density. The Kirkwood correlation factor 'g' is measured via the relative permittivity. This parameter displays short-range molecular association between molecules. This measurement demonstrates short-range molecular that attributed to hydrogen bonding base on deviation g from unity. The Kirkwood correlation factor 'g' evaluated with the Kirkwood correlation equation. The dipole correlation expressed by the Kirkwood correlation factor 'g' for pure liquids can be calculated according to the Kirkwood–Frohlich equation [4,6,7].

$$\frac{(\varepsilon_0-\varepsilon_\infty)(2\varepsilon_0+\varepsilon_\infty)}{\varepsilon_0(\varepsilon_\infty+2)^2}=g\mu^2\frac{4\pi N\rho}{9KTM} \qquad (1)$$

To evaluate the value of 'g', we have derived μ_{CPO} = 3.27 D, $\mu_{1,3\text{-BD}}$ = 2.52 D and $\mu_{1,4\text{-BD}}$ = 2.7 D for CPO, 1,3-butanediol and 1,4-butanediol respectively from the previous literatures. We have taken ε_∞ value from refractive index ($\varepsilon_\infty = n^2$) data. The value calculated for CPO is g = 0.61. This calculation demonstrated that g less than 1 for the CPO and suggests the strong self-association between CPO molecules with the antiparallel dipole orientation.
The modified Kirkwood-Frohlich equation utilized for understanding associating result in this binary mixtures [3].

$$\frac{4\pi N}{9kT}\left[\frac{\mu_{BD}^2\rho_{BD}}{M_{BD}}X_{BD}+\frac{\mu_{BD}^2\rho_{BD}}{M_{BD}}(1-X_{BD})\right]g_{eff}=\frac{(\varepsilon_{0m}-\varepsilon_{\infty m})}{\varepsilon_{0m}}\frac{(2\varepsilon_{0m}+\varepsilon_{\infty m})}{(\varepsilon_{\infty m}+2)^2} \qquad (2)$$

The g_{eff} data are higher than unity display the parallel dipole orientation between CPO and BD mixtures. The g_{eff} data for various concentrations at 25 ˚C are presented in Table 1.

Table 1: Kirkwood correlation factor (g_{eff}) for 1,3- and 1,4-BD and CPO mixtures at 298 k

1,3-BD + CPO		1,4-BD + CPO	
Mol fraction of 1,3-BD	g_{eff}	Mol fraction of 1,4-BD	g_{eff}
0.000	0.552	0.000	0.611
0.099	0.630	0.1	0.700
0.198	0.718	0.2	0.792
0.298	0.823	0.3	0.896
0.398	0.942	0.4	1.018
0.497	1.066	0.5	1.156
0.598	1.245	0.6	1.312
0.698	1.442	0.7	1.485
0.798	1.677	0.8	1.685
0.899	1.962	0.9	1.920
1.000	2.316	1.000	2.180

Evidence indicate 1,3-, 1,4-BD g_{eff} are greater than unity that it attributed to interaction between the similar molecules with the parallel dipole orientation. So this parameter displays that g less than 1 for the CPO and suggests the strong self-association between CPO molecules with the antiparallel dipole orientation.

C. Excess permittivity (ε^E)

The plots of excess permittivity of BD–CPO mixtures against the mole fraction of CPO are shown in Fig. 3. The plots display pronounced minima. The negative values excess permittivity for BD–CPO mixtures exhibit the certain hetero molecular interaction therefore the dipole moment of the molecules decreased in the binary mixture.

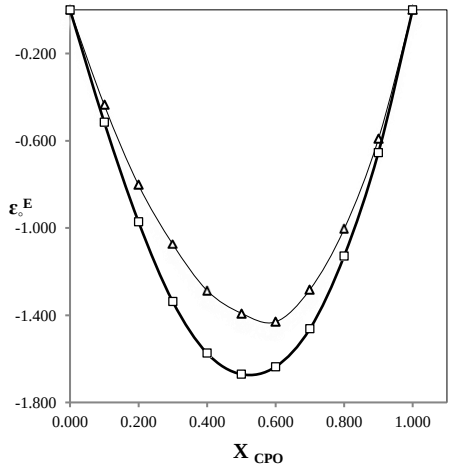

Fig. 3: Comparing of the excess permittivity ($\varepsilon_{\circ}^{E}$) of the (1,3-BD (Δ) and 1,4-BD (□) + cyclopentanone) binary systems as a function of mole fraction at T = 298.15 K

IV. CONCLUSION

Relative permittivities for the binary systems including 1,3-butanediol and Cyclopentanone and 1,4-butanediol and cyclopentanone were measured over a wide concentrations range at T = 298.15 K. For the investigated systems, the Kirkwood correlation factor (g_{eff}) and the excess permittivity (ε^E) were determined. In the investigated systems, the excess permittivity (ε^E) indicates negative values, which explain the certain hetero molecular interaction by decreasing the dipole moment of the molecules in the binary mixture. Evidence displayed BD molecules constitute multimers with the parallel ordering of their dipole because g_{eff} is larger than unity. This occurrence displays the homo interaction between the similar molecules with the parallel dipole orientation.

REFERENCES

[1] A. Ghanadzadeh. Gilani, Sh. Ramezani. Journal of Chemical & Engineering Data, vol 63, pp 2888-2903, **2018.**

[2] U. aatze, Journal of Molecular Liquids, pp 56-95, **1993**.

[3] S. havan, A. C. Kumbharkhane, and S. C. Mehrotra, Journal of the Chinese Chemical Society Vol 54, pp 14-5, **2007.**

[4] S. S. Kadam1, K. S. Kanse, Y. S. Joshi, D. N. Rander and A. C. Kumbharkhane, Indian Journal of Physics, vol 92, pp 1367–1372, **2018.**

[5] A. Ghanadzadeh. Gilani, Sh. Ramezani. Journal of Chemical & Engineerind Data, vol 63, pp4703-4719, **2018.**

[6] R. J. Sengwa, V. Khatri and S. Sankhala, Journal of Molecular Liquids, vol 144, pp 89-96, **2009.**

[7] D. A. G. Bruggeman, Journal of annalen der physik, vol 5, pp 34-39, **1995**.

The Aqueous Solubility of Indomethacin in the Presence of Tetrabutylammonium Bromide Based Deep Eutectic Solvents at Various Temperatures

Masumeh Mokhtarpour[a], Hemayat Shekaari*[a], Mohammed Taghi Zafarani-Moattar[a], Saied Faraji[a]

[a]Department of Physical Chemistry, University of Tabriz, Tabriz, Iran
Email address: Masomeh64_m@yahoo.com
**Corresponding author: Hemayatt@yahoo.com*

Abstract*:* Deep eutectic solvents (DESs) have recently been getting a great deal of attention in many fields of science and technology. The objective of this study was to peruse the solubility of indomethacin (IMC) as sparingly soluble drug in some tetrabutylammonium bromide (TBAB) based DESs (TBAB/ethylene glycol and TBAB/glycerol). The shake flask method has been employed in this study at temperature range T = (298.15-313.15) K and atmospheric pressure (P = 86.6 kPa). The results showed that the solubility of IMC was obtained approximately 17000-fold more than its solubility in water. The solubility data were accurately correlated by the famous local composition activity coefficient models including e-NRTL and UNIQUAC.

Keywords Deep eutectic solvents; Solubility; Indomethacin; Activity coefficient model.

I. INTRODUCTION

Deep eutectic solvents (DES) were introduced in 2003 [1] and are widely applied because they are cheap, easy to prepare and well characterized. DES is a homogeneous mixture composed of two or more substances at particular molar ratios and the mixture shows a melting point depression compared to the original components. Because of their unique features, these new green solvents are a proper alternative to organic solvents and ionic liquids and have been used in wide variety of fields, including pharmaceutical industries [2].

The co-solvency method is addition of a second solvent in small quantities to enhance the solvent power of the primary solvent and is very much used for convenience and cheapness [3]. In the last decades, to replace these organic solvents, several efforts have been made such as using non-volatile systems including ionic liquids (ILs), DESs and low-melting mixtures (LMMs) [4]. The great advantage of ILs is that they can be tuned by combining different cations and anions. However, the controversial environmental acceptability concerning their application and synthesis is considered as one of their big drawback [5, 6]. DESs as a new class of IL analogues were discovered to overcome these disadvantages. Although they represent a different type of solvent, DESs share many characteristics and properties with ILs [2]. However, because DESs as new solvents are green and sustainable solvents, scientific community especially in the green chemistry area give more attention to these solvents. Therefore, the use of green solvents instead of organic and toxic solvents is considered as an important issue in the pharmaceutical industry.

Indomethacin (IMC) is a tocolytic agent from the non-steroidal anti-inflammatory drugs (NSAID) family, which acts by reducing prostaglandin production. It is in the biopharmaceutics classification system (BCS) class II of drugs and its poor aqueous solubility (2.5 mg per mL to 4.0 mg per mL) needs to be improved in pharmaceutical science.

In the present study, we examined the solubility of this poorly water soluble drug in tetrabutylammonium bromide (TBAB) based DESs with ethylene glycol (EG) and glycerol (G) at various concentrations (ranging from 0 to 1 weight fraction of DES) and different temperatures (298.15, 303.15, 308.15, 313.15) K. In addition, the activity coefficient models such as e-NRTL [7], and UNIQUAC [8] have been applied to fit the solubility data.

II. METHODS

Chemical

Tetra butyl ammonium bromide, ethylene glycol and glycerol were purchased from MERCK Company and indomethacin was provided by Zahravi Pharmacy, Tabriz, Iran.

DES preparation

The purified compounds of TBAB and G or EG were mixed with the molar ratio 1:4 [9] to form the homogeneous liquid with mixing at 353.15 K for 3 hours.

Solubility measurement

Mixtures of water with DES were weighed by an analytical balance with precision 1×10^{-4} g (AW 220, GR220, Shimadzu, Japan). The shake flask method is one of the most common methods for measuring solubility [10] and we used this method in our study.The term of drug mole fraction

solubility, x_1, in (IMC (1) + water (2) + DESs (3)) systems was attained by Eq. (1) [11]:

$$x_1 = \frac{\frac{w_1}{M_1}}{\frac{w_1}{M_1} + \frac{w_2}{M_2} + \frac{w_3}{M_3}} \quad (1)$$

where M_i and w_i denote the molar mass and weight fractions of *i* component in the saturated solution, respectively.

Modeling

The main purpose of the present work is to illustrate improvement of solubility of IMC for pharmaceutical applications. Recently, some of the academic researchers have been tried to correlate and calculate solubility data of solid in mixed solvents. The following equation is gained through solid-liquid equilibrium (SLE):

$$-\ln x_1 = \frac{\Delta_{fus}H}{R}\left(\frac{1}{T} - \frac{1}{T_{fus}}\right) + \ln \gamma_1 \quad (2)$$

where T_{fus} , $\Delta_{fus}H$, T , x_1 and γ_1 refer to: melting temperature and enthalpy of fusion for the pure IMC, the experimental temperature, equilibrium mole fraction, and the activity coefficient of the IMC in the saturated solution, respectively. In addition, the enthalpy of melting assumed to be temperature independent. To correlate the solubility data of the studied drug and to generalize the UNIQUAC and e-NRTL models for a multi component systems consisting of electrolytes, the molar excess Gibbs energy, G^{ex}, is considered as following equation:

$$\frac{G^{ex*}}{RT} = \frac{G^{ex*,LR}}{RT} + \frac{G^{ex*,SR}}{RT} \quad (3)$$

superscript *is asymmetric convention, *LR* (long range) and *SR* (short range) represent interactions. The extended version of the Pitzer Debye–Hückel model, $G^{ex*,PDH}$, introduced by Pitzer [12] can be used for the long-range interaction contribution. In this article, the activity coefficient models such as e-NRTL and UNIQUAC [8] were applied for representing short-range interactions, G^{ex*SR}.

Electrolyte-NRTL model

One of the convenient utilized activity coefficient model for industrial systems is the electrolyte-NRTL model (e-NRTL) by Chen (1982) and Chen and Evans (1986). For any species appear in the investigated system, the sum of the Pitzer–Debye–Hückel and the NRTL is:

$$\ln(\gamma_i^*) = \ln(\gamma_i^{*PDH}) + \ln(\gamma_i^{*NRTL}) \quad (6)$$

UNIQUAC model

$\ln \gamma_i$ in UNIQUAC model (the Universal Quasi-Chemical theory) contains two parts: a residual part due to intermolecular forces which represents the enthalpy of mixing and a combinatorial part which describes the entropic contribution. System composition, the size and the shape of the molecules identifies combinatorial part. The residual part can be recognized by intermolecular forces. The UNIQUAC equation which is considered the temperature-dependent parameters is written as follows:

$$\ln \gamma_i = \ln \gamma_i^C + \ln \gamma_i^R \quad (7)$$

In this study the average relative deviation percent (*ARD%*) is used to evaluate the accuracy and applicability of the mentioned models. This calculation can be done using the subsequent equation:

$$ARD = 100\left(\frac{\sum_{i=1}^{N}\frac{\left|x_i^{\exp} - x_i^{cal}\right|}{\left|x_i^{\exp}\right|}}{N}\right) \quad (8)$$

where $x_i^{\exp}$, x_i^{cal} and N are experimental and calculated solubility mole fraction and the number of experimental data, respectively.

III. RESULTS AND DISCUSSION

Determination of drug Solubility

Available measured solubility data of IMC in {DES + water} solvents at studied temperatures are collected in Table 4. Almost all investigated experiments show a similar solubility profile in which IMC solubility increases with increasing weight fraction of DES. The relationship between solubility of IMC, x_1 , versus absolute temperature and weight fractions of DESs in the aqueous DES solutions has been drawn in Fig. 1. These figures demonstrate that at higher DES concentrations and temperatures, IMC solubility becomes 17000-fold more than its solubility in water.

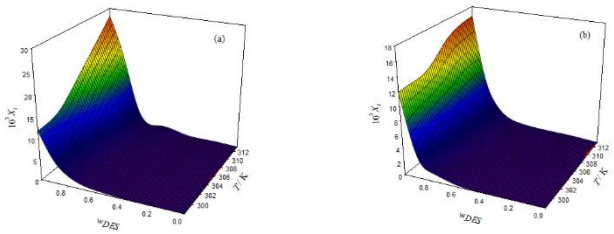

Fig. 1. The relationship between solubility of IMC, mole fraction x_1, versus weight fraction of DES, w_{DES}, and temperature in aqueous DES solutions, the solid lines obtained from e-NRTL model a) solutions with EG DESs and a) solutions with G DESs.

Correlation results

In the next step, the e-NRTL and UNIQUAC activity coefficient models were used to correlate the experimental solubility data of IMC in the aqueous solutions. The best

fitting results were obtained from the e-NRTL model based on the *ARD%* values (Table 1).

Table 1:The calculated average relative deviation percent (*ARD%*) from different models.

	ARD%	
T / K	e-NRTL	UNIQUAC
IMC (1) + water (2) + TBAB / EG (3)		
Average	1.49	1.96
IMC (1) + water (2) + TBAB / G (3)		
Average	2.37	2.38

IV. CONCLUSION

In recent years, deep eutectic solvents have been extensively investigated as promising materials for several processes in numerous fields of science and technology. In this work the aqueous solubility data of indomethacin in two tetrabutylammonium bromide based deep eutectic solvents (TBAB/EG or TBAB/G) in full ranges of deep eutectic solvent concentration were obtained experimentally at temperatures (298.15 to 313.15) K by using the shake flask method. The indomethacin mole fraction of solubility in the studied systems increased approximately 17000-fold. At a certain temperature and concentration of co-solvents, TBAB/EG is more effective on the solubility of IMC rather than TBAB/G. The solubility data was correlated with some activity coefficient models and their performance was e-NRTL>UNIQUAC for studied systems.

REFERENCES

[1] A.P. Abbott, G. Capper, D.L. Davies, R.K. Rasheed, V. Tambyrajah, Chemical Communications (2003) 70.
[2] E.L. Smith, A.P. Abbott, K.S. Ryder, Chemical reviews 114 (2014) 11060.
[3] X. Chen, H.M. Fadda, A. Aburub, D. Mishra, R. Pinal, International journal of pharmaceutics 494 (2015) 346.
[4] J.H. Clark, S.J. Tavener, Organic process research & development 11 (2007) 149.
[5] M. Petkovic, K.R. Seddon, L.P.N. Rebelo, C.S. Pereira, Chemical Society Reviews 40 (2011) 1383.
[6] M. Deetlefs, K.R. Seddon, Green Chemistry 12 (2010) 17.
[7] H. Renon, J.M. Prausnitz, AIChE journal 14 (1968) 135.
[8] D.S. Abrams, J.M. Prausnitz, AIChE Journal 21 (1975) 116.
[9] M. Mohan, P.K. Naik, T. Banerjee, V.V. Goud, S. Paul, Fluid Phase Equilibria 448 (2017) 168.
[10] J. Larsson, (2009).
[11] A. Forte, C.I. Melo, R. Bogel-Łukasik, E. Bogel-Łukasik, Fluid Phase Equilibria 318 (2012) 89.
[12] K.S. Pitzer, Journal of the American Chemical Society 102 (1980) 2902.

Selective Partitioning of Alkaloids in Alcohol- Carbohydrate Aqueous Two-Phase Systems

Nosaibah Ebrahimi*[a], *Rahmat Sadeghi*[b]

[a] *Department of Chemistry, University of Kurdistan, Sanandaj, Iran, Email: no.ebrahimi@gmail.com*

[b] *Department of Chemistry, University of Kurdistan, Sanandaj, Iran, Email: rsadeghi@uok.ac.ir*

Abstract: The new aqueous two-phase systems (ATPS) composed of saccharides and propanol was produced in this work. The main elements that control the phase splitting aptitude of these systems were studied. Two alkaloids (caffeine and codeine) and a flavoring antioxidant (vanillin) were used as target biomolecules for evaluating the extraction performance of propanol-carbohydrate ATPS. Because of the difference in the electric charge of caffeine and codeine in the produced ATPS, and also due to the difference in the water content and hydrophilic nature of the coexisting phases, the propanol- carbohydrate ATPS showed a proper selectivity for separation of these alkaloids. The partitioning experiments revealed that caffeine and vanillin are present as neutral species and preferentially concentrate in the alcohol-rich phase, however, codeine is present mostly in the cationic form and has a preferable orientation for the carbohydrate-rich phase. In order to optimize the selectivity of propanol-carbohydrate ATPS to separate similar biomolecules, factors such as the chemical structure of saccharides, temperature, and tie-line length were addressed.

Keywords: Alkaloids, Aqueous two-phase systems, Partitioning, Propanol, Carbohydrate

I. INTRODUCTION

One of the main limitations in the analysis and quantification of different target compounds is the high detection limit of conventional analytical apparatus. Therefore, a pretreatment step to concentrate target compounds from original samples is essential for satisfactory quantification [1,2]. The liquid-liquid extraction based on aqueous two-phase systems (ATPS), because of environmental adaptability, easiness, diversity, significant efficiency, and low time- and cost- consumption has been remarkably studied as a pretreatment approach for a large range of samples [3]. ATPS, which is a kind of soluting-out appearance, forms when combinations of two hydrophilic solutes show incompatibility in aqueous mixtures above critical concentrations. The appropriate selection of the phase forming components (soluting-out inducer and soluted-out agent) leads to the adjustable nature of ATPS, allowing thus the development of reasonable extraction platforms [4]. Saccharides are polyhydroxy aldehydes or ketones with high hydrophilic nature, which because of biodegradability, electrical neutrality, and non-toxicity are able to act as green and gentle soluting-out inducer instead of salts [5]. Herein, for the first time, the aptitude of carbohydrates and their polyols to solute-out the fully water-soluble aliphatic alcohols from aqueous media and form alcohol-carbohydrate ATPS is established. Then, the liquid-liquid separation performance of these new ATPS is explored through the investigation of the partition coefficients of three model biomolecules, namely caffeine, codeine, and vanillin among the coexisting phases.

II. METHODS

Materials: 1-propanol (99.9 wt %) was obtained from DUKSAN. D-(+)-xylose (≥99.0 wt %), L-(+)-arabinose (≥ 99.0 wt %), D-(+)-glucose (≥99.5 wt %), D-(+)-galactose (≥98.0 wt %), D-(-)-fructose (≥99.0 wt %), sucrose (≥98.0 wt %), maltose monohydrate (≥99.0 wt %), caffeine (≥98.0 wt %) and vanillin (≥99.0 wt %) were purchased from Merck. Xylitol (≥99.0 wt %) and maltitol (≥97.0 wt %) were obtained from Alfa Aesar. Codeine (≥0.98 wt %) was obtained from Shafa Pharmaceutical, Tehran, Iran. All chemicals were used without further purification. The water used was double distilled, with a specific conductivity of 1.2 $\mu S \cdot cm^{-1}$ at 298 K.

Methods: The turbidity titration method [5] was used to determine the binodal curves of the produced ATPS at T = (298.2 and 318.2) K, and atmospheric pressure. For determination of tie-lines (TLs), the concentration of carbohydrates was determined using a Gyromat digital polarimeter supplied by Anton Paar. This apparatus is an automatic circular polarimeter with a resolution of 0.001^0 optical rotation. An Anton Paar Abbemat refractometer, with a resolution of ±0.000001, was used to measure the concentration of 1-propanol in each sample. The quantification of the partitioning solutes was performed by UV spectroscopy using a SPEKOL-2000 Analytik Jena UV-VIS spectrophotometer at the wavelengths of 272 nm (for caffeine), 284 nm (for codeine) and 280 nm (for vanillin). The balance engaged in all the experiments was Sartorius CP124S precisely within ± 1.10^{-7} kg.

III. RESULTS AND DISCUSSION

This paper performs a broad experimental study on the formation of the new ATPS composed of carbohydrates and fully water-soluble alcohols, and also their aptitude as cost-

effective and proficient extractive platform. The results obtained from solubility experiments show that ethanol + carbohydrate aqueous solutions are not prone to form stable ATPS. However, propanol + carbohydrates aqueous solutions form permanent alcohol-sugar ATPS above critical concentrations. Comparing all the binodal curves obtained shows that the capability of sugars to solute-out propanol follows the order: Maltose (m_A > 9 mol.kg^{-1}) > Maltitol > Maltose (9 mol.kg^{-1} > m_A) > Sucrose > D-Galactose > D-Glucose > D-Fructose ≥ L-Arabinose > Xylitol > D-Xylose. This sequence which can be arranged as disaccharides hexose monosaccharides > pentose monosaccharides is i agreement with the general order of the sugars' hydrophili nature, and also their capacity to produce ATPS wit polypropylene glycol [5]. Details on the role of number an spatial position of carbohydrates' hydroxyl groups on the hydrophilicity and soluting-out ability were discussed, b examining several carbohydrates, in our previous work [5]. decrease in temperature increases the potential of propanol carbohydrate aqueous solutions to form ATPS. This propert provides opportunity to design scaled-up strategies involvin propanol-sugar ATPS, in terms of energetic inputs.

In order to investigate the extraction applicability of th novel ATPS produced here, the partition coefficients (K = C_{t} / C_{bot}) of two alkaloids (caffeine and codeine) and a flavorin antioxidant (vanillin) in the ATPS composed of ternary 1-propanol + glucose / sucrose / maltitol aqueous solutions were studied. The extraction experiments were performed at different mixture compositions (different tie-line lengths) of each ATPS, at T = (298.2 and 318.2) K. The obtained results are given in Table 1. Fig. 1 sketches the logarithm of the partition coefficients (log K) of the studied biomolecules in different TLL of 1-propanol-maltitol ATPS, at 298.2 K, as an example of the investigated systems. The similar behavior was observed for the other systems.

Table1: Initial mixtures compositions (mass fraction of carbohydrate (w_C) and alcohol (w_A)), and tie-line length (TLL) of 1-propanol-sugar ATPS, along with the experimental partition coefficients of caffeine (K_{Caf}), codeine (K_{Cod}), and vanillin (K_{Van}), at P = 845 hPa.

Sugar	w_C	w_A	TLL	K_{Caf}	K_{Cod}	K_{Van}
			T = 298.2 K			
D-Glucose	0.2263	0.3554	0.4646	1.6955	0.3956	5.2407
	0.2384	0.3776	0.5941	2.1053	0.2640	8.3090
	0.2545	0.4018	0.7116	2.5011	0.1940	12.5579
Sucrose	0.2786	0.3630	0.5793	2.0569	0.3175	6.5460
	0.2948	0.3848	0.6908	2.4096	0.2635	8.1019
	0.3122	0.4104	0.8196	3.2584	0.1825	12.8441
Maltitol	0.2445	0.3218	0.4828	1.9611	0.3401	6.0130
	0.2716	0.3427	0.6431	2.7874	0.2303	9.7984
	0.2926	0.3594	0.7449	3.2590	0.2044	11.5090
	0.3152	0.3850	0.8532	4.1527	0.1647	15.5886
			T = 318.2 K			
D-Glucose	0.2394	0.3646	0.4795	1.9285	0.3338	4.7141
	0.2530	0.3801	0.6091	2.3226	0.2448	7.0039
	0.2665	0.3996	0.7097	2.6851	0.2007	10.0126
	0.2840	0.4228	0.8103	3.0252	0.1729	12.6886
Sucrose	0.2781	0.3629	0.5105	1.9080	0.3530	4.0293
	0.2943	0.3850	0.6563	2.4579	0.2642	6.5901
	0.3127	0.4107	0.7869	3.1411	0.1954	9.4010
	0.3288	0.4304	0.8775	3.9007	0.1691	11.9870
Maltitol	0.2447	0.3216	0.4683	2.2054	0.3115	5.0863
	0.2719	0.3429	0.6395	3.0569	0.2304	7.9235
	0.2921	0.3591	0.7377	3.9915	0.2001	10.3647
	0.3143	0.3834	0.8377	4.6354	0.1797	12.5910

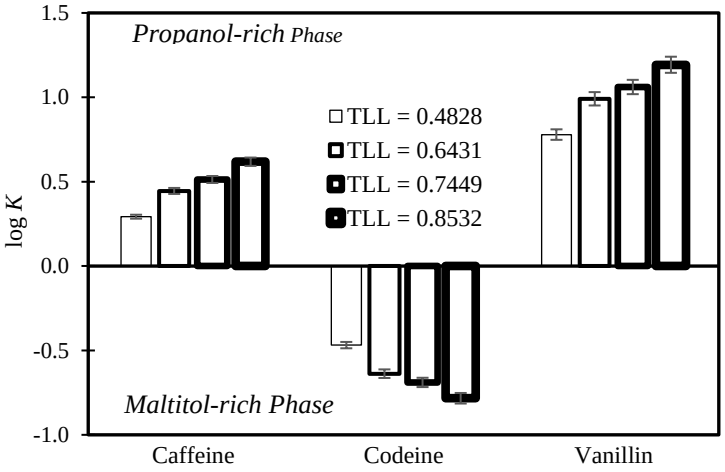

Fig. 1: Logarithm of the biomolecules partition coefficients (log K) at different TLLs of 1-propanol-Maltitol ATPS, at 298.2 K.

As observed from Table 1 and Fig. 1, in all cases vanillin and caffeine preferentially concentrate in the top propanol-rich phase (K > 1 and log K > 0), while codeine is willing to migrate for the bottom carbohydrate-rich phase (K < 1 and log K < 0). An increase in TLL facilitates the immigration of vanillin and caffeine into the propanol-rich phase, as well as the preferred partition of codeine to the carbohydrate-rich phase. In fact, according to the TLs data, the amount of water molecules existing in the bottom phase is higher than that in the top phase, and as TLL increases the water content of the top phase decreases. Therefore, it can be concluded that vanillin and caffeine concentrate in the more hydrophobic phase, while codeine migrates to the more hydrophilic phase, and this behavior becomes more preferred by increasing the difference in the hydrophobic/hydrophilic nature of the coexisting phases via the rise in TLL. As Table 1 shows, the K values obtained for caffeine vary from 1.7 to 4.6, while those for vanillin vary from 4.7 to 15.6. Vanillin ($C_8H_8O_3$, log K_{ow} =1.21) is more hydrophobic than caffeine ($C_8H_{10}N_4O_2$, log K_{ow} =-0.07). Hence, the partition coefficients of vanillin for the alcohol-rich phase are more than those of caffeine. The open question is that why codeine ($C_{18}H_{21}NO_3$) with log K_{ow} = 1.19 preferentially migrates for the more hydrophilic

carbohydrate-rich phase. In fact, codeine ($pK_a = 8.3$) owing to an amine functional group has a positive charge in the medium of the investigated ATPS, in which the pH values are lower than the pK_a of codeine (pH varies between 5.01 and 6.28 in the studied systems). Therefore, despite an expected preferential migration to the more hydrophobic alcohol-rich phase, codeine being present generally as a cation in all the studied ATPS, concentrates in the more hydrophilic carbohydrate-rich phase. The reverse partition trend of caffeine and codeine verifies the inherent aptitude of the propanol-sugar ATPS for selective separation of these two alkaloids. The selectivity index ($S = K_{Caf} / K_{Cod}$) of the investigated 1-propanol-carbohydrate ATPS decreases in the order: maltitol > sucrose > glucose, and in each ATPS its values increase by the increase in both TLL and temperature.

IV. CONCLUSION

This paper addressed the possibility of forming new ATPS by mixing propanol and a variety of carbohydrate (mono- and di-saccharides, and their polyols) in aqueous solutions. A comprehensive database regarding the liquid-liquid phase splitting behavior and their relative properties was established. The promising results were acquired for the partitioning behavior of caffeine, codeine, and vanillin in the produced ATPS. Propanol- carbohydrate ATPS are able to provide the selective separation of similar biomolecules. Partition coefficients vary from 1.7 to 4.6 for caffeine, 0.16 to 0.4 for codeine, and 4.7 to 15.6 for vanillin.

REFERENCES

[1] D.P. Mohapatra, S.K. Brar, R.D. Tyagi, P. Picard, and R.Y. Surampalli, Sci. Total Environ., vol. 470, pp. 58–75, **2014**.
[2] T.B. V Dinis, H. Passos, D.L.D. Lima, A.C.A. Sousa, J.A.P. Coutinho, V.I. Esteves, and M.G. Freire, J. Chromatogr. A. vol. 1559, pp. 69-77, **2018**.
[3] G. de Brito Cardoso, I.N. Souza, T. Mourão, M.G. Freire, C.M.F. Soares, and Á.S. Lima, Sep. Purif. Technol. vol. 124, pp. 54–60, **2014**.
[4] F.A. e Silva, R.M.C. Carmo, A.P.M. Fernandes, M. Kholany, J.A.P. Coutinho, and S.P.M. Ventura, ACS Sustain. Chem. Eng. vol. 5, pp. 6409–6419, **2017**.
[5] R. Sadeghi, N. Ebrahimi, M.D. Tehrani, Polymer, vol. 98, pp. 365–377, **2016**.

Study of the liquid-liquid equilibrium for aqueous systems containing choline bitartrate and 1-propanol at different temperatures and their performances in acetaminophen separation

Elnaz Pourbagherian [a]*, Mohammed Taghi Zafarani–Moattar [b], Hemayat Shekaari [b]
Affiliation (*Department of Chemistry, Tabriz University*)
Email: elnnazi.pb@gmail.com

Abstract*:* The purpose of this research is study of the aqueous two-phase system composed of (1- propanol+ choline bitartrate + water) at T = (298.15, 308.15 and 318.15) K and atmospheric pressure (≈ 85 kPa). The use of this system for separation of acetaminophen, as a model drug was examined. First, the binodal data and tie-lines were determined for this system at the above mentioned temperatures. The effects of the tie-line length and temperature on the drug separation were also investigated. The Gibbs energies, enthalpies, and entropies are calculated from the cloud points at working temperatures in order to investigate the driving force of phase separation. In addition, the Merchuk equation and an empirical equation were used to show binodal results. The Setschenow equation and the non-random two-liquid (e-NRTL) model were used to fit the tie-line values.

Keywords: Liquid–liquid equilibrium; choline bitartrate; separation of acetaminophen; non-random two-liquid model.

I. INTRODUCTION

The design of the separation process related to liquid mixtures containing alcohol and water has important role in the chemical industry [1]. 1-propanol and 2-propanol are used as extraction solvents for chemical and biological processes, natural proteins and biological processes. In these processes, alcohols form a mixture of azeotropic with water. So, the separation of alcohol with simple distillation is not useful; instead, liquid-liquid extraction, which is one of the most important industrial and scientific options, is replaced. In order to separate alcohols by liquid - liquid extraction, use of ionic liquids instead of conventional solvents is known for their azeotropes breaking capacity [2]. Ionic fluids are salts with a melting point below 100 ° C, which include organic or inorganic anions and organic cations and are used as green solvents. The main advantages of aqueous two-phase systems (ATPSs) are their speed, phase equilibrium, the possibility of continuous processing, low power requirements, etc. ATPS can be used in applied biotechnology for the separation and purification of enzymes such as lipase, antibiotics, and drugs such as acetaminophen.

II. METHODS

The chemicals used in this work are: choline bitartrate,1-propanol, acetaminophen. A glass vessel, volume 50 cm^3, was used to determine the phase equilibrium. The glass vessel was provided with an external jacket in which water at constant temperature was circulated using a thermostat. The temperature was controlled to within ± 0.05 K. The binodal curves were determined by clouding point titration method. For determination of the tie-lines, feed samples (about 2×10^{-5} m^3) were prepared by mixing appropriate amounts of polymer, salt and water in the vessel. The thermostat was set to optimum temperature and the sample was placed in the thermostat for 1 hour. The mixture was then allowed to be separated into two clear phases for 48 hours. After the separation of the two phases, the concentrations of choline bitartrate in the top and bottom phases were determined by using conductivity measurements. The concentration of alcohol in both phases was determined by refractive index measurements performed at T = 298.15 K using a refract meter. To investigate the extraction of acetaminophen, UV-Visible method was used.

III. RESULTS AND DISCUSSION

For the ternary {1-propanol (m) + choline bitartrate (s) + water (w)} system, the binodal data and tie-line compositions were determined experimentally at T = (298.15, 308.15 and 318.15) K and atmospheric pressure (≈ 85 kPa).

A. Figures and Tables

The effect of different temperatures on the binodal curves for the studied system and the effect of temperature on the phase-forming ability is shown Fig. 1 which demonstrates

that the two-phase area is expanded with an increase in temperature. For the studied system, the experimental binodal data were fitted using the least-squares regression method with the following empirical nonlinear expression proposed by Zafarani-Nemati [3]:

$$w_a = \alpha + \beta \ln(w_s) + \gamma w_s \qquad (1)$$

Using eq. 1, the fitting parameters α, β, and γ obtained from the correlation of experimental binodal data along with the corresponding standard deviations are given in Table 1.

In this work, the obtained tie-line data were fitted with the Othmer-Tobias and Bancroft [4] and Setschenow equations [5].

Finally, the use of this alcohol-based ATPS has been investigated for acetaminophen extraction. The partition coefficient and percentage of acetaminophen extraction were obtained in this ATPS, as shown in Fig. 2; and it was found that by increasing temperature, the partition coefficients K_{acet} and separation efficiency E_{acet} are increased.

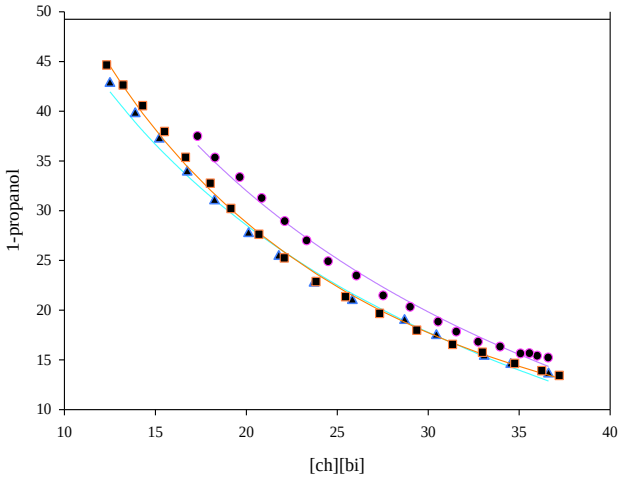

Fig.1: Experimental binodal results for the {1-propanol (m) + choline bitartrate (s) + water (w)} system at different temperatures.

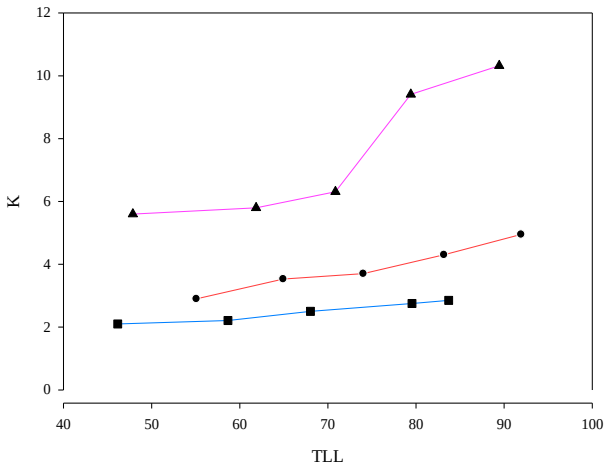

Fig. 2. Effect of temperature and *TLL* on the acetaminophen partitioning for {1-propanol (m) + choline bitartrate (s) + water (w)} system: ( ) T = 298.15 K; ( ) T = 308.15 K and ( ) T = 318.15 K.

Table1: Values of Parameters of eq 1 for {1-propanol (m) + choline bitartrate (s) + water (w)} at different temperatures.

T/K	*α*	*β*	*γ*	$10^2 sd$
298.15	-0.34	-0.37	0.30	0.60
308.15	-0.57	-0.32	0.22	0.65
318.15	-0.27	-0.44	0.70	0.54

IV. CONCLUSION

Liquid–liquid equilibrium for the {1-propanol (m) + choline bitartrate (s) + water (w)} system was studied at T = (298.15, 308.15 and 318.15) K and the experimental binodal and tie-line data at the mentioned temperatures were reported. The experimental binodal data were satisfactorily correlated using an empirical equation. An acceptable experimental lines is obtained using Equation Othmer - Tobias and Bancroft. In addition, the Seteschenow type and e -NRTL model are used to investigate phase behavior of the studied system. The use of this alcohol- based ATPS for acetaminophen partitioning has been studied. From the specified values found for acetaminophen partitioning, we conclude that the partition coefficient increases with increasing temperature.

REFERENCES

[1] Asenjo, J. A., & Andrews, B. A. (2011). Aqueous two-phase systems for protein separation: a perspective. J.Chrom A, 1218(49), 8826-8835.

[2] A. Marciniak, Ternary liquid–liquid equilibria of bis (trifluoromethylsulfonyl)-amide based ionic liquids + 2-propanol +di-iso-propyl ether, Fluid Phase Equilib. 378 (2014) 102-106.

[3] Zafarani-Moattar, M. T., Emamian, S., & Hamzehzadeh, S. (2008). Effect of temperature on the phase equilibrium of the aqueous two-phase poly (propylene glycol)+ tripotassium citrate system. J. Chem.Eng, 53(2), 456-461.

[4] D.F. Othmer, P.E. Tobias, Ind. Eng. Chem. 34 (1942) 690-692.

[5] M.J. Hey, D.P. Jackson, Hong Yan, Polymer 46 (2005) 2567-2572.

Thermodynamic Behaviour Of Lithium Chloride Solutions Containing Deep Eutectic Solvent in The Dilute Region at T = (288.15 to 303.15) K

Mohammed Taghi Zafarani-Moattar, Hemayat Shekaari, Asma Sadr-Mousavi*
Department of Physical Chemistry, University of Tabriz, Tabriz, Iran
**Email: asmamousavi58@gmail.com*

Abstract: Deep eutectic solvents (DESs) have getting a much attention in many areas of science and technology in the last decade. In this respect we have studied thermodynamic behaviour of aqueous Lithium Chloride solution + Deep Eutectic Solvent in the dilute region at different temperatures (T=288.15-318.15 K) under atmospheric pressure (≈ 85 kPa). To obtain some information regarding the solute-solvent interaction in this system the densities (d) were measured for Lithium Chloride aqueous solutions of the DESs based on choline chloride (ChCl) with urea. On the basis of calculated apparent molar volume values calculated from the measured density data, solute-solvent and solvent-solvent interactions are discussed.

Keywords: Apparent molar volume, deep eutectic solvents (DESs), Excess molar volumes, Lithium Chloride.

I. INTRODUCTION

Deep eutectic solvents (DESs) composed of two or more substances that can form a liquid phase through hydrogen bonding. This new phase typically has a much lower freezing point than any of its component parts. Deep eutectic solvents (DESs) have all of the requirements for a green solvent. They are cheap, easy to prepare, and well characterized [1]. These features make new green solvents a proper alternative to ionic liquids and organic solvents [2]. Deep eutectic solvents are used in a wide range of technologies such as catalysts, pharmaceutical industries and energy storage. In the field of power storage, lithium-ion batteries are widely used. But the safety, environmental, and cost is a major concern for researchers. This problem mostly arises from their nonaqueous electrolytes. The use of aqueous alternatives can expand the electrochemical stable window [3]. Therefore, in the present study we have investigated the use of the thermodynamic properties of Lithum salt with DES in aqueous solution. A few studies have been made on the thermodynamic properties of these solvents in the literature. To design and production of new electrolytes, understanding the interaction between solute-solute, solvent- solute and solvent- solvent are essential. In this work the thermodynamic properties of LiCl+DES systems in aqueous solutions have been measured and correlated. Density have been measured for Lithium Chloride+ choline chloride/urea in water at T = (283.15 – 318.15) K and atmospheric pressure. The density measurements were used to calculate the apparent molar volumes (V_φ) and standard partial molar volumes ($V_\varphi{}^0$).

II. METHODS

In the present study, the deep eutectic solvent of ChCl/Urea was prepared at molar ratios of 1:2 [4]. The binary solvent mixtures (DES + water) were prepared by mixing the appropriate amounts (in grams) of solvents. Solutions were provided in glass vials and in molal base concentration by weighting using an analytical balance with an uncertainty $\pm 1\times10^{-4}$ g and closed firmly with parafilme. The density (d) of solutions was measured with a vibrating tube densimeter (Anton Paar DSA 5000, Austria) at frequency (approximately 3 MHz) [5].

III. RESULTS AND DISCUSSION

The densities, d, for LiCl in aqueous DES solutions (0.06-0.14 mol.Kg^{-1}) in aqueous DES solutions are measured. According to the obtained data densities increase with LiCl concentrations as well as with DES concentrations but decrease with rise in temperature. These data were used to compute apparent molar volume. The apparent molar volume, V_φ, and standard partial molar volume $V_\varphi{}^0$ were computed with Eqs (1) and (2) respectively.

$$V_\phi = \frac{M}{d} - \left[\frac{(d-d_0)}{mdd_0}\right] \quad (1)$$

$$V_\phi = V_\phi{}^0 + S_v m \quad (2)$$

where, m, M, d and d_0 are molality (in mol.kg^{-1}), molar mass (in kg.mol^{-1}), densities (in kg.m^{-3}) of solution and pure solvent, respectively. Also S_v is the experimental slope explain solute−solute interactions. These parameter was used to obtain some information in regard to interactions between ChCl/Urea and LiCl in water. The apparent molar volumes of LiCl in aqueous ChCl/Urea solution (0.02 w/w) at experimental temperatures T = (288.15, 298.15, 308.15, 318.15) K are plotted in Fig.1. The positive V_ϕ values show intensive solute-solvent interactions. Also, we observed that the apparent molar volumes decrease with increasing of the LiCl concentration. In addition, it was found that increasing the temperature increased V_ϕ. The values of standard partial

molar volume for aqueous DES solutions is plotted in Fig.2. It is observed that due to enhanced solute-solvent interactions, the positive values of standard partial molar for aqueous DES solutions increase with increasing temperature. This increase of standard partial molar with temperature indicates the presence of strong (solute-solvent) interactions at elevated temperatures.

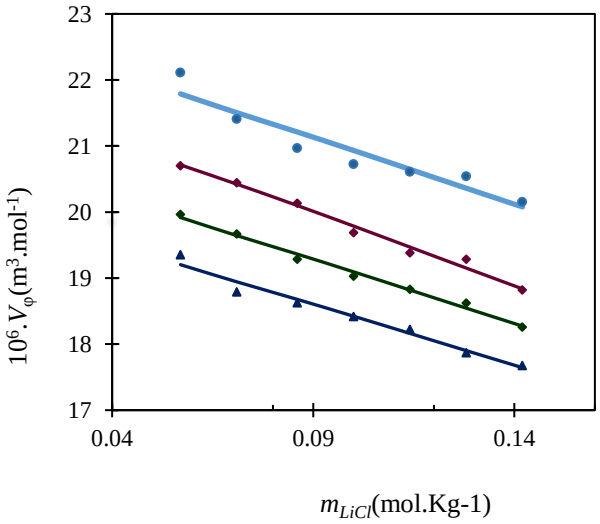

Fig.1: Experimental and calculated apparent molar volume ($V\varphi$) of [ChCl/urea][H_2O] versus molality of LiCl (m_{LiCl}) in at T = (288.15 to 318.15) K. (▲), T = 288.15 K; (■), T = 298.15 K; (▲), T = 308.15 K; (●), T = 318.15 K.

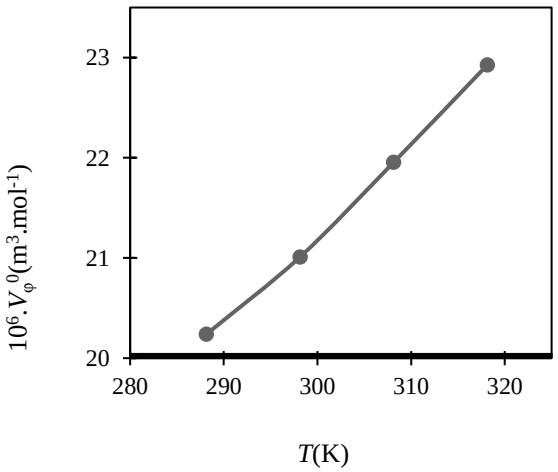

Fig.2: The comparison of the standard partial molar volumes, V_ϕ^0, of LiCl+ ChCl /urea in aqueous solutions at different temperatures.

IV. CONCLUSION

Densities were experimentally measured for ternary (ChCl/Urea + LiCl + water) solutions at T = (288.15, 298.15, 308.15 and 318.15) K under atmospheric pressure (≈ 85 kPa). Volumetric parameters of LiCl in aqueous ChCl / Urea solutions have been used to study the interactions between Lithum salt and the deep eutectic solvents in aqueous solutions. The standard partial molar volumes, show that their values have increased by increasing the temperature. This observation indicates that the interactions of the deep eutectic solvent with LiCl in aqueous solutions become stronger with increasing the temperature. Also, standard partial molar volumes are decreased by increasing the concentration of Lithium chloride. There results indicate that the interaction between the solute-solute is reduced and the interaction between the solvent- solute is increased.

REFERENCES

[1] Wang, H., Jia, Y., Wang, X., Yao, Y., & Jing, Y. (2014). Physical–chemical properties of nickel analogs ionic liquid based on choline chloride. *Journal of Thermal Analysis and Calorimetry*, *115*(2), 1779-1785.

[2] Abbott, A. P., Capper, G., Davies, D. L., Munro, H. L., Rasheed, R. K., & Tambyrajah, V. (2001). Preparation of novel, moisture-stable, Lewis-acidic ionic liquids containing quaternary ammonium salts with functional side chainsElectronic supplementary information (ESI) available: plot of conductivity vs. temperature for the ionic liquid formed from zinc chloride and choline chloride (2: 1). See http://www. rsc. org/suppdata/cc/b1/b106357j. Chemical Communications, (19), 2010-2011.

[3] Suo, L., Borodin, O., Gao, T., Olguin, M., Ho, J., Fan, X., ... & Xu, K. (2015). "Water-in-salt" electrolyte enables high-voltage aqueous lithium-ion chemistries. *Science*, *350*(6263), 938-943.

[4] Zhang, Q., Vigier, K. D. O., Royer, S., & Jérôme, F. (2012). Deep eutectic solvents: syntheses, properties and applications. *Chemical Society Reviews*, *41*(21), 7108-7146.

[5] Fortin, T. J., Laesecke, A., Freund, M., & Outcalt, S. (2013). Advanced calibration, adjustment, and operation of a density and sound speed analyzer. *The Journal of Chemical Thermodynamics*, *57*, 276-285.

Volumetric Properties of Ternary Mixtures for Choline Salicylate (API-IL) + Amino acids + Water at T = 298.15 K

***H. Shekaari*[a] *, N. Ammari*[a]**

[a] *Department of Chemistry, University of Tabriz, Tabriz, Postal code :5166616471, Iran*

**Email:hemayatt@yahoo.com, ammari.ngn@gmail.com*

Abstract The knowledge of physicochemical properties of third generation of ionic liquids, active pharmaceutical ingredients ionic liquid (API-IL), in the presence of amino acids are attractive and essential for various applications in biological activities including efficacy, penetration and rapid solubility of drugs. In this work, density of choline salicylate ([Chol][Sal]) as API-IL in 0.2 mol·kg^{-1} aqueous amino acids (L-alanine and L-arginine) solutions have been measured at room temperature. Standard partial molar volumes, V_φ^0, have been calculated using measured data. The calculated parameters have been used to interpret the present interactions between [Chol][Sal] and amino acids which are essentially dependent on the structure of amino acids and contribution of the charged end groups and the length of alkyl chain. Results indicate the presence of strong ion-polar interactions between [Chol][Sal] and L-alanine. The amount of this interaction has been decreased for another amino acid L-arginine.

Keywords: Choline salicylate, Amino acids, Standard partial molar volumes

I. INTRODUCTION

In the classification of pharmaceutical dosage forms, unit solid and bulk dosage forms have series of problems among the process of dissolving and absorbing which results in limited stability, so increasing need for patients to take such medications has led to improve the quality, effectiveness with minimal side effects [1]. In recent years, conversion of the drug into the form ionic liquid has been proposed. The ionic liquids with outstanding solvation properties and less toxicity are considered as an active pharmaceutical ionic liquid (API-IL) [2]. Choline salicylate as (API-IL) consists two cationic and anionic drug components that choline is used as vitamin B4 and salicylate is used as an anti-inflammatory, rheumatism treatment and analgesic drug. Understanding behavior of [Chol][Sal] with amino acids gives us useful information about the interactions in these types of solutions. In the present study, density of [Chol][Sal] in aqueous solutions of some amino acids (L-alanine and L-arginine) are presented. Apparent molar volume v_φ, has been computed resulting from the mentioned experimental data to interpret the present interactions between solute-solvent molecules [3].

II. METHODS

Choline chloride > 0.99, Sodium salicylate ≥0.995, Acetone >0.998 and Dichloromethane >0.996 were used for synthesis of the Choline salicylate. Both amino acids have initial mole fraction purity of >0.99. Densities ρ of solutions were measured with a vibrating tube densimeter (Anton Para, DSA 5000 densimeter). Double distilled deionized and degassed water and also dry air at atmospheric pressure were used to calibrate the apparatus.

III. RESULTS AND DISCUSSION

The experimental densities and apparent molar volumes (v_φ) for [Chol][Sal] in water with approximate concentration 0.2 mol/lit of aqueous (L-alanine, and L-arginine) solutions at T=298.15 K are measured. Comparisons of values of v_φ for [Chol][Sal] in aqueous solutions of (L-alanine, L-proline and L-arginine) with 0.2 molality is plotted in Figure 1. As can be seen in Fig.1, values of v_φ have a rising trend with increasing in L-alanine concentration but for L-arginine this trend is completely reversed. Standard partial molar volume, v_φ, is obtained by using a least-squares treatment of the following Redlich-Mayer equation demonstrated as Eq.1 below:

$$V_\varphi = V_\varphi^0 + S_v m^{1/2} + b_v m \qquad (1)$$

It is remarkable that all values of (V_φ^0) as a scale of the solute-solvent interactions are positive and it increases at higher concentration of L-alanine, apart from the fact that another amino acid L-arginine has a decreasing trend with an increase in concentration [4].

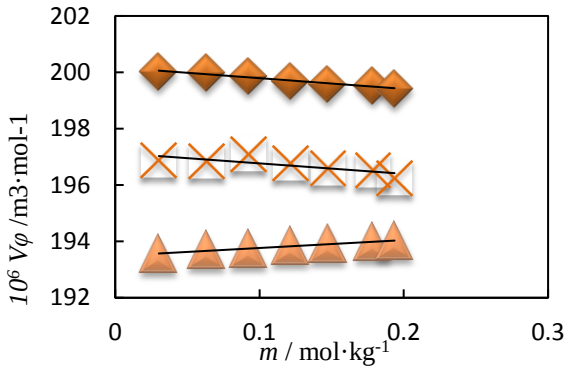

Fig1. Apparent molar volumes of [Chol][Sal] in aqueous solutions of amino acids with approximately 0.2 molality: (×), 0.0000; (◆), L-alanine; (▲), L-argenine; at 298.15 K.

IV. CONCLUSION

According to the results obtained from the volumetric measurements the values of standard partial molar volumes, (V_φ^0), are positive and it has increasing trend for L-alanine and decreasing trend for L-arginine. The possible reason for this feature could be due to the presence of long alkyl chain in the structure of L-argenine. Generally, it is concluded that an addition of amino acids with non-polar structures (CH2) in aqueous solutions of [Chol][Sal] changes the types of interactions from (hydrophilic-hydrophilic, hydrophilic-ions) to the (hydrophobic-hydrophobic, hydrophobic-ions).

REFERENCES

[1] J .Shamshina, and R. Rogers, Journal of therapeutic delivery, vol 5, pp. 489-491, **2014**.
[2] J. Wang, Y. Pei, Y, Zhao, and Z. Hu, Journal of green chemistry, vol 7, pp. 196-202, **2005**.
[3] H. Shekaari, and F. Jebali, Journal of solution chemistry, vol 39, pp. 1409-1427, **2010**.
[4] S. Panda, V. Singh, N. Islam, and R. L. Gardas, Journal of fluid phase equilibria, vol 445, pp. 35-44, **2017**.

Gibbs energies of transfer of NH_4SCN from water to aqueous solution of Butanol using Potentiometric Method

Vahideh Masumi*[a], *Rahman Salamat–Ahangari*[b]

[a,b,]*Department of Chemistry, Faculty of Basic Sciences, Azarbaijan Shahid Madani University, Tabriz, Iran*

[a] *E-mail: v.masoomy63@gmail.com*, [b] *E-mail: r.a.salamata@gmail.com*

Abstract*:* In This work, the thermodynamic properties of (NH_4SCN+BuOH+H_2O) system were experimentally studied by emf measurements at 25 ºC. Mean activity coefficients and Gibbs energies of transfer of NH_4SCN in mixed-solvent systems containing (0.05, 0.1, 0. 15 and 0.2) mass fractions (w) of BuOH in water were determined using the Pitzer ion-interaction model. The results of optimization by Pitzer model were meaningful.

Keywords: Activity Coefficients, Emf, Gibbs energies of transfer, Pitzer ion-interaction model.

I. INTRODUCTION

Ion–ion and ion–solvent interactions play an important role in the solution chemistry of solutes [1]. Investigation of activity coefficients prepares a good way to study ion-solvent interactions and solvation of the electrolytes and non-electrolytes solutes [2]. For example, Hernandez-Luis et al. obtained the activity coefficients of NaCl in ethanol + water and PEG 4000 + water mixtures [3-6]. Koh et al determined the activity coefficients of the alkali metal chlorides in methanol + water mixtures at 25 °C [7].

Lopes et al. investigated the activity coefficients of KCl or NaCl in ethanol + water mixtures [8,9]. Moreover, Deyhimi et al. measured the activity coefficient of NH_4Cl in some mixed solvents [10].

Butanol is considered as a potential biofuel (butanol fuel). Butanol at 85 percent strength can be used in cars designed for gasoline (petrol) without any change to the engine. Moreover, Butanol is used as a solvent for a wide variety of chemical and textile processes, in organic synthesis, and as a chemical intermediate. It is also used as a component of hydraulic and brake fluids.

We present herein the activity coefficients and standard transfer Gibbs energy for NH_4SCN at different Concentrations of BuOH + water mixtures from (0 to 0.20) mass fraction BuOH.

II. METHODS

The analytical grade NH_4SCN salt (mass percent fraction >99.5%) is obtained from merck. Butanol was analytical grade high purity (purity >99.5%, Fluka). Each time, prior to use, the NH_4SCN was dried under vacuum (110 ^{0}C) to constant weight and stored in desiccators. All primary stock solutions are prepared by weight using an electronic balance (Model Sartorius) with a resolution of 0.0001 mg. in this research, also Double-distilled deionized water was used. All measurements were performed in a double-walled glass container, and temperature of the work solution was kept constant at T = 298.2 K ± 0.1 K by employing a Model Julabo circulation water bath. Cell potentials were obtained with a PH/ISE meter (Model 781, with a resolution of 0.1 mV). In the present study, we have used a bi-ISE system formed by an electrochemical cell with an ammoniumion selective electrode (NH_4–ISE) versus a thiocyanate (solid state) ion selective electrode (SCN–ISE) as a reference electrode to determine the activity coefficients for NH_4SCN–alcohol (Butanol) systems in water at 298.15 K.Pitzer and modified Pitzer ion-interaction model has been used for correlating the data and some thermodynamic results were achieved.

III. RESULTS AND DISCUSSION

As shown in the figure (1) the Mean ionic activity coefficients values for NH_4SCN in (Butanol +water) were determined from the emf measurements of the following galvanic cells:

NH4-ISE | NH_4SCN(m), H_2O (1- wt%), Butanol (wt%)| SCN-ISE

Applying the Nernst equation, the following expression is obtained:

$$E = E^{0}* + S \log m\gamma_{\pm} \quad (1)$$

where E is the emf of cell, S is the theoretical Nernst slope and E0*is standard potential. An excellent linear relationship is obtained when E vs. log(mɣ±) is plotted. In order to obtain a good estimation of E^0*, one further equation was employed.

A typical slope (S) of the electrodes response obtained by a least-squares regression analysis is 117.88 mV, with a correlation coefficient of 0.9999. The experimental data thus

obtained were fitted to a virial expansion series similar to that suggested by Pitzer equation(1973).

A. Figures and Tables

Prior to having a more detail analysis of an aforementioned system the standard potential in the cell, E^{0*} for each mixture studied, must be determined.

Since this affects the accuracy of the activity coefficient and the other thermodynamic functions consequently could be calculated on this basis. Consequently, Gibbs free energy of transfer and solvation number could be evaluated using potential of standards. The pitzer ion-interaction model was used for the experimental thermodynamic properties for data correlation and calculation of the investigated systems.

Gibbs free energy of transfer is expressed as:

$$\Delta G^0 = -nF(E^0s - E^0w) \qquad (2)$$

Where E^0s stands for the standard potential in the mixed solvent and E^0w is the corresponding value in the pure water, other quantities have their usual significance [4].

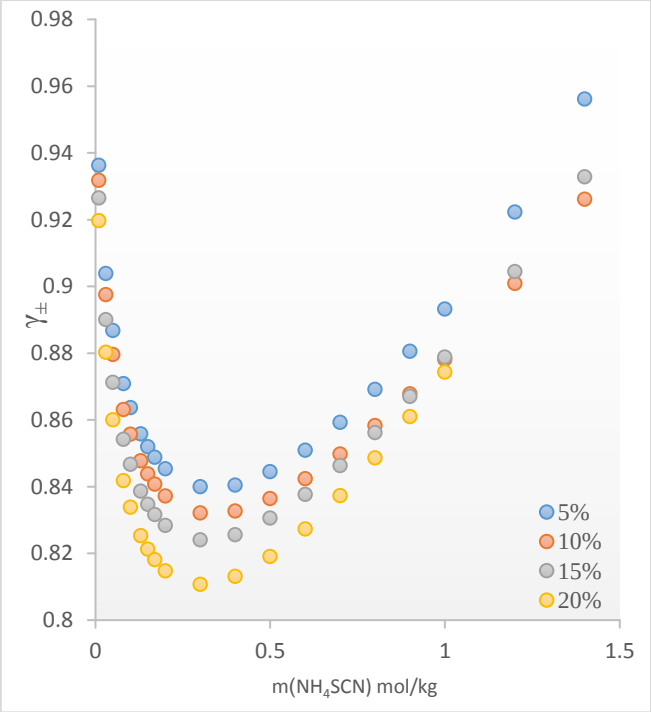

Fig.1: Activity coefficients versus molality of KBr in the ternary NH_4SCN+ Butanol + H_2O + Water at 298.15 K.

B. Equations

for 1:1 electrolyte, the pitzer equation [12] can be written as[2] :

$$\ln\gamma_{\pm} = F^{\gamma} + B^{\gamma}m + C^{\gamma}m2, \qquad (3a)$$

Where:

$$F^{\gamma} = -A^{\Phi}m^{1/2} / (1 + bm^{1/2}) + (2/b) \ln (1 + bm^{1/2}) \qquad (3b)$$

$$B^{\gamma} = 2\beta^0 + (2\beta^1 / \alpha^2m) \{1 - (1+ \alpha m^{1/2} - \alpha^2m / 2(\exp) \alpha m^{1/2})\} \qquad (3c)$$

In these equations α and b are assumed fixed parameters with values of 2.0 and 2.1, respectively; A^{Φ} is the Debye-Huckel constants for osmotic coefficient. β^0, β^1 and C^{γ} denote solute-specific interaction Pitzer parameters for the electrolyte solution so that their values were found by fitting with the experimental data. For the 10% mass fraction, the measured values of β^0, β^1 and C^{γ} were β^0 = 0.1152, β^1 = 0.1402 and C^{γ}=-0.00321 with an average standard deviation of ±0.23 mV.

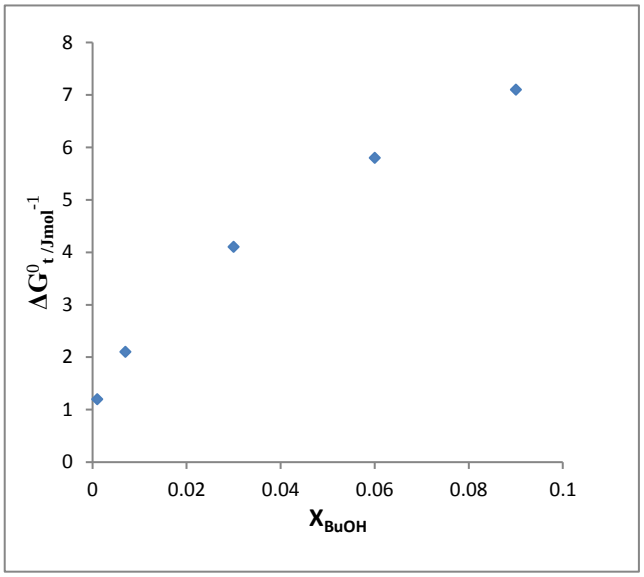

Fig .2: Variation of ΔG^0_t for the NH_4SCN as a function of mole fraction of alcohol in (Butanol + water) mixtures.

IV. CONCLUSION

The activity coefficients have descending trend and are quite similar to those concluded by Hernandez-Luis et al. and resembling the results by Zhuo et al. [5,11]. Modeling implemented by using, the Pitzer (P) equation.

A comparison of the results with similar systems of references shown that agreement is excellent Gibbs free energy of transfer and in addition ion-solvent interactions

were evaluated. The values of standard potentials decrease by increasing water weight percent in the mixed solvent and as illustrated in the figure (2) Gibbs energy of transfer has an increasing trend as mole fraction of Butanol increases.

REFERENCES

[1] R.G. Bales, Pure Appl. Chem, vol. 54, pp. 229, **1982**.
[2] J. P. Morel, and C. Lhermet, Can. J.Chem, vol. 63, pp. 263, **1985.**
[3] M. A. Esteso, O. M. Gonzalez-Diaz, F. Hernandez-Luis, and L. Fernandez-Merida, J. Solution Chem, vol. 18, pp. 277–288, **1989.**
[4] F. Herna´ndez-Luis, M. V. Va´zquez, and M. A. Esteso, Carbohydr. Res, vol. 338, pp. 1415–1424, **2003**.
[5] F. Herna´ndez-Luis, H. R.Galleguillos, L. Ferna´ndez-Me´rida, and O. Gonza´lez-Dı´az, Fluid Phase Equilib, vol. 275, pp. 116–126. **2009**.
[6] J. W. Morales, H. R, Galleguillos, M. E.Taboada, and F. Herna´ndez-Luis, Fluid Phase Equilib, vol. 281, pp.120–126. **2009.**
[7] D. S. P. Koh, K. H. Khoo, and C. Y. Chan, J. Solution Chem, vol. 14, pp. 635–651**, 1985**.
[8] A. Lopes, F.Farelo, and M. I. Ferra, J. Solution Chem, vol. 28 , pp. 117–131, **1999**.
[9] A. Lopes, F.Farelo, and M. I. Ferra, J. Solution Chem, vol. 30, pp. 757–770, **2001**.
[10] F. Deyhimi, B. Ghalami-Choobar, and R. Salamat Ahangari ,J. Mol. Liq, Vol, 116, **2005**.
[11] k. Zhuo, J. Wang, and H.Wang, Carbohydrate Research, vol. 325 pp. 46–55,**2000**.
[12] K. S. Pitzer, J. Phys. Chem, Vol. 77, pp. 268, **1973.**

Salting Effect of Amino Acids and Surfactants on the Clouding Behavior of Polypropylene Glycol in Aqueous Media

Nosaibah Ebrahimi*[a], *Rahmat Sadeghi*[b]

[a] *Department of Chemistry, University of Kurdistan, Sanandaj, Iran, Email: no.ebrahimi@gmail.com*

[b] *Department of Chemistry, University of Kurdistan, Sanandaj, Iran, Email: rsadeghi@uok.ac.ir*

Abstract*:* The clouding behavior of aqueous polypropylene glycol 725 (PPG725) solutions in the absence and presence of various anionic surfactants and amino acids were studied. It was found that, all of the investigated amino acids reduce the water-solubility of PPG725 and so induce a reduction in the cloud point temperatures (salting-out effect). However, anionic surfactants with long alkyl chain length induce the salting-in effect on the aqueous PPG725 solutions and increase the cloud point temperatures. The thermodynamic parameters of clouding process in the investigated systems were computed and it was found that entropy is the main motive force for clouding process in aqueous PPG solutions.

Keywords: Amino acids, Clouding process, PPG, Salting effects, Surfactants

I. INTRODUCTION

Thermo-regulated polymers, a class of intelligent water-soluble polymers, have gained significant attention due to their reversible conformational changes in response to small external stimuli [1]. Thermo-regulated polymers are able to act as simple models to imitate the water-solubility of proteins and other biopolymers. Hence, the research on the solution behavior of thermo-regulated polymers in aqueous media, and study the impact of different additives on their solutions is important [2]. Aqueous solutions containing thermo-regulated polymers become cloudy by elevating temperature to critical values known as cloud points. These systems have a great potential for cloud point extraction processes which provide more gentle nature and higher performance as compared with outdated techniques involving volatile organic solvents. Moreover, temperature responsiveness of these systems simplifies the recovery and reusability of PPG, thus making them cheap and suitable for designing large scale processes [3]. Additives affect the polymer cloud point temperatures (T_C), and both enhancement (salting-in effect) and reduction (salting-out effect) of T_C in the presence of them have been reported [4]. This paper reports the T_C values of binary polypropylene glycol of molecular weight 725 (PPG725) + water solutions. Then, the effect of several amino acids and surfactants as additives on the phase formation ability of PPG725 aqueous solutions was explored. The obtained results discuss in terms of salting effects occurring in these systems.

II. METHODS

Materials: PPG725 was obtained from Sigma-Aldrich. Proline ($C_5H_9NO_2$, purity > 99.0 w/w) was obtained from BDH. Sodium n-hexyl sulfonate (SHSu, C_6SO_3Na, purity > 99.0 % w/w), sodium n-dodecyl sulfonate (SDSu, $C_{12}SO_3Na$, purity > 99.0 % w/w), sodium n-octyl sulfate (SOS, C_8SO_4Na, purity > 98.0 % w/w), sodium n-dodecyl sulfate (SDS, $C_{12}SO_4Na$, purity > 98.0 % w/w), glycine ($C_2H_5NO_2$, purity > 99.7 % w/w), $_{S(+)}$-alanine ($C_3H_7NO_2$, purity > 99 % w/w), $_L$-serine ($C_3H_7NO_3$, purity > 99 % w/w) and $_{S(+)}$-isoleucine ($C_6H_{13}NO_2$, purity > 99 % w/w) were obtained from Merck. Double distilled water, with a specific conductivity of 1.2 $\mu S \cdot cm^{-1}$ at 25 $^\circ$C, was used.

Methods: Solutions were prepared by mass with the use of a Sartorius CP124S balance precisely within ± 1.10^{-7} kg. A double-shell glassy cell was used as solution container in the cloud point measurements. The Julabo thermostat with a precision of ±0.1 K was used to circulate water at a certain temperature around solutions. The visual detection method [4] was used to determine cloud point temperatures (T_C) of PPG725 in water, and in aqueous solutions of amino acids and surfactants.

III. RESULTS AND DISCUSSION

In an attempt to study the salting-in or salting-out effects of amino acids and surfactants on the aqueous PPG725 solutions, cloud point diagrams (liquid-liquid demixing temperature as a function of polymer mass fraction) were determined for: (i) PPG725 in pure water; (ii) PPG725 in aqueous solutions of 0.2 $mol.kg^{-1}$ of amino acids including alanine, glycine, serine, proline, and isoleucine; and (iii) PPG725 in aqueous solutions of anionic surfactants including SOS (0.011 $mol.kg^{-1}$), SDS (0.002, 0.005, 0.008 and 0.011 $mol.kg^{-1}$), SHSu (0.011 $mol.kg^{-1}$) and SDSu (0.011 $mol.kg^{-1}$). The obtained results are presented in Fig. 1. It can be seen from Fig. 1a that the values of cloud point temperature decrease by increasing PPG725 mass fraction (w_p), and at each w_p follow the order: water > isoleucine ≈ proline > alanine > serine ≈ glycine. An increase

in the hydrophilic nature of amino acids reduces the temperature at which phase separation takes place. In other words, the more hydrophilic amino acids obviously induce the dehydration of PPG polyether groups at lower temperatures. Fig. 1b shows that for the same molality (0.011 mol.kg^{-1}) of the anionic surfactants, the values of cloud point temperature follow the order: $C_{12}SO_4Na$ (SDS) > $C_{12}SO_3Na$ (SDSu) > water > C_6SO_3Na (SHSu) > C_8SO_4Na (SOS). This result shows that anionic surfactants with long alkyl chain length (SDS and SDSu) act as salting-in inducer agents and thus increase the values of T_C. However, anionic surfactants with short alkyl chain length (SOS and SHSu) play the role of salting-out inducer and decrease the values of T_C. In fact, the complex behavior of salting effects produced by the addition of surface-active ions to aqueous PPG solutions originates from a delicate balance between hydrophobic and hydrophilic nature of ions. The longer chain length surface-active ions provide stronger van der Waals interactions with PPG and charge the polyether chains more simply than shorter chain length ones. Therefore, it is reasonable that SDS and SDSu are able to increase the water-solubility of PPG and thus increase its cloud point temperature.

It should be noted that the values of critical micelle concentration of SOS, SDS, SHSu and SDSu in pure water at 298.15 K are 0.134, 0.0083, 0.571 and 0.011 mol.kg^{-1}, respectively. Therefore, the molality engaged for anionic surfactants (aqueous solutions of 0.011 mol.kg^{-1}) is much smaller than critical micelle concentrations of SOS and SHSu. Hence, it can be concluded that SOS and SHSu don't favorably interact with the polymer chain when they are in their monomeric state. The salting-in ability of SDS on the PPG725 aqueous solutions is higher than that of SDSu, which is in agreement with our previous results [5] obtained from conductance, volumetric and compressibility measurements indicating stronger SDS-polymer interactions than SDSu-polymer interactions. Fig. 1b also shows that the salting-in strength of SDS on the aqueous polymer solution intensifies by increasing surfactant concentration.

The energetic thermodynamic functions of clouding process in the investigated systems have been calculated by the following equations:

$$\Delta G_{m,C} = RT_C \ln X_p \qquad (1)$$

$$\mathrm{d}\left(\frac{\Delta G_{m,C}}{T_C}\right) / \mathrm{d}\left(\frac{1}{T_C}\right) = \Delta H_{m,C} \qquad (2)$$

$$\Delta S_{m,C} = (\Delta H_{m,C} - \Delta G_{m,C}) / T_C \qquad (3)$$

where X_p is the mole fraction of PPG at T_C. The obtained results showed that the clouding process in the binary and all the ternary PPG725 aqueous solutions is endothermic ($\Delta H_{m,C} \rangle 0$), but because of entropy increase ($\Delta S_{m,C} \rangle 0$), the phase separation takes place spontaneously ($\Delta G_{m,C} \langle 0$). The values of $\Delta G_{m,C}$ for ternary PPG725 + SDS / SDSu + water systems are less negative than those values for binary PPG725 + water system. It is due to the salting-in effect of SDS and SDSu on the aqueous polymer solution. However, phase separation in PPG725 + amino acids / SOS / SHSu + water

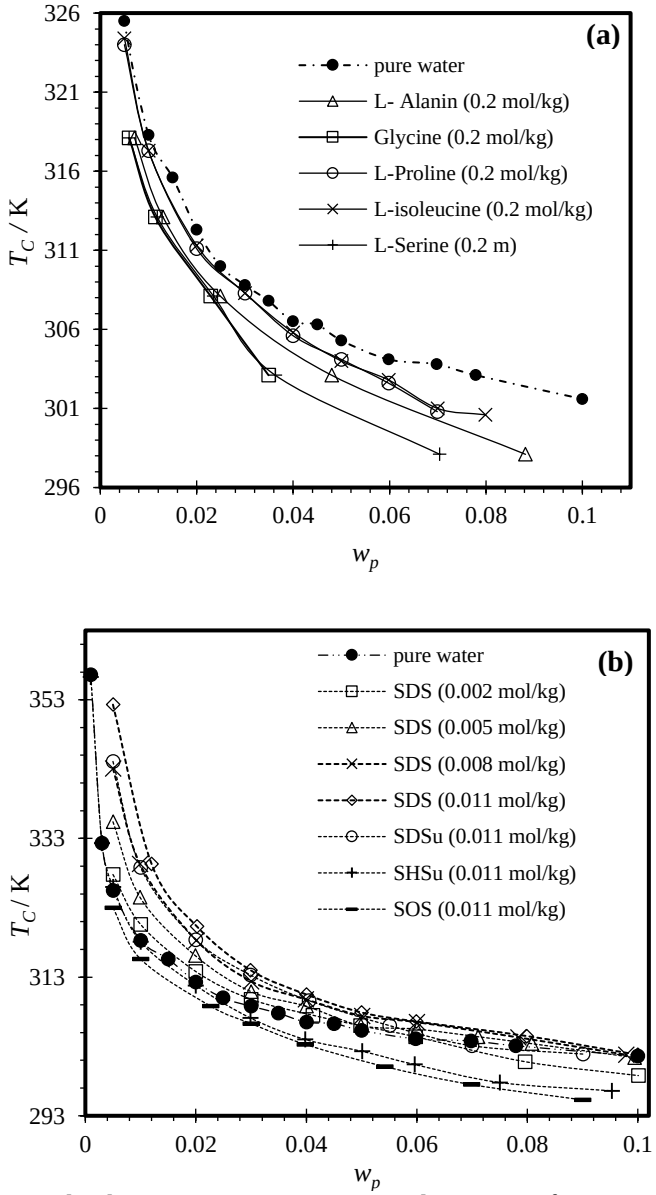

Fig. 1: cloud point temperature against polymer mass fraction for PPG725 in pure water and in the aqueous solutions of amino acids (a) and anionic surfactants (b).

systems is more spontaneous than that in pure water resulting from the salting-out phenomenon occurring in these systems.

IV. CONCLUSION

Salting effects of different amino acids and anionic surfactants on the PPG aqueous solution were investigated by visual observation of cloud points. The T_C values of PPG725 aqueous solutions decrease by the addition of amino acids or small amounts of anionic surfactants with short hydrocarbon proportion (salting-out effect). However, anionic surfactants with long alkyl chain length leads to an increase in T_C (salting-in effect). The calculated values of Gibbs free energy, enthalpy and entropy of clouding process revealed that entropy is the main motive force for spontaneous liquid-liquid demixing in both polymer-amino acid and polymer-surfactant aqueous solutions.

REFERENCES

[1] I.Y. Galaev, and B. Mattiasson, Trends Biotechnol. vol. 17, pp. 335–340., **1999**
[2] R. Umapathi, P.M. Reddy, A. Rani, and P. Venkatesu, Phys. Chem. Chem. Phys. vol. 20, pp. 9717–9744, **2018**.
[3] Z. Li, X. Liu, Y. Pei, J. Wang, and M. He, Green Chem. Vol. 14, pp. 2941-2950, **2012**.
[4] N. Ebrahimi, B. Farahbod, and R. Sadeghi, J. Chem. Thermodyn., vol. 123, pp. 86-98, **2018**.
[5] R. Sadeghi, and S. Shahabi, J. Chem. Thermodyn., vol. 43, pp. 1361-1370, **2011**.

Determination of Kamlet-Abboud-Taft solvatochromic parameters in some green solvent mixtures

Fatemeh Pasham*, Morteza Jabbari
School of Chemistry, University of Damghan, Damghan, Iran
Email: m_jabari@du.ac.ir

Abstract: The solvatochromism is a simple and suitable method to study solvent-solute interactions (special and nonspecial interactions). Structural and intermolecular interactions of solvatochromic indicators Reichardt's dye (RD), 4-nitroaniline (PNA) and *N*,*N*-Dimethyl-4-nitroanilin (DMNA) were investigated in the green solvent mixtures of *N*-Formylmorpholin with water, ethanol, 1-propanol and 2-propanol. The solvatochromic parameters (α, hydrogen -bond donor acidity; β, hydrogen-bond acceptor basicity; π^*, dipolarity/polarizability; $E_T(30)$, Reichardt's polarity parameter) were determined in these mixtures at 298 K using UV/Vis spectrophotometric method. Finally, the variation of Kamlet-Abboud-Taft (KAT) parameters of the solvatocoromic dyes by changing the solvent percentage are discussed.

Keywords: UV/Vis spectroscopy, Solvatochromism, Kamlet-Abboud-Taft's parameters, Green solvent mixture.

I. INTRODUCTION

The use of UV/Vis spectrophotometry for the characterization of pure solvents through solvatochromic indicators has been widely performed over the last decades, but fewer studies involved two solvents and even fewer addressed three or more component solutions. The intricacy of solvent/solvent interactions increases considerably with the number of components in the mixture. Although several models have been developed and used to address mixed solvents, most of them encompass only two components or, at the most, to be able to deal with three components.

Solvatochromic indicators which their spectroscopic behavior is strongly affected by solvents, allow on the involved specific and nonspecific molecular interactions. These indicators on the determination of different polarity parameters such as the Kamlet-Abboud-Taft (KAT) solvatochromic parameters and Reichardt's polarity parameter, via the measurement of the wavenumbers of one or more indicators, which enables a accurated understanding of indicator/solvent/solvent interactions [1]. The KAT solvatochromic parameters are α, β and π^*, which quantify hydrogen-bond donating ability (acidity), hydrogen bond accepting ability (basicity) and polarity/polarizability, respectively. Together these three parameters, Reichardt's polarity parameter, $E_T(30)$, can be used to predict a wide range of observables such as rate constants, equilibrium constants, solubilities and spectral frequencies, based upon data acquired with only a few solvents. $E_T(30)$ is a measure of both polarity and acidity together, but is not dependent on polarizability [2].

II. METHODS

The pure solvents *N*-Formylmorpholin, ethanol, 1-propanol and 2-propanol were obtained as spectral grade (≥99.5%) from Merck. Reichardt's betaine dye (RD, purity ≥ 90%), 4-nitroaniline (PNA, purity ≥ 99%), and *N*,*N*-dimethyl 4-nitroaniline (DMPNA, purity ≥ 98%) were obtained from Sigma–Aldrich. The spectrophotometric measurements were done at 298 K.

Briefly, first a 5.0 mL of the stock solution of each indicator was prepared in acetone with concentration 1×10^{-2} mol dm^{-3} and then about 30 µL (for 4-nitroaniline and *N*,*N*-dimethyl-4 nitroaniline) and 300 µL (for Reichard's dye) of the stock solution were transferred to 10 mL glass volumetric tubes. After evaporation of the solvent under reduced pressure, 8.0 mL of the pure solvents under study was pipetted into the tubes. For each binary system, a 2 mL solution of the dye prepared in solvent 1 (solution A) and placed in a cuvette were then weighed (the weight of empty cuvette has been previously measured). After recording the electronic absorption spectrum (over the wavelength range of 300–700 nm), a 0.2 mL solution of the same dye prepared in solvent 2 (solution B) was added, the cuvette weighed and the spectrum of the new solution was recorded. The procedure was repeated after adding further volumes of solution B until the final cuvette volume reached 3.5 mL. Subsequent sets of experiments were performed starting with solution B and adding volumes of solution A or starting with selected solution A/solution B mixtures and adding volumes of one or the other solution. The different sets of solvent mixtures were overlapped in composition to ensure concordance of the results. Finally, the wavelength of the maximum absorbance, λ_{max}, of each sample was recorded for subsequent calculations. At least three independent measurements were performed for each indicator starting from the solution preparation

III. RESULTS AND DISCUSSION

The spectral changes of solvatochromic indicators PNA, DMNA, and RD were investigated in some green solvent binary mixtures to obtain KAT solvatochromic parameters together $E_T(30)$.

A. *Figures and Tables*

Figures 1-3 show the spectral changes of 4-nitroaniline, *N*,*N*-Dimethyl-4-nitroanilin, and Reichardt's dye, respectively, in the mixture of *N*-Formylmorpholin with water. The wavenumber maxima, $\bar{\upsilon}$, of three solvatochromic indicators in mixtures were determined for obtaining the solvatochromic parameters.

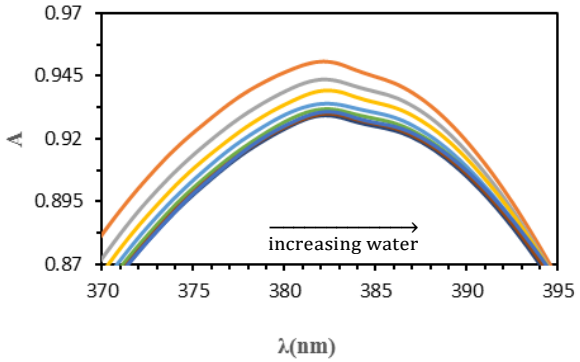

Fig. 1: The spectral changes of 4-nitroanilin in the mixture of *N*-Formylmorpholin with water. $[PNA]_0 = 5 \times 10^{-5}$ mol dm^{-3}. T=25°C.

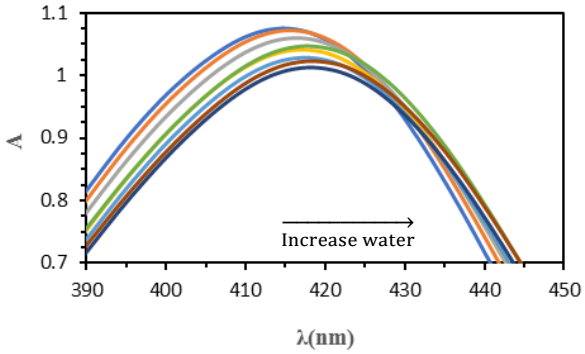

Fig. 2: The spectral changes of *N*,*N*-Dimethyl-4-nitroanilin in the mixture of *N*-Formylmorpholin with water. $[\mathbf{DMPNA}]_0 = 5.6 \times 10^{-5}$ mol dm^{-3} . T=25°C.

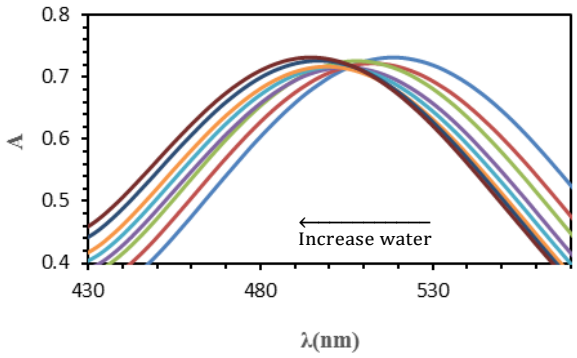

Fig. 3: The spectral changes of Reichardt's dye in the mixture of *N*-Formylmorpholin with water. $[RD]_0 = 2.8 \times 10^{-4}$ mol dm^{-3}. T=25°C.

B. *Equations*

Reichardt's parameter, $E_T(30)$, well-known as solvent polarity scale, was determined from the wavenumber maxima of RD, $\bar{\upsilon}_{RD}$, using Eq. (1) [3]:

$$E_T(30) = 28591 \times \bar{\upsilon}_{RD} \quad (1)$$

The KAT parameters are calculated from equations (2, 3 and 4) [4,5]:

$$\pi^* = \frac{28.18 - \bar{\upsilon}_{DMPNA}}{3.52} \quad (2)$$

$$\beta = \frac{0.9841 \times \bar{\upsilon}_{PNA} + 3.49 - \bar{\upsilon}_{DMPNA}}{2.759} \quad (3)$$

$$\alpha = \frac{E_T(30) - 14.60\pi^* - 30.30}{16.50} \quad (4)$$

where $\bar{\upsilon}_{DMPNA}$ and $\bar{\upsilon}_{PNA}$ are wavenumber maxima of N,N-Dimethyl-4-nitroanilin and 4-nitroaniline, respectively.

The determined values for $E_T(30)$, π^*, α and β are presented as a function of mixture composition in Table 1.

Table 1: The maximum wavelength of DMPNA, PNA and RD together with the polarity parameter $E_T(30)$, and Kamlet-Abboud-Taft (KAT) parameters α, β and π^* in the mixtures of *N*-Formylmorpholin (NFM) and ethanol at 298 K.

x_{NFM}	$x_{ethanol}$	λ_{DMPNA}	λ_{PNA}	λ_{RD}	$E_{T(30)}$	π^*	α	β
1.00	0.00	400.1	377.4	640.7	44.63	0.91	0.58	0.07
0.90	0.10	399.3	376.7	612.5	46.68	0.89	0.58	0.20
0.80	0.20	398.6	376.0	596.3	47.95	0.88	0.57	0.29
0.70	0.30	397.7	375.3	586.0	48.79	0.86	0.58	0.36
0.60	0.40	397.1	374.8	576.6	49.59	0.85	0.58	0.41
0.50	0.50	395.8	374.3	568.6	50.28	0.83	0.59	0.48
0.40	0.60	394.7	373.9	564.4	50.66	0.81	0.61	0.52
0.30	0.70	394.1	373.4	560.2	51.04	0.80	0.61	0.55
0.20	0.80	392.8	372.8	556.2	51.41	0.77	0.62	0.59
0.10	0.90	390.7	372.0	552.7	51.73	0.73	0.65	0.65
0.05	0.95	388.8	371.5	552.3	51.77	0.70	0.68	0.68
0.00	1.00	386.9	371.0	552.6	51.74	0.66	0.71	0.71

IV. CONCLUSION

From the solvatochromism behavior of three indicators, the empirical solvent parameters α, β, π^* and $E_T(30)$ were determined for the mixtures of *N*-Formylmorpholin with ethanol, 1-propanol, 2-propanol and water. For the first three parameters, the values increase as alcohols and water are added to *N*-Formylmorpholin. The value π^* for the mixtures decreases with increasing mole fraction of alcohols and water, while values of $E_T(30)$, α, β increase as alcohols are added to *N*-Formylmorpholin. Synergistic effects were observed for all binary mixtures in the solvation shell of RD in alcohol-rich regions, indicating that pure solvents make complexes more polar than themselves. Synergism is heightened more with higher chain length and branching in alcohols that is concomitant with the decrease in α values of alcohols and the $E_T(30)$ difference in the pure solvents.

REFERENCES

[1] Nunes, N., Elvas-Leitão, R., Martins, F. UV–Vis spectroscopic study of preferential solvation and intermolecular interactions in methanol/1-propanol/acetonitrile by means of solvatochromic probes. Spectrochimica Acta Part A: Molecular and Biomolecular Spectroscopy, vol. 124, pp. 470-479, **2014.**

[2] Jessop, P. G., Jessop, D. A., Fu, D., Phan, L. Solvatochromic parameters for solvents of interest in green chemistry. Green Chemistry, vol. 14, pp. 1245-1259, **2012**.

[3] Reichardt, C. Solvatochromic dyes as solvent polarity indicators. Chemical Reviews, vol.94, pp.2319-2358, **1994**.

[4] Marcus, Y.: The properties of organic liquids that are relevant to their use as solvating solvents. Chemical Society Reviews. vol.21, pp. 409–416, **1993**.

[5] Helburn, R., Bartoli, M., Pohaku, K., Maxka, J., Compton, D., Creedon, B., Stimpson, C.: Solvatochromic properties of long alkyl chain π* indicators: comparison of N, N-dialkyl-4-nitroanilines and alkyl 4-nitrophenyl ethers. Journal of Physical Organic Chemistry. vol.20, pp.321–331**, 2007**.

Study on the protonation equilibria of drug naproxen in different surfactant media

Yeganeh Nachari*, Morteza Jabbari
School of Chemistry, University of Damghan, Damghan, Iran
** Email: m_jabari@du.ac.ir*

Abstract: Naproxen is a drug with very low solubility in aqueous solution. In the present work, the acid-base equilibria for this drug was studied pH-potentiometrically in ethanol-water mixtures (25% v/v) at constant ionic strength of 0.15 mol dm^{-3} NaCl and the temperature of 25°C. The potentiometeric measurements were carried out in presence of three micelle-forming surfactants with different concentrations, namely sodium dodecylsulfate (anionic SDS), dodecyltrimethylammonium bromide (cationic DTAB) and polyethylene glycol dodecyl ether (non-ionic Brij 35). The results obtained indicate that, irrespective of the surfactant type, the protonation constant of the drug naproxen decreases with increasing concentrations of the surfactants.

Keywords: *Protonation equilibria, Naproxen, surfactant effect, Potentiometery*

I. INTRODUCTION

Naproxen ($C_{14}H_{14}O_3$) is an anti-inflammatory and non-steroidal drug that is chemically called (S) -6-methoxy-R-methyl-2-naphtaleneacetic acid. The drug naproxen is practically insoluble in water (0.025 mg/mL at 25 °C). Therefore, the expansion of a drug delivery system allowing the controlled release of naproxen would be useful, especially in high-dose-dependent treatments, including chronic diseases such as rheumatoid arthritis [1].

It is well known that micelle-forming surfactants have a very important application in pharmaceutical science, especially in the aqueous solubility and delivery of the drugs in medicine [2]. There are few reports about protonation process of the drug in micellar media. The core-corona structure of a micelle is very important for solubilizing insoluble water species [1].

The protonation constant is one of the physico-chemical parameters that plays an important role in recognizing the ionic behavior of many biological compounds. Thus, a precise knowledge about this property and its determination is of interest in a large range of research fields as well as pharmacy sciences that helps understanding the mechanism of drug function in several processes. Most of drugs have acidic or basic functionalities in their molecular structures and hence include one or more protonation step(s). This causes in an extensive pH range, different type of a drug may exist in the solution, including cationic, neutral or anionic forms [3].

In this research, the protonation of naproxen in was investigated using potentiometric method at different concentrations above the critical micelle concentration (CMC) of SDS, DTAB and Brij 35. Since naproxen is a water-insoluble drug, all the experiments were done in aqueous solution of 25% (v/v) ethanol. The micellar effects (base on structure and concentration of the surfactants) on the acid-base constants of naproxen were discussed.

II. METHODS

The pure solvent ethanol was obtained as spectral grade (≥99.5%) from Merck. Titrasol HCl and NaOH solutions, NaCl (purity ≥ 99.5%), Sodium dodecyl sulphate (SDS, purity ≥ 99%), Dodecyltrimethyl-ammonium bromide (DTAB, purity ≥ 99%) and Polyoxyethylene glycol dodecyl ether (Brij 35, purity ≥ 98%) were obtained from Sigma. The drug naproxen (purity ≥ 99.9%) was obtained from Damavand Darou Co. (Iran).

The potentiometric measurements were done using a Metrohm model 827 pH lab meter, equipped with a combined glass-pH electrode. The electrode response in terms of the potential can be read with a precision typically of the order of ±0.1mV.

The potentiometric measurements to evaluate the pH (-log $[H^+]$) of the solution were carried out in different concentrations of the surfactants SDS, DTAB and Brij 35 at an ionic strength 0.15 mol dm^{-3} of NaCl. During all the acid-base titrations the temperature was kept at 25°C using a constant-temperature thermostat.

Before the beginning of each titration, the glass electrode was calibrated in the ethanol–water mixture (25% v/v) in each of micellar solutions according to the Gran's method [4]. For this purpose, a known volume of an acidic solution (0.10 mol dm^{-3} HCl) was placed in a double-wall glass vessel. The electrode was immersed in the acidic solution and then the solution was titrated with a strong base (0.20 mol dm^{-3} NaOH). In general, 10 or 15 additions of NaOH solution were enough to determine calibration constants accurately.

In the next step, to obtain protonation constants, a suitable volume of naproxen solution was added to the pre-titrated background solution. By continuing the titration, from the recorded potential values and volume added of NaOH

solution, the protonation constants were evaluated. All experiments including the glass electrode calibration and the potentiometric titrations were repeated at least three times.

III. RESULTS AND DISCUSSION

The protonation constant values of naproxen were evaluated by titration of micellar naproxen solutions using NaOH solution as titrant. The drug naproxen was entirely protonated at the starting of the titration by adding a known value of HCl. If H_nL denotes the fully protonated form of naproxen (where L is neutral naproxen), the protonation equilibria studied were represented with the following equation:

$$H_nL \rightleftharpoons H_{n-1}L^- + H^+ \quad (1)$$

Based on Eq. (1), the protonation constants (K_n) are defined by

$$K_n=[H_{n-1}L^-][H^+]/[H_nL] \quad (2)$$

The typical potentiometric titration curves (a plot of pH or E against V) for naproxen in the concentration 15 mM of SDS is shown in Fig. 1. Using a suitable computer program the potentiometry data were processed for estimating the protonation constants of naproxen in water and in different aqueous solutions of the micelles under study.

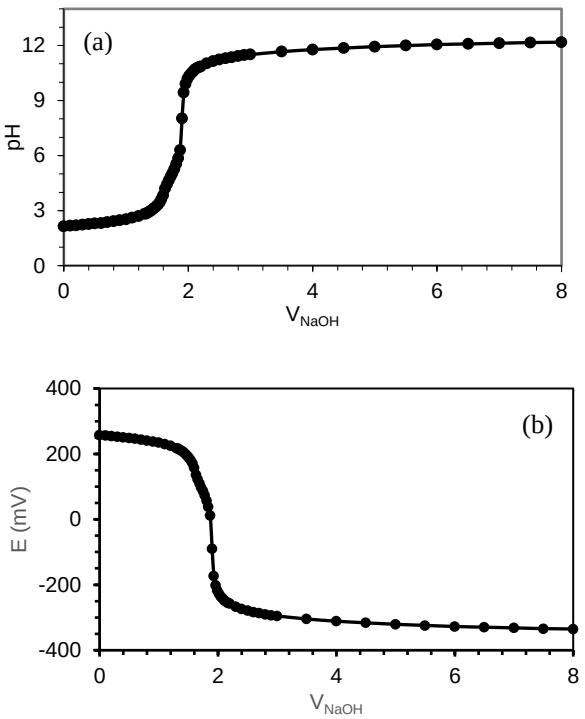

Fig. 1: The typical potentiometric titration curves for naproxen in the concentration 15 mM of SDS at 25 °C.

The experimental values of protonation constant for the drug naproxen in ethanol aqueous and micellar aqueous solutions of SDS, DTAB, Brij 35 are listed in Table 1.

Table1: Experimental values of protonation constant for the drug naproxen in ethanol aqueous and micellar aqueous solutions of SDS, DTAB and Brij 35 at the temperature 25°C.

Micelle free medium		p*K*=5.654			
Micellar media					
[SDS] (mM)	p*K*	[DTAB] (mM)	p*K*	[Brij 35] (mM)	p*K*
12	5.372	18	5.346	0.15	5.228
15	5.367	20	5.211	0.3	5.148
18	5.349	22	5.105	0.5	5.074

From Table 1 it can be observed that the protonation constant for the drug in all micellar media under study is less than that in free micelle medium. Moreover, regardless of the surfactant type, the protonation constants for the drug naproxen in the aqueous micellar media of SDS, DTAB and Brij 35, decrease by the increasing concentration of micelle-forming surfactants. This probably is related to the possible interactions between the dissociated drug naproxen and the micelle systems as electrostatic and hydrophobic interactions and hydrogen bonding. The naproxen in anionic SDS medium has the highest protonation constant due to electrostatic repulsions of the drug and the negative charge of surfactant head group, whereas the cationic DTAB and non-ionic Brij 35 media provided lower protonation constant. This is maybe due to the different extent of interactions of the drug with the surfactant systems.

IV. CONCLUSION

In this work, we study the protonation process of the drug naproxen as an organic acid with ionizable carboxylic group, in micellar medium by using potentiometric titration. The p*K* values obtained experimentally in various concentrations of SDS, DTAB and Brij 35 were related to the possible interactions of the dissociated drug naproxen with the micelle systems under study.

REFERENCES

[1] P. A. Baht, G. M. Rather, A. A. Dar, Effect of surfactant mixing on partitioning of model hydrophobic drug,

naproxen, between aqueous and micellar phases. The Journal of Physical Chemistry, 113, 997-1006, **2009**.

[2] S. D. Bhattamishra, R. K. Padhy, Estimation of Ibuprofen solubilization in cationic and anionic surfactant media: Application of micelle binding model, Indian Journal Chem. Technol, 16, 426-430, **2009**.

[3] H. Chahiyan Boroujeni, F, Gharib, Thermodynamic investigation on acid-base equilibria of deferiprone and deferasirox at different ionic strengths and various temperatures. Journal of Chemical Thermodynamics, 103, 366-373, **2016**.

[4] M. Jabbari, Solvent dependence of protonation equilibria for gallic acid in water and different acetonitrile–water cosolvent systems, Journal of Molecular Liquids, 208, 5-10, **2015**.

Densities and derived thermodynamic properties study for the binary mixtures of (Ethyl methyl ketone, N,N-Dimethylbenzylamine) at different temperature

Maryam Kebriaei Amjad, Hossein Iloukhani, and Khatereh Khanlarzadeh

Department of Chemistry, Faculty of Chemistry, Bu-Ali Sina University, Hamedan, Iran:
Email:Maryam_k_amjad10@yahoo.com

Abstract*:* In this study, the density and refractive index of binary system including ethylmethylketone, *N, N*-dimethylbenzylamine in *T*= (298.15 – 318.15) K was investigated. Using these values, the thermodynamic properties such as excess molar volume,V_m^E, partial expansion molecular volume, $\bar{V}_{m,i}^E$excess expansion coefficient, α^E, isothermal coefficient of pressure excess molar enthalpy, $(\partial H^E_m / \partial P)_{x.T}$ and refractive index deviation, Δn_D ,are also calculated. The excess molar volume and refractive index deviation of the binary mixtures were correlated with the Redilich-Kister equation. The excess molar volume of this system { *N, N*-dimethylbenzylamine, and ethylmethylketone } have a negative deviation of the ideal state. This trend for the refractive index deviation of the system, *N, N*-dimethylbenzylamine and ethylmethylketone , is negative and deviates with increasing temperature. but with increasing the temperature, these values in all of the molar fractions finds a positive deviation. Also, four experimental quantitative equations were used to calculate the deviation of the refractive index of binary systems using the refractive index of pure compounds.

Keywords: Excess molar volume,binary mixturedensity, Refractive index deviation, Redlich-Kister,

I. INTRODUCTION

In the present work, densities, ρ, for binary mixture of (Ethyl methyl ketone) + 2N,NDimethylbenzylamine) have been measured at atmospheric pressure and in the entire composition range. These quantities have been used to calculate excess molar volumes, . The obtained correlations were used to calculate the other thermodynamic functions such as thermal expansion coefficient, α, and its excess value, αE, and isothermal coefficient of excess molar enthalpy (∂ /∂P)T,x,refractive index deviation, Δn_D,. These excess and deviation quantities have then been fitted to the Redlich–Kister equation [1].

II. METHODS

The densities of the pure components and their binary mixture were measured with an Anton Paar DMA 4500 Oscillating U-tube densitometer, the temperature in the cell was regulated to ±0.01K with a solid state thermostat Each mixture was immediately used, after it was mixed by shaking. All the weightings were performed on an electronic digital balance (AB 204-N Mettler) accurate to ±0.1 mg. The uncertainty in the mole fraction is estimated to be lower than ±1×10−4 [2]. The excess molar volumes for the binary mixtures were calculated from the measured densities using the following equation, where Mi and ρi are the molar mass and density of pure component, respectively, and ρ is the density of the binary mixture. Results of such calculations for excess molar volumes are listed in Fig.1 illustrate these results, graphical from Redlich- Kister correlation.

III. RESULTS AND DISCUSSION

Results of such calculations were used for interpreting intermolecular interactions that exist between molecules of the binary mixture, qualitatively. Results of these calculations were used for interpreting intermolecular interactions that exist between molecules of the binary mixture [3]. The increase in the magnitude of the positive values with increasing temperature can be attributed to the decreasing importance of hydrogen bonding with increasing temperature. If interactions between unlike molecules are stronger than those exist between like molecules, as a consequence negative will be observed

Table 1.

x	ρ	V_m^E	$\bar{V}_1^E$	$\bar{V}_2^E$	$^E\alpha 10^3$	$(\partial H^E_m/\partial P)_{T,x}$
	g. cm^{-3}	cm^3. mol^{-1}	cm^3. mol^{-1}	cm^3. mol^{-1}	(K^{-1})	J. MPa^{-1}. mol^{-1}
x Ethyl methyl ketone + $(1-x)$ *N*,*N*-dimethylbenzylamine						
			T = 298. 15 K			
0	0. 89699		-1. 695	0		
0. 0710	0. 89342	-0. 111	-1. 285	-0. 021	0. 012	-0. 556
0. 1780	0. 88716	-0. 208	-0. 857	-0. 067	-0. 390	0. 563
0. 3197	0. 87759	-0. 290	-0. 538	-0. 173	-0. 416	0. 009
0. 4503	0. 86728	-0. 324	-0. 359	-0. 295	-0. 593	0. 310
0. 5585	0. 85742	-0. 317	-0. 240	-0. 415	-0. 774	0. 807
0. 6512	0. 84782	-0. 283	-0. 147	-0. 538	-0. 778	0. 805
0. 7368	0. 83804	-0. 247	-0. 088	-0. 692	-0. 598	0. 336
0. 8099	0. 82870	-0. 191	-0. 041	-0. 831	-0. 527	0. 331
0. 8819	0. 81866	-0. 133	-0. 018	-0. 990	-0. 417	0. 331
0. 9439	0. 80914	-0. 069	-0. 006	-1. 125	-0. 210	0. 122
1	0. 79978		0	-1. 235		

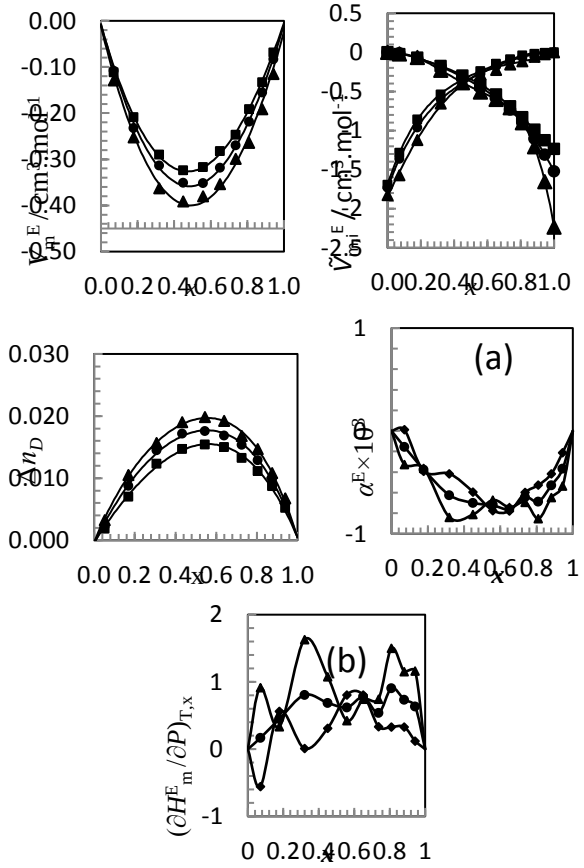

Figs. excess molar volume,V_m^E, partial expansion molecular volume, $\bar{V}^E_{m,i}$excess expansion coefficient, α^E, isothermal coefficient of pressure excess molar enthalpy, $(\partial H^E_m/\partial P)_{x,T}$ and refractive index deviation, Δn_D of binary mixture of a){x1 Ethyl methyl+ x2 N,NDimethylbenzylamine}, at different temperatures. Lines from Redlich- Kister correlation

$$Y^E = x_1(1-x_1)\sum_{i=0}^{p} A_k(2x_1-1)^k \quad (1)$$

$$A_i = \sum_{j=0}^{q} B_{ij}T^j$$

IV. CONCLUTION

The excess molar volumes of both binary mixtures are negative within the entire composition range and become more negative with increasing temperature from (298.15 to 318.15) K. The increase in the magnitude of the values with increasing temperature can be attributed to the decreasing importance of hydrogen bonding with increasing it, Other factors that affect the volume are molecular shap and size of components in the mixture the addition of ketones causes the rupture of intramolecular and intermplecular hydrogen bonding in amin and this will be followed by association of unlike molecules through intermolecular hydrogen bonding .A negative value of V_m^E and α^E indicates strong interaction between the components of the mixtures while their positive values are indicative of weaker intraction . when the strength of intraction between the unlike molecules increases, V_m^E and α^E become increasingly negative.

REFERENCES

[1] O. Redlich, A.T. Kister, Ind. Eng. Chem, 1948, 40, 345
[2] H. Iloukhani, K. Khanlarzadeh, Thermochim. Acta, 2010, 502, 77
[3] G. P. Dubey, K. Kumar, Thermochim. Acta, 2011, 524, 7
[4] F. Kermanpour, H. Z. Niakan, J. Chem. Thermodynamics, 2012, 54, 10
[5]A. Heintz, J. Chem. Thermodynamics, 2005, 37, 525

Solid-Liquid and Vapor-Liquid Equilibria Measurements for the Aqueous Ionic Liquid/Carbohydrate Systems

Bahman Jamehbozorg*[a], *Rahmat Sadeghi*[b]

[a] *Department of Chemistry, University of Kurdistan, Sanandaj, Iran, bahman_jame@yahoo.com*

[b] *Department of Chemistry, University of Kurdistan, Sanandaj, Iran, rsadeghi@uok.ac.ir*

Abstract*:* In order to study the soluting-effect of imidazolium-based ionic liquids (ILs) on sugar in aqueous systems, systematic experiments on the solid-liquid equilibria (SLE) and vapor-liquid equilibria (VLE) of ternary IL + sugar + water systems were carried out at different temperatures. The ILs 1-butyl-3-methylimidazolium hydrogen sulfate ([Bmim][HSO_4]) and 1-butyl-3- methylimidazolium bromide ([Bmim][Br]) and carbohydrates including L-(+)-arabinose, D-(+)-xylose, D-(+)-glucose, D-(-)-fructose, maltose, sucrose, and maltitol were selected. The negative departures of the constant water activity lines from the semi-ideal behavior for [Bmim][Br]/sugar systems were somewhat smaller than [Bmim][HSO_4]/sugar systems. The order of these departures was agreement with the obtained soluting-out coefficients, k_s, from the solid-liquid equilibria experiments.

Keywords: Carbohydrate, Ionic liquid, Isopiestic, Solubility, Solute effect

I. INTRODUCTION

Recently, ILs gained attention for their wonderful natures such as very low vapor pressures, nonflammability, and good thermal and electrochemical steadiness. But, as far as we know there is very limit experimental data about the ternary aqueous sugar-ionic liquid solutions in the literature [1,2].

II. METHODS

Materials. All sugars and NaCl, were obtained from Merck. Maltitol and [Bmim][HSO_4] were purchased from Alfa Aesar and IoLiTec, respectively. [Bmim][Br] was synthesized and purified based on processes designated in the literature [3].

Vapor-Liquid equilibria measurements. VLE measurements of the considered systems were conducted by the enhanced isopiestic technique. The isopiestic device consisted of a multi-leg manifold connected to round-bottom flasks. The instrument was held in a constant-temperature bath for several days to reach equilibrium. From the water activity (a_w) of a standard solution (NaCl solution), the activity of water for all the mixtures within the isopiestic system can be calculated. The measurements were performed in a fixed temperature water bath at three temperatures: 298.15, 303.15 and 308.15 K.

Solubility measurements. The solubilities (S) of the carbohydrates in pure water and in water/[Bmim][Br] and water/[Bmim][HSO_4] solutions were obtained at 298.15 K. First, aqueous mixtures of ionic liquids with definite concentration were constructed in the cell. Carbohydrates were added to each solution in a small excess value over the expected solubility. Samples were remained for one day at 298.15 K to allow any suspended solid bits to settle down. After the equilibrium was achieved, sampling as performed by syringes from liquid phase of each tube and then the concentrations of sugars were determined by the Anton Paar Gyromat Digital Automatic Polarimeter.

III. RESULTS AND DISCUSSION

For a better understanding of the molecular mechanism of the soluting-effect phenomenon of ionic liquids on saccharides in aqueous mixtures, the experimental vapor-liquid equilibria data including water activity (a_w) and the constant a_w lines and as well as the solid-liquid equilibria data were gained for several aqueous saccharide/ionic liquid systems. At the same condition, the values for the a_w of aqueous binary systems increase in the trend: [Bmim][HSO_4] < [Bmim][Br] ≤ sugars, which is reverse order of hydrophilicity power of the solutes. From these data, the hydrophilicity of these ionic liquids and sugars is independent of temperature. The SLE experiments were conducted for the aqueous [Bmim][Br]/sugars and [Bmim][HSO_4]/sugars systems at 298.15 K. In fact the soluting-out effect phenomenon in these systems is leading to sequestration of carbohydrates from aqueous medium by ionic liquids. Soluting-out effects are usually quantified by fitting the experimental solubility data to the Setschenow relation:

$$\ln\frac{S_0}{S} = k_s C_s \qquad (1)$$

In which S and S_0 are the solubilities of the nonelectrolyte in a salt solution of concentration C_S and pure water, respectively and k_S, is the soluting-out coefficient (Table 1). As can be seen, [Bmim][Br] because of its smaller hydrophilicity, has the weaker soluting-out effect on the

aqueous carbohydrate solutions than [Bmim][HSO_4] (larger values of k_s).

Table 1: The values of the soluting-out coefficients, k_s, obtained from SLE data for the investigated systems at 298.15 K

Carbohydrate	[Bmim][Br]		[Bmim][HSO_4]	
	k_s / kg.mol^{-1}	R^2	k_s / kg.mol^{-1}	R^2
Sucrose	0.0699	0.9230	1.0323	0.9420
Glucose	0.0501	0.9980	0.2454	0.9676
Fructose	0.0674	0.9992	0.2563	0.9880
Arabinose	0.1087	0.9530	0.1052	0.9479

Zdanovskii-Stokes-Robinson rule (ZSR rule) is a linear concentration relation between equilibrated isopiestic concentration of solutes in ternary and binary aqueous mixtures in which both components have similar hydrophilic strength (semi-ideal behavior) [4]. The measured isopiestic concentrations of the investigated sugar / ionic liquid / water systems were examined with the following ZSR low:

$$\frac{m_{IL}}{m^0_{IL}} + \frac{m_C}{m^0_C} = 1 \quad (a_w\text{=constant}, 0 \le \frac{m_{IL}}{m^0_{IL}} \le 1 \text{ and } 0 \le \frac{m_C}{m^0_C} \le 1) \qquad (2)$$

where m^0_i and m_i are the molality in the binary and ternary mixtures under isopiestic equilibrium, respectively. In Table 2, the experimental deviations ($\Delta_0 = \frac{m_{IL}}{m^0_{IL}} + \frac{m_C}{m^0_C} - 1$) from this equation have been presented for some of the studied systems. From table 2, all the investigated IL/sugar systems show the negative deviation from the ZSR law (Eq. (2)).The negative departure from the semi-ideal model shows that the soluting-out effect happens in all the investigated systems. The hydrophilicity of all the studied solutes conform the order: [Bmim][HSO_4] > [Bmim][Br] ≥ carbohydrates. Because of the unfavorable sugar-ionic liquid interaction, when the ILs are added to the aqueous carbohydrate mixtures, the sugar molecules exclude themselves from the neighborhood of ionic liquid ions or vice versa by strengthen their interactions with water molecules. Consequently, in the ternary ionic liquid + sugar aqueous mixtures, the smaller ionic liquid and sugar concentrations are required for the isopiestic equilibrium with certain binary sugar/water and IL/water mixtures in respect to the ZSR rule (straight line). Therefore these systems show the negative deviation from the semi-ideal behavior. For example, Fig. 1 shows the experimental constant a_w lines for aqueous [Bmim][HSO_4] + sucrose and [Bmim][Br] + sucrose systems. As can be seen from Table 2 and Fig. 1, for all the aqueous [Bmim][HSO_4] + sugar systems, the negative deviations are slightly more than [Bmim][Br] containing systems.

Table 2: Isopiestic equilibrium concentrations, a_w and deviations from the semi-ideal behavior, Δ_0, for several IL + carbohydrate (C) + water (w) solutions.

m_{IL} / mol.kg^{-1}	m_C / mol.kg^{-1}	a_w	Δ_0
[Bmim][HSO_4] + Sucrose + water at 298.15 K			
1.7736	0.4535	0.9237	-0.1485
1.0311	0.9886	0.9237	-0.2868
1.5068	0.3851	0.9353	-0.1316
0.8815	0.8448	0.9353	-0.2781
1.0964	0.2803	0.9536	-0.1102
[Bmim][Br] + Sucrose + water at 298.15 K			
3.6850	1.3608	0.8837	0.0090
2.0740	2.7906	0.8837	-0.0073
1.8791	0.8670	0.9377	-0.0029
0.8767	1.8621	0.9377	-0.0132

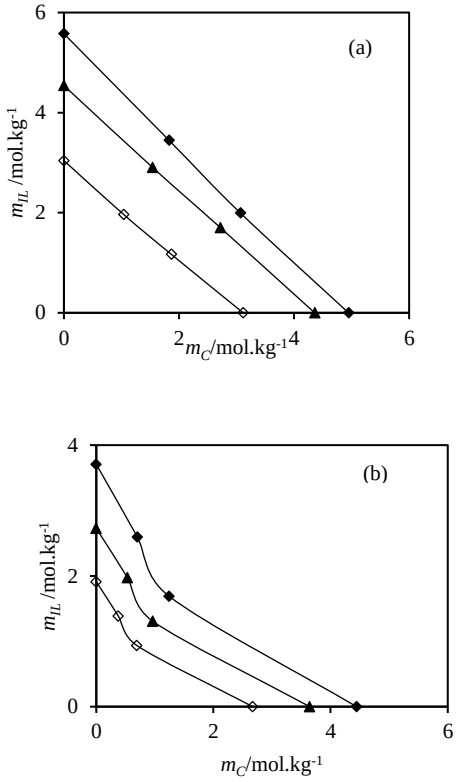

Fig. 1: Plot of the molality of ILs, m_{IL}, against the molality of sucrose, m_C, for the constant water-activity lines at T = 308.15 K. (a): [Bmim][Br] + sucrose + H_2O system, ◆, a_w = 0.8816; ▲, a_w = 0.8960; ◇, a_w = 0.9297 and (b): [Bmim][HSO_4] + sucrose + H_2O system, ◆, a_w = 0.8916; ▲, a_w = 0.9161; ◇, a_w = 0.9417.

IV. CONCLUSION

Aiming to achieve a finer understanding of the mechanism of the soluting-effect phenomenon in aqueous systems, a systematic study including solid-liquid equilibria and vapor-liquid equilibria experiments were carried out for aqueous mixtures of two groups [Bmim][Br]/sugar, and [Bmim][HSO_4]/sugar aqueous systems at various temperatures. In these systems with the small difference of hydrophilicity power between ionic liquids and carbohydrates the very slight deviation from the semi-ideal manner were seen. On the other hand, SLE results showed that the soluting-out effect appears in the form of precipitation of carbohydrates from the aqueous solution by hydrophilic ionic liquids. The more hydrophilic ionic liquid ([Bmim][HSO_4]) showed the stronger soluting-out effect and thereby more negative departure from ZSR rule than [Bmim][Br].

REFERENCES

[1] Y. Zhang, S. Zhang, Y. Chen, J. Zhang, Fluid Phase Equilib. 257, 173–176, **2007**.
[2] M.G. Freire, C.L.S. Louros, L.P.N. Rebelo, J.A.P. Coutinho, Green Chem. 13, 1536–1545, **2011**.
[3] L. Cammarata, S.G. Kazarian, P.A. Salter, T. Welton, Phys. Chem. Chem. Phys. 3, 5192–5200, **2001**.
[4] A.B. Zdanovskii, Tr. Solyanoi Lab. Akad. Nauk. 6, 5, **1936**.

Volumetric and Compressibility Studies of Tetraalkylammonium Bromide Salts in Aqueous Solutions at Different Temperatures

Shadieh Yadollahzadeh*[a], *Rahmat Sadeghi*[b]

[a]*Department of Chemistry, University of Kurdistan, Sanandaj, Iran, shadi.ydz1994@gmail.com*
[b]*Department of Chemistry, University of Kurdistan, Sanandaj, Iran, rsadeghi@uok.ac.ir*

Abstract: In order to study the thermodynamic of aqueous solutions of tetraalkylammonium bromide (TAAB) salts and to better understanding of ion-ion, ion-solvent, and solvent-solvent interactions, the systematic studies included the volumetric and compressibility, were carried out on these systems. The salts tetramethylammonium bromide (TMAB), tetraethylammonium bromide (TEAB), tetrapropylammonium bromide (TPAB), and tetrabutylammonium bromide (TBAB) were selected. The volumetric and compressibility measurements were carried out for the aqueous solutions of these salts at different temperatures. The experimental density and sound velocity data were used to calculate the apparent molar volume ($V_{\varphi,s}$) and apparent molar isentropic compressibility of the solutes ($\kappa_{\varphi,s}$), and isentropic compressibility of solutions (κ_S). In order to investigate the solute-solvent interactions, the infinite dilution quantities such as the infinite dilution apparent molar volume ($V^0_{\varphi,s}$), infinite dilution apparent molar isentropic compressibilities ($\kappa^0_{\varphi,s}$), and the partial molar expansibilities ($E^0{}_\Phi$) were calculated.

Keywords: Apparent molar volume, Compressibility, Density, Hydrophobic hydration, Tetraalkylammonium bromide

I. INTRODUCTION

Tetraalkylammonium salts have been extensively used in research work on water and aqueous solutions because the salts have nonpolar groups (hydrocarbon chains) that strongly interact with water and have notorious structural influence. Solute partial molal volume, V_i^0 , has been useful in understanding solute-solvent interactions. The temperature dependence of V_i^0 and some extra thermodynamic assumptions can be used to calculate ionic contributions to the volumes and to get partial molal expansibilities at infinite dilution. These limiting quantities depend on ion size and ion-solvent interaction. In particular, hydrophobic interactions can be studied this way. Volumetric properties have been widely investigated for this purpose. Most of the work has been done at 298.15 K; much less work has been done above 298.15 K and very little work has been done below 298.15 K [1,2]. In this work, in order to study the thermodynamic of aqueous solutions of tetraalkylammonium bromide (TAAB) salts and to better understanding of ion-ion, ion-solvent, and structural interactions, the systematic studies included the volumetric and compressibility were carried out on these systems. For this propose, four TAAB salts with common anion (Br^-) and different cations including TMAB, TEAB, TPAB, and TBAB were selected. The experimental density and sound velocity data are reported at 288.15–308.15 K and atmospheric pressure.

II. METHODS

All tetraalkylammonium bromide salts including TBAB, TPAB, TEAB, and TMAB were obtained from Merck. All the solutions were prepared by mass on a Sartorius CP225D balance precise to within $\pm10^{-5}$ g. The density and sound velocity of the mixtures were measured at different temperatures with a digital vibrating-tube analyzer (Anton Paar DSA 5000, Austria) with proportional temperature control that kept the samples at working temperature within $\pm10^{-3}$ K. The apparatus was calibrated with double distilled deionized, and degassed water, and dry air at atmospheric pressure. Densities and ultrasonic velocities can be measured to $\pm10^{-6}$ g.cm^{-3} and $\pm10^{-2}$ m.s^{-1}, respectively, under the most favorable conditions. The uncertainties of density and ultrasonic velocity measurements were $\pm3 \times 10^{-6}$ g.cm^{-3} and $\pm10^{-1}$ m.s^{-1}, respectively.

III. RESULTS AND DISCUSSION

Apparent molal volumes ($V_{\varphi,s}$) of various salts in aqueous binary solutions at different temperatures have been calculated from the experimental values of densities using the following equation [3]:

$$V_{\varphi,s} = \frac{M}{d} + \frac{1000}{mdd_0}(d_0 - d) \quad (1)$$

where M, m, d, and d_0 are the molar mass of salt, molality, density of solution, and density of solvent, respectively. Based on our results, for all studied TAAB salts in aqueous solution the value of $V_{\varphi,s}$ is increased by increasing temperature. This can be explained with releasing water molecule from

hydration zone of solutes to the bulk and thereby increasing the volume of solute at higher temperatures. However, the $V_{\varphi,s}$ – m_s behavior is quite different for each salt. For TBAB/water system, the $V_{\varphi,s}$ isotherms are decreased slowly with concentration that shows that hydrophobic hydration plays an important role. In other systems especially for TMAB/water system at lower concentrations, the apparent molar volume of salt increases with increasing solute molality. At the low concentrations, the produced ions can be hydrated strongly by electrostatic interactions. By increasing the salt concentration due to destructive overlap between hydration co-spheres of ions, the net hydration of solutes is reduced and the solute volume will increase. The infinite dilution apparent molar volumes ($V^0_{\varphi,s}$) for salts were obtained by least-squares fitting of the following relations to $V_{\varphi s}$ data by using Redlich–Mayer type of equation as [4]:

$$V_{\varphi,s} = V^0_{\varphi,s} + S_v m_s^{0.5} + B_v m_s \quad (2)$$

The obtained results show that for all salts, the values of $V^0_{\varphi,s}$ are increased by temperature in the temperature range studied. The partial molar volumes ($V^0_{\varphi,s}$) were fitted to a polynomial of the following type in terms of temperature [5]:

$$V^0_{\varphi,s} = a_0 + a_1 T + a_2 T^2 \quad (3)$$

The partial molar expansibilities ($E^0_{\varphi,s}$) can be obtained by the following equation:

$$E^0_{\varphi,s} = (\frac{\partial V^0_{\varphi,s}}{\partial T})_P = a_1 + 2a_2 T \quad (4)$$

As can be seen from Fig. 1, the values of $E^0_{\varphi,s}$ for all investigated TAAB salts in aqueous solution are positive. For TMAB and TBAB decrease by increasing temperature, while for TEAB and TPAB increase by increasing temperature. The positive values for $E^0_{\varphi,s}$ depicts that the presence of strong salt – water interaction in solution. In the temperature range studied, the values of $E^0_{\varphi,s}$ follow the order: TBAB > TPAB > TEAB> TMAB.

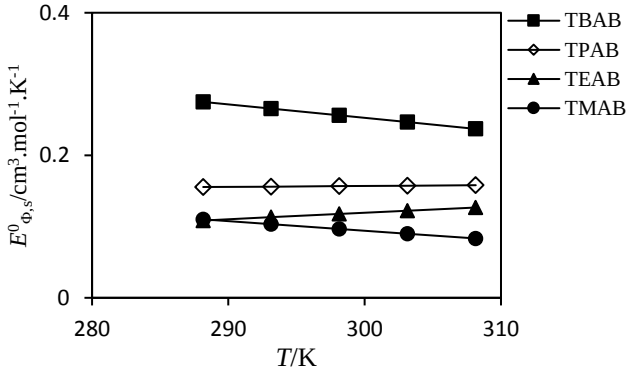

Fig. 1: Plot of infinite dilution apparent molar expansibilities of the investigated salts, $E^0_{\varphi,s}$, in aqueous solutions against the temperature.

Isentropic compressibility of aqueous salt solutions (κ_S), can be calculated from the experimental density (d) and sound velocity (u) data by using the Laplace – Newton equation:

$$\kappa_S = \frac{1}{du^2} \quad (5)$$

As an example, the variation of κ_S values with the molality of salt (m_S) for aqueous TBAB solutions at different temperatures are shown in Fig. 2. From this Figure, it can be seen that the κ_S isotherms decrease with increasing the concentration of solute, and the slope of these isotherms becomes smaller with increasing temperature. Figure 2 also shows that, at a certain molality of solute, the values of κ_S are decreased with increasing temperature. In fact, in aqueous TAAB solutions the isentropic compressibility is sum of two contributions, κ_S (solvent intrinsic) and κ_S (solute intrinsic). κ_S (solvent intrinsic) is related to compression of three-dimensional network of water structure and dependent on the temperature. κ_S (solute intrinsic) is compressibility due to compression of hydration layer and intramolecular empty spaces of solute which increases by temperature. On The other hand, for pure water at a certain temperature there are two structured aggregates with $\frac{\partial \kappa_S}{\partial T} < 0$ (which is stable below 373 K) and less structured aggregates with $\frac{\partial \kappa_S}{\partial T} > 0$ (which is stable above 373 K). At the studied temperature range, the structured aggregates are dominant and compressibility of water is decreased with temperature. For all salt/water systems in the studied concentration range, participation of solvent is dominant and since the compressibility of the structured form of water is reduced in studied temperature range, therefore compressibility of aqueous salt solutions is diminished by temperature. At high concentrations, the term of solute intrinsic in κ_S becomes dominant and the isentropic compressibility of solutions is increased with increasing temperature.

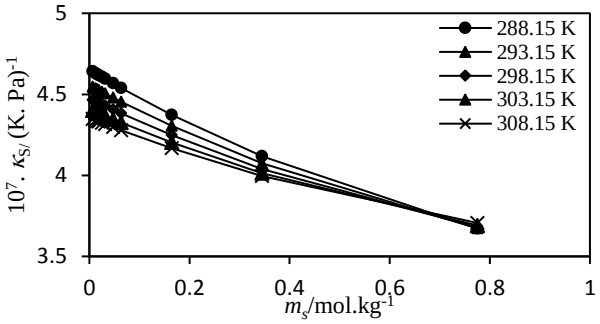

Fig. 2: Variation of isentropic compressibility, κ_S, with the molality of salt, m_s, for aqueous TBAB solutions at different temperatures

The apparent molar isentropic compressibility ($\kappa_{\varphi,s}$),

of salts in water as a function of their concentration were calculated by using equations given below:

$$\kappa_{\varphi,s} = \frac{\kappa_S M_s}{d} + \frac{1000(\kappa_S d_0 - \kappa_S{}^0 d)}{m_s d d_0} \quad (6)$$

The values of infinite dilution apparent molar isentropic compressibility of salts ($\kappa^0{}_{\varphi,s}$) in water were obtained by least-squares fitting of the following relations to $\kappa_{\varphi,s}$ data by using Redlich–Mayer type of equations as:

$$\kappa_{\varphi,s} = \kappa^0_{\varphi,s} + S_\kappa m^{0.5} + B_\kappa m$$

The results show that the values of $\kappa^0_{\varphi,s}$ in pure water are increased by increasing temperature for all salts and at a certain temperature follows the order: TMAB > TEAB > TPAB > TBAB.

IV. CONCLUSION

Volumetric and compressibility behavior of tetraalkylammonium bromide salts including TMAB, TEAB, TPAB, and TBAB in aqueous solutions have been studied at different temperatures. The results show that the values of $\kappa^0_{\varphi,s}$ are increased by increasing temperature for all solutes and at a certain temperature follows the order: TMAB > TEAB > TPAB > TBAB. The results show by reducing the length of the alkyl chain of cation, the solvation behaviors of these salts become closer to the 1:1 electrolytes and with increasing the length of alkyl chain more deviation has been observed for 1:1 electrolytes.

REFERENCES

[1] C. Klofutar, J. Horvat, D. Rudan-Tasič,., Acta Chim. Slov. 54 **2007**.

[2] L.H. Blanco, E.F. Vargas, J. Solution Chem. 35, 21–28, **2006**.

[3] C. Marignac, *Ann. Chim. (Paris)*,22, 415, **1871**

[4] L.M. V Pinheiro, A.R.T. Calado, J.C.R. Reis, C.A.N. Viana, s, J. Solution Chem. 32, 41–52, **2003**.

[5] H. Shekaari, Y. Mansoori, R. Sadeghi, Density, J. Chem. Thermodyn. 40, 852–859, **2008**.

Prediction of Water Content in Poly (Para-Phenylene terephthalamide) Based on Non-Electrolyte Flory-Huggins Theory

Maryam Abedi

Department of Chemical Engineering, Faculty of Imam Mohammad Bagher, sari branch, Technical and Vocational University (TVU), Mazandaran, Iran.

Email: m.abedi85@gmail.com

Abstract: In this study, the water content was predicted in type of aromatic polyamides at high degrees of polymerization at high temperatures .To model the experimental results, a semi-experimental Flory-Huggins theory was used. The model contains only two fitted parameters, and is able to describe the available data for the effects of temperature on the water concentration in the polymer at various water partial pressures.

Keywords*:* Flory-Huggins theory; water content; high temperatures; non-electrolyte model; partial pressure; poly-para-phenylene terephthalamide.

I. INTRODUCTION

poly-para-phenylene terephthalamide is an important group of commercial polymers known as aramid. This polymer is one of the first synthetic polymer fibers that is very light and has high tensile strength and has good thermal resistance. It is used in aerospace and military applications, for ballistic-rated body armor fabric and ballistic composites, in bicycle tires, marine cordage, marine hull reinforcement [1-3].

Environmental factors such as humidity and temperature can affect polyamides and cause them to degrade. Most polymer fibers swell due to moisture absorption. During the polymerization and in the presence of Low amounts of water, the equilibrium progresses to the amidation of the end-group and, as a result, we will have a high average molecular weight of the polymer; But in environments where the amount of water is high, the equilibrium progresses to hydrolysis of amide bonds, resulting in low molecular weight polymerization. Since molecular weight has a profound effect on the physical properties and polymer efficiency, as a result, the concentration of water in polyamides is an important quantity, and modeling the water content in polyamides is of particular importance.

II. METHODS

To perform experiments, a stainless-steel reactor was used to maintain polymers at high temperatures and to create a Phase equilibrium. Also, moisture analyzer was used to determine the moisture content of each sample and deionized water was used to create steam in the reactor [4].

III. RESULTS AND DISCUSSION

Various analytical techniques can be used to measure the amount of water in aramid polymers. One of these methods is to heat the sample under a vacuum or stream of neutral carrier gas to separate the water, then the header is represented by Karl Fischer reagent. Karl Fischer's titration is one of the common methods for determining the moisture content of polymer samples. The aramid polymer pieces are placed in the stainless-steel reactor to provide a high-temperature, high-pressure water vapor pressure equilibrium between the liquid-vapor phase. The samples are placed very quickly on glass walls and analyzed with a moisture analyzer. The empirical data was used to model the solubility of water in poly-para-phenylene terephthalamide using the Flory-Huggins theory.

A. Figures and Tables

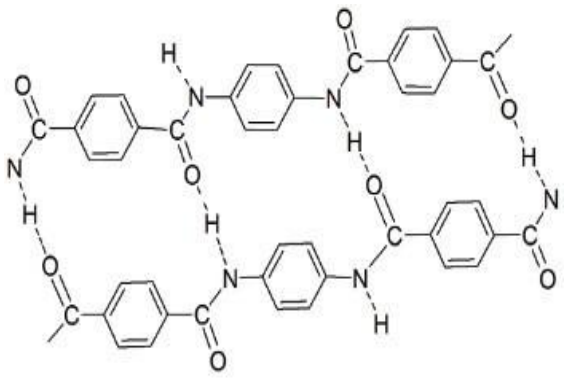

Fig.1: structure of poly-para-phenylene terephthalamide.

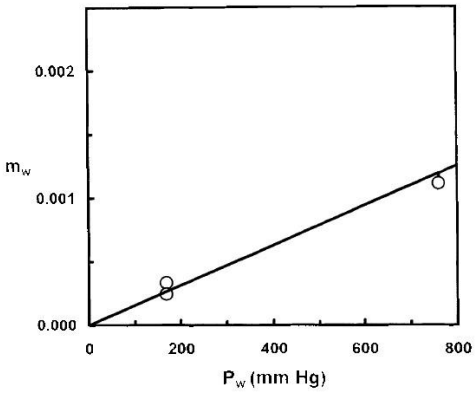

Fig.2 : Comparison of the results obtained from model predictions and experimental data for water solubility in poly-para-phenylene terephthalamide.

B. Equations

The study of the thermodynamic properties of non-electrolytic systems has always been of interest to scientists. During the extensive research, various models have been presented.

In 1941, Flory and Huggins independently worked on systems containing large polymeric macromolecules in the presence of a smaller solvent and provided a model for studying the thermodynamic properties of these systems.

The relation that describes the activity of water in the equilibrium of liquid-vapor in the polymer-water system is:

$$\ln a_w = \ln \nu_w + \left[1 - \frac{1}{DP}\right] \nu_P + \chi_{wp} \nu_p^2 \qquad (1)$$

The Flory-Huggins interaction parameter is temperature dependent and has an inverse relationship with temperature variations and is often modeled as follows [3]:

$$\chi = A + \frac{B}{T} \qquad (2)$$

IV. CONCLUSION

To study the thermodynamics of non-electrolytic systems including high molecular weight soluble molecules, the Flory-Huggins model was used. This model requires only two adjustable parameters and is a simple and widely used model for studying the compression reaction of the aramids and the phase equilibrium. For types of poly-aramids (with different amide groups ratio to different benzene groups), knowing the values of temperature and vapor pressure, and using this model, we can predict the water content, as well as the obtained values with the values obtained with Experimental methods.

REFERENCES

[1] J.N .Boss, V.K .Ganesh, Composite Structures, 274, 289,**2006**.
[2] Dawelbeit Ahmed, Zhong Hongpeng, Kong Haijuan, Liu Jing, Ma Yua, Yu Muhuo, Materials Research. **2014**; 17(5): 1180-1200
[3] Zhaoqing Lu, Wanbin Dang, Yongsheng Zhao, Lamei Wang, Meiyun Zhanga and Guodong Liua, RSC Adv., **2017**, 7, 7293–7302
[4] M .A .SchaEer, E .K .Marchildon, K .B .McAuley .and M. F .Cunningham, Chem Erg .TechnoL, 401,**2001**.
[5] N .Schuld and B .A .Wolf, in J .Brandrup, E .H . Imrnergutand E .Grulke, eds., Polymer Handbook Fourth Edition, p .vII/247 .Wiley and Sons, NewYork **1999**.

Butyric Acid-based Deep Eutectic Solvent as a novel catalyst for esterification Reaction

Karzan Abdulkareem Omar [a,b], ***Rahmat Sadeghi*** [b]*

[a,b] *Department of Chemistry, Faculty of Science, University Koya, Koya KOY45, Kurdistan Region – F.R, Iraq*
[b] *Department of Chemistry, University Kurdistan, Sanangaj, Iran*
Email: rsadeghi@uok.ac.ir, karzan.abdulkareem@koyauniversity.org

Abstract*:* The green esterification carried out for the first time by using deep eutectic solvents as replacement of harmful sulfuric acid, which was commonly used as a catalyst in the esterification reactions. The catalytic activity of DES1 and DES2 observed for producing 25%, 54% and 76% of ester at the optimum temperature(140 ^{0}C).

Keywords: Quaternary ammonium salts, butyric acid, DES, and green catalyst.

I. INTRODUCTION

A deep eutectic solvent has been synthesized in 2001and introduced as a new type of green solvent [1, 2]. Such a novel solvent showed great green potential over other solvents by their non-toxicity, non-flammability, sustainability, biodegradability, lower vapor pressure, low-cost, and easy preparation methods. Basically, DESs mixture is composed of hydrogen bond acceptors (HBAs) and hydrogen bond donors (HBDs) interacting through hydrogen bond interactions between each other. The melting point of DESs mixtures is lower than pure individual component. Moreover, deep eutectic solvents exhibited interesting physicochemical properties such as high depression freezing point, polarity, viscosity, density, surface tension, conductivity, and pH[3]. Such attracting properties made them applicable in different type of applications such as cosmetics[4], pharmaceutical[5], food industry[6], catalyst[7], reaction media[8], adsorbing carbon dioxide[9] and sulfide dioxide[10], solubilizing metal oxides[11], extraction and separation of organic phenolic compounds[12], and antioxidant[13]. Esters are a significantly interesting type of compounds due to their uses of food and cosmetics[14], pharmaceutics, and polymer industry[15]. Generally, esters are prepared by condensation of alcohol with carboxylic acids[16] along with the presence of alkylating agents such as triazine[17], dimethylcarbonate[18]. All these methods required acids as catalysts which causing long time reaction and dealing with toxic solvents. Recently, researches defined deep eutectic solvent have the capability to replace organic toxic solvents[19]. A few studies reported the activity of DES as an effective catalyst in the esterification processes[20]. In this work, for the first time, we used super acidic DESs as a catalyst, solvent, and alkylating agent for the preparation of ester without adding other additives.

II. METHODS

Quaternary ammonium salts (ChCl, TEAB, and TPAB) and butyric acid (BA) was the raw materials of the deep eutectic solvents (Aldrich 99%). The eutectic solvents such as DES1(ChCl-BA), DES2 (TEAB-BA), and DES3 (TPAB-BA) was formed at a certain molar ratio by mixing the two HBAs and HBDs components together at 80^{0}C until a homogeneous, colorless liquid form. The esterification carried out according to literature[16].

III. RESULTS AND DISCUSSION

The prepared deep eutectic solvents were kept for three weeks to ensure their stability, after that their physical characteristics studied.

A. Density

The density measurement of prepared deep eutectic solvents examined in the range of 293.15 to 333.15 K at 5 K interval with an average uncertainty of ±0. 0001 g cm−3. Figure 1 presents measured densities of the DES1-DES3. The obtained results revealed that the temperature-dependent behavior of DESs mixtures. DES densities were decreased with increases temperature as shown in figure 1a.

B. Speed of sound

The speed of sound for all three DESs measured as a function of temperature. Figure1 shows the variation of the speed of sound with temperature. It can be the observed speed of sound decreases with increasing temperature. The rising temperature made the medium less dense and retarding traveling wave of sound as presented in figure 1b.

C. Refractive index

The measurement of the refractive index of DESs carried

Batch	Catalyst	T(°C)	t(h)	DES(ml)	Yield
1	DES1	100	2	1	0
1	DES2	100	2	1	0
1	DES3	100	2	1	0
1	DES1	120	2	1	0
1	DES2	120	2	1	0
1	DES3	120	2	1	0
1	DES1	120	2	1	54
1	DES2	120	2	1	25
1	DES3	120	2	1	0
2	DES1	100	2	1	76
2	DES2	100	2	1	0

out at a temperature range of 293.15 K to 333.15 K. The variation of refractive index plotted as a function of temperature presented in Figure 1. The impact of temperature can be observed on the refractive index of DESs. The refractive index value of DESs decreased as temperature increases as shown in figure 1c.

D. Esterification

In this work, the catalytic activity studied all for three deep eutectic solvents. in the present work, we screened temperature and avoided long time reaction to preventing an undesirable side products [21]. The esterification reaction carried out at two hours of reaction time and different temperature. The experimental condition is shown in table 1. There was no ester product observed from 100 to 120 °C. But when reaction performed at 140 °C for DES1, DES2, and DES3. The desirable esters formed by using DES1 and DES2 as a catalyst from 25 to 76%, and except for the DES3 in the first batch and DES2 in the second batch showed no catalytic activity may be due to their long alkyl chain.

Batch 1

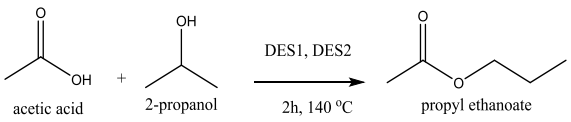

Batch 2

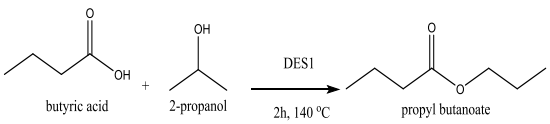

Table 1 Catalytic condition for esterification reactions

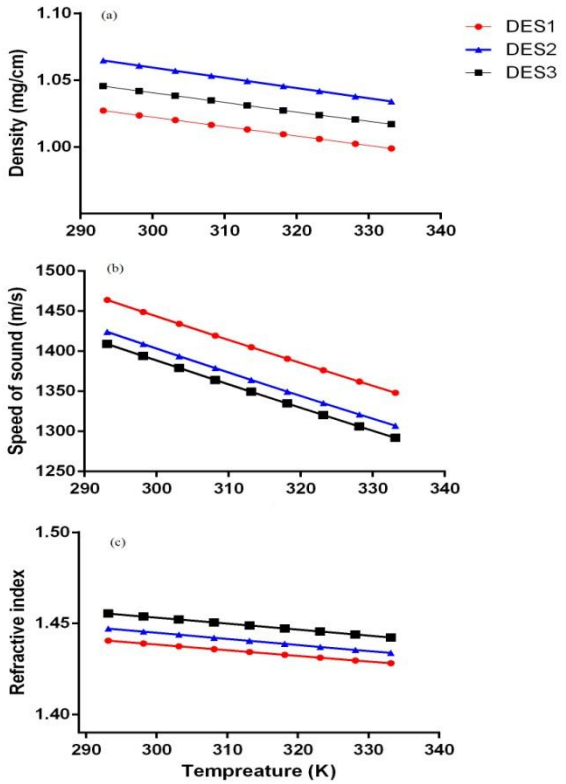

Figure 1. Physical properties of prepared DESs, (a) density, (b) speed of sound, and (c) refractive index.

III. CONCLUSION

In this work, we are reporting a new green catalyst for the production of the ester from carboxylic acid and alcohol. We indicated catalytic activity for DESs under the performed conditions. Therefore, from now on, the harmful sulfuric acid can be replaced by proper deep eutectic solvents.

REFERENCES

[1] Liang H, Li H, Wang Z, Wu F, Chen L, Huang X. 2001. *The Journal of Physical Chemistry B* 105:9966-9

[2] Abbott AP, Capper G, Davies DL, Munro HL, Rasheed RK, Tambyrajah V. 2001. *Chemical Communications*:2010-1

[3] AlOmar MK, Hayyan M, Alsaadi MA, Akib S, Hayyan A, Hashim MA. 2016. *Journal of Molecular Liquids* 215:98-103

[4] Jeong KM, Ko J, Zhao J, Jin Y, Yoo DE, et al. 2017. *Journal of Cleaner Production* 151:87-95

[5] Choi YH, van Spronsen J, Dai Y, Verberne M, Hollmann F, et al. 2011. *Plant Physiology* 156:1701-5
[6] Dai Y, Verpoorte R, Choi YH. 2014. *Food Chemistry* 159:116-21
[7] Gotor-Fernández V, Paul CE. 2019. *Journal of Biotechnology* 293:24-35
[8] De Santi V, Cardellini F, Brinchi L, Germani R. 2012. *Tetrahedron Letters* 53:5151-5
[9] Ali E, Hadj-Kali MK, Mulyono S, Alnashef I, Fakeeha A, et al. 2014. *Chemical Engineering Research and Design* 92:1898-906
[10] Jiang B, Zhang H, Zhang L, Zhang N, Huang Z, et al. 2019. *ACS Sustainable Chemistry & Engineering*
[11] Rodriguez Rodriguez N, Machiels L, Binnemans K. 2019. *ACS Sustainable Chemistry & Engineering* 7:3940-8
[12] Warrag SEE, Rodriguez NR, Nashef IM, van Sint Annaland M, Siepmann JI, et al. 2017. *Journal of Chemical & Engineering Data* 62:2911-9
[13] Wan Mahmood WMA, Lorwirachsutee A, Theodoropoulos C, Gonzalez-Miquel M. 2019. *ACS Sustainable Chemistry & Engineering* 7:5018-26
[14] Pacheco BS, Nunes CFP, Rockembach CT, Bertelli P, Mesko MF, et al. 2014. *Green Chemistry Letters and Reviews* 7:265-70
[15] Hou F, Wang X-C, Quan Z-J. 2018. *Organic & Biomolecular Chemistry* 16:9472-6
[16] Zheng Y, Song W-B, Xuan L-J. 2015. *Organic & Biomolecular Chemistry* 13:10834-43
[17] Gholap S, Gunjal N. 2017. *Arabian Journal of Chemistry* 10:S2750-S3
[18] Zeng H, Shao H. 2013. *Green Chemistry Letters and Reviews* 6:222-7
[19] Francisco M, van den Bruinhorst A, Kroon MC. 2013. *Angewandte Chemie International Edition* 52:3074-85
[20] Alhassan Y, Kumar N. 2016. *Waste and Biomass Valorization* 7:1055-65
[21] Yasmin S, Sheng W-B, Peng C-Y, Rahman A-u, Liao D-F, et al. 2018. *Synthetic Communications* 48:68-75

Effect of fructose on conductivity of choline chloride/urea deep eutectic solvent as a green and sustainable solvent

Elmira Behboudi[a], Hemayat Shekaari*[a]
[a]Department of Physical Chemistry, University of Tabriz, Tabriz, Iran
Email address: elmira74221@yahoo.com *Corresponding author: Hemayatt@yahoo.com

Abstract*:* Deep eutectic solvents (DESs) have recently received a great interest in diverse fields due to their unique properties as new green solvents. In this paper, we studied the effect of choline chloride (ChCl)/urea on conductivity of aqueous fructose solutions at (288.15-308.15) K. The physical properties such as conductivity, limiting molar conductivities, Λ_0, and ion association constants, K_a, for the fructose in aqueous DES solutions have been estimated using low concentration Chemical Model (lcCM).

Keywords: Fructose; Deep eutectic solvents; Molar conductivity; Limiting molar conductivity.

I. INTRODUCTION

The concept of deep eutectic solvents (DES) was first introduced by Abbott *et al.* as a mixture of two or more components that forms a eutectic. The melting point of this eutectic mixture is lower than both of the individual components [1].The most popular component among all DESs is choline chloride (ChCl) which is similar to B vitamins, and it is a biodegradable and non-toxic salt. Over the last decade, there has been a rapid development in DES systems as designer solvents for various applications [2]. Furthermore, DESs as new type of green solvents, have some recognized properties, such as high viscosity, high thermal stability and low vapor pressure. The purpose of this work is providing the values of molar conductivity of in the aqueous fructose solutions in presence of DES based on ChCl and urea, at T = (288.15 to 308.15) K and atmospheric pressure.

II. METHODS

Chemicals

Choline chloride, urea and fructose were purchased from Merck (Germany) (Table 1).

Table1. Sample provenance of the chemicals and purity.

Chamical Name	Source	Final purity
ChCl	Merk	>0.99
Urea	Merk	>0.99
Fructose	Merk	>0.99

Synthesis the DES

Firstly, choline chloride (ChCl) was mixed with urea with a mole ratio of 1:2 [3]. Briefly, the corresponding mixtures were stirred and heated at 353.15 K for 1 h until homogeneous and transparent liquid was obtained.

Conductivity

The electrical conductivity of the synthesized DES was measured by a multi parameter analyzer (DZS-708, Cheetah) with a resolution of 0.001 ($S.cm^{-1}$). The cell constant was calibrated by measuring the conductivities of aqueous solutions of KCl at different concentrations according to the IUPAC recommendation [1]. The accuracy of the cell constant was found to be 0.2%. The DES electrical conductivity in this study was measured at temperature range of (288.15-308.15) K with 5K intervals. The variation of the temperature was achieved by using a water bath with temperature control. For each measurement three replicates were carried out and the uncertainties of the electrical conductivity and temperature values were within the range of ±0.003 $mS.cm^{-1}$ and ±0.1K, respectively.

III. RESULTS AND DISCUSSION

The electrical conductivities of this DES were successfully measured over a wide temperature range (from 288.15 to 308.15 K with 5 K interval) at normal atmospheric pressure. The experimental data were analyzed using the low concentration Chemical Model (lcCM) by the following set of equations:

$$\Lambda = \alpha\left[\Lambda_0 - S(c\alpha)^{1/2} + Ec\alpha\ln(c\alpha) + J_1 c\alpha + J_2(c\alpha)^{3/2}\right] \quad (1)$$

Table 2 shows the experimentally measured electrical conductivities of this DES in the aqueous fructose solutions. It was found that the electrical conductivity of synthesized DES increased exponentially with raising temperature. This can be attributed to the decrease of viscosity of the DES

exponentially with increasing the temperature. If a solvent is to be used for any particular electrochemical process its electrical conductivity should be higher than a certain limit. So the ChCl/urea DES will be used in electrochemical processes and their conductivity must be more than 10^{-1} $mS.cm^{-1}$.

Table 2**:** Electrical conductivity dataset for choline chloride-based DES.

DES	T/k		
	288.15	298.15	308.15
	Conductivity($mS^{-1}cm^{-1}$)		
ChCl/urea	90.01	96.89	100.55

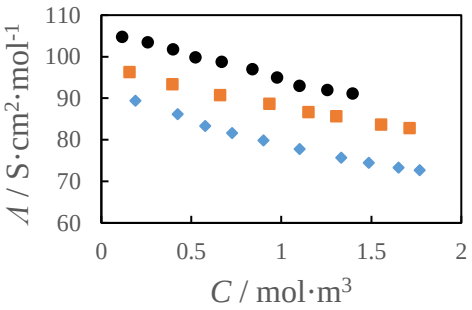

Fig.1: Molar conductivities (Λ) of ChCl/urea in aqueous fructose solution.

IV. CONCLUSION

In this study, we reported the electrical conductivities of DES made from choline chlorid/urea salts in aqueous fructose solutions over a wide range of temperature (288.15–308.15 K at 5 Kinterval) at atmospheric pressure. The results revealed that the electrical conductivities of the synthesized DES demonstrate a strong temperature-dependent behavior. The electrical conductivities of the DES increased exponentially with the increase in temperature.

REFERENCES

[1] A.P. Abbott, G. Capper, D.L. Davies, R.K. Rasheed, V. Tambyrajah, Novel solvent properties of choline chloride/urea mixtures, Chemical Communications (1) (2003) 70-71.

[2] E.L. Smith, A.P. Abbott, K.S. Ryder, Deep eutectic solvents (DESs) and their applications, Chemical reviews 114(21) (2014) 11060-11082.

[3] Q. Zhang, K.D.O. Vigier, S. Royer, F. Jérôme, Deep eutectic solvents: syntheses, properties and applications, Chemical Society Reviews 41(21) (2012) 7108-7146.

Study of molecular interactions between choline chloride/urea deep eutectic solvent and meloxicam

Salva Golgoun [a], ***Hemayat Shekaari*** [a]*, ***Masumeh Mokhtarpour*** [a]
[a]*Department of Physical Chemistry, University of Tabriz, Tabriz, Iran*
**Email:Hemayatt@yahoo.com*

Abstract*:* In the present study, we have investigated a comprehensive assessment of interactional behavior between the choline chloride/urea (ChCl/U) and meloxicam (MEL). Dynamic light scattering (DLS) measurements have been employed to get insight into interactions among DES and drug in the interfacial region.

Keywords**:** Deep eutectic solvents; Solubility; Dynamic light scattering; Meloxicam.

I. INTRODUCTION

Deep eutectic solvents (DESs) have recently been getting a great deal of attention in many fields of science and technology. With a growing interest in this field, there is an urge to understand their effect on the solubility of drugs, which in turn would assist in further designing of drug formation. Nowadays, one of the major problems of pharmaceutical sciences is drug solubility and permeability, which result in an insufficient pharmacokinetics and poor bioavailability of the active pharmaceutical ingredient (API) [1, 2]. According to the biopharmaceutics classification system (BCS) the drugs can be classified in four main groups based on their solubility and permeability [3]. To increase the permeability of class II drugs, their solubility should be increased. In this regard the potential to reduce the environmental impact in pharmaceutical processes has led to investigations on greener solvents for a variety of applications that conventionally use organic compounds. In recent years, Deep Eutectic Solvents (DESs) have emerged as a promising new class of solvents and have opened a new field of research, also they are considered a green alternative to ionic liquids (ILs) in various applications such as pharmaceuticals, organic reactions and nano-science [4, 5]. Also, in some point of view, DESs are deemed new generation of ILs due to their resemblance such as low vapor pressure, wide liquid range, low flammability, easy preparation and low cost [6, 7]. In addition, there are some advantages in DESs, that make them distinguished from ILs, such as, non-toxicity, biodegradability and so on. DESs have emerged as a desirable solvent in view of minimal toxicity and they can be used to overcome the low solubility of drugs. This work was carried out to understand the nature of intermolecular interactions of DESs and meloxicam (MEL). In this regard, dynamic light scattering (DLS) measurements have been employed in order to get deep insight into the molecular interactions between the DES and drug.

II. METHODS

Materials

Choline chloride and urea were acquired from Merck (Darmstadt, Germany). The studied drug was produced by Zahravi Pharmaceutical Co. (Tabriz, Iran). All other chemical reagents were used as analytical grade.

Preparation of DES

The used DES was prepared by weighing using an electronic balance with a precision of $\pm 10^{-4}$ g. The DES can be prepared with the specific mole ratio by stirring at 373.15 K and 1 atm. The stirring was continued for 1 h after a homogeneous liquid was formed. The mixture was cooled naturally to room temperature for further use.

Dynamic light scattering measurements (DLS)

Static light scattering measurements were carried out with a commercial light scattering plate reader (Malvern, model zeta potentiometer) equipped with a diode laser.

III. RESULTS AND DISCUSSION

DLS measurements have been performed to analyze the size of aggregates formed due to drug-DES and drug-drug interactions. The size of aggregates signifies the strength of the interactions between drug and DES as a function of their varying composition. These measurements are carried out for MEL in aqueous ChCl/U solutions at 4 different temperatures (298.15, 308.15, 318.15 and 328.15) K with three different weight fractions of DES. The Fig. 1 represents particle size distribution of aqueous mixtures of meloxicam and DESs at different weight fractions of DES. From the number distribution of particles in these figures (a, b, c), it may be stated that drug-DES interactions are main contributor and large size of aggregates are negligible at lower concentration of DES. The DES-DES interactions may be weakening to a

large extent due to the stronger ion-dipole interaction between meloxicam and DES.

The hydrodynamic radius (d_H) values for smaller aggregates increase by increasing the weight fraction of DES which may put emphasis on the increased drug-DES interactions (w_3= 0.10, 0.30, 0.50). The results are collected in Table for two sampled drugs. There is no doubt that large size aggregates are also increased in size with enhancing the weight fraction of DES.

Additionally, the figures illustrate the d_H of the drug molecules as a function of temperature in the range of 298.15–328.15 K. The value of this parameter showed an apparently decrease with rising of temperature. This temperature dependent size variation could be assigned to the thermo-sensibility of molecules in the hydrophilic shell. Once heating, the particles are moving rapidly in the solution and the drug-DES is separated from each other leading to the reduction of the hydrodynamic radius.

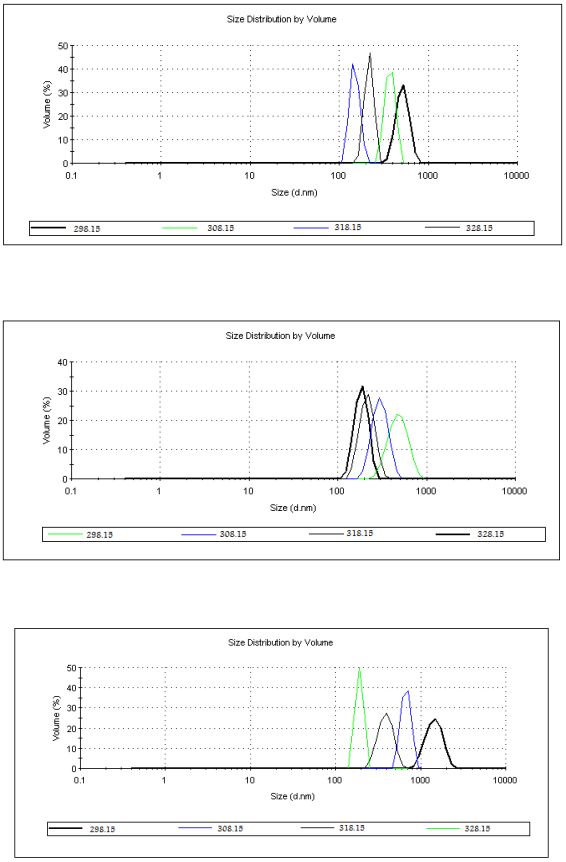

Fig.1: The size distribution of particles of mixtures by volume at three weight fractions of DES and different tempratures.

IV. CONCLUSION

The interaction behavior of DESs and drugs in aqueous solutions has been performed using dynamic light scattering. The hydrodynamic radius (d_H) values for smaller aggregates increase by increasing the weight fraction of DES which may put emphasis on the increased drug-DES interactions (w_3= 0.10, 0.30, 0.50). There is no doubt that large size aggregates are also increased in size with enhancing the weight fraction of DES. The temperature dependent size variation could be assigned to the thermo-sensibility of molecules in the hydrophilic shell. Once heating, the particles are moving rapidly in the solution and the drug-DES is separated from each other leading to the reduction of the hydrodynamic radius.

REFERENCES

[1] C. Loschen, A. Klamt, Journal of Pharmacy and Pharmacology 67 (2015) 803.
[2] U. Tehler, J.H. Fagerberg, R. Svensson, M. Larhed, P. Artursson, C.A. Bergström, Journal of medicinal chemistry 56 (2013) 2690.
[3] N. Tampal, H. Mandula, H. Zhang, B.V. Li, H. Nguyen, D.P. Conner, AAPS PharmSciTech 16 (2015) 5.
[4] A. Shishov, A. Bulatov, M. Locatelli, S. Carradori, V. Andruch, Microchemical Journal 135 (2017) 33.
[5] L. Duan, W.-H. Zhang, Z.-H. Zhang, E.-H. Liu, L. Guo, Microchemical Journal 145 (2019) 180.
[6] B.-Y. Zhao, P. Xu, F.-X. Yang, H. Wu, M.-H. Zong, W.-Y. Lou, ACS Sustainable Chemistry & Engineering 3 (2015) 2746.
[7] S.E. Warrag, C.J. Peters, M.C. Kroon, Current Opinion in Green and Sustainable Chemistry 5 (2017) 55.

Effect of choline lactate as novel green solvent on the aqueous solubility of acetaminophen

Negar Oliya[a], Hemayat Shekaari[*a], Mohammed Taghi Zafarani-Moattar[a], Masumeh Mokhtarpour[a]
"Department of Physical Chemistry, University of Tabriz, Tabriz, Iran
**Corresponding author: Hemayatt@yahoo.com*

Abstract*:* In this work the choline lactate ionic liquid as a green solvent in concentration ranges of 0-0.15 in mol fraction scale has been used to overcome the low solubility of acetaminophen at *T* = (298.15 to 313.15) K. By increasing the concentration of choline lactate the solubility was increased. The obtained solubility data were satisfactorily correlated by modified Apelblat, λh (Buchowski), Yalkowsky models.

Keywords*: Ionic Liquid, Solubility, Acetaminophen, Choline Lactate*

I. INTRODUCTION

Ionic liquid (IL) are a great alternative to organic solvents and are used in different processes [1,2]. The ILs are widely used in the pharmaceutical applications especially in the field of solubility of drugs, recrystallizations, as extractants of pharmaceutical compounds from aqueous solutions. The advantages of these solvents are negligible vapor pressure, low melting point and good thermal stability which making them liquid over large temperature ranges. Furthermore, ILs are non-flammable and easy to recycle. These properties have made them very attractive for use in pharmaceutical industry [3]. The low solubility of many drugs in water is one of the important issues in pharmacy which pharmacists persuade looking for some ways to increase the solubility of drugs [4]. Co-solvency is usually used to increase the solubility of many drugs, including the common drugs such as acetaminophen (ACP). ACP is a painkiller and antipyretic drug which is widely used in modern therapeutics. This drug presented by pediatric patients is especially indicated in the treatment of several minor diseases [5]. However, this drug has a low solubility in water (14 $g \cdot L^{-1}$ at 298.15 K) [6]; and research for a suitable solvent is needed to overcome this problem. In this work, the role of choline lactate [ChLa] as a co-solvent was studied in regard with improving the solubility of ACP at T = (298.15 to 313.15) K and the atmospheric pressure. [ChLa] is a liquid at the environment temperature. The obtained experimental solubility data were correlated with some frequently used models including the modified Apelblat [7], λh (Buchowski) [8], Yalkowsky[9] models.

II. METHODS

First the solutions of IL in water in mass fraction ranges of 0.00 to 0.15 were prepared accurately by using an analytical balance (AW 220, GR220, Shimadzu, Japan) with precision of 1×10^{-4} g. Then using the saturation shake-flask method the solubility of ACP was determined at different temperatures.
When the equilibrium was reached, the top clear solutions were withdrawn and diluted with water. For determining mass fractions of the drug the double beam UV–vis spectrophotometer (Shimadzu, Japan) were used at 248 nm. Each experimental data point was determined as averages of three measurements. In using this method the necessary calibration curve with correlation coefficient of 0.9998 was obtained using diluted known concentrations of aqueous drug solutions.

III. RESULTS AND DISCUSSION

For calculating the aqueous solubility of ACP in the studied IL as mole fraction, X_{ACP}, the following relation was used (1):

$$X_{ACP} = \frac{\frac{W_{ACP}}{M_{ACP}}}{\frac{W_{ACP}}{M_{ACP}} + \frac{W_{IL}}{M_{IL}} + \frac{W_{H2O}}{M_{H2O}}} \qquad (1)$$

In the above equation, M_i and w_i respectively represent the molar mass and the mass fraction of the *i* component in saturated solution [10]. In this research, for the correlation of the experimental solubility data at dilute region, the Apelblat [7], λh [8] and Yalkowsky's [9] modified equations have been used.

The obtained average relative deviation percent (*ARD*%) of the models are used to evaluate the accuracy and applicability of the mentioned models. To calculate (*ARD*%) values the relation (2) was used:

$$\%ARD = 100\left(\frac{\sum_{i=0}^{last(x1exp)} \frac{\left|x1exp_i - x1cal_i\right|}{\left|x1exp_i\right|}}{N}\right) \quad (2)$$

In this equation, x^{exp} and x^{cal} are respectively the experimental and theoretical mole fraction, and *N* is the number of samples. The *ARD*% for the used models are Apelblat (1.43), λh (2.03) and Yalkowsky (5.29).

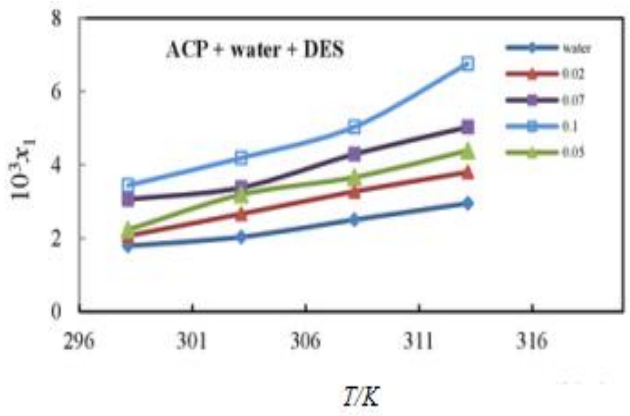

Fig. 1. The solubility mole fraction of ACP in aqueous [ChLa] solutions at different temperatures.

IV. CONCLUSION

The aqueous solubility of acetaminophen in the presence of ionic liquid choline lactate (ChLa), as co-solvent was investigated at the different temperatures *T*= (298.15 to 313.15) K. The results of this study show that with increasing the concentration of this green solvent (ChLa) and temperature, the solubility mole fraction of acetaminophen is increased. In addition, some popular models were satisfactorily used to correlate the solubility data.

REFERENCES

[1] D.H. Zaitsau, G.J. Kabo, A.A. Strechan, Y.U. Paulechka, A. Tschersich, S.P. Verevkin, A. Heintz, Experimental vapor pressures of 1-alkyl-3-methylimidazolium bis (trifluoromethylsulfonyl) imides and a correlation scheme for estimation of vaporization enthalpies of ionic liquids, J. Phys. Chem. A 110 (2006) 7303–7306.

[2] L. Rebelo, J. Lopes, J.M.S.S. Esperança, E. Filipe, J. Phys. Chem. B 53 (2008) 6040–6043.

[3] K.R. Seddon, Ionic Liquids for clean technology, J. Chem. Technol. Biotechnol. 68 (1997) 351-356.

[4] I. Marrucho, L Rebelo, ionic liquids in Pharmaceutical applications, Ann. Rev. Chem. Biomol. Eng. 5 (2014) 527-546.

[5] J.G. Hardman, L.E. Limbird, Gilman's the pharmacological basis of therapeuticsChapter 27 2001 712.

[6] S.H. Yalkosky, R.M. Dannenfelser, Aquasol database of aqueous solubility, College of Pharmacy, University OArizona, Tucson, AZ, 1992 DOI.

[7] A. Apelblate, E. Manzurola, Solubilities ofo-acetylsalicylic, 4-aminosalicylic, 3, 4, 5-dinitrosalicylic, andp-toluic acid, and magnesium-DL-aspartate in water from T= (278 to 348)K, J. Chem. Eng. Data 50 (2005) 1684-1686.

[8] H. Buchowski, A. Ksiazczak, S. Pietrzyk, Solvent activity along a saturation line and solubility of hydrogen-bonding solids, J. phys. Chem. 84 (1980) 975-979.

[9] S.H. Yalkowsky, Y.He,P.Jain, Handbook of aqueous solubility data, CRC press, 2016.

[10] A. Forte, CL Melo, R, Bogel-Lukasik,E. Bogel-Lukasik, A favourable solubility of isoniazid, an antitubercular antibioticdrug. In alternative solvents, Fluid phase Equilib. 318 (2012) 89-95.

Prigogine–Flory– Patterson theory to correlate the excess molar volume and study of interactions for aqueous solutions of some choline chloride based deep eutectic solvents

***Saeid Faraji*[a], *Hemayat Shekaari**[a], *Mohammed Taghi Zafarani-Moattar*[a], *Masumeh Mokhtarpour*[a]**
[a]*Department of Physical Chemistry, University of Tabriz, Tabriz, Iran*
**Corresponding author: Hemayatt@yahoo.com*

Abstract: The excess molar volumes (V^E) for aqueous solutions of the deep eutectic solvents (DESs) based on choline chloride (ChCl) as hydrogen bond acceptor (HBA) with some hydrogen bond donors (HBDs), ethylene glycol (EG), oxalic acid (OA), and malonic acid (MA) were calculated from the density measurements. To develop and design processes and understand molecular interactions the excess properties of aqueous DESs solutions are needed. The obtained values of V^E in the whole concentration range are negative and needless to say that they increase with increasing temperature which indicates strong interactions between DESs and water. The excess molar volumes values were correlated with the use of Prigogine–Flory–Patterson (PFP) theory.

Keywords: Excess molar volumes, Deep eutectic solvents (DESs), Prigogine–Flory–Patterson (PFP) theory.

I. INTRODUCTION

Recently, to overcome the limitations of organic solvents and ILs usage, deep eutectic solvents (DESs) have been introduced. These neoteric green solvents have unique properties including greener replacement to conventional solvents, being as a lower cost, desirable environmental impact, and simple preparation methods. In addition, biodegradable and natural components have been widely used in many processes [1-3].

The applications of these green solvents have been reported in different aspects including NH3 absorbents, SO2 absorption, CO2 capture, and environmental fields. In recent years, many studies have been done on DESs and their physicochemical properties [4,5].

In continuation of our previous studies, the densities (ρ) for aqueous solutions of DESs including ChCl as hydrogen bond acceptor (HBA) with some hydrogen bond donors (HBDs), ethylene glycol (EG), oxalic acid (OA), and malonic acid (MA) were measured in the whole concentration range at T = (293.15 – 308.15) K. The excess molar volume (V^E) for the mentioned systems were calculated. To correlate the obtained V^E values, Prigogine-Flory-Patterson (PFP) theory is used.

II. METHODS

The chemicals used in this work including choline chloride (ChCl), ethylene glycol (EG), oxalic acid (OA), and malonic acid (MA). An analytical balance with precision $1 \cdot 10^{-4}$ g (AW 220, GR220, Shimadzu, Japan) was used to prepare the aqueous solutions with various mole fractions.

Chemical materials	Molar mass ($g \cdot mol^{-1}$)	CAS No.	Resource	Mass fraction Purity
Choline chloride	139.62	67-48-1	Sigma-Aldrich	≥ 0.99
Ethylene glycol (EG)	62.07	107-21-1	Merck	≥ 0.99
Malonic acid (MA)	104.06	141-82-2	Merck	≥ 0.99
Oxalic acid (OA)	90.03	144-62-7	Merck	0.998

Table 1

Chemicals used in the study.

The density of the studied systems was measured with the use a digital vibrating-tube densimeter and speed of sound analyzer (Anton Paar DSA 5000, Austria) at frequency (approximately 3 MHz).

III. RESULTS AND DISCUSSION

In this study, the density measurements were used to calculate the excess molar volume quantity. From this quantity the interactions in the solutions studied are represented at the experimental temperatures.

$$V^E = \sum_{i=1}^{2} x_i M_i \left(\frac{1}{\rho} - \frac{1}{\rho_i} \right) \quad (1)$$

where x, M, and ρ indicate the mole fraction, molar mass, and density of component i, respectively. The negative V^E values for the aqueous DESs solutions at all concentrations and temperatures indicate stronger interactions of DESs with water compared to solvent-solvent and solute- solute interactions.

When pure water is mixed with DESs molecule and with the replacement of DES molecules in the water network, structure of the hydrogen bonds are breakdown which is the reason for the increase in the volume and negativity of the V^E values.

The values of the excess molar volumes for the mentioned systems are as follows; ChCl:OA + water > ChCl:EG + water > ChCl:MA + water. Fig. 1 illustrates the comparison of the V^E values for the systems at T = 298.15 K. It is known that interactions between unlike molecules such as ion-dipole and hydrogen bonding, or structural effects such as packing lead to negative values of V^E, while interactions between like molecules increase these values.

In recent years, the contributions of the structure of the compounds, as well as the structure of the neighboring sites have been used to correlate the excess molar volumes with the help of Prigogine-Flory-Patterson theory (PFP) [6].

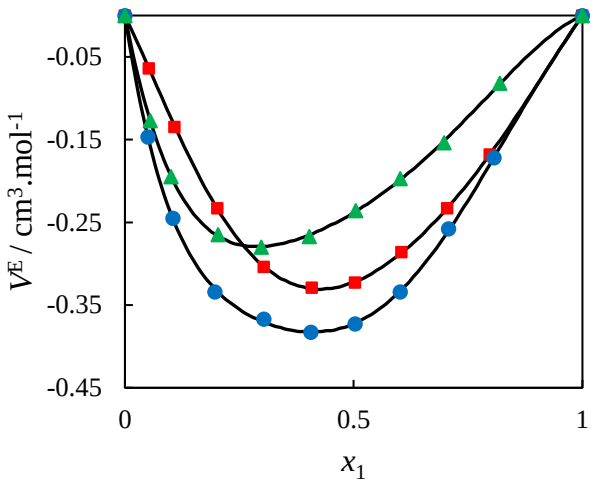

Fig. 4. Comparison of the excess molar volume (V^E) for aqueous DES solutions as a function of DES mole fraction (x_1) at T = 298.15 K: ChCl:EG (■); ChCl:MA (●); ChCl:OA (▲).

The molecular interactions between the compounds of solution have been determined with interaction parameter (χ12) values. The negative values of this parameter describe the stronger interactions between DES molecules and water. The results obtained in Table 2 show that this parameter has become more positive by increasing the temperature, which indicates weaker interactions between DES and water. The values of this parameter for considered systems are as follows; ChCl:OA > ChCl:EG > ChCl:MA, which represents the stronger interactions of ChCl:MA with water.

Table 2
The values of Prigogine–Flory–Patterson (PFP) theory interaction parameter χ_{12} and corresponding the standard deviations (σ (V^E)).

Components	T / K	$10^{-3}\chi_{12}$	σ (V^E)[a]
ChCl:EG (1) + water (2)	293.15	2.382	0.025
	298.15	3.157	0.019
	303.15	3.798	0.017
	308.15	4.315	0.016
ChCl:MA (1) + water (2)	293.15	0.830	0.049
	298.15	2.230	0.049
	303.15	3.293	0.042
	308.15	4.154	0.036
ChCl:OA (1) + water (2)	293.15	4.050	0.044
	298.15	4.975	0.037
	303.15	5.704	0.032
	308.15	6.208	0.026

[a] Standard deviation; $$\sigma = \left(\frac{\sum_{i=1}^{n_{Dat}} \left(V^E_{\exp} - V^E_{cal} \right)^2}{n_{Dat}} \right)^{1/2}$$

IV. CONCLUSION

The excess molar volumes (V^E) were calculated for the mentioned solutions. The values of V^E for DESs are as follows; ChCl:OA + water > ChCl:EG + water > ChCl:MA + water. The more negative values indicate the stronger interactions between DES and water. Prigogine–Flory–Patterson (PFP) theory was also used to illustrate the logical results of excess molar volumes. The parameter (χ12), which represents the molecular interaction of DES with water, describes the more negative values of this parameter and the stronger interactions between solvent and solute. The values of this parameter for DESs are as follows; ChCl:OA + water > ChCl:EG + water > ChCl:MA + water.

REFERENCES

[1] A.P. Abbott, G. Capper, D.L. Davies, R.K. Rasheed, V. Tambyrajah, Novel solvent properties of choline chloride/urea mixtures, Chem. Commun. (2003) 70-71.
[2] A.P. Abbott, G. Capper, D.L. Davies, H.L. Munro, R.K. Rasheed, V. Tambyrajah, Preparation of novel, moisture-stable, Lewis-acidic ionic liquids containing quaternary ammonium salts with functional side chainsElectronic supplementary information (ESI) available: plot of conductivity vs. temperature for the ionic liquid formed from zinc chloride and choline chloride (2: 1). Chem. Commun. (2001) 2010-2011.
[3] M. Hayyan, M.A. Hashim, A. Hayyan, M.A. Al-Saadi, I.M. AlNashef, M.E. Mirghani, O.K. Saheed, Are deep eutectic solvents benign or toxic?, Chemosphere, 90 (2013) 2193-2195.
[4] E. Ali, M.K. Hadj-Kali, S. Mulyono, I. Alnashef, A. Fakeeha, F. Mjalli, A. Hayyan, Solubility of CO2 in deep eutectic solvents: experiments and modelling using the Peng–Robinson equation of state, Chem. Eng. Res. Des. 92 (2014) 1898-1906.
[5] M.T. Zafarani-Moattar, H. Shekaari, Application of Prigogine–Flory–Patterson theory to excess molar volume and speed of sound of 1-n-butyl-3-methylimidazolium hexafluorophosphate or 1-n-butyl-3-methylimidazolium tetrafluoroborate in methanol and acetonitrile, J. Chem. Thermodyn. 38 (2006) 1377-1384.
[6] J. Chen, L. Chen, Y. Lu, Y. Xu, Physicochemical properties of aqueous solution of 1-methylimidazolium acetate ionic liquid at several temperatures, J. Mol. Liq. 197 (2014) 374-380.

Experimental study on the calorimetric data of Aniline + Alkylamine (C4 and C6) at 303.15 K

Mehdi Dadkhah Tehrani*, Khatereh Khanlarzadeh, Hossein Iloukhani
Department of Chemistry, Bu-Ali Sina University, Hamedan, 6517838695, Iran,
Email: m.dadkhahtehrani@che.basu.ac.ir

Abstract: Excess molar enthalpies, H_m^E, of two binary mixtures of Aniline (ANL) + {Butylamine (BUT) or Hexylamine (HEX)} were measured over the whole range of the composition at T = 303.15 K and ambient pressure using a Parr 1455 solution calorimeter. The H_m^E data were negative for all systems over the whole range of composition which become less negative with increasing the chain length. The trend of the H_m^E data was interpreted in terms of the self-association of pure alkylamines, dipole–dipole interactions between ANL molecules and cross-association between unlike molecules (Aniline–alkylamine). Finally, the experimental results were correlated by the Redlich–Kister[1] equation and the two thermodynamic models (Wilson[2] and NRTL[2]) based on the local composition theory.

Keywords: excess molar enthalpy; Aniline; Butylamine; Hexylamine; Redlich–Kister; Wilson; NRTL.

I. INTRODUCTION

The study of thermodynamic properties of binary mixtures is important for the investigation of inter-molecular interactions such as hydrogen bonding, bipolar - bipolar, ion - ion, multipolar and dispersive forces [3,4]. The excess molar enthalpy, H_m^E, is one of the most important thermodynamic properties that provide useful and valuable resources for intermolecular interactions from microscopic and macroscopic point of view in liquid solutions. According to type of geometric connections of hydrogen bonding, steric hindrance, component size, different functional groups, hydrophobic groups, spacial deformation from linear to spherical or vice versa[5,6]. H_m^E can be shown three types of trends: positive deviation, negative deviation and sigmoidal. In this research work, as a continuation of our studies on calorimetric data of mixtures, binary systems of BUT + ANL and HEX+ ANL have been examined. Experimental data were fitted with the Riddle-Kister equation and analyzed by using two thermodynamic models Wilson and NRTL

II. METHODS

A. Materials

Butylamine (w > 0.99), Hexylamine (w > 0.99) and Aniline (w > 0.99) where w is mass fraction, were purchased from Merck and were used without any purification.

B. Apparatus and Procedure

The excess enthalpy of binary mixtures have been measured by using a Parr 1455 solution calorimeter in the isolated room at 303.15 K. All solutions were prepared by mass on a Mettler AB204-N analytical balance precisely within ± 0.1 mg.

III. RESULTS AND DISCUSSION

A. Equations

Experimental values for four binaries mixture were calculated due to the temperature changes during the mixing process and the following equation was calculated:

$$H_m^E = -\left(C_P + \frac{C_V}{n}\right)\Delta T$$

Because of limitation in the volume of the cell and vessel of calorimeter, it is not possible to measure the heat directly from pure reagents, therefore a mixture was used in Dewar vessel whose H_m^E was previously determined, and the value of H_m^E is calculated by:

$$H_m^E = -\left(C_P + \frac{C_V}{n}\right)\Delta T + \frac{n_0}{n}H_{m,0}^E$$

where C_P, C_V, , n_0, n, $H_{m,0}^E$ and ΔT represent the molar heat capacity of the mixture, heat capacity of the calorimeter, amount of substance in the previous mixing process, amount of substance in the Dewar vessel of the calorimeter, excess molar enthalpy and the difference in the temperature after and before the mixing process, respectively. The experimental data were fitted by Redlich–Kister polynomial equation:

$$H_m^E = x_i x_j \sum_{K=0}^{N} A_k (x_i - x_j)^k$$

The experimental and theoretical excess molar enthalpies values of the binary mixture of BUT + ANL as a function of the mole fraction are presented in“ Figure 1”.

By Using the Redlich−Kister polynomial, values of H_m^E for each binary system have been correlated and their standard deviations, σ, determined. Binary mixture of HEX + ANL also shows a similar behavior to the above were mentioned system.

The interactions in the four binary systems of BUT and HEX with solvents of ANL were shown a negative deviation for them. Viewing these values reflects this fact that negative chemical (value of mutual-association between the unlike-molecules + self-association between the like-molecules is negative) contribution is greater than the positive amount of physical contribution in these binary systems and that's why negative deviation for H_m^E is observed. The Redlich–Kister polynomial equation and three thermodynamics models (Wilson and NRTL) were used to correlate the H_m^E data and adjustable parameters of the Wilson and of the NRTL were reported in "Table 1".

Table 1: Adjustable parameters of the Wilson (λ12; λ21) and of NRTL (Δg_{12}; Δg_{21}; α_{12}), models for {BUT(1) + ANL (2)} and {HEX(1) + ANL (2)} at T = 303.15 K together with their standard deviations.

λ_{12}	λ_{21}	Δg_{12}	Δg_{21}	α_{12}	$\sigma(H_m^E)$/J.mol^{-1}	
(J.mol^{-1})					Wilson	NRTL
BUT(x$_1$) + ANL (1-x$_1$)						
-4275.44	401.266	1083.42	-4321.15	0.509	126.131	106.707
HEX(x1) + ANL (1-x1)						
-4651.17	1393.72	940.207	-3898.83	0.592	227.58	217.51

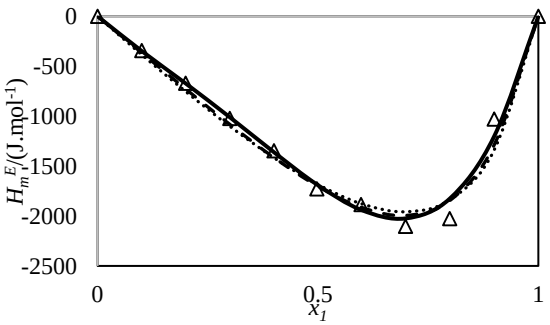

Figure 1: Experimental excess molar enthalpies at T = 303.15 K for {BUT (1) + ANL (2)} mixtures, (△). The point line (…), dash line (---) and solid line were calculated from Wilson model, NRTL model and Redlich-Kister equation respectively.

IV. CONCLUSION

Isothermal excess molar enthalpies, H_m^E, values are negative for all binary mixtures of BUT and HEX with ANL over the whole composition range at T = 303.15 K. In the mixing process, the self-association of alkylamines and ANL are broken and cross-association happens between the unlike molecules. The negative values of H_m^E m due to interactions of unlike molecules are stronger than that of like molecules Analyses of experimental data of all binary systems using the Wilson and NRTL models show that both models were generally satisfactory.

REFERENCES

[1] O. Redlich, A.T. Kister, Ind. Eng. Chem., vol. 40, pp. 345-348 **1948**.

[2] H. Iloukhani, K. Khanlarzadeh, Phys. Chem. Liq., vol. 53, pp. 559-573, **2015**.

[3] R. Checoni, J. Therm. Anal. Calorim., vol. 101, pp. 349-357, **2009**.

[4] H. Zarei, E. Parvini, M. Behroozi, J. Chem. Thermodyn., vol. 51, pp. 139-143, **2012**.

[5] T. Kimura, T. Suzuki, K. Takata, A. Soga, Y. Nomoto, T. Kamiyama, Y. Nakai, H. Matsui, M. Fujisawa, J. Therm. Anal. Calorim., vol. 113, pp. 1467-1474, **2013.**

[6] E. Matteoli, L. Lepori, A. Spanedda, Fluid Phase Equilib., vol. 212, pp. 41-52, **2003**.

Mathematical modeling of liquid phase equilibria for the systems (water + phosphoric acid + linear alcohols) using the GMDH-type neural network

Kh. Kazemi*, S. Shekarsaraee
Department of Chemistry, University of Guilan, Rasht, Iran
*Email:**dkazemi7375@gmail.com***

Abstract: A GMDH type-neural network was applied to predict ternary equilibrium data for the {water + phosphoric acid + linear alcohol (1-nonanol or 1-undecanol)} ternary systems at T = 298.2 K. In order to achieve modeling, the experimental points were divided into train and test parts. The data set was separated into two sections: 70% were utilized for ‘‘training’’ and 30% were applied as test. The forecasted values were compared to experimental values in order to evaluate the ability of the GMDH neural network method. The results predicted by GMDH type neural network were in excellent agreement with the experimental results.

Keywords: phosphoric acid, GMDH model, Liquid equilibria

I. INTRODUCTION

The exact LLE data of ternary aqueous systems containing phosphoric acid (PA) and organic solvents are important and required for design of competent separation treatments, which should be prepared from straight measurement of LLE data [1]. Usual activity coefficient models such as NRTL and UNIQUAC have been effectively used to explain many LLE systems. Lately, new forecasting methods were improved using artificial neural networks (ANNs). ANNs are nonlinear and highly flexible models that have been effectively applied in various systems mainly in predicting vapor-liquid equilibrium (VLE) and LLE data [2]. In this research, a model for LLE forecasting was improved by GMDH algorithm.

II. METHODS

The feed-compositions of the ternary systems {water + phosphoric acid + organic solvents (1-nonanol or 1-undecanol)} were generated using formerly published experimental points [1 and 3]. For both the ternary systems, the data set includes 6 points for each ternary mixture. For all the systems, the data were separated into two sections: nearly 70 % was applied as training data (4 points) and 30% was utilized as test one (2 points). The three feed compositions in the mass fractions were employed as inputs of the GMDH-type network. The two mass fractions in the water phase (w_{11}, w_{21}) and solvent phase (w_{13}, w_{23}) were employed as output data of the neural network.

III. RESULTS AND DISCUSSION

For the three ternary systems, the data set include 6 points for two different solvents. The three feed compositions were used as inputs of the GMDH-type network. The two mass fractions in the aqueous phase (w_{11}, w_{21}) and organic phase (w_{13}, w_{23}) were applied as demandable outputs of the neural network. Our suggested model deal in prediction of the LLE of the studied systems is presented in Figs. 1-4. These figures belong to (water + PA + 1-Nonnol) system and the rest of figures were not presented here. An example of obtained equations for w11 of 1-Nonanol containing system is given in Table 1.

The root-mean-square deviation (RMSD) could be calculated as a parameter of the precision of the predictions. The RMSD values were calculated from the dissimilarity between the experimental and estimated mass fractions. The following equation shows how to calculate the RMSD values:

$$\mathrm{rmsd} = \sqrt{\frac{\sum_{k=1}^{n}\sum_{j=1}^{2}\sum_{i=1}^{3}\left(w_{ijk}^{\exp} - w_{ijk}^{cal}\right)^2}{6n}}$$

where n is the number of tie-lines, w^{exp} indicates the experimental mass fraction, w^{cal} is the calculated mass fraction, and subscript I indexes components, j indexes phases and k = 1, 2,. . ., n (tie-lines). The results of rmsd calculations for both the ternary systems are tabulated in Table 2. As can be seen from the table, the results of the improved models give a close contract between measured and estimated points of the LLE.

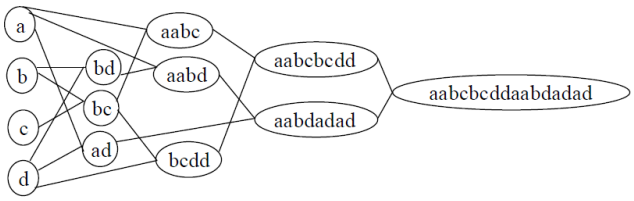

Fig.1. Plot of the Mass Fractions against Data Set Number in the Aqueous Phase w_{11} for Water + PA + 1-Nonanol system

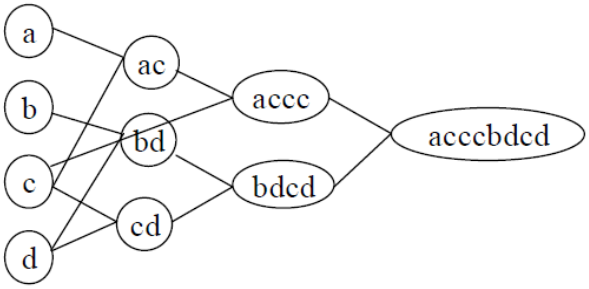

Fig.2. Plot of the Mass Fractions against Data Set Number in the Aqueous Phase w_{21} for Water + PA + 1-Nonanol system

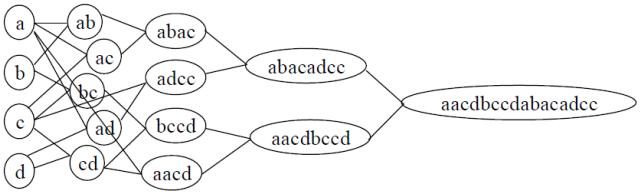

Fig.3. Plot of the Mass Fractions against Data Set Number in the Aqueous Phase w_{13} for Water + PA + 1-Nonanol system

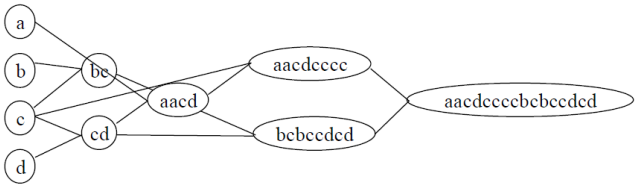

Fig.4. Plot of the Mass Fractions against Data Set Number in the Aqueous Phase w_{23} for Water + PA + 1-Nonanol system

Table 1: Equations of W11 for Water + PA + 1-Nonanol system

w_{11} (mass fraction of water in aqueous phase)	
Y_1=	0.0022 + 0.0442 T – 4.8970 Z_1 – 0.0006 T^2 + 8.7850 Z_1^2 + 0.0326 (T)(Z_1)
Y_2=	1.5342 – 1.6738 Z_2 – 3.0024 Z_3 + 0.2104 Z_2^2 + 3.9381 Z_3^2 + 0.7752(Z_2)(Z_3)
Y_3=	0.0007 + 0.0134 T – 0.4693 Z_3 – 0.0005 T^2 + 0.1717 Z_3^2 + 0.0761 (T)(Z_3)
Y_4=	0.0025 + 0.0493 T – 1.4495 Z_2 – 0.0006 T^2 + 0.7905 Z_2^2 – 0.0075 (T)(Z_2)
Y_5=	0.0708 + 1.2529 Z_1 – 0.9743 Z_3 + 0.2104 Z_1^2 + 3.3733 Z_3^2 – 0.3543(Z_1)(Z_3)
Y_6=	-2.66e-10 + 0.0003Y_1 + 0.9997 Y_2 – 0.0001 Y_1^2 + 0.0004 Y_2^2 – 0.0001 (Y_1)(Y_2)
Y_7=	– 0.3241 – 2.9447 Y_3 + 7.9984 Z_1 – 4.1242 Y_3^2 – 29.1114 Z_1^2 +23.4103 (Y_3)(Z_1)
Y_8=	– 6.25e-9 + 5.89e-8 Y_3 + 1 Y_5 – 7.54e-7 Y_3^2 + 2e-6 Y_5^2 – 2.21e-6 (Y_3)(Y_5)
Y_9=	– 5.48e-8 + 0.4950 Y_6 + 0.50 Y_7 + 0.0005 Y_6^2 – 0.0006 Y_7^2 – 0.00004 (Y_6)(Y_7)
Y_{10}=	12.7e-8 – 2.8e-5 Y_4 + 1 Y_8 – 0.0032 Y_4^2 – 0.0073 Y_8^2 + 0.0004 (Y_4)(Y_8)
w_{11}=	4.6e-8 + 1 Y_9 + 2 Y_{10} – 6.5e-5 Y_9^2 – 0.0007 Y_{10}^2 + 0.0015 (Y_9)(Y_{10})

Table 2: Experimental and calculated tie-lines and RMSD values for the ternary systems (water + PA + 1-Nonanol or 1-Undecanol) at 298.2 K and 303.2 K, respectively.

w_{11}		w_{21}		w_{13}		w_{23}	
Exp.	Calc.	Exp.	Calc.	Exp.	Calc.	Exp.	Calc.
water + PA + 1-Nonanol							
0.779	0.772	0.219	0.224	0.040	0.041	0.019	0.021
0.709	0.711	0.289	0.293	0.042	0.047	0.032	0.030
0.651	0.634	0.347	0.346	0.039	0.044	0.049	0.048
0.594	0.593	0.404	0.405	0.041	0.045	0.071	0.072
0.558	0.555	0.439	0.446	0.045	0.051	0.106	0.112
0.507	0.503	0.490	0.491	0.048	0.053	0.164	0.175
% RMSD: 0.53		% RMSD: 0.61		% RMSD: 0.84		% RMSD: 1.21	
water + PA + 1-Undecanol							
0.831	0.832	0.167	0.169	0.024	0.019	0.005	0.006
0.783	0.788	0.215	0.216	0.025	0.024	0.014	0.015
0.699	0.700	0.299	0.289	0.026	0.025	0.023	0.022
0.623	0.609	0.375	0.374	0.030	0.031	0.051	0.051
0.566	0.561	0.431	0.433	0.032	0.030	0.074	0.077
0.515	0.523	0.482	0.481	0.035	0.035	0.118	0.121
% RMSD: 1.02		% RMSD: 0.76		% RMSD: 0.31		% RMSD: 0.18	

IV. CONCLUSION

In this research, a GMDH-type neural network model was improved by use of published LLE data for the (water + PA + linear alcohols) ternary systems. The equilibrium data were predicted by the GMDH model, the predictions compared with the experimental points and also those previously obtained using the UNIQUAC model. In spite of the difficulty of the studied systems, the GMDH model performed a good prediction of the phase equilibrium. Thus, the GMDH model is appropriate for predicting the LLE data. The agreements between the experimental and estimated data were found to be admirable.

REFERENCES

[1] S. Shekarsaraee. Phase Equilibria of the Ternary System Water + Phosphoric Acid + 1-Nonanol at Different Temperatures, Phys. Chem. Res. 4 (2016) 507-518.

[2] H. Ghanadzadeh, S. Fallahi, M. Ganji, Liquid-Liquid Equilibrium Calculation for Ternary Aqueous Mixtures of Ethanol and Acetic Acid with 2-Ethyl-1-hexanol Using the GMDH-Type Neural Network, Ind. Eng. Chem. Res. 50 (2011) 10158–10167.

[3] S. Shekarsaraee, B. Kolachahi Sabet, F. Moradi, M. Kazemi and Y. Parvandi, Measurement and Correlation of LLE Data for the Ternary System Water + Phosphoric Acid + 1-Undecanol at 303.2 K, Phys. Chem. Res. 7 (2019) 425-434.

Correlation of Celecoxib Solubility in Aqueous Solutions Containing Some Choline Based Deep Eutectic Solvents as Sustainable Solvents

Masumeh Mokhtarpour*[a], Hemayat Shekaari[a], Mohammed Taghi Zafarani-Moattar[a], Saied Faraji[a]

[a]Department of Physical Chemistry, University of Tabriz, Tabriz, Iran
**Email address: Masomeh64_m@yahoo.com*

Abstract*:* Deep eutectic solvents (DESs) have a wide variety of potential and existing applications. Based on the fact that the choline chloride (ChCl) is a complex B vitamin and widely used as food additive, the choline-based DESs are generically regarded as environmentally "harmless" and thus, accepted as "non-toxic". This work provides the solubility measurement of celecoxib (CLX) in binary solvent mixture of water and two DESs at various temperatures (298.15 K, 303.15 K, 308.15 K and 313.15 K). The observed solubility data was subjected to evaluate the relative performance of a number of models including Apelblat, Yalkowsky and Jouyban–Acree, e-NRTL and Wilson models for their correlation efficacy. It was found that the used models can satisfactorily correlate the solubilities of CLX in the mixture solvents under different temperatures.

Keywords: Deep eutectic solvent; Wilson model; Solubility; Celecoxib.

I. INTRODUCTION

Celecoxib (CLX) is a COX-2 selective non-steroidal anti-inflammatory drug and it is used clinically to treat pain and inflammation, and rheumatoid arthritis [1]. However, CLX is a lipophilic drug with very poor water solubility (about 3μg/mL) and a slow dissolution rate, which could limit the efficacy of its formulation in dry powder for inhalation. It should be mentioned that water solubility of CLX should be increased because poor solubility is a persistent challenge in drug discovery which represents the most frequent causes of limited bioavailability [2, 3].

The solubilization of drugs in co-solvents is a technique for enhancing the solubility of poorly soluble drugs. It is well-known that the addition of an organic co-solvent or ionic liquids (ILs) to water can dramatically change the solubility of drugs [4-9]. But ILs are expensive, sometimes highly toxic, poor biodegradable and barely biocompatible, whereas, Volatile organic solvents are a class of chemical solvents in the environment that can cause severe health problems [10]. By contrast, deep eutectic solvents (DESs) have lower costs and environmental impacts. Secondly, the synthesis methods of IL and DES are different. While DES are prepared by simply mixing the components, without waste and no purification step of the solvent is required, Preparation of ILs is difficult and costly. Finally, ILs are organic salts that are wholly composed of ions; DES are the result of complexation between a hydrogen bond acceptor (HBA) and a hydrogen bond donor (HBD), whose interactions, as discussed above, involve mostly hydrogen bonds [11-13].

In this work, the CLX was used for investigation of its solubility in two DESs (ChCl/urea, malonic acid) using UV spectrophotometry and shake flask method for drug quantification at T = (298.15 to 313.15) K. for correlation of the experimental solubility data of CLX in these solvents, the Apelblat [14], Yalkowsky [15] and Jouyban–Acree [16], e-NRTL [17] and Wilson [18] models were used. Comparison and discussion of the solubility and used equations were carried out.

II. METHODS

1. Experimental

1.1. Materials

material	company
Celecoxib	Zahravi (Tabriz, Iran)
Choline chloride	Merck
Urea	Merck
Malonic acid	Merck

1.2. Synthesis of the choline chloride based DESs

Accurate amounts of choline chloride (ChCl) and, urea and malonic acid were mixed with each other [11]. Briefly, the corresponding mixtures were stirred and heated at 353.15 K for 1 h till a transparent homogenous solution was obtained.

1.3. Solubility determination

In this study, for solubility measurement, the shake flask method was chosen. In order to measure the solubility of drug in the aqueous solutions of DESs, an excess amount of drug with 5 g of solvent was poured to a glass tube. Then the vials with the (solid + liquid) mixture and a magnet were stirred in a system with thermostat (ED, Julabo Co., Germany, temperature variation ± 0.1 K). Then the vials were placed in water bath thermostat that was equipped with a temperature-controlling system for 3 days to reach equilibrium. Samples were centrifuged for 15 min at to remove the solid phase (D-7200 Tuttlingen, Hettich Co., U.S.A.) in addition, the undissolved crystals was removed by filteration at isothermal condition through a membrane filters (Durapore® membrane filters, type HV, 0.45 µm, Millipore, MA, U.S.A.). A certain amount of solution depending on temperature and composition was taken and diluted with a certain amount of ethanol/water mixtures. The concentration of the drug was measured using double beam spectrophotometers model T80 UV-vis spectrometer PG instruments, U.K. The λ_{max} (wavelength of maximum absorption) for CLX was at 254 nm. The aqueous solubility of CLX in terms of mole fraction, x_1, in {CLX (1) + water (2) + DESs (3)} systems are calculated by using of Eq. (1):

$$x_1 = \frac{\frac{w_1}{M_1}}{\frac{w_1}{M_1} + \frac{w_2}{M_2} + \frac{w_3}{M_3}} \qquad (1)$$

III. RESULTS AND DISCUSSION

Solubility of CLX in aqueous solutions of DESs

The result of the CLX solubility experiment in terms of mole fraction, x_1, at two concentration areas of co-solvent (dilute and concentrated region) at temperature ranges from 298.15 to 313.15 K is shown graphically in Fig. 1 for w_3 = 0.90. The results show that the solubility of CLX in three aqueous DESs solutions increased with the increasing of DESs weight fraction and temperature. However, the increasing extent of solubility differs in the studied co-solvents. At same temperature, the mole fraction solubility is highest in the presence of ChCl / malonic acid, and lowest in neat water. The solubility of the drug in the presence of co-solvent containing ChCl / malonic acid has increased 62,700-fold than its solubility in pure water. In general, the solubility of CLX in different co-solvents decreases according to the order: ChCl / malonic acid > ChCl / urea. The solubility is determined by the competition of the interaction between the solute-solvent and solvent-solvent.

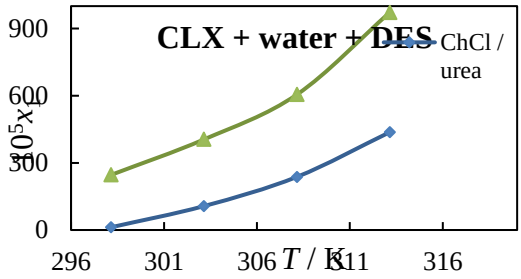

Figure. 3. The relationship between mole fraction solubility of CLX (x_1) in the aqueous DESs mixtures versus temperature (T) at w_3 = 0.90 of DESs.

Modeling results

In the next step, the generated solubility data points were correlated with the Apelblat and Yalkowsky equations, e-NRTL, Wilson and Jouyban-Acree models. the overall %*ARD* (average relative deviation) results for these models are Apelblat (2.58), Yalkowsky (3.20), e-NRTL (11.79), Wilson (22.14) and Jouyban-Acree (1.08). As one can see the Jouyban-Acree model presents better results in respect to the other models, even this model is more accurate than the modified Apelblat and Yalkowsky correlations. Thus, the performance of these models in correlation of the experimental solubility data can be ordered as Jouyban-Acree > modified Apelblat > Yalkowsky > e-NRTL > Wilson.

IV. CONCLUSION

The solubilities of the celecoxib in two aqueous DESs solutions, namely, ChCl / urea and ChCl / malonic acid, were determined experimentally in an equilibrium glass tube at different temperatures using an ultraviolet spectrometer. The solubility of the drug in the presence of co-solvent containing ChCl / malonic acid has increased 62,700-fold regarding its solubility in pure water. Some empirical correlations such as the modified Apelblat, Yalkowsky and Jouyban-Acree models were used. Moreover, to take into account the

nonideality of the liquid mixture, the local composition activity coefficient models, e-NRTL and Wilson were applied to correlate the solubility data. It turned out that the Jouyban-Acree model could give a better satisfactory correlation results compared with those obtained by using the other models.

REFERENCES

[1] C.-C. Tsai, H.-m. Lin, M.-J. Lee, The Journal of Supercritical Fluids 95 (2014) 17.
[2] V. Jouyban-Gharamaleki, J. Soleymani, K. Jouyban-Gharamaleki, T.A. Suleymanov, A. Jouyban, Journal of Molecular Liquids 243 (2017) 715.
[3] S. Rawat, S.K. Jain, European journal of pharmaceutics and biopharmaceutics 57 (2004) 263.
[4] X. Zhang, Z. Zhang, Z. Yang, J. Chai, C. Liu, L. Zhang, X. Zhou, Fluid Phase Equilibria 374 (2014) 20.
[5] K. Zhang, H. Shen, S. Xu, H. Zhang, M. Zhu, P. Shi, X. Fu, Y. Yang, J. Gong, The Journal of Chemical Thermodynamics 112 (2017) 204.
[6] A. Mehrdad, S. Taeb, S. Ehsani-Tabar, Physics and Chemistry of Liquids (2016) 1.
[7] H. Shekaari, M.T. Zafarani-Moattar, M. Mokhtarpour, S. Faraji, Journal of Molecular Liquids (2018).
[8] M. Barzegar-Jalali, A. Jouyban, F. Martinez, H. Shekaari, S.N. Mirheydari, Chinese Journal of Chemical Engineering (2019).
[9] M. Barzegar-Jalali, E. Rahimpour, F. Martinez, A. Jouyban, Chemical Engineering Communications (2018) 1.
[10] E.L. Smith, A.P. Abbott, K.S. Ryder, Chemical reviews 114 (2014) 11060.
[11] Q. Zhang, K.D.O. Vigier, S. Royer, F. Jérôme, Chemical Society Reviews 41 (2012) 7108.
[12] A.P. Abbott, D. Boothby, G. Capper, D.L. Davies, R.K. Rasheed, Journal of the American Chemical Society 126 (2004) 9142.
[13] W. Jiang, L. Dong, W. Liu, T. Guo, H. Li, S. Yin, W. Zhu, H. Li, Chemical Engineering and Processing: Process Intensification 115 (2017) 34.
[14] A. Apelblat, E. Manzurola, The Journal of Chemical Thermodynamics 19 (1987) 317.
[15] S.H. Yalkowsky, Solubility and solubilization in aqueous media. American Chemical Society, 1999.
[16] A. Jouyban, W.E. Acree Jr, Journal of Molecular Liquids 256 (2018) 541.
[17] C.C. Chen, H.I. Britt, J. Boston, L. Evans, AIChE Journal 28 (1982) 588.
[18] G.M. Wilson, Journal of the American Chemical Society 86 (1964) 127.
[19] V. Jouyban, M. Khoubnasabjafari, F. Martinez, A. Peña, A. Jouyban, Journal of Drug Delivery Science and Technology 22 (2012) 545.
[20] C.H. Gu, D.J. Grant, Journal of pharmaceutical sciences 90 (2001) 1277.